UNIVERSIDAD COMPLUTENSE DE MADRID

Facultad de Ciencias Físicas

TESIS DOCTORAL

Rotating objects in general relativity and gauge theories

Objetos rolantes en relatividad general y teorías gauge.

MEMORIA PARA OPTAR AL GRADO DE DOCTOR

PRESENTADA POR

José Luis Blázquez Salcedo

Directores

Luis Manuel González Romero
Francisco Navarro Lérida

Madrid, 2014

Rotating objects in General Relativity and gauge theories

Objetos rotantes en Relatividad General y teorías gauge

by

Jose Luis Blázquez Salcedo

under the supervision of

Dr. Luis Manuel González Romero

and

Dr. Francisco Navarro Lérida

Thesis submitted for the Degree of Doctor in Physics in the
Universidad Complutense de Madrid

· March 2014 ·

CONTENTS

ACKNOWLEDGMENTS

Esta Tesis Doctoral ha sido posible gracias al trabajo y apoyo de mucha gente, cuya contribución, directa o indirecta, quiero agradecer a continuación. Ha sido una etapa de mi vida estupenda, que no habría sido posible sin estas personas.

Lo primero de todo, quiero dar las gracias a mis directores de Tesis, Luis Manuel González Romero y Francisco Navarro Lérida. Los dos han sido unos grandes directores, y sin ellos esta Tesis no habría sido posible. Se han preocupado por que tuviera a mi disposición los medios materiales necesarios para realizar estas investigaciones (en particular, gracias a ellos conseguí la beca de Formación de Personal Investigador de la Universidad Complutense de Madrid (2009), y he podido participar en el proyecto FIS2011-28013 del Ministerio de Ciencia e Innovación). Pero sobre todo, les estoy agradecido por la cantidad de tiempo que me han dedicado. Han sido muchas horas de discusiones y de trabajo personal. Son excelentes personas además de investigadores, y su dedicación y esfuerzo han sido impresionantes y muy motivadores. He aprendido muchísimo de ellos.

También quiero dar las gracias a toda la gente del Departamento de Física Teórica II. En particular a Francisco Guil, por iniciarme en las tareas docentes y facilitarme tanto la colaboración. A Ángela Lera por su constante apoyo e interés. A mis compañeros de despacho, Giovanni, Ricardo, Miguel, Jacobo, Jenifer, Guillermo, Juan y Gerardo, por los buenos momentos y a quienes todavía debo alguna vigilancia...

Quiero dar las gracias a la gente del grupo de Física Teórica de la Universidad de Oldenburg, con quien he realizado dos estancias y visitas extraordinarias: Jutta Kunz, Eugen Radu, Burkhard Kleihaus, Valeria Kagramanova, etc. Especialmente a Jutta Kunz, quien además de ser una científica excepcional, es una gran persona, y me ha ayudado muchísimo, poniendo a mi disposición todo tipo de recursos y dedicándome

todo el tiempo que he necesitado (durante las estancias y después de ellas). He aprendido muchísimo de ella. Tampoco quiero olvidarme de mis compañeros en Oldenburg (Bintoro, Sindy, Olga, Saskia, Keno, Christian, etc), y de la gente del grupo de Astrofísica Teórica de la Universidad de Tübingen. Le estoy muy agradecido a Kostas Kokkotas. Su ayuda fue decisiva en parte de la investigación de esta Tesis, y me procuró los medios necesarios para realizar una visita a su grupo durante la primera estancia en Oldenburg.

No quiero olvidarme de los amigos que han estado a mi lado durante estos años, tanto en los momentos buenos como en los menos buenos. Tengo la suerte de conocer a gente divertida e inquieta, que me ha contagiado su fuerza cuando la he necesitado.

También quiero agradecer a mi madre y a mi padre su apoyo y cariño. Ellos fueron los que incentivaron en mí la capacidad de asombro y el amor por la ciencia. Si he llegado hasta aquí, ha sido por ellos.

Finalmente, quiero dar las gracias a Elena por estar a mi lado constantemente. Su cariño y sus consejos me han dado energías a lo largo de todos estos años. Con ella he compartido esta etapa de mi vida tan feliz.

LIST OF PUBLICATIONS

The research performed in this Thesis has been published in the following peer-reviewed papers:

- Jose Luis Blázquez-Salcedo, Luis Manuel González-Romero, and Francisco Navarro-Lérida, *Phenomenological relations for axial quasinormal modes of neutron stars with realistic equations of state*, Physical Review D **87** (2013) 104042

- Jose Luis Blázquez-Salcedo, Luis Manuel González-Romero, and Francisco Navarro-Lérida, *Polar quasi-normal modes of neutron stars with equations of state satisfying the 2 $M_{\odot}$ constraint*, Physical Review D **89** (2014) 044006

- Jose Luis Blázquez-Salcedo, Jutta Kunz, and Francisco Navarro-Lérida, *Angular momentum – area – proportionality of extremal charged black holes in odd dimensions*, Physics Letters B **727** (2013) 340–344

- Jose Luis Blázquez-Salcedo, Jutta Kunz, and Francisco Navarro-Lérida, *Properties of rotating Einstein-Maxwell-Dilaton black holes in odd dimensions*, Physical Review D **89** (2014) 024038

- Jose Luis Blázquez-Salcedo, Jutta Kunz, Francisco Navarro-Lérida, and Eugen Radu, *Sequences of Extremal Radially Excited Rotating Black Holes*, Physical Review Letters **112** (2014) 011101

- Jose Luis Blázquez-Salcedo, Luis Manuel González-Romero, Francisco Navarro-Lérida, and D. H. Tchrakian, *Non-Abelian Chern-Simons-Higgs vortices with a quartic potential*, Physical Review D **88** (2013) 025026

In addition, several proceedings have been published in peer-reviewed publications:

- Luis Manuel González-Romero and Jose Luis Blázquez-Salcedo, *Core-crust transition pressure for relativistic slowly rotating neutron stars*, AIP Conference Proceedings **1458** (2012) 419-422

- Luis Manuel González-Romero and Jose Luis Blázquez-Salcedo, *New model of relativistic slowly rotating neutron stars with surface layer crust: application to giant glitches of Vela Pulsar*, Journal of Physics: Conference Series **314** (2011) 012088

- Jose Luis Blázquez-Salcedo, Luis Manuel González-Romero, and Francisco Navarro-Lérida, *Axial quasi-normal modes of neutron stars with exotic matter*, Progress in Mathematical Relativity, Gravitation and Cosmology, Springer Proceedings in Mathematics and Statistics **60** (2014) 147-151

INTRODUCTION

In this Thesis we have studied different configurations which are solutions of classical field theories. These objects are neutron stars, black holes, and vortices. The physical interpretation of these objects, and the field theories where they are found, is very different. Neutron stars are solutions of the Einstein equations, and correspond to astrophysical objects which allow us to study the properties of space-time and matter at extremely high densities. The higher dimensional black holes we have studied are very interesting solutions of state-of-the-art low energy effective field theories coming from string theory. Vortices of Yang-Mill-Higgs theories are useful in the phenomenological description of superconductivity.

We have divided these three studies (neutron stars, black holes, and vortices) in three chapters. The link between these three studies is in the methods we have used to generate the solutions, and the tools we have used to study their properties. Although, as we will see, each particular problem has its own peculiarities, the tools used are almost the same ones. In particular, since we have treated axially symmetric and stationary objects, or small perturbations of such objects, we will find that the mathematical problems are very similar in the three cases. We give more detail of this in Chapter 1, where we briefly explain the mathematical and numerical tools we have used throughout the Thesis.

From there we proceed to each particular study. Chapter 2 is devoted to neutron stars, Chapter 3 is devoted to higher dimensional black holes, and Chapter 4 is devoted to vortices. Each one of these chapters includes a brief introduction to each topic. These introductions will help the reader situate the importance and interest of the work. In addition in each Chapter we include the papers that have resulted from these investigations. Together with the introductions presented in each Chapter, the

reader will be able to understand the results obtained in each study.

Finally in Chapter 5 we present some conclusions and an outlook of future continuations of this research.

As we have mentioned, our investigation has led to interesting, original results, which have been published in international front-line journals. Let us enumerate the main results of this Thesis and the corresponding papers where they have been published.

Neutron stars. In papers [1] and [2] (which are included in sections 2.3.2 and 2.3.3, respectively) we have studied axial and polar quasi-normal modes of neutron stars. To do so, we have considered several realistic matter compositions of the neutron star. That is, realistic equations of state that include exotic matter. These equations of state have never been considered before in this context. We have studied several phenomenological relations concerning the spectrum of neutron stars, and we have obtained new ones which are highly independent of the model, and hence could be very useful for asteroseismology.

Regarding neutron stars, we have also studied the slow rotation limit in the presence of a surface energy density enveloping the star. We have applied this model to the study of pulsar glitches. This model allows us to interpret jumps in the rotation velocity of the pulsar as variations in the transition pressure of the core-crust interface. The results of this work can be found in the references [3] and [4], which are included in sections 2.4.2 and 2.4.3, respectively.

Black Holes. Higher dimensional black holes have been obtained in two different theories. In Einstein-Maxwell-dilaton theory, we have studied odd-dimensional black holes, with spherical topology and equal-magnitude angular momenta. We have considered a general dilaton coupling, and hence we also include the case of pure Einstein-Maxwell theory. We have obtained that in the extremal case, Einstein-Maxwell theory features two branches of black holes, with very special relations between the entropy and the global charges (in one of them the entropy is independent of the electric charge). In Einstein-Maxwell-dilaton theory, only the branch of black holes with entropy independent of the electric charge is found. The numerical analysis is supplemented with the use of the near horizon formalism. This work can be found in references [5] and [6], and are included in sections 3.5.1 and 3.5.2, respectively.

In Einstein-Maxwell-Chern-Simons theory we have studied five dimensional black holes, where we also assumed spherical topology and equal-magnitude angular momenta. We have considered a general Chern-Simons coupling constant. Surprisingly, we have obtained an infinite branch structure in the extremal case for certain values of

this coupling constant. In this branch structure we find a sequence of radially excited extremal solutions. We also find infinite non-uniqueness of some solutions with respect to the global charges. The study of the near-horizon geometry has also been used to complement the numerical analysis. The results can be found in [7], which is included in section 3.6.1.

Vortices. We have studied non-Abelian vortices in an $SU(2)$ Chern-Simons-Higgs theory with a quartic Higgs potential. We have obtained a branch structure which is dependent on the topological index n, and non-uniqueness with respect the global charges for $n > 3$. This results can be found in paper [8], which is included in section 4.4.1.

Let us begin by giving some insight on which tools and methods have been used throughout this Thesis.

CHAPTER 1

DESCRIPTION OF THE NUMERICAL METHODS

In this chapter we will make some comments on the methods and tools we have used to perform the analysis of the different problems. Although the topics treated in this Thesis are very different (black holes, neutron stars, and vortices), the mathematical tools we have used are very similar in all of them. Since all these three objects are axially symmetric, stationary solutions of relativistic field theories, essentially the system of differential equations, and the corresponding numerical analysis, were mainly equivalent.

1.1 Systems of ordinary differential equations

In this Thesis we will be interested in studying some subset of solutions of a theory. We will see that in every particular case we have been able to reduce the problem to a system of ordinary differential equations. Let us explain briefly how this has been possible.

The theories we have considered can be expressed in terms of a Lagrangian, which is a functional of the matter fields and metric of the space-time. Variations with respect to these fields lead to the Euler-Lagrange equations of the theory, which yield the differential equations we need to solve.

Essentially, we will obtain the Einstein equations together with some matter field equations in the case of gravity (that is, when we study neutron stars and black holes), or just the matter field equations in the case of vortices (which are essentially ruled by the coupling of the Higgs scalar field with the gauge field in our case). All the theories we have considered will yield second order differential equations.

We will consider two different problems: in some cases we will be interested in obtaining some configurations with certain symmetry requirements, and in other cases, our interest will be in studying perturbations of a given solution.

In the first case, we are interested in obtaining a solution of a particular theory. This solution is known to satisfy some symmetry constraints, and hence we are able to write an Ansatz for it. This has been the case for higher dimensional black holes. In this case we are interested in stationary axisymmetric black holes, with event horizon of spherical topology, and all the angular momenta of equal magnitude. In this case, although in general the solution will depend on D coordinates ($D = 2N + 1$), the symmetries allow us to write the metric without any time dependence, or dependence on the azimuthal angles φ_i. Even more, the equal-magnitude angular momentum constrain increases the symmetry to cohomogeneity-1, and we are able to write explicitly the dependence of the metric and field functions on the polar coordinates θ_i. Hence, the only unknown is the dependence of the functions on the radial coordinate r. We are able to reduce the field equations to a system of ordinary differential equations. For more detail see Chapter 3.

Chern-Simons-Higgs vortices are also obtained using an Ansatz. In this case we are interested in vortices in Chern-Simons-Higgs theory in 2 space dimensions. Since we are treating stationary configurations, the fields can be written independently of the time. We are interested in configurations with rotational symmetry on the plane. Even more, we will consider configurations of n vortices pinned up at a certain point (the origin if we center the polar coordinates here). Hence we can explicitly write the angular dependence of the components of the fields in terms of the polar angle φ and the topological index (which coincides with n). Again we have reduced the problem to a system of ordinary differential equations, since the only unknown dependence is on the radial dependence of the field components. This is presented in detail in Chapter 4.

To obtain rotating neutron stars, we have used the Hartle-Thorne approximation [9], where the star is assumed to be in rigid slow rotation (Chapter 2). In this case, the perturbative expansion (which is controlled by the order of the angular velocity), is independent of time (stationary configurations) and the angular dependence can be explicitly written. Hence this problem can also be reduced to a system of ordinary differential equations.

We will also be interested in studying time dependent perturbations of neutron stars, considering non-radial perturbations associated with gravitational waves (quasi-normal modes). The details can be found in Chapter 2. We consider perturbations

of static spherically symmetric neutron stars. Quasi-normal modes are resonant oscillation modes that can be obtained by studying the spectrum of resonances of small perturbations applied on the metric and matter functions. The perturbations are supposed to be small in terms of their contributions to the total energy and curvature. Although the perturbations are in general not spherical, and hence they depend in principle on (t, r, θ, φ), they can be expanded in spherical harmonics, so that we explicitly know the angular dependence for each contribution to the expansion. The perturbation is then indexed with some harmonic indices (l, m). Axial symmetry prevents the perturbation from being dependent on the m number. We will restrict to $l = 2$ perturbations. Hence we have a system of second-order partial differential equations in terms of t and r.

We will be able to write the system of equations of the perturbation functions like

$$\frac{\partial^2 \Psi}{\partial t^2} - \frac{\partial^2 \Psi}{\partial x^2} + \mathcal{D}(\Psi, \frac{\partial \Psi}{\partial x}) = 0 \ , \tag{1.1}$$

where Ψ is some vector containing the perturbation functions that depends on some (redefined) radial coordinate x and the time t. We will find that the system is supplemented with some extra algebraic relations or first-order differential equations.

The time dependence of the solution can be extracted by performing the following transformation

$$\Psi(t, r) = \int e^{i\omega t} \Psi(\omega, r) d\omega \ . \tag{1.2}$$

If ω, the eigen-value, is real, then this is just a Fourier transform. If it is complex, like in quasi-normal modes, then the perturbation is damped, and this is a Laplace transformation. The resulting system of differential equations can be written like

$$\frac{d^2 \Psi}{dx^2} = \mathcal{D}(\Psi, \frac{d\Psi}{dx}) - \omega^2 \Psi \ . \tag{1.3}$$

This is a set of ordinary, second-order differential equations. Although at first sight we have been able to reduce the problem considerably, the cost of this transformation is that now we have introduced into the system ω, which must be determined by studying the boundary conditions of each particular problem. Essentially, we will need to solve the system of equations for random values of ω, and test if the solution satisfies all the necessary boundary and junction conditions. If it does, then ω is an eigen-value, and the solution is a quasi-normal mode.

Thus we have seen that, in all the problems we will study, we will need to solve a system of ordinary differential equations. It will always consist of non-linear second-order differential equations, coupled to some first-order differential equations and algebraic constraints.

Typically we will find that the system of equations is over-determined, meaning that there are more differential equations than unknown functions. In this case we must explicitly show that all the differential equations are compatible with each other. Then we must choose which differential equations to be used to generate the numerical solution. The remaining equations are used as a test which this numerical solution must satisfy.

1.2 Boundary conditions

The system of differential equations must be supplemented with some boundary conditions. The boundary conditions of each type of solution will be characteristic of each object (neutron stars, black holes, and vortices). The domain of integration of neutron stars and vortices is all space-time, while we only need to generate the black hole configuration outside the outer event horizon.

Since we are interested only in asymptotically flat space-time (neutron stars and black holes) or fully flat space-time (vortices), essentially we will see that we must impose a certain decay on the field and metric functions towards infinity.

In addition, the solutions must be regular at the center of the neutron stars and the vortices ($r = 0$), or satisfy symmetry conditions at the event horizon when we consider black holes ($r = r_H$).

We perform a series expansion of the unknown functions around these points. The series expansion is in terms of the radial coordinate. We use the differential equations to constraint the series expansion, in particular, the expansion coefficients and power index. A good parametrization of the unknown functions will allow us to impose the correct dominant term dependence to the numerical programs.

In some cases, the number of constraints that we will be able to obtain from the power expansion and the asymptotical analysis will be bigger than the number of free integration constants. Of course, all these constraints must be satisfied by the numerical solution. We must perform a numerical analysis to decide which set of boundary conditions is more efficient (better precision, shorter integration times, code stability ...). Nevertheless the remaining constraints must be tested in order to ensure that the numerical configuration is correct.

A specially interesting case are extremal black holes of Einstein-Maxwell-dilaton and Einstein-Maxwell-Chern-Simons theories. We will see that in these cases the dominant term of the series expansion (isotropic coordinates) has a non-integer power index (Chapter 3).

1.3 Continuation method

In this section we will give some generalities on the uniqueness of the configurations we are considering. In the next section we will see that we generate a solution by slowly deforming an initial solution, which is assumed to be close enough to the target solution in the space of solutions of the theory. The idea is to start at a known solution or a solution previously generated (initial guess). By small variations of the parameters of the initial guess boundary conditions, we can obtain a new configuration. This is called the continuation method. The numerical procedure does only converge if the final configuration is close enough to the initial one, and if there is uniqueness of the solution with respect to the space of parameters that are changed in the procedure.

Let us note that the boundary conditions are typically given in terms of some parameters, that can be some global charges like mass and angular momentum, or internal parameters of the functions like derivatives or expansion coefficients.

When using the continuation method, we assume to have local uniqueness, in the sense that with the set of boundary conditions used and some fixed values of the parameters, there is one and only one solution of the differential equations in a region near the initial guess. The set of these parameters and boundary conditions must uniquely characterize a solution, at least in a region close enough to the initial configuration.

If this is not the case, then the programs will not converge. If in a region close enough to the initial configuration the parameters and the boundary conditions do not uniquely characterize one solution, then in principle the numerical algorithm will not be able to converge towards one solution, and typically it will oscillate between the possible final solutions.

We find this behavior sometimes, and it can be due to two main reasons. First, it can happen if the boundary conditions we have chosen do not uniquely characterize one solution, and hence, we have to select another more constraining subset of boundary conditions. This happens in systems with over-determined boundary conditions. It can also happen because the initial solution is not close enough to the, otherwise well defined, solution of the differential equations. This can be solved if we select

parameters closer to the ones of the initial solution, or if we try as an initial guess another solution.

Let us finish this section by noting that we will refer sometimes in this Thesis to non-uniqueness of the theory with respect the global charges. This is not to be confused with what we have talked here. When we say there is global non-uniqueness we refer to the inability to uniquely characterize a solution by its global charges (mass, electric charge, angular momentum). In this case, there are various solutions to the differential equations with the same global charges. But the solutions can be uniquely characterized by other parameters, i.e, different boundary conditions. Hence we still have local uniqueness in the space of configurations, and we can safely apply the continuation method.

1.4 Free boundary problems and compactification

We will usually find that the domain of existence of the functions to be determined is not known neither. In mathematics, this is called a free boundary problem.

Typically this problem is found in systems which present phase transitions (Stefan problem). For example, we can imagine a system out of thermal equilibrium composed by ice and water. If in some element of ice the temperature increases above the melting point, the volume of ice decreases and the boundary between both phases moves. Hence the matching surface is determined by the dynamics of the different phases.

In this Thesis we will find this kind of problem when studying neutron stars.

We will see that neutron stars have two different regions. The interior region is formed by matter in different states. The density drops to zero at a certain surface. Beyond this surface we have the exterior region where the space is empty.

We will have two different sets of differential equations for the interior region and the exterior region. In fact, in the interior region the components of the metric will be coupled to the energy density and pressure, but in the exterior region the energy density and the pressure will vanish. The two regions will be separated by a surface (the border of the star) where certain continuity requirements must be imposed to the functions.

The practical problem is that, a priori, the border of the star cannot be determined. The border of the star can only be determined once the pressure distribution is known.

When non-rotating stars are considered, one possible approach is to integrate the pressure distribution, localize the border, and once the border is obtained, proceed to the full integration of the system with the appropriate boundary conditions.

We have used another approach. First we rescale the radial coordinate to the radius of the star $r = a \cdot x$. Hence the radius of the star shows up in the differential equations as a parameter. Then we introduce a trivial differential equation for the radius of the star into the system of equations, $\frac{da}{dx} = 0$. The border of the star is localized at $x = 1$, and the radius can be obtained from the solution of this differential equation.

Compactification of the domain of integration is used in order to be able to impose the boundary conditions without any need to perform approximations. Since the radial coordinate r tends to infinity, and we need to impose certain behaviors of the functions asymptotically, we compactify the radial coordinate so that the integration domain is a compact space. Then we can treat radial infinity as just the endpoint of the domain of integration.

1.5 Colsys

As we have seen, we will need to solve numerically some systems of differential equations. In every problem we will be dealing with, we will make use of symmetries of the system in order to reduce its complexity. We will always reduce the system to a set of ordinary differential equations. The integration variable will typically correspond to some sort of radius.

We will need to supplement this system of differential equations with some boundary conditions. The boundary conditions will be crucial in order to obtain a numerical solution corresponding to the particular configurations we will be looking for (neutron stars, black holes, ...). Essentially, the behavior of the functions at the origin or asymptotically as they approach infinity must be imposed via some boundary conditions at these points. Even more, for neutron stars we will find that two different regions, the interior of the star, and the outside, must be solved and appropriately matched. This will be accomplished by including in addition some important boundary conditions at the surface of the star.

To obtain these numerical solutions we will use Colsys [10]. This software allows to numerically solve boundary value problems for systems of ordinary differential equations. In this section we will give some details on how it works.

We will need to solve numerically some set of unknown functions $u_i(x)$, where $i = 1, \ldots, d$ and $x \in [a, b]$. The system of ordinary differential equations can be written as

$$\frac{d^{m_i} u_i}{dx^{m_i}} = f_i(x, z(u)) \ , \tag{1.4}$$

where m_i refers to the order of the differential equation for the function u_i, and $z(u)$ is the set of all functions and lower order derivatives,

$$z(u) = \left[u_1,\ \frac{du_1}{dx}, \ldots,\ \frac{du_1^{m_1-1}}{dx^{m_1-1}}, \ldots,\ u_d,\ \frac{du_d}{dx}, \ldots,\ \frac{du_d^{m_d-1}}{dx^{m_d-1}}\right] \ . \tag{1.5}$$

Hence, in general we will have a system of d differential equations for d unknown functions. The order of the i-th differential equation is m_i. In general the system will be non-linear and will depend on (not necessarily all) the functions and lower-order derivatives $z(u)$.

This system of differential equations could be written as a system of first-order ordinary differential equations. In this case we will have a system of m^* differential equations, where $m^* = \sum_{i=1}^{d} m_i$. Nevertheless, we will see that the preparation of the system into first-order form will not be necessary. In any case we will need m^* boundary conditions in order to define a solution.

The boundary conditions can be written as

$$g_j(z(u(\eta_j))) = 0 \ , \tag{1.6}$$

where $j = 1, \ldots, m^*$ and $\eta_j \in [a, b]$, $\eta_1 \leq \eta_2 \leq \ldots \leq \eta_{m^*}$. These are the points where the boundary conditions are required to be satisfied. We will assume that each boundary condition only depends on one point η_i (separated boundary conditions). That is, although the conditions could be non-linear in the functions and derivatives, they must relate to values of these quantities only at a single point of the integration domain η_i.

We will assume that this system has a numerical solution such that $u_i(x) \in C^{m_i-1}$ in the interval of integration $[a, b]$.

Since we are dealing with boundary value problems, the method of numerical integration must be global [11]. This means that, contrary to what can be done for initial value problems, where some local approximation can be extended iteratively in order to generate the global solution, for a boundary value problem we will need to solve the approximation globally at once. This is a much harder task than for initial value problems, specially if we seek to control the error. Several methods can be used.

A straight forward generalization of an initial value problem is the shooting method [11]. In this method, a solution is generated satisfying boundary conditions at a single point (say at η_1). Then by randomly guessing values for the rest of free integration constants (always imposed at η_1) different solutions for the system of equations are

obtained. Eventually, the solution which satisfies the appropriate boundary conditions at the remaining points η_i is hit. This "simple" method has the advantage of easy implementation, and use of very well-established algorithms for the initial value problem. But if the parameter space to explore is very large, obtaining the right solution satisfying some particular boundary conditions could be hard and slow.

Hence, one has to rely on finite difference methods (Runge-Kutta methods [11]). The implementation of these methods on boundary value problems is harder than for initial value problems. For initial value problems (no matter whether the method is one-step or multi-step), full information on the solution is available at the initial condition point. The global solution is built locally, and the global error can be estimated using the local error. In boundary value problems, in principle no function u_i is going to be completely determined at any point of the mesh, because the boundary conditions are defined in different points of the mesh. Hence we cannot build the solution locally (there are no explicit Runge-Kutta methods). The method must solve in each iteration all the values of the functions at the mesh points at once (multi-step method). The approximate solution must be obtained globally.

We will make use of Colsys (Collocation Software for Boundary-Value ODEs). This is a state-of-the-art software for boundary value problems [12] that implements several algorithms to solve optimally these kinds of problems. Here is a brief description on how it works.

Collocation method. Let π be a mesh on the integration domain $[a, b]$, with

$$\pi = (a = x_1,\ x_2, \ldots,\ x_N,\ x_{N+1} = b)\ , \tag{1.7}$$

$$h_j = x_{j+1} - x_j,\ j = 1 \ldots N\ , \tag{1.8}$$

$$h = \max h_i\ . \tag{1.9}$$

In each sub-interval, the collocation points are defined using the Gauss-Legendre distribution [13],

$$x_{jl} = \frac{x_j + x_{j+1}}{2} + \frac{1}{2} h_j \rho_l, \tag{1.10}$$

where $j = 1 \ldots N$, $l = 1 \ldots k$ and ρ_l are k Gauss-Legendre points on $[-1, 1]$.

The approximate solution can be written as $u_i = \sum_{n=1}^{M} \alpha_{i,n} \phi_n(x)$, where ϕ_n are some basis of linearly independent functions, and $\alpha_{i,n}$ some coefficients of this approximate solution that remain to be chosen once we assume that $u_i \in C^{m_i - 1}$ [14]. Colsys

uses as basis functions piecewise polynomials which probe to enhance stability and efficiency of the algorithms [12].

There are $M = kN + m^*$ free parameters $\alpha_{i,l}$, which must be determined by requiring the m^* boundary conditions [10], and the differential equations all along the collocation points in the whole interval $[a, b]$. The points where the approximate solution is evaluated are precisely the k collocation points inside each sub-interval.

Linearization. The non-linear problem is linearized by expanding both the ODEs system and the boundary conditions in a first-order Taylor series [14]. In each iteration of the procedure, the collocation procedure is made on this linearized system. The conditions that determine the unknown coefficients can be obtained from the linearized system.

Let us call $u_i^{(0)}$ an initial guess solution of the system, and $u_i^{(\nu)}$ the approximate solution at the ν-th iteration. The linearized system reads

$$\frac{d^{m_i} w_i^{(\nu)}}{dx^{m_i}} - \sum_{l=1}^{m^*} \frac{\partial f_i(x, z(u^{(\nu)}))}{\partial z_l} \cdot z_l(w^{(\nu)}) = \hat{f}_i(x, z(u^{(\nu)})) \ , \tag{1.11}$$

$$\sum_{l=1}^{m^*} \frac{\partial g_j(x, z(u^{(\nu)}))}{\partial z_l} \cdot z_l(w^{(\nu)}) = \hat{g}_i(x, z(u^{(\nu)})) \ , \tag{1.12}$$

with $i = 1 \ldots d$ and $j = 1 \ldots m^*$. $\hat{f}$ and $\hat{g}$ correspond to the non-linear contribution of the differential equations and boundary conditions respectively,

$$\hat{f}_i(x, z(u^{(\nu)})) = f_i(x, z(u^{(\nu)})) - \sum_{l=1}^{m^*} \frac{\partial f_i(x, z(u^{(\nu)}))}{\partial z_l} \cdot z_l(u^{(\nu)}) \ , \tag{1.13}$$

$$\hat{g}_i(x, z(u^{(\nu)})) = \sum_{l=1}^{m^*} \frac{\partial g_j(x, z(u^{(\nu)}))}{\partial z_l} \cdot z_l(u^{(\nu)}) - g_i(x, z(u^{(\nu)})) \ . \tag{1.14}$$

Note this non-linear terms are evaluated using the aproximate solution $z(u^{(\nu)})$. $z_l(u)$ refers to the l-th component of the set $z(u)$ of functions and lower order derivatives. The approximate solution in the $(\nu + 1)$-th iteration is then

$$u_i^{(\nu+1)} = u_i^{(\nu)} + w_i^{(\nu)}. \tag{1.15}$$

Although Colsys does not need the ODE system in first-order form, it does need these Jacobians explicitly [14]. From the differential equations we have to implement into Colsys $\frac{\partial f_i(x, z(u^{(\nu)}))}{\partial z_l}$, and from the boundary conditions, $\frac{\partial g_j(x, z(u^{(\nu)}))}{\partial z_l}$.

Newton's method is used, so that the coefficients of the approximate solution are obtained applying the collocation method to the corresponding linearized problem. But the pure Newton's method tends to perform poorly if the initial approximation is far away from the solution. Hence Colsys actually can make use of a modified (damped) Newton's method [11]. The approximate solution is then

$$u_i^{(\nu+1)} = u_i^{(\nu)} + \lambda^{(\nu)} w_i^{(\nu)}. \tag{1.16}$$

The scalar $\lambda^{(\nu)}$ is the relaxation factor. Colsys implements a method of prediction and correction of the relaxation factor in each iteration. Typically, Colsys only needs a damped Newton's method in the first iteration, since in the subsequent iterations the approximation is good enough to allow the use of the pure Newton's method. The user can control how carefully to estimate the relaxation factor, depending on the sensitivity of the problem [13]. If the problem is not very sensitive to the initial guess, or the approximate behavior is very well known from the beginning, the relaxation factor does not need to be finely estimated as in a more sensitive problem.

Error estimation and mesh selection. Colsys is able to estimate the global error of each function and the derivatives. Essentially, in each iteration two solutions are obtained, one of them with the mesh halved. If the number of Gauss points k is large enough, then the error can be estimated in terms only of this two approximate solutions [14].

The user must introduce some tolerances for each function. If the estimated error is lower than the required tolerance, then Colsys stops. If not, the iteration process continues.

The halving of the mesh is not only useful for error estimation but also for mesh adaptation. If the tolerances have not been satisfied, then Colsys is able to adapt the mesh in order to equidistribute the local error. Hopefully, the equidistribution of the local error leads to a reduction of the estimated global error, and eventually, to the satisfaction of the tolerances required [14]. This adaptive mesh selection is very useful, and allows Colsys to introduce more points in regions where the functions could be more problematic (i.e. fast oscillations of the functions in some regions).

CHAPTER 2

NEUTRON STARS

2.1 Outline and objectives

In this chapter we will study two important properties of neutron stars: quasi-normal modes and the slow rotation regime.

We are interested in studying the resonant modes of oscillation of neutron stars. These oscillations couple to the space-time dynamics and give rise to the emission of gravitational waves. Since neutron star space-time is intrinsically dissipative, these modes are characterized by a spectrum of dominant frequencies and damping times. We cannot apply a standard normal mode analysis. The appropriate tools to study dissipative systems are quasi-normal modes.

The spectrum is sensitive to the size of the star, its mass and its composition. Hence the study of quasi-normal modes of neutron stars with realistic equations of state (EOS) is interesting in order to identify which equation of state describes effectively the matter composition at the densities of neutron stars.

We have performed this analysis in two complementary papers. In the paper Physical Review D **87** (2013) 104042 [1], which is included in section 2.3.2, we have studied the axial component of the spectrum. In paper Physical Review D **89** (2014) 044006 [2], which is also included in section 2.3.3, we have studied the polar component. Both studies have used 15 state-of-the-art equations of state. These equations of state include models for pure nuclear matter, quark-nucleon matter, hyperon matter, and pure quark matter. Most of them are compatible with the recent measurements of $2M_{\odot}$ pulsars. We have studied well-known phenomenological relations, whose purpose is to obtain universal empirical relations between the eigen-modes and some global

properties of the star like the compacity or the mean density. We have also considered some new universal phenomenological relations that are very well satisfied for nuclear, hybrid and hyperon stars. These new phenomenological relations could be used to determine the radius of a neutron star emitting gravitational waves, provided that its mass is known.

We will also study the slow rotation approximation of neutron stars. Since neutron stars are found in nature as pulsars, it is important to study the effect of rotation on the global properties of the star. We will be interested in neutron stars with rigid rotation, where we will study the effect of a surface layer of energy density enveloping the star. We will find that this is an appropriate way of modeling the outer layers of the neutron star. We have applied this model to study the impact of glitches of pulsars on the outer layers of the star. The results of this work can be found in AIP Conference Proceedings **1458** (2012) 419-422 [4] and Journal of Physics: Conference Series **314** (2011) 012088 [3], which are also included in 2.4.2 and 2.4.3 respectively.

2.2 Brief introduction to neutron stars properties

We begin with a brief exposition on the origin of neutron stars. So far, these objects have been observed in nature as pulsars, and we present some properties of these important astrophysical objects. Then we present the internal structure of neutron stars and composition of matter at those densities (higher than nuclear density).

2.2.1 The origin of neutron stars: late-stage stars

Neutron stars are cold compact astrophysical objects, which are found at the final stages of massive stars [15]. During the main sequence phase of a star of mass between 6 $M_\odot$ and 40 $M_\odot$, the star burns mainly hydrogen and helium at its core. The star remains in this stage for several million years, but as the time passes, the chemical composition at the central regions of the star becomes more and more heterogeneous. When the star depletes the hydrogen at the core, it shrinks, increasing the temperature and pressure in the core, and the necessary thermonuclear energy to maintain the star from collapsing is obtained mainly from the fusion of helium. The fusion of hydrogen continues at a thin layer above the core.

Eventually, helium is also depleted from the core, and the star shrinks and heats even more, being able to burn higher and higher elements (carbon, oxygen, silicon...) as the pressure rises at its core. When the core of the star is able to use another

element as nuclear fuel, the thermal energy radiated can even re-expand the outer layers of the star, forming a super red giant with radius bigger than 10^8 km, between 100 and 1000 times the radius of the Sun [16].

As we said, the phase of hydrogen-helium burning at the core maintains the massive star for most of its main sequence life (10^9 years). But higher elements are burnt faster [17]. The carbon fusion stage lasts only 100 years, neon is depleted in 1 year, oxygen in months, and silicon in less than a day [18].

The massive star develops a shell structure composed of different nuclei species. In the deepest shells, temperature and pressure is high enough so that fusion processes can also be found. Eventually, the most exterior layers of the star (mostly of hydrogen and helium) are ejected because of the thermal energy released on them. Massive stars loose mass as soon as the burning of helium in the outer layers starts [17].

Eventually, the core of the star is composed essentially of iron nuclei [18]. Since the fusion of iron and higher elements is an endothermic reaction, no thermal energy can be extracted from the fusion of this element in order to maintain the stability of the star. The core now is maintained by the pressure of non-degenerate electrons. This core has a size of the order of 10^3 km.

In the outer layers of the star, temperature and pressure increase and the fusion can continue. Since the core of the star keeps growing and heating, the central density of the massive star increases, and the core eventually becomes unstable. The neutronization begins [17], and electrons and protons of the iron nuclei interact conversing protons into neutrons. This reaction releases high energy neutrinos which are absorbed in the outer layers. Iron nuclei can also photodisintegrate by absorption of high energy gamma rays [18].

Since the supporting electrons vanish, gravity becomes unbalanced and the core of the star collapse. The core implodes in less than a second and heats beyond 10^{11} K. The densities at the core increase beyond nuclear densities 10^{12} $\mathrm{g \cdot cm^{-3}}$. The supernova explosion begins.

The outer layers free-fall into the core and heat its outer envelopment. But these in-falling layers of matter are rebounded from the core, and shock waves are originated in the interior of the core. These shock waves, together with other mechanisms like the diffusion of high energy neutrinos and convection, interplay so that the gravitational binding energy of the core of the star is transported to the outer layers. A small percentage of this energy (less than 1%) is converted into kinetic energy on the outer layers and electromagnetic radiation, while the rest is lost as high-energy neutrinos. This kinetic energy is responsible for the ejection of all of the outer layers of the star.

The rest of the energy is radiated mainly in electromagnetic form. A single supernova could be more luminous than an entire galaxy for several days. The energy released during the supernova is order 10^{44} J [17].

Only the degenerate core of the progenitor star survives the supernova explosion. This proto-neutron star has a temperature of 10^{11} K. But the heat is radiated by high energy neutrinos which are able to escape the inner regions of the proto-neutron star. The star cools down quickly (in seconds) to temperatures of 10^{10} K. In a matter of years, the neutron star cools down to 10^6 K. The resulting neutron star has a stable structure, and a mix of neutrons, hyperons and quarks could be found in their interior. We will discuss in detail the composition in the following sections.

The outer layers of the progenitor star continue to expand across the interstellar medium. Supernova remnants can have velocities of 10^4 km/s. These remnants can be visible in multiple wavelengths for periods of thousands of years. The composition of these clouds is very rich, since elements heavier than iron can be formed during the supernova phase [18].

As a side note, it is important to notice that the mass ejection during the supernova phase could fail. If the core of the star is not able to eject enough mass, the core could be beyond the Chandrashekar limit (over 2 $M_\odot$), and the collapse of the core could not be stopped. A black hole is then formed. This is though to be the case for very massive stars (over 40 $M_\odot$) [17].

2.2.2 Pulsars

Neutron stars are thought to be realized in nature as pulsars. Pulsar are detected as Pulsating Radio Sources (PSR) in the sky [19]. They radiate in extremely regular pulses, mainly in the radio wavelength. But some pulsars do emit also in other wavelengths like X-rays [20].

The periods of pulsars are essentially found in two groups. Most of the pulsars present periods of the order of a second. The other group radiates with faster periods of the order of milliseconds [17].

The pulse periodicity is highly regular. In fact millisecond pulsars rival with atomic clocks. The amplitude and shape of each individual pulse nevertheless is very variable, probably because of complicated phenomena taking place in the regions of the pulse emission. But when a number of pulses are averaged, typically around one hundred, the mean pulse structure becomes very characteristic of each pulsar. In some pulsars the mean structure can abruptly change from time to time, returning eventually to the original form, indicating again some complicated phenomenology happening in the

outer regions of the pulsar or in its vicinity [17].

Although the averaged pulse is highly stable, the periods can be measured to change over time. In every pulsar, it has been observed that the pulse period increases with time, typically as $\dot{P} = 10^{-15}$. Since the pulsar is braking, we can define a characteristic time of the process $\tau_b = P/\dot{P}$, which in most braking models can be used as an estimation for the age of the pulsar.

Current models of pulsar evolution divide the evolution of the period in two main ages. In the first phase, pulsars spend thousands of years with the period changing very little. Then after a transition epoch, the period starts to grow in a second phase, which can last for some millions of years. Hence pulsars spend most of their life with much larger periods than their initial ones [17].

Millisecond pulsars are very old (10^9 years). The most probable scenario is that these pulsars have been recycled, meaning that the accretion of matter from a companion star has transferred angular momentum to the rotating star. This theory is sustained by the observation of binary systems composed of a millisecond pulsar and a low mass white dwarf companion [19].

In some pulsars, the period presents another interesting feature. Sometimes the period of the pulsar presents sudden jumps, speeding up in a very short time, and increasing the breaking rate until the previous value is reached [19]. These jumps are called glitches, and are thought to be connected with some phenomena happening in the outer layers of the neutron star.

Nowadays there have been detected more than 1000 pulsars. Most of them belong to our own galaxy. But pulsars have also been observed in the Magellanic clouds.

Although pulsars are thought to be the final stage of very massive stars, as we explained in the previous section, only in a few cases pulsars have been observed in the neighborhood of a supernova remnant. Pulsars velocities are very high (10^3 km/s). The supernova remnant, although initially moving fast (10^4 km/s), is slowed down by the interstellar medium. Hence pulsars can move very far away from their corresponding supernova remnant, which finally fades out after times of 10^4 years. As long as supernova remnants are detectable, their signal is much stronger than pulsars signals. Pulsars, on the other hand are much fainter objects. Most of the detected pulsars are found only within 5 kps of the Sun [17].

When a pulsar is found on a binary system, the mass of the object can be calculated. Current masses are between 1 $M_\odot$ and 2 $M_\odot$. Most of the pulsars have a mass of 1.4 $M_\odot$. A model of neutron star must explain why the value of the mass is found in this range, with the current maximum value for a neutron star mass being 2 $M_\odot$ as

we will discuss later.

Because during the collapse of the red giant star, the total magnetic flux is conserved, neutron stars have a very energetic magnetic field (10^{12} Gauss, whereas a normal star has 10^2 Gauss). The axis of the magnetic field in general will not coincide with the axis of rotation of the star.

The current model of pulsar, first considered by Goldreich and Julian [21] and later by Kapoor and Shukre [22], is based on this image of a rotating neutron star with a very intense magnetic field. Apart from the thermal radiation that can be observed in X-ray emission at the surface of the neutron star, the pulsar presents two main regions of emission: the polar cap, where the radio emission is produced, an the outer magnetospheric gap, where the high energy radiation takes place [19].

Basically, electric charges are ejected from the surface and fill the pulsar magnetosphere (from 10^5 km for slow pulsars, to 100 km for millisecond pulsars), until there is electromagnetic equilibrium along the magnetic lines. The axis of rotation would be generally different to the magnetic axis, so there is a complicated structure for the magnetic lines. Because far enough from the star, some of the magnetic lines must move faster than the velocity of light in order to be closed (light cylinder), some of them will be open, giving rise to very intense electric fields. The polar cap is the region around the magnetic poles, where the lines are open, and intense electric fields appear. Similarly, the outer gap is the region near the light cylinder where the magnetic lines are open and strong electric fields are also found. Different interactions of accelerated charges give rise to radio emission near the polar cap, and to high energy electromagnetic emission near the outer gap [19].

2.2.3 Structure and composition of neutron stars

The interior regions of the neutron star support very high densities, higher than nuclear density. Nevertheless, very little is known about the behavior of matter in this regime. Since the behavior of matter at high densities have an impact on the neutron star structure, the observation of the global properties of neutron stars can shed light into the behavior of matter at these energies.

Most of the neutron stars models have a layer structure. Each layer is related to different phase transitions, particle population and interactions appearing as the energy increases. The most probable layer structure, from the surface of the star to the center, is the following [23]:

Atmosphere. A layer of plasma at high temperatures $10^6 - 10^5$ K surrounded by the intense magnetic field of the neutron star near the surface 10^{11} Gauss. Hottest

neutron stars may have an atmosphere of centimeters, while the coldest only of millimeters. Because of the importance of the magnetic field in this region, the equation of state here is not completely understood.

Outer crust. Up to densities of $\rho = 4 \cdot 10^{11}$ g $\cdot$ cm^{-3}, and with sizes around 100 m, it is essentially composed of a mixture of electrons and ions. Ions become fully ionized at $\rho > 10^4$ g $\cdot$ cm^{-3} by the electron pressure. At $\rho > 10^6$ g $\cdot$ cm^{-3} the ultra-relativistic electrons form a strongly degenerate gas. Ions are strongly coupled to the electrons in the most internal regions of the outer crust. Hence most of the outer crust is solidified, forming a crystalline envelopment similar to a metal. The high density favors beta captures in the ions nuclei, enriching the nuclei with neutrons. At the base of the outer crust the neutron rich nuclei becomes unstable, and the neutrons start to drip out, producing a free neutron gas.

Inner crust. This region extends along one kilometer with densities ranging from $\rho = 4 \cdot 10^{11}$ g $\cdot$ cm^{-3} to $0.5\rho_0$, where $\rho_0 = 2.9 \cdot 10^{14}$ g $\cdot$ cm^{-3} is the mass density of nuclear matter in heavy atomic nuclei. It is essentially composed of electrons, free neutrons and neutron-rich atomic nuclei. The fraction of free neutrons increase as the density increases, and at the lower layers, the nuclei may become non-spherical. Different models predict different forms for the nuclei (flat, cylindrical, ...), changing at different phase transitions as the density increases. Superfluidity of the free neutrons confined in the atomic nuclei is likely. In the innermost layer, the nuclei disappear (core-crust interface).

Outer core. Several kilometers long, and densities between $0.5\rho_0$ and $2\rho_0$. Composed essentially by neutrons, and a percentage of protons, electrons and muons (npeμ composition). There is equilibrium of muon decay into neutrons (beta equilibrium), which is density dependent. Since all the components of the npeμ plasma are strongly coupled by nuclear forces, the description of this region must deal with a model of many-body nucleon interaction.

Inner core. This region can have several kilometers long, and reach densities beyond $10\rho_0$. The composition of this region is very model-dependent. Several hypotheses exist: Hyper-ionization, the appearance of hyperon matter like Σ^- and Λ particles; pion and kaon condensation, that is, excitations of pion and kaon condensates; and quark matter deconfinement, essentially light u and d quarks, and strange s quarks. Some results on hyper-ionization can be obtained from experiment, while pion and kaon condensation have not been observed. Quark deconfinement is the most probable scenario for exotic matter. Of course, it is also likely that a mixed phase of these phenomena may happen in the central regions of the inner core of the neutron

star.

Another possibility is that (some) pulsars are really pure quark stars. Essentially naked cores of self-bounded quark matter. We will consider this possibility in our calculations.

2.2.4 Equation of state

In order to build models of neutron stars, we will need to parametrize the matter content in some way. Some properties of the matter inside the neutron star can be used to constrain the way this parametrization is realized.

First, we will always assume that matter inside the star can be described as a continuous medium. The fluid velocity u will be assumed to be continuous in most of the interior of the star, except possibly in some surfaces where a jump may occur.

We will consider that the matter can be described as a perfect fluid [24]. Hence the pressure in a fluid comoving frame will be observed as isotropic. If we denote ρ and p as the energy density and pressure of the fluid observed in this comoving frame, the stress-energy tensor of this perfect fluid could be written such as

$$T^{\mu\nu} = (p + \rho)u^{\mu}u^{\nu} - pg^{\mu\nu}. \tag{2.1}$$

Conservation of energy density flux give us the integrability condition for the Einstein's equations $\nabla_{\nu}T^{\mu\nu} = 0$.

In the interior regions of the star, the temperature of a neutron star falls below 10^{10} K after a few seconds of its formation. Although this is a remarkably high temperature, we can consider the matter to be in a cold state when compared to the energy of the nuclear interactions taking place in most of the neutron star layers (10 MeV). But of course, as we approach the surface of the star, below the neutron drip density, the temperature has important effects and may alter the behavior of the most external layers.

Most of the global properties of the star, like mass, radius, etc., can be very accurately calculated assuming cold matter at the exterior layers of the star. But the temperature of the matter at these layers plays some important effects on some specific properties of the neutron star. For example, the magnetosphere of the neutron star is very sensitive to the Fe^{56} nuclei at the outer layers of the star, which is found at a temperature well beyond its evaporation point [23]. Another example are glitches, which may be triggered by the liberation of thermal energy into the outer layers of the crust [25]. Hence the effect of temperature on the equation of state at these lower

densities is important in the description of some phenomena.

Nevertheless, for the core and inner crust regions, the assumption of cold catalyzed matter is a perfectly valid approximation: cold matter because the thermal energy in the interior regions can be neglected when compared to the interaction energy taking place at nuclear densities. Catalyzed matter because, since we are dealing with late stage stars, all nuclear reactions admissible at the given thermodynamic state of the star have been completed [25].

In general the pressure and the energy density are given in terms of the baryon density n and entropy per baryon s, $p = p(n, s)$, $\rho = \rho(n, s)$. But we are supposing that the thermal degrees of freedom are frozen (Fermi energy is order 10 MeV at nuclear densities, and the star core has thermal energy below 1 MeV $= 10^{10}$ K and decreasing over time). Hence the pressure and energy density are just given by the baryon density $p = p(n)$, $\rho = \rho(n)$. In principle we could always find a relation $\rho = \rho(p)$, the equation of state [23]. The adiabatic index $\Gamma = \left(\frac{\delta \log \rho}{\delta \log n}\right)_s$ is also an important parameter that typically characterizes the behavior of the equation of state at the different regions.

So, in order to build a model of neutron star, we will need to know the equation of state. The way the energy density is related to the pressure depends on the exact material content and interactions present as the density increases. As we have said in the previous section, once the nuclear density is surpassed, the uncertainty in the exact matter behavior is very high, and hence the equation of state for very high densities is very model dependent [23].

Essentially an equation of state can be described in terms of its stiffness or softness. In a certain range of densities, an equation of state is said to be soft if lower pressures are reached, and stiff if higher pressures are reached. In principle, the presence of exotic matter has the effect of softening the equation of state, while the pure nucleonic matter equations of state are much stiffer ones. State-of-the-art equations of state including exotic matter can also become as stiff as pure nucleonic matter EOS. In general, stiff EOS is able to reach higher maximum masses than softer EOS, essentially because for these equations of state the compressibility of matter is higher, and the stars are able to sustain more mass.

Any realistic equation of state must be compatible with recent measurements for the mass of massive neutron stars (1.97 ± 0.04 $M_\odot$ for PSR J1614-2230 [26] and 2.01 ± 0.04 $M_\odot$ PSR J0348+0432 [27]). In particular, the maximum mass of neutron stars [28] cannot be lower than 2 $M_\odot$. Recently several equations of state with exotic matter in the core satisfying the 2 $M_\odot$ condition have been proposed [29, 30, 31, 32], and we will use them in our work.

Typically the equation of state is obtained by extremizing an action that incorporates the couplings between the particle species [17]. Hartee-Fock methods and other mean field methods are used in order to obtain a numerical table relating the energy density, the pressure and the baryon density. A third order monotonic b-spline can be enough to calculate a desired pair of $\rho,\ p$ values, since this interpolation allows us to have continuity in the equation of state and its derivative (the adiabatic index).

The implementation of the equation of state can be made using another interesting method where the adiabatic index Γ is assumed to be piecewise constant. An equation of state with constant adiabatic index is called a polytrope. Hence, if we approximate an equation of state by considering the adiabatic index to be constant in different density intervals, we can build a piecewise polytrope approximation of the equation of state. In the paper by Read et al. [33], this piecewise polytrope approximation is made for 34 equations of state. We will make use of this piecewise polytrope approximation, together with a b-spline of more recent state-of-the-art tabulated EOS.

2.3 Quasi-normal modes

We have seen that the origin of neutron stars is related to a catastrophic event, the supernova explosion, that liberates large amounts of energy. Pulsations of the proto-neutron star are expected as a result of this event. Even more, other catastrophic phenomena, like neutron star collisions, are expected to produce as a result pulsating neutron stars [34].

Neutron stars tend to pulse at a characteristic frequency. This can be understood if we consider the Newtonian limit, where we find that the fluid making up the star rings with a certain spectrum of frequencies determined by the composition, geometry, etc. If viscosity is considered in the Newtonian regime, damping of the oscillation is found.

But since neutron stars are very compact objects, the appropriate description of them must be done in the context of General Relativity. Hence, space-time is a dynamical object, coupled to matter via the Einstein equations. Pulsation of the neutron star couples to the oscillations of the space-time. This causes a very interesting fact, i.e., neutron star pulses are damped, even if viscosity is ignored. The reason is that the energy of the non-spherical oscillation is carried away from the neutron star as gravitational radiation maintained by its own space-time dynamics. The mechanism is similar to, for example, a vibrating string surrounded by a medium. The energy of the vibration couples to the medium, dissipating towards infinity [35].

In the case of non-damped waves, the appropriate way of describing a wave is by a normal modes analysis (Fourier transformation). In this case the wave equation determines the spectrum of frequencies (real numbers) of the system. Typically in these systems the perturbation is localized, and outside this region, the boundary conditions must guarantee that the perturbation vanish.

Neutron star pulsations are quite different. The damping of the oscillation prevents the use of standard normal mode analysis. Even more, since the wave will propagate throughout all the space-time, boundary conditions will be special. Since we are considering that the neutron star is perturbed by an external event, we must impose boundary conditions such that the gravitational wave is outgoing with respect the neutron star [36]. That is, the neutron star radiates gravitational waves, but not incoming gravitational waves are producing the pulsation.

Consider the metric describing the space-time inside and around a static neutron star. This is a spherically symmetric space-time

$$ds^2 = e^{2\nu}dt^2 - e^{2\lambda}dr^2 - r^2(d\theta^2 + \sin^2\theta d\varphi^2). \tag{2.2}$$

The functions ν and λ are functions of r. The matter inside of the star is considered a perfect fluid with a barotropic equation of state. At zero order we have to solve the Tolman-Oppenheimer-Volkov equations inside the star

$$\frac{dm}{dr} = 4\pi r^2 \rho, \tag{2.3}$$

$$\frac{dp}{dr} = -(\rho + p)\frac{m + 4\pi r^3 p}{(r - 2m)r}, \tag{2.4}$$

$$\frac{d\nu}{dr} = -\frac{1}{\rho + p}\frac{dp}{dr}. \tag{2.5}$$

Outside we have the Schwarzschild solution with gravitational mass M.

If we assume that the pulsation of the star is small, we can use perturbation theory to describe the oscillation

$$g_{\mu\nu} = g^0_{\mu\nu} + h_{\mu\nu}. \tag{2.6}$$

Here $g^0_{\mu\nu}$ is the metric of the static configuration, and $h_{\mu\nu}$ the perturbation on the static metric which we will assume satisfies $\max|h_{\mu\nu}| << \max|g^0_{\mu\nu}|$ in order to work with perturbation theory up to first order.

Of course, the matter description must also be perturbed. The 4-velocity is modified by the Lagrangian displacement of a fluid element ξ, and the energy density and pressure are also perturbed up to first order [36]

$$p = p^0 + \delta p, \tag{2.7}$$

$$\rho = \rho^0 + \delta\rho, \tag{2.8}$$

$$u = u^0 + \xi_{,t}. \tag{2.9}$$

We will consider that the pressure and density perturbations are not affected by any dissipative processes. The perturbed stress-energy tensor is given by $T^{\mu\nu} = (p+\rho)\, u^\mu u^\nu - p g^{\mu\nu}$, where we must retain only terms up to first order in the perturbation.

At zeroth order the space-time is static and spherically symmetric, hence the functions only depend on the radial coordinate. In general for a non-radial oscillation, the perturbation functions will be dependent on the radial and angular coordinates, and time. But nevertheless, and following the standard procedure for normal mode analysis, we can expand in harmonic functions the angular dependence of the functions [36]. Essentially, under a parity transformation of the θ coordinate ($\theta \to \pi - \theta$), the components of the metric and stress-energy tensor undergo a scalar, a vectorial, or a tensorial parity transformation. We need a basis of 10 tensor harmonics in order to appropriately expand the angular dependence of the perturbation functions. As a result, the perturbations are indexed with integer numbers (l, k). Since we are assuming axial symmetry, the perturbations do not depend on the k number.

It is interesting to note that we can group the perturbations into two groups, axial and polar perturbations [34]. Under a parity transformation, the axial perturbations transform like $(-1)^{l+1}$ and the polar perturbations like $(-1)^l$. Hence, polar perturbations do not couple to axial perturbations (this is not true if we consider perturbations of rotating stars).

Since energy density and pressure perturbations transform like polar perturbations, the axial component of the oscillation is in fact decoupled from the matter perturbation. The spectrum of axial oscillations is composed only by space-time modes. These modes are related to the space-time curvature and are sustained only by oscillations of the neutron star space-time. In fact, we will see later that polar modes also have a space-time mode component. This is a result of space-time in General Relativity having its own dynamics.

Hence we can consider axial and polar perturbations separately. Second-order

differential equations can be obtained from the Einstein equations for each one of the harmonic components of the perturbation equations. It can be demonstrated that the perturbations outside of the star can be parametrized by a single function that must satisfy the equation

$$\frac{\partial^2 Z^{lk}}{\partial r_*^2} - \frac{\partial^2 Z^{lk}}{\partial t^2} - V(r) Z^{lk} = 0, \tag{2.10}$$

where l and k are the spherical harmonic indexes, r_* is the tortoise coordinate

$$r_* = \int_0^r e^{\lambda - \nu} dr. \tag{2.11}$$

Z^{lk} is a function of the radial coordinate and time.

If Z^{lk} refers to axial perturbations it is called the Zerilli function, and

$$V(r) = \frac{e^{2\nu}}{r^3}\left[l(l+1)r + 4\pi r^3(\rho + p) - 6M\right]. \tag{2.12}$$

Note that for axial perturbations this parametrization also holds inside the star. If Z^{lk} refers to polar perturbations, then it is called the Regge-Wheeler function, and

$$V(r) = 2(r-2M)\frac{n^2(n+1)r^3 + 3Mn^2r^2 + 9M^2nr + 9M^3}{r^4(nr+3M)^2}, \tag{2.13}$$

where $n = (l+2)(l-1)/2$. In the polar case, inside the star a more complicated system of equations must be solved. In any case, a set of algebraic relations and matching conditions (obtained from the imposition of Einstein equations) completely determines all of the perturbation components.

So any initial pulse will propagate throughout the star and the space-time according to (2.10). The spectrum of this equation will be in general continuous. Nevertheless, a pulse propagating will have two distinct phases. In the first phase, the pulse evolves into an oscillatory regime, with a very regular frequency and decay with a very characteristic damping time. After this, the pulse decay with a power law tail. The striking feature is that the configuration does not ring with any arbitrary frequency, but instead it has characteristic frequencies (resonances). The decay of the pulse is a power law at late times, because, as the signal travels away from the star, the dominating term in the potential of (2.10) does not decay exponentially, but as a power of r.

We are interested in this spectrum of characteristic frequencies and damping times found in the first phase of the pulsation. The necessary formalism to obtain these frequencies is the study of quasi-normal modes. The term quasi-normal modes comes

from the parallelism with normal modes. If we perform a Laplace transformation on the Z function

$$Z^{lk}(t,r) = \int_0^\infty e^{i\omega t} Z^{lk}(\omega, r) d\omega \tag{2.14}$$

we can obtain the quasi-normal modes by solving the eigen-value equation

$$\frac{d^2 Z^{lk}}{dr_*^2} + \left[\omega^2 - V(r)\right] Z^{lk} = 0. \tag{2.15}$$

Let us note that in both axial and polar perturbations we will be interested in the $l = 2$ case, and we will drop the (l, k) indices in the following discussion.

There are important differences between normal modes and quasi-normal modes. Note that for quasi-normal modes, the eigen-value ω is a complex number. The real part is the frequency and the imaginary part the damping time. Note that in general a solution of (2.10) will have two independent components, a composition of incoming and outgoing waves, i.e.

$$\lim_{r_*\to\infty} Z^{in} \sim e^{i\omega r_*}, \tag{2.16}$$

$$\lim_{r_*\to\infty} Z^{out} \sim e^{-i\omega r_*}. \tag{2.17}$$

Note that, while the real part of ω determines the oscillation frequency of the wave, the imaginary part of the eigen-value determines the asymptotic behavior of the quasi-normal mode: If we call $\tau = 1/\omega_I$, the ingoing and outgoing modes will behave, respectively, as:

$$\lim_{r_*\to\infty} Z^{in} \sim e^{-r_*/\tau}, \lim_{r_*\to\infty} Z^{out} \sim e^{r_*/\tau}, \tag{2.18}$$

Outgoing quasi-normal modes are divergent at radial infinity, while ingoing ones tend exponentially to zero as the radius grows.

Since we are interested in pulses evolving as outgoing waves, with no incoming gravitational wave exciting the neutron star, we must find a way to eliminate the incoming wave component of solutions of (2.15).

Note that an outgoing solution of (2.15) diverges towards spatial infinity. Hence its energy is also divergent. In fact, since the time dependence of the solution is like $e^{i\omega t}$, we can see that the energy is divergent also as we go back in time. Hence, quasi-normal modes are not physically feasible solutions. Normal modes are perfectly valid physical solutions (plane waves), whereas quasi-normal modes are only an approximation of a signal, valid for a certain period of time (the first phase of the pulse ringing). Quasi-

normal modes must be seen as a tool to extract the resonant frequencies and damping times of the configuration.

The purely outgoing wave condition is not appropriate for numerical analysis. In principle, the purely outgoing quasi-normal mode condition could be imposed at a very distant point, but because of the quick vanishing of the ingoing signal, which tends exponentially to zero at radial infinity, every small numerical error in the imposition of this behavior will be amplified as we approach the border of the star, resulting in a mixture of outgoing with ingoing waves. This is precisely what happens when attempting to calculate strongly damped modes.

Before commenting the methods used to calculate the quasi-normal modes, let us first present the different families of modes that can be found on neutron stars. We will follow [34] and distinguish them into space-time modes and fluid modes. Let us make some comments on the modes we have considered in our work.

Fluid modes:

They correspond to modes associated to energy and pressure oscillations. They are only found in polar modes.

Fundamental mode. The fundamental mode or f-mode, is a single stable mode of non-radial oscillations. With frequencies typically around 1 kHz and damping times of the order of 0.1 s, it is called fundamental because it has no nodes inside the star.

Pressure modes. Also known as p or acoustic modes, these modes arise as a result of pressure fluctuations. They present both radial and non-radial components. They are infinite in number. The fundamental p-mode is usually found around 5 kHz, with damping times of the order of 1 s, but both the frequency and damping time increase with the order of the mode. These modes are very sensitive to the equation of state of the star.

Other families of fluid modes we will not consider are gravity modes and rotational modes. The gravity modes or g-modes arise as a result of possible material inhomogeneities. There are an infinite amount of g-modes. The stability of this mode is related to the stability of the star under convection. Typically, these modes have frequencies of 10 Hz and damping times of 1 year. The rotational modes or r-modes arise as a result of the rotation of the star. Some modes could be counter-rotating. These counter-rotating modes are unstable (r-unstability) and prevent young neutron stars from very fast rotation rates.

Space-time modes:

They are often called w-modes. Space-time modes can be found both in the axial and the polar component.

Curvature modes. Also known as wI-modes, they are the standard space-time modes. They exist in every neutron star, and are associated to the space-time curvature. There are infinite curvature modes. The fundamental mode usually has frequencies around 10 kHz and damping times of 0.01 μs, and both quantities increase with the order of the mode. If the neutron star is highly compact ($R \leq 3M$), the surface of the star is inside the potential peek of $V(r)$. The first curvature modes become trapped, and the damping times can become very slow. Nevertheless, for realistic equations of state, such compactness is not realized, and curvature modes do not become trapped.

Interface modes. Also known as wII-modes, they are much rapidly damped than the curvature modes. They are probably finite in number. Typically, they have frequencies around 10 kHz and damping times of 0.1 ms

There are several methods that can be used in order to calculate quasi-normal modes of neutron stars. In [34] and [36], the most important methods are commented.

The time dependent equations inside and outside of the star can be integrated, using as initial data some pulse. Inside the star, specially for the polar modes, the system of equations is much more complicated than outside. Nevertheless, this method has the advantage of not needing to deal with the perturbation behavior at radial infinity, and from the evolution of the initial pulse, the quasi-normal modes can be extracted. Nevertheless, only a few excited modes can be observed on the evolution of a pulse, so it is difficult to study the complete spectrum using this method.

The use of the Laplace transform allows us to treat the problem as a time independent problem. The WKB method [37, 38] and the continued fraction method [39, 40, 41, 42, 43] have been extensively used with very good results specially in the calculation of frequencies of slowly damped modes. Other more sophisticated methods study the phase function [44] and its boundary conditions. Also, an analytical continuation of the perturbation function into the complex plane [45, 38, 46, 47], can be used to control in a better way the boundary conditions needed to completely suppress any incoming wave contribution.

In our studies, we have developed a method based on exterior complex scaling, making use of both previously used and new techniques. Essentially this technique complexifies the radial coordinate. The new radial variable takes its values along a line in the complex plane (we assume that an analytical continuation of a solution of the perturbation equation can be done). If this path in the complex plane is chosen

appropriately, it can be demonstrated that the outgoing wave behavior can be imposed as a boundary condition.

Even more, we combine the exterior complex scaling to the study of the phase function. The phase function of the perturbation contains enough information in order to obtain the quasi-normal modes eigen-values. With an appropriate junction condition with the interior solution, the complete problem can be reduced to the calculation of a determinant, whose zeros are reached at the resonances.

To construct this determinant, we require precise control of the junction conditions at the surface of the star [48]. Continuity of the fundamental forms across the surface of the star, allowing for possible jumps in the stress-energy tensor, gives us the necessary conditions in order to completely determine the problem. In the following papers, we will give more details on the method we have developed.

2.3.1 Results

In this section we will present our results on quasi-normal modes of realistic neutron stars. Our research has been published in two papers. The axial spectrum is analyzed in Physical Review D **87** (2013) 104042 [1], which is included in the following section 2.3.2. Polar modes are studied in Physical Review D **89** (2014) 044006 [2], which is also included in section 2.3.3.

Let us present the main results obtained for axial modes of realistic neutron stars:

- Since we are interested in axial quasi-normal modes of neutron stars including realistic equations of state, we have to rely on numerical methods in order to integrate the differential equations. We have to integrate the Tolman-Openheimer-Volkov (TOV) equations for the zeroth order, and the Zerilli equation for the perturbations. We integrate both systems of equations at the same time. This allows us to adapt the static solution to the precision we need for the perturbation.

- The perturbation function is a complex function which diverges towards infinity (outgoing wave). We use the exterior complex scaling method. This method allows us to study an analytical extension of the perturbation function, where well-defined boundary conditions for the phase function of the perturbation, more appropriate for the numerical integration, can be obtained.

- We have studied the fundamental wI mode (space-time mode), and its first excitation. We have also studied the fundamental wII mode (interface mode).

No trapped modes are found for these equations of state.

- We use 18 realistic equations of state and two different methods of interpolation in order to implement them. One of them is a piecewise polytropic interpolation (different regions of the equation of state are approximated as specific polytropes). This interpolation was developed in [33]. The other method consist of a piecewise monotone cubic Hermite interpolation satisfying the local thermodynamic condition. This interpolation is performed on a numerical table of density-pressure values. The equations of state considered satisfy the 2 $M_\odot$ condition (except in two cases included for comparison), and include various compositions: plain nuclear matter, mixed hyperon-nuclear matter, hybrid quark-nuclear matter, and pure quark matter. Most of the equations of state are state-of-the-art results of high energy nuclear theory.

- We have studied phenomenological scaled relations, following [49, 50, 51, 41]. If these relations are independent of the equation of state, then they can be very useful in order to determine, from a quasi-normal mode measurement, other parameters of the star, like the radius, the mass or the compacity. For axial modes we obtain that they are quite independent of the equation of state, except in the case of pure quark matter stars, which present different scaled phenomenological relations (the same functional dependence but with different parameters).

- We have also studied new phenomenological relations. In this case the idea is to relate the frequency with the damping time of a quasi-normal mode. We scale both quantities to the central pressure. The relations obtained are very independent of the equation of state. We propose that these phenomenological relations can be used to estimate the central pressure of the neutron star.

In a later paper included in section 2.3.3 we have performed an equivalent study to the polar component of the quasi-normal mode spectrum. Let us present a summary with the main results and discussion:

- Essentially the numerical procedure is equivalent to the one performed on axial modes. We integrate the TOV system of equations together with the polar perturbation equations. The difference is that the system of equations necessary to describe the perturbation is more complicated in the interior region, because the system of equations cannot be redefined into a single ordinary differential equation like it can be done in the exterior region (Regge-Wheeler equation).

- Nevertheless, in the exterior region, since the ordinary differential equation is basically the same one as in the axial case, we apply the exterior complex scaling method to the Regge-Wheeler function, so that we can impose boundary conditions to the phase function and obtain pure outgoing wave functions.

- In this paper we use 15 realistic equations of state, which are the same equations of state of 2.3.2 that satisfy the 2 $M_{\odot}$ condition. The same procedures of equation of state interpolation are used.

- We study the fundamental wI mode of the polar spectrum, the fundamental pressure mode, and the fundamental mode. Again, we follow [49, 50, 51, 41] and study scaled phenomenological relation. In this case the scaled relations are not as useful as in the axial component since the spectrum is more dependent on the physics of the equation of state (except of course, for the w modes). Again the pure quark stars are the most different ones.

- We propose new phenomenological relations that relate the frequency to the damping time of a quasi-normal mode. We scale both quantities to the central pressure. We obtain relations for the w modes and the fundamental modes. The relations obtained are very independent of the equation of state. We propose that this phenomenological relations can be used to estimate the central pressure of the neutron star, and the radius (provided that the mass is known, and the detection is good enough to have the real and the imaginary part of both the w mode and the fundamental mode).

We think that the results of these works could be very useful in future neutron star asteroseismology. Because the analysis is realized on a wide range of realistic state-of-the-art equations of state, the information contained in these papers could be used in future gravitational wave measurements in order to constrain the equation of state of neutron stars.

2.3.2 Publication: Jose Luis Blázquez-Salcedo, Luis Manuel González-Romero, and Francisco Navarro-Lérida, *Phenomenological relations for axial quasinormal modes of neutron stars with realistic equations of state*, Physical Review D 87 (2013) 104042

PHYSICAL REVIEW D **87,** 104042 (2013)

Phenomenological relations for axial quasinormal modes of neutron stars with realistic equations of state

J. L. Blázquez-Salcedo,[1] L. M. González-Romero,[1] and F. Navarro-Lérida[2]

[1]*Departamento Física Teórica II, Facultad de Ciencias Físicas, Universidad Complutense de Madrid, 28040 Madrid, Spain*
[2]*Departamento Física Atómica, Molecular y Nuclear, Facultad de Ciencias Físicas, Universidad Complutense de Madrid, 28040 Madrid, Spain*

(Received 20 July 2012; published 31 May 2013)

Here we investigate the axial w quasinormal modes of neutron stars for 18 realistic equations of state, most of them satisfying the $2M_\odot$ condition. In particular, we study the influence of the presence of hyperons and quarks in the core of the neutron stars. We have obtained that w modes can be used to distinguish between neutron stars with exotic matter and without exotic matter for compact enough stars. We present phenomenological relations for the frequency and damping times with the compactness of the neutron star for wI and wII modes showing the differences of the stars with exotic matter in the core. Also, we obtain a new phenomenological relation between the real part and the imaginary part of the frequency of the w quasinormal modes, which can be used to estimate the central pressure of the neutron stars. Finally, we study the low compactness limit configuration of fundamental wII modes, and the influence of changes in the core-*crust* transition pressure. To obtain these results we have developed a new method based on the exterior complex scaling technique with variable angle.

DOI: 10.1103/PhysRevD.87.104042 PACS numbers: 04.40.Dg, 04.30.−w, 95.30.Sf, 97.60.Jd

I. INTRODUCTION

Considerable progress has been made in the last years on the development of gravitational wave detectors. Large-scale interferometric gravitational wave detectors, such as LIGO, GEO, TAMA, and VIRGO, have reached the original design sensitivity, and are currently beginning to operate with frequencies between 1 Hz to 1 kHz. The sensitivity is continuously being enhanced [1]. First, detections are expected to happen within the next five years. These observations are of huge importance because they can be used to perform stringent tests of general relativity. But also because gravitational wave detection opens a new window to observations of the insights of numerous, and probably also new, astrophysical processes. Possible sources of gravitational waves are interacting black holes, coalescing compact binary systems, stellar collapses, and pulsars [2].

Neutron stars are major candidates to detectable gravitational wave sources because of their rich emission spectrum, which lays inside the frequency range of current detectors. A recent review about gravitational waves from neutron stars can be found in [3]. The study of the signature of the equation of state on gravitational radiation from neutron star has been developed in [4–9]. The first direct search for the gravitational-wave emission associated with oscillations of fundamental quadrupole mode excited by a pulsar glitch has been presented in [10].

Neutron stars are found inside pulsars, and are thought to originate after the collapse of massive star cores. The supernova explosion causes violent oscillations of the resulting compact star. Similarly, the coalescence of compact bodies like white dwarfs leaves behind an oscillating neutron star. The resulting excess of energy that causes the star to oscillate is radiated in the form of gravitational radiation [2].

It is well known that although the spectrum of neutron star oscillations is continuous, general perturbations cause the star to ring with concrete oscillation frequencies that dominates over the rest of possible frequencies for a certain period of time after the perturbation. These resonant frequencies can be studied introducing the concept of quasinormal modes, that is, eigenmodes of oscillation, which, although they do not form a complete set of functions in which to expand every possible perturbation evolution, are very useful in the determination of the eigenfrequencies for which the star tends to oscillate [11–13]. These eigenfrequencies are given by a complex number. The real part gives us the oscillation frequency of the mode, while the imaginary part gives us the inverse of the damping time. The quasinormal mode spectrum is quite dependent on the properties of the star, i.e., the equation of state.

Neutron stars are compact objects of very high density. Inside of them matter is found at extreme densities (10^{15} g/cm^3). Current theories predict a layer structure for the neutron star, essentially composed by the core and the *crust*. The properties of the crust are very different from those of the core, and it is thought that this region has a solid crystalline structure similar to a metal. Although the high density matter inside the star has exotic properties, the resulting relativistic fluid that composes the neutron star can be described as a perfect fluid. What we need to know is the equation of state for the neutron star matter; but beyond the nuclear densities this relation is not well understood. The inner part of the core is very model dependent, essentially because different populations of particle states may appear at those densities. The composition is not

exactly known and several hypotheses exist [14,15]. Along the core of the star and especially in the core-crust interface, first order phase transitions are expected to be found in realistic equations of state. These phase transitions result in small discontinuities in the energy density of the star matter [14,16].

The measurement of $1.97M_\odot$ for PSR J1614-2230 imposes a stringent condition on the equations of state, in particular to those with exotic matter in the core [17]. Recently, several equations of state with exotic matter in the core satisfying the $2M_\odot$ condition have been proposed [18–21].

In order to systematize the study of constraints placed by astrophysical observations on the nature of neutron star matter, several parametrizations of high-density equations of state (EOS) have been introduced: a piecewise polytropic approximation by Jocelyn *et al.* [22] and Lindblom spectral decomposition [23]. The advantage of these parametrizations is that they reduce the total amounts of parameters which modelize the equation of state to a more tractable quantity, allowing us to constrain with observational data the values of the parameters, and also usually they enhance a numerical integration scheme allowing better precision. Let us note that a very large family of equations of state can be fitted to these parametrizations with a very good precision. From a practical or numerical point of view, another possibility to describe the equation of state, satisfying local thermodynamic conditions, is a monotone piecewise cubic Hermite interpolation.

The detection of gravitational radiation from neutron stars can be a very useful tool to determine the neutron star equation of state. The extraction of the spectrum of quasinormal modes (frequency and damping time) from these signals could give important constrains to the equation of state, and, in consequence, information about the behavior of matter at densities beyond nuclear matter [24–30].

The theoretical study of the quasinormal mode spectrum considering different models of neutron stars with different equations of state is then well justified. The necessary formalism was developed first for quasinormal modes of black holes by Regge and Wheeler [31] and by Zerilli [32]. Quasinormal modes can be differentiated into polar and axial modes. In these papers it is found that the equation describing the quasinormal mode perturbation of the Schwarzschild metric is essentially a Schrödinger-like equation: the Regge-Wheeler equation for axial perturbations and the Zerilli equation for polar ones. For black holes, both types of modes are space-time modes. The formalism was studied in the context of neutron stars first by Thorne [33–37], Lindblom [38,39], and then reformulated by Chandrasekhar and Ferrari [40–42], and Kojima [43]. In neutron stars, axial modes are purely space-time modes of oscillation (w modes), while polar modes can be coupled to fluid oscillations (although a branch of w modes can be found also in polar oscillations). In this paper we will consider only axial modes of oscillation.

The study of the quasinormal modes spectrum is complicated because of several reasons. Quasinormal modes can only be studied numerically. No analytical solutions are known for physically acceptable configurations of neutron stars. Another reason is that quasinormal modes are found as isolated points scattered on the complex plane, so that usually an exhaustive scan of this plane is necessary in order to find the complete spectrum. Also the numerical study is hindered by the very definition of quasinormal mode itself, that as we will see explicitly in the following sections, gives rise to diverging functions that oscillate an infinite number of times towards spatial infinity. These functions are not well handled numerically.

Several methods have been developed to deal with these and other difficulties. For a complete review on the methods see the review by Kokkotas and Schmidt [11].

Chandrasekhar and Ferrari [40–42] used a slowly damped approximation ($\mathrm{Im}[\omega] \ll \mathrm{Re}[\omega]$), which reduces the system of equations needed to resolve the problem, so that the damping time of the quasinormal mode can be given in terms of the real part. This method was also used in the determination of w modes on polar perturbations of constant density neutron stars by Kojima *et al.* [44]. It is only valid for slowly damped modes, which are present in highly compact stars, and is not appropriate for realistic configurations, although it can be used to obtain a first approximation of the fundamental frequencies.

In an interesting paper [45], Kokkotas studied the axial spectrum integrating the exterior solution up to a finite radius, which allows us to impose the outgoing wave behavior to the exterior solution. The matching between the interior and exterior solutions results in the construction of a Wronskian at the matching surface, which must be zero when both solutions correspond to a quasinormal mode.

The Wentzel-Kramers-Brillouin method [46] can be used to approximate the outer solutions provided that no backscattering is found in the exterior region. This condition usually is satisfied when the imaginary part of the mode is small compared with the real part [47].

The phase function can be studied in order to deal with the oscillatory nature of the perturbation function. Studied for black holes by Chandrasekhar and Detweiller [48], the phase function plays a fundamental role in the numerical approach made by Andersson *et al.* in [47] and in [49] for neutron stars. The phase is usually a well-behaved function if there is not backscattering contamination in the numerical solution.

The divergence of the outgoing wave solution of the perturbation equations makes the avoidance of incoming wave contamination a difficult task. This problem was dealt with for black holes by Andersson in [50] by rotating the radial variable into a complex variable parallel to the anti-Stokes line. This approach was used for constant density

neutron stars in [47,49] together with the phase function approach. More recently, Samuelsson *et al.* [51] used a similar complex-radius approach for a constant density configuration which dealt with the divergence at infinity by integrating the Bondi-Sachs phase along a fixed path for the complexified radius parallel to the anti-Stokes line.

Another approach is based on the Leaver continued fraction method [52], which allows us to impose the outgoing wave behavior on the border of the star as a self-consistent equation that can be satisfied iteratively [53]. This method has been used successfully with realistic models of neutron stars [24,26,30]. As commented above, for fluid modes there is also a branch of w modes. As these are purely space-time modes, they do not couple to matter, and the inverse Cowling approximation can be used to obtain this part of the spectrum [49].

In this work we present a new approach to calculate quasinormal modes of realistic neutron stars. We make use of several well-known techniques, like the use of the phase for the exterior solution and the use of a complexified coordinate to deal with the divergence of the outgoing wave. We also introduce some new techniques not used before in this context: freedom in the angle of the exterior complex path of integration, implementation of realistic equations of state in a piecewise polytrope approximation or by monotone piecewise cubic Hermite interpolation, use of the COLSYS package to integrate all the system of equations at once with proper boundary and junction conditions and possibility of implementation of phase transition discontinuities. These new techniques allow us to enhance precision, to obtain more modes in shorter times, and also to study several realistic equations of state, comparing results for different compositions.

In Sec. II we will start presenting the well-known general formalism of quasinormal modes. In Sec. III we will present a study of the junction conditions for a general matching that can include first-order phase transitions or surface energy layers. In most of the results of the paper we will make use of the junction conditions without phase transitions or energy layers. In Sec. IV we describe the numerical method we have used to obtain our results, testing the algorithm to obtain already known modes for a simple model. In Secs. V, VI, and VII we present our results, focusing on 18 different equations of state: for pure nuclear matter (Sly, APR4), mixed hyperon-nuclear matter (GNH3, H1, H4, BGN1H1,WCS1, WCS2, BHZBM), hybrid stars (ALF2, ALF4,WSPHS3), hybrid stars with hyperons and quark color-superconductivity (BS1, BS2, BS3, BS4), and quark stars (WSPHS1, WSPHS2). In Sec. VIII we finish the paper with a summary of the main points of the work.

II. QUASINORMAL MODE FORMALISM

In order to fix the notation we will present a brief review of the formalism used to describe axial quasinormal modes. In the following we use geometrized units ($c = 1$, $G = 1$).

We consider a static spherical space-time with metric $ds^2 = e^{2\nu}dt^2 - e^{2\lambda}dr^2 - r^2(d\theta^2 + \sin^2\theta d\varphi^2)$. The matter inside of the star is considered perfect fluid with stress-energy tensor $T^{\mu\nu} = (p + \rho)u^\mu u^\nu - pg^{\mu\nu}$, where p is the pressure, ρ is the energy density and u is the 4-velocity. At zero order the equations obtained are well known. Inside the star we have

$$\frac{dm}{dr} = 4\pi r^2 \rho, \tag{1}$$

$$\frac{dp}{dr} = -(\rho + p)\frac{m + 4\pi r^3 p}{(r - 2m)r}, \tag{2}$$

$$\frac{d\nu}{dr} = -\frac{1}{\rho + p}\frac{dp}{dr}, \tag{3}$$

where we must provide an equation of state. Outside, we have the Schwarzschild solution with gravitational mass M.

Following the original papers [33–43], we make perturbations over this metric, expanding the perturbation in tensor harmonics, and taking into account only the axial perturbations. It can be demonstrated that the axial perturbations must satisfy the well-known Regge-Wheeler equation [32].

$$\frac{d^2Z^{lk}}{dr_*^2} + [\omega^2 - V(r)]Z^{lk} = 0, \tag{4}$$

where l and k are the spherical harmonic indexes, r_* is the tortoise coordinate

$$r_* = \int_0^r e^{\lambda - \nu}dr, \tag{5}$$

and the eigenfrequency of the axial mode is a complex number $\omega = \omega_{\mathrm{Re}} + i\omega_{\mathrm{Im}}$. The potential can be written as

$$V(r) = \frac{e^{2\nu}}{r^3}[l(l + 1)r + 4\pi r^3(\rho + p) - 6m]. \tag{6}$$

In this work we will consider only the $l = 2$ case.

Axial oscillations do not modify the energy density or the pressure of the fluid. Hence, for axial modes, inside the star only the perturbations on the 4-velocity of the matter have to be taken into account (Lagrangian displacement).

Note that in general the perturbation function Z is a complex function. Hence, we have a system of two real second-order differential equations (one for the real part Z_{Re}, and another for the imaginary part Z_{Im}).

Z has to satisfy a set of boundary conditions that can be obtained from the following two requirements [40]: (i) the perturbation must be regular at the center of the star, and (ii) the resulting quasinormal mode must be a pure outgoing wave.

The second requirement imposes the quasinormal modes to behave as purely outgoing waves at radial infinity. In general a quasinormal mode will be a composition of incoming and outgoing waves, i.e.,

$$\lim_{r_*\to\infty} Z^{\text{in}} \sim e^{i\omega r_*}, \qquad \lim_{r_*\to\infty} Z^{\text{out}} \sim e^{-i\omega r_*}. \tag{7}$$

Note that, while the real part of ω determines the oscillation frequency of the wave, the imaginary part of the eigenvalue determines the asymptotic behavior of the quasinormal mode: If we call $\tau = 1/\omega_I$, the ingoing and outgoing modes will behave, respectively, as

$$\lim_{r_*\to\infty} Z^{\text{in}} \sim e^{-r_*/\tau}, \qquad \lim_{r_*\to\infty} Z^{\text{out}} \sim e^{r_*/\tau}. \tag{8}$$

Outgoing quasinormal modes are divergent at radial infinity, while ingoing ones tend exponentially to zero as the radius grows.

In the next sections we will present our numerical method, which is able to deal with this problem.

III. JUNCTION CONDITIONS

To determine completely the problem, we must study the junction conditions between the interior solution and the exterior solution on the boundary of the star. The junction conditions between two space-times have been considered in classical works by Darmois [54], Lichnerowicz [55], O'Brien and Synge [56], and Israel [57], and, more recently, in [58–60]. In the context of relativistic rotating stars, it has been considered in [61–63].

We will impose the usual junction conditions. But, in order to have the possibility to study the influence of small changes in the core-*crust* transition pressure, we will include the more general case in which the star is surrounded by a surface layer of energy density.

We use Darmois conditions, the intrinsic formulation of these junction conditions, which imposes certain constrains on the continuity of the fundamental forms of the matching hypersurface S [64].

This surface S is defined by the points where the pressure is null, or more generally, constant. As we have seen previously the axial oscillations do not modify the pressure or the density, so the surfaces of constant pressure of the perturbed star are essentially the same as the surfaces of constant pressure of the static star.

Let us consider a surface S of constant pressure inside the star, and a surface layer on top of S described by a surface stress-energy tensor of a perfect fluid of the following form:

$$T_S^{\mu\nu}(R) = \varepsilon u_S^{\mu}(R) u_S^{\nu}(R), \tag{9}$$

where, S is defined by the points where $r = \text{const} = R$, ε is the surface energy density of the fluid moving in S, and $u_S^{\mu}(R)$ is its velocity. The continuity of the first fundamental form gives us two conditions: the continuity of ν

$$\nu_{\text{int}} = \nu_{\text{ext}}, \tag{10}$$

and the continuity of perturbation function Z:

$$Z^{lk}_{\text{int}} = Z^{lk}_{\text{ext}}. \tag{11}$$

The second fundamental form conditions impose a jump in the pressure if $\varepsilon \neq 0$. Let the pressure in the inner part of the surface S, be p_{int}, and in the outer part be p_{ext} with $p_{\text{ext}} < p_{\text{int}}$.

Making the same steps as with the first fundamental form, we obtain the following conditions for the zero order functions:

$$M_{\text{ext}} = M_{\text{int}} + 4\pi R^2 \sqrt{1 - \frac{2M_{\text{int}}}{R}}\varepsilon - 8\pi^2 R^3 \varepsilon^2, \tag{12}$$

$$\frac{M_{\text{ext}} + 4\pi R^3 p_{\text{ext}}}{R^2\sqrt{1 - \frac{2M_{\text{ext}}}{R}}} - \frac{M_{\text{int}} + 4\pi R^3 p_{\text{int}}}{R^2\sqrt{1 - \frac{2M_{\text{int}}}{R}}} = 4\pi\varepsilon. \tag{13}$$

In this work we will consider $p_{\text{ext}} = 0$. That is, the surface of star with pressure $p = p_{\text{int}}$ is being matched directly to the empty exterior surface of the star, in which case, M_{ext} is just the Schwarzschild mass M. If we choose p_{int} as the core-crust transition pressure, this matching condition is equivalent to approximating exterior layers of the star to a surface layer energy density that envelops the core of the star (surface crust approximation). The Eq. (12) can be interpreted as giving the total mass of the star to zero order (M_{ext}), as the addition of three terms, the first one representing the core mass ($M_{\text{int}} \equiv 4\pi \int_0^R \rho r^2 dr$), the second one representing the mass of the crust, and the third one being a negative bounding energy term. The radius of the resulting configuration will be the radius of the core of the star. Equation (13) can be seen as a condition for the determination of the radius of the core of the star when approximating the crust of the star to a thin surface energy density.

In the surface crust approximation, these relations allow us to use the core-crust transition pressure p_{int}, as a new parameter of the resulting configuration.

Up to first order in the perturbative expansion we obtain junction conditions for the axial functions. Essentially we obtain the following condition for the derivative of the Z function:

$$\left.\frac{dZ^{lk}}{dr}\right|_{\text{ext}} = \frac{e^{\lambda_{\text{ext}}}}{e^{\lambda_{\text{int}}}} \left.\frac{dZ^{lk}}{dr}\right|_{\text{int}} + \left[\frac{e^{\lambda_{\text{ext}}}}{e^{\lambda_{\text{int}}}} - 1\right]\frac{Z^{lk}}{R}. \tag{14}$$

Together with condition (11) we have enough information to perform correctly the matching of the perturbation.

Let us note that, the usual treatment without surface crust approximation is recovered by making in the previous conditions $p_{\text{int}} = p_{\text{ext}} = 0$ and $\varepsilon = 0$, in which case the continuity of the metric functions and of their derivatives is obtained. This is what we do in almost the entire paper except in the final part of Sec. VII, where the influence of the changes in the core-crust transition pressure is analyzed.

IV. NUMERICAL METHOD

In this section we will explain the numerical method we use to obtain outgoing quasinormal modes of realistic stars. We implement this method into different Fortran programs and routines, making use of the COLSYS package [65] to solve numerically the differential equations. The advantage of this package is that it allows the utilization of quite flexible multiboundary conditions, that, as we will see in the following sections, are important in our method of quasinormal mode determination. On the other hand, COLSYS allows us to construct an adaptative mesh of points depending of the precision we would like to achieve. In this manner, the more precision we need on the perturbation function, the more points COLSYS introduces into the mesh. The static solution is calculated at the same time as the perturbation, so the static solution functions will be also adapted to the precision we require for the Regge-Wheeler function. COLSYS additionally allows the use of the continuation method: we can use as an initial guess for a new numerical solution another numerical solution with parameters close enough to the parameters of the new solution.

We will start explaining how the outgoing modes are determined in the exterior region of the metric.

Quasinormal modes present an oscillating part given by the real part of the eigenfrequency, that remains towards infinity, as can be seen in relation (7).

In order to deal with this issue we will follow [50,51], and we will study the phase function. The phase function (logarithmic derivative of the Z function),

$$g = \frac{Z'}{Z}, \tag{15}$$

does not oscillate towards asymptotic infinity.

The other important issue we have seen is that quasinormal modes diverge towards spatial infinity because of their pure outgoing wave behavior. This problem can be treated using the phase function together with a rotation of the radial coordinate into the complex plane.

This technique of complexification of the integration variable is called exterior complex scaling [66–68]. An analytical extension of the g function, which is a function of r, is made into a g function that is dependent of the generalized complex coordinate. This new function has no physical meaning, but the eigen-values obtained by integrating the equation along the extended radius will remain unaltered.

We parametrize the complex coordinate along a line in the complex plane. We will take a straight line with an angle α with respect to the real axis.

$$r = R + ye^{-i\alpha}, \tag{16}$$

with $y \in [0, \infty)$. The g function has the same limits in the case of a purely outgoing or a purely ingoing wave than with the real coordinate. But the mixed waves now depend on the angle of the path of integration α.

In our method, the angle of the integration path is treated as a free parameter of the solution. This angle can be chosen appropriately to increase precision and integration time, but always remaining in the region where $g \rightarrow -i\omega$. This boundary condition imposes to the obtained solution a

TABLE I. Frequency and damping time of the trapped modes (t), the spatial modes and the interface modes (i), in central density units, for axial $l = 2$ modes, $2M/R = 0.885$.

ω_{Re}	ω_{Im}	ω_{Re}	ω_{Im}
(t)0.213 863 87	$2.432\,045\,9 \times 10^{-9}$	1.683 478 76	$6.024\,371\,6 \times 10^{-2}$
(t)0.291 011 53	$7.747\,252\,3 \times 10^{-8}$	1.767 048 36	$6.193\,009\,9 \times 10^{-2}$
(t)0.367 998 64	$1.072\,527\,9 \times 10^{-6}$	1.850 665 83	$6.339\,002\,4 \times 10^{-2}$
(t)0.444 634 93	$9.518\,752\,2 \times 10^{-6}$	1.934 298 17	$6.469\,996\,1 \times 10^{-2}$
(t)0.520 639 03	$6.339\,319\,4 \times 10^{-5}$	2.017 934 47	$6.589\,768\,6 \times 10^{-2}$
0.595 579 00	$3.380\,600\,6 \times 10^{-4}$	2.101 577 98	$6.701\,936\,1 \times 10^{-2}$
0.668 960 67	$1.432\,266\,6 \times 10^{-3}$	2.185 223 98	$6.808\,051\,0 \times 10^{-2}$
0.740 909 53	$4.508\,007\,7 \times 10^{-3}$	2.268 880 71	$6.909\,887\,8 \times 10^{-2}$
0.812 802 72	$1.013\,574\,2 \times 10^{-2}$	2.352 547 74	$7.007\,604\,2 \times 10^{-2}$
0.885 903 97	$1.725\,926\,4 \times 10^{-2}$	2.436 225 99	$7.101\,810\,2 \times 10^{-2}$
0.960 373 07	$2.448\,019\,5 \times 10^{-2}$	(i)1.451 159 09	$5.401\,141\,9 \times 10^{-2}$
1.036 081 10	$3.102\,748\,4 \times 10^{-2}$	(i)1.734 339 05	$1.394\,506\,6 \times 10^{-2}$
1.113 081 52	$3.668\,522\,1 \times 10^{-2}$	(i)2.011 068 06	$2.290\,268\,7 \times 10^{-2}$
1.19147020	$4.155\,931\,3 \times 10^{-2}$	(i)2.293 936 79	$3.197\,562\,5 \times 10^{-2}$
1.271 223 30	$4.583\,803\,1 \times 10^{-2}$	(i)2.579 829 76	$4.106\,780\,2 \times 10^{-2}$
1.352 192 68	$4.963\,653\,2 \times 10^{-2}$	(i)2.866 336 83	$5.015\,580\,9 \times 10^{-2}$
1.434 156 22	$5.297\,614\,4 \times 10^{-2}$	(i)3.152 744 66	$5.923\,420\,4 \times 10^{-2}$
1.516 855 60	$5.584\,164\,1 \times 10^{-2}$	(i)3.437 120 11	$6.830\,781\,3 \times 10^{-2}$
1.600 033 82	$5.824\,412\,1 \times 10^{-2}$		

purely outgoing wave behavior. Exterior complex scaling with variable angle is widely used in other contexts like atomic and molecular physics, where it gives excellent results [69].

The use of the phase and exterior complex scaling with variable angle allows us to compactify, so we can impose the outgoing quasinormal mode behavior as a boundary condition at infinity without using any cutoff for the radial coordinate.

Inside the star the Regge-Wheeler equation (4) can be solved without any problem. The perturbation function is oscillating, but the number of oscillations will be finite between $r = 0$ and $r = R$.

We must provide an equation of state. We implement the realistic EOS in two different ways: (i) A piecewise polytrope approximation, done by Read *et al.* [22]. In this approximation the equation of state is approximated by a polytrope in different density-pressure intervals. For densities below the nuclear density, the SLy equation of state is considered. (ii) A piecewise monotone cubic Hermite interpolation satisfying the local thermodynamic condition [70].

We generate two independent solutions of the Regge-Wheeler equation inside the star. The junction conditions (11) and (14) can be written in the form of a determinant making use of these two solutions together with the exterior phase function. The determinant can be calculated numerically from the integrated solutions.

We must explore the plane $(\omega_{\mathrm{Re}}, \omega_{\mathrm{Im}})$ looking for null determinants. This process can be automated so that the program looks for minima of the determinant on the plane.

We have made several tests on our method using simpler equations of state. We successfully reproduce data from previous works. For example, in Table I we show our results for a star of constant density and $2M/R = 0.885$, in perfect agreement with [51].

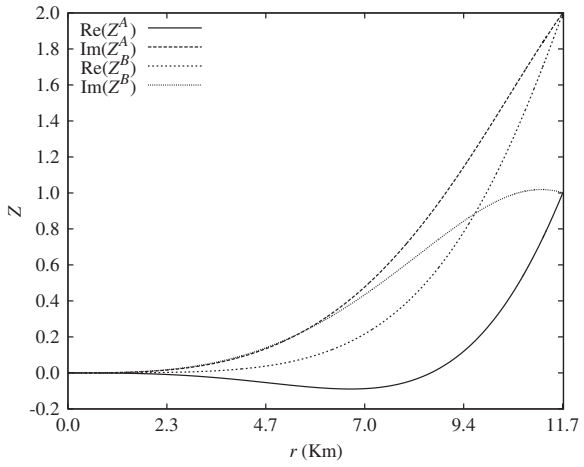

FIG. 1. Example of the Regge-Wheeler function inside the star vs radius.

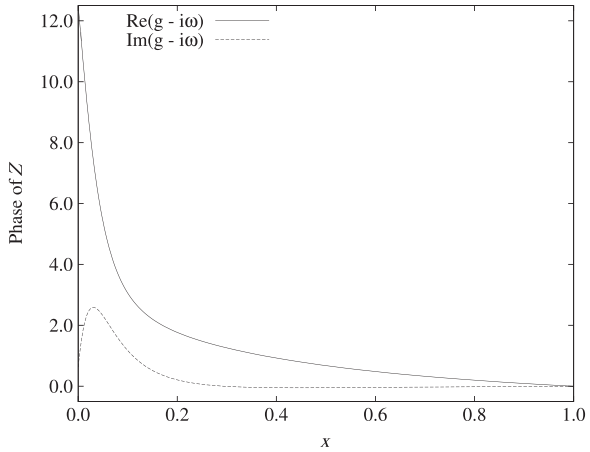

FIG. 2. Example of phase function g outside the star vs the compactified rotated coordinate x.

In Figs. 1 and 2 we show an example of calculated perturbation functions. These functions correspond to a star of $1.4M_\odot$, with Sly equation of state. The quasinormal mode is the first axial mode w_I with frequency $\nu = 8.034$ kHz and damping time $\tau = 29.31$ μs. In Fig. 1 we plot the real and imaginary parts of the two interior solutions for Z vs r. In Fig. 2 we plot the real and imaginary parts of the calculated phase function outside the star vs the compactified rotated coordinate x.

In the next sections we will show the results obtained for realistic equations of state.

V. RESULTS FOR REALISTIC EQUATIONS OF STATE

In this section we present our results for the axial quasinormal modes of neutron stars with realistic equations of state. We consider a wide range of equations of state in order to study the influence of exotic matter in the core of the star on the axial quasinormal modes.

Using the parametrization presented by Read *et al.* [22], which is implemented in our code, we can study the 34 equations of state they considered. For this paper we have used, following their notation, SLy, APR4, BGN1H1, GNH3, H1, H4, ALF2, ALF4.

After the recent measurement of the $1.97M_\odot$ for the pulsar PSR J164-2230, several equations of state have been proposed. These new equations allow the presence of exotic matter in the core of the neutron star, and the maximum mass for stable configurations is over this value. We have considered the following ones: two equations of state presented by Weissenborn *et al.* with hyperons in [20]; we call them WCS1 y WCS2, three EOS presented by Weissenborn *et al.* with quark matter in [21]; we call them WSPHS1, WSPHS2, WSPHS3, four equations of state presented by Bonanno and Sedrakian in [19]; we

call them BS1, BS2, BS3, BS4, and one EOS presented by Bednarek *et al.* in [18]; we call it BHZBM.

In Fig. 3 we plot the 18 equations of state we have studied in order to give an idea of the range considered. Let us describe briefly the characteristics of the equations of state we have used: For plain $npe\mu$ nuclear matter, we use

(i) SLy [71] with $npe\mu$ using a potential method to obtain the EOS.

(ii) APR4 [72] with $npe\mu$, obtained using a variational method.

For mixed hyperon-nuclear matter we use

(i) GNH3 [73], a relativistic mean-field theory EOS containing hyperons.

(ii) H1 and H4 [74], two variants of the GNH3 equation of state.

(iii) BGN1H1 [75], an effective-potential equation of state including hyperons.

(iv) WCS1 and WCS2 [20], two equations of state with hyperon matter, using "model $\sigma\omega\rho\phi$", and considering ideal mixing, SU(6) quark model, and the symmetric-antisymmetric couplings ratio $\alpha_v = 1$ and $\alpha_v = 0.2$, respectively.

(v) BHZBM [18], a nonlinear relativistic mean field model involving baryon octet coupled to meson fields.

For hybrid stars we use

(i) ALF2 and ALF4 [76], two hybrid EOS with mixed APR nuclear matter and color-flavor-locked quark matter.

(ii) WSPHS3 [21], a hybrid star calculated using the bag model, mixed with NL3 RMF hadronic EOS. The parameters employed are $B_{\rm eff}^{1/4} = 140$ MeV, $a_4 = 0.5$, and a Gibbs phase transition.

For Hybrid stars with hyperons and quark color superconductivity we use

(i) BS1, BS2, BS3, and BS4, [19], four equations of state calculated using a combination of phenomenological relativistic hypernuclear density functional and an effective NJL model of quantum chromodynamics. The parameters considered are vector coupling $G_V/G_S = 0.6$ and quark-hadron transition density $\rho_{\rm tr}/\rho_0$ equal to 2, 3, 3.5, and 4, respectively, where ρ_0 is the density of nuclear saturation.

For quark stars we use

(i) WSPHS1 and WSPHS2 [21]. The first equation of state is for unpaired quark matter, and we have considered the parameters $B_{\rm eff}^{1/4} = 123.7$ MeV, $a_4 = 0.53$. The second equation of state considers quark matter in the CFL phase (paired). The parameters considered are $B_{\rm eff}^{1/4} = 130.5$ MeV, $a_4 = 0.66$, $\Delta = 50$ MeV.

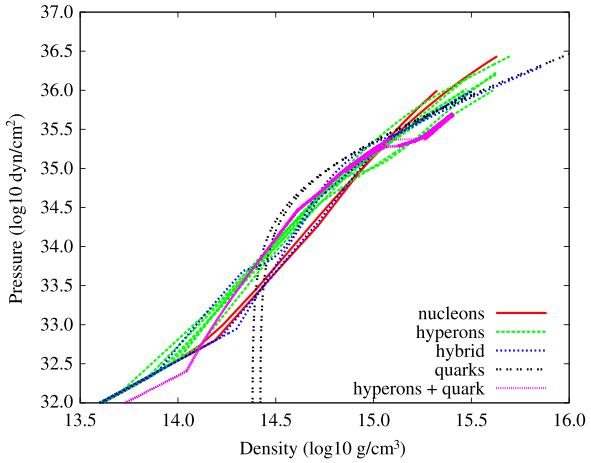

FIG. 3 (color online). Pressure vs density in logarithmic scale for the 18 equations of state considered, in the high density region.

A. Nuclear and hyperon matter

We will start studying the impact of hyperon matter on the quasinormal mode spectrum, comparing with configurations with plain nuclear matter EOS.

In Figs. 4 and 5 we plot the mass-central pressure and mass-radius relation, respectively. For the study of the quasinormal modes we have considered only stable configurations below the maximum mass of each equation of state. It can be seen that the introduction of a hyperon core changes the mass radius relation and we will see that this has an imprint on the quasinormal mode spectrum of these configurations. Note that all the EOS considered are near or beyond the $1.97M_\odot$ limit, except the BGN1H1 and H1 equations of state, which are included for comparison. In the following we will consider only stable configurations

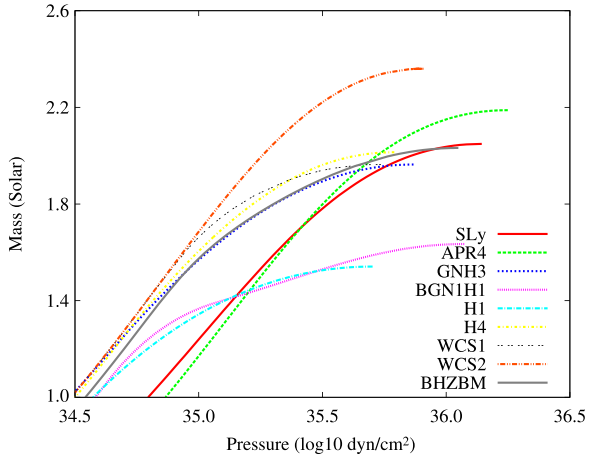

FIG. 4 (color online). Mass vs central pressure for the equations of state considered in Sec. VA. We plot configurations up to the maximum stable mass. Note that all the EOS have a maximum mass nearby or beyond $2M_\odot$, except H1 and BGN1H1, which are included for comparison.

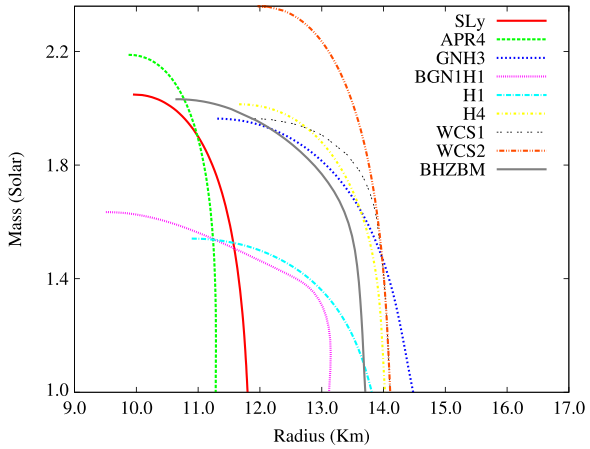

FIG. 5 (color online). Mass vs radius for the equations of state considered in Sec. VA. Typically, stars with hyperon matter have bigger radius than nuclear matter stars of the same mass.

between $1M_\odot$ and the maximum mass of the particular equation of state. We will study the fundamental and first excited wI modes, as well as the fundamental wII mode.

Fundamental wI mode: In Figs. 6 and 7, we plot the frequency and damping time of the fundamental wI mode as a function of the central pressure of the star in logarithmic scale, for the different equations of state. There is no significant difference between the two pure nuclear matter equations of state considered, except for the bigger maximum mass of the APR4 EOS. On the other hand, we observe that the presence of hyperon condensates has a clear impact on the frequencies of the fundamental

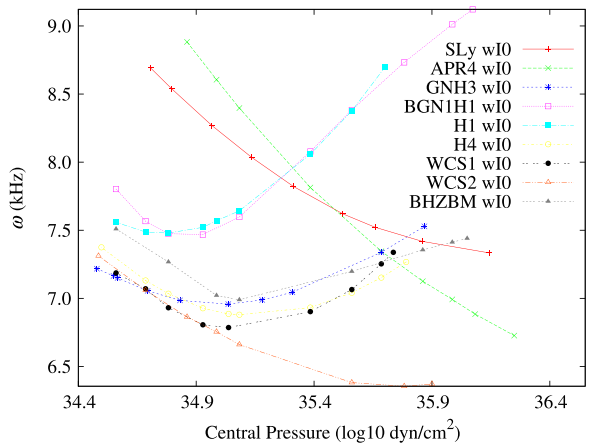

FIG. 6 (color online). Frequency of the fundamental wI mode vs central pressure in logarithmic scale, for the EOS considered in Sec. VA. While there is no significant difference between the SLy and the APR4, the hyperon core changes the relation of the frequency with the central pressure for high densities (p_c above $\sim 10^{35}$ dyn/cm^2).

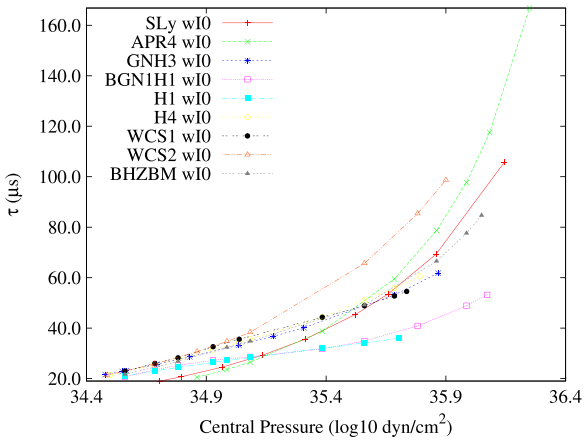

FIG. 7 (color online). Damping time of the fundamental wI mode vs central pressure in logarithmic scale, for the EOS considered in Sec. VA. The behavior is quite similar for all the equations of state considered. At high density, the lowest values of the damping time are reached by the H1 and BGN1H1 EOS.

w modes. Note that the hyperon core is changing the frequency relation for high mass configurations, increasing with the central pressure above $\sim 10^{35}$ dyn/cm^2, where the hyperon phases are more important due to the high density of the star core. Essentially, this effect is related to the softening of the EOS by the introduction of hyperon matter at the inner regions of the star.

This result is in agreement with a recent work by Chatterjee and Bandyopadhyay [29].

In order to use future observations of gravitational waves to estimate the mass and the radius of the neutron star, as well as to discriminate between different families of equations of state, we obtain empirical relations between the frequency and damping time of quasinormal modes and the compactness of the star, following [4,25,77,78]. In Fig. 8 we present the frequency of the fundamental mode scaled to the radius of each configuration. It is interesting to note that even with this scaling, the softest equations of state that include hyperon matter, H1 and BGN1H1, present a quite different behavior than the rest of EOS considered. Nevertheless, as the detection of the recent $2M_\odot$ pulsar suggest, these two particular EOS cannot be realized in nature, so the behavior of the scaled frequency is quite similar for hyperon matter or plain nuclear matter stars.

A linear fit can be made to each equation of state. We fit to the following phenomenological relation:

$$\omega(Khz) = \frac{1}{R(Km)}\left(A\frac{M}{R} + B\right). \tag{17}$$

In Table II we present the fit parameters A, B for each one of the equations of state studied. For the Sly and for the APR4 equations very similar results are obtained.

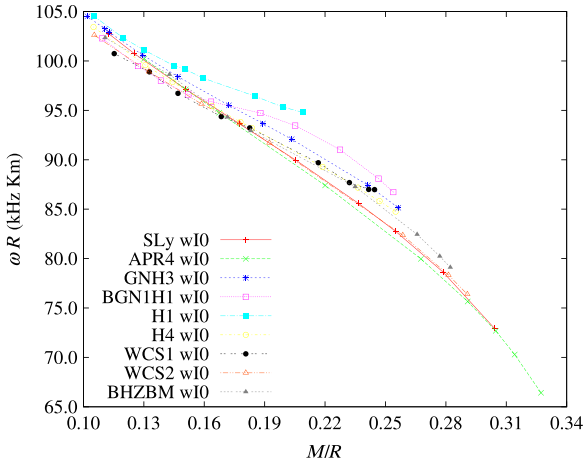

FIG. 8 (color online). Scaled frequency of the fundamental wI mode vs M/R, for the EOS considered in Sec. VA. Except for H1 and BGN1H1 EOS, which present a quite different behavior, all the scaled frequencies can be fitted to a linear relation with the compactness (17). The fits can be found in Table II.

The empirical parameters for SLy and APR4 are compatible with the empirical relation obtained by Benhar *et al.* [78] for six equations of state.

In general, for hyperon matter EOS, we still obtain a linear relation, but with slightly different parameters, as can be seen in Table II. As commented before, quite remarkable is the case of the H1 and BGN1H1, where the linear relation is almost lost.

Our results show that the introduction of hyperon matter changes very little the dependence of the frequency with the compactness. Even for M/R bigger than 0.18, the difference between equations of state with and without hyperon matter is quite small. As these empirical relations depend minimally on the equation of state, they could be used, applying the technique from [77] to measure the radius of the neutron star and constrain the equation of state.

In Fig. 9 we present the damping time of the fundamental mode scaled to the mass of each configuration. In this case, the results can be fitted to an empirical quadratic relation on M/R, as follows

$$\frac{10^3}{\tau(\mu s)} = \frac{1}{M(M_\odot)}\left[a\left(\frac{M}{R}\right)^2 + b\frac{M}{R} + c\right]. \quad (18)$$

In Table II we present the fit parameters a, b, and c. Note that for SLy and APR4 the fits are quite similar, and in accordance with the results obtained in [78]. All of the equations of state are well fitted to a quadratic relation with the compactness. For compactness beyond 0.18 the presence of hyperon matter slightly changes the dependence of the scaled damping time with M/R, specially for the BGN1H1 EOS.

First excited wI mode.—In Figs. 10 and 11 we plot the scaled frequency and damping time for the first excited wI modes. We make fits to the empirical relations (17) and (18). In Table III we present the corresponding empirical parameters.

Fundamental wII mode.—In Fig. 12 we plot the frequency of the fundamental wII mode scaled with the mass vs the metric function $e^{2\lambda(R)}$. It can be seen that for all the equations of state studied, there is a minimal compactness below which the wII mode does not exist. The scaled frequency is quite linear with $e^{2\lambda(R)}$ nearby this minimal compactness. Our numerical scheme allows us to obtain explicitly these limit configurations with vanishing real part of the mode with a precision of the order of 10^{-5}. The limit configuration has compactness between $M/R = 0.1044$ and $M/R = 0.1066$, so it is quite independent of the particular equation of state, and in consequence independent of the presence of hyperon matter. For example, the GNH3 equation of state limit configuration has compactness $M/R = 0.1051$, and for the BGN1H1, $M/R = 0.1061$, and the SLy has compactness $M/R = 0.1056$ and the APR4 compactness $M/R = 0.1046$. The reason why the limit configuration is independent of the EOS is because, for these values of the compactness, the mass of the stars considered are below $1M_\odot$. In these low mass configurations the presence of hyperons at the core is small or null, depending of the equation of state, and so we are comparing plain nuclear matter stars with slightly different EOS at the core.

These limit configurations were conjectured by extrapolation in Wen *et al.* in [30]. Our results are in agreement with their extrapolation.

TABLE II. Fits for the wI0 modes. Parameters A and B correspond to the linear empirical relation for the frequency (17). Parameters a, b, and c correspond to the quadratic empirical relation for the damping time (18).

wI0	SLy	APR4	GNH3	BGN1H1	H1	H4	WCS2	WCS1	BHZBM
A	-148.7 ± 4.5	-164.2 ± 5.8	-122.1 ± 1.4	-95.5 ± 5.4	-89.9 ± 5.1	-120.6 ± 1.8	-139.7 ± 3.6	-107.1 ± 2.2	-132.8 ± 3.6
B	119.8 ± 1.0	122.4 ± 1.4	116.67 ± 0.25	111.9 ± 1.0	113.06 ± 0.81	115.50 ± 0.35	117.83 ± 0.75	112.81 ± 0.43	117.35 ± 0.78
χ^2	0.760	0.039	1.56	0.689	0.260	0.0812	0.430	0.096	0.388
a	-1221 ± 22	-1112 ± 19	-1444 ± 23	-1690 ± 49	-1539 ± 42	-1385 ± 47	-1244 ± 23	-1450 ± 64	-1401 ± 41
b	365.1 ± 9.3	331.1 ± 9.0	425.4 ± 8.3	506 ± 18	448 ± 13	414 ± 17	371.4 ± 9.6	437 ± 24	418 ± 17
c	21.63 ± 0.89	24.16 ± 0.94	17.87 ± 0.68	11.2 ± 1.6	16.6 ± 1.0	18.2 ± 1.5	21.4 ± 0.9	16.2 ± 2.1	17.9 ± 1.6
χ^2	0.050	0.034	0.027	0.084	0.016	0.091	0.044	0.083	0.097

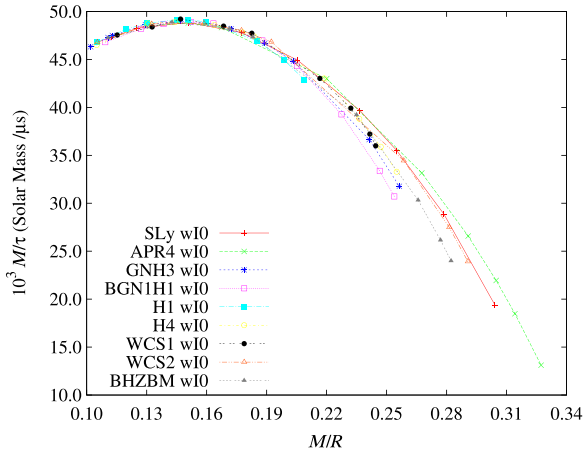

FIG. 9 (color online). Scaled damping time of the fundamental wI mode vs M/R, for the EOS considered in Sec. VA. The scaled damping times can be fitted to a quadratic relation with the compactness (18). The fits can be found in Table II.

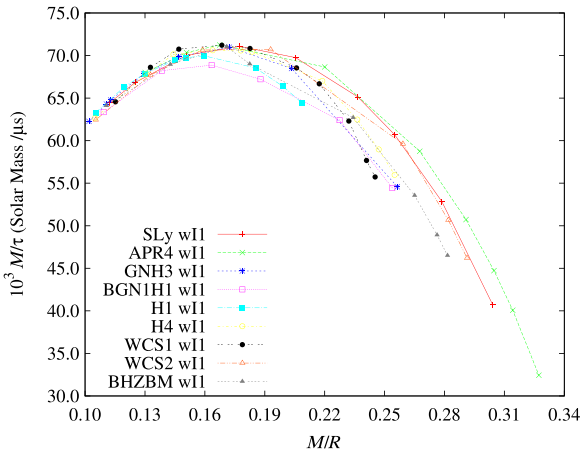

FIG. 11 (color online). Scaled damping time of the first excited wI mode vs M/R, for the EOS considered in Sec. VA. The quadratic relation (18) is valid for every EOS considered. The empirical parameters are more sensitive to the hyperon core, especially at high densities. The fits can be found in Table III.

In Fig. 13 we show the damping time of the wII mode scaled with the mass. Although for low compactness the damping time is quite independent of the equation of state and linear in M/R for the reasons mentioned before, for compactness above 0.18 it is very sensitive to the presence of hyperon matter, changing completely the linear behavior. The damping time does not vanish in the limit compactness as the frequency does. On the contrary, it tends to a limit τ.

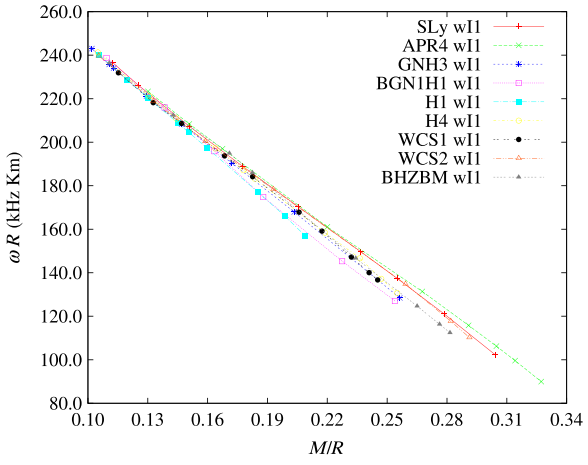

FIG. 10 (color online). Scaled frequency of the first excited wI mode vs M/R, for the EOS considered in Sec. VA. In this case the linear relation (17) is found for all these EOS. If we exclude the H1 and BN1H1 EOS, the presence of hyperons is not affecting strongly the scaled frequency. The fits can be found in Table III.

B. Quark matter

In this subsection we will present our results for the axial quasinormal modes of compact stars with quark matter at the core. We consider the following equations of state: ALF2, ALF4, WSPHS1-3, BS1-4, already described previously. In the following figures we will always include the results for the SLy EOS for comparison.

In Fig. 14 we present the equations of state at the high density region. In Fig. 15 we present the mass-radius relation for these equations of state and in Fig. 16 the mass-central pressure relation. Only stable configurations below the maximum mass of each equation of state have been considered. Note that all the equations of state considered are near or above the $1.97M_\odot$ limit. We will repeat the analysis for these new equations, studying the fundamental and first excited wI modes, and, finally, the fundamental wII mode.

Fundamental wI mode.—In Fig. 17 we plot the frequency of the fundamental wI mode as a function of the central pressure of the star in logarithmic scale. In Fig. 18 we make a similar plot for the damping time of these configurations. Note the similitude between the SLy modes and the ALF4 modes for both the frequency and damping time. These two equations of state cannot be differentiated by the observation of the fundamental *w* mode. This is not the case if the EOS for hybrid matter is softer, as it happens for the other EOS considered, which present smaller frequencies.

In Figs. 17 and 18 we also plot the fundamental mode for the two pure quark matter EOS considered (WSPHS1 and WSPHS2). The configurations near the maximum mass limits of these EOS have much lower frequencies than the rest of the EOS studied, around 5.5 kHz.

TABLE III. Fits for the wI1 modes. Parameters A and B correspond to the linear empirical relation for the frequency (17). Parameters a, b, and c correspond to the quadratic empirical relation for the damping time (18).

wI1	SLy	APR4	GNH3	BGN1H1	H1	H4	WCS2	WCS1	BHZBM
A	-689.5 ± 5.2	-667.9 ± 3.9	-736.5 ± 6.8	-779.4 ± 6.8	-797 ± 12	-703.7 ± 5.5	-684.2 ± 6.8	-723.5 ± 7.0	-727.7 ± 6.2
B	312.5 ± 1.1	309.35 ± 0.97	317.2 ± 1.4	323.3 ± 1.4	324.4 ± 0.7	316.2 ± 1.1	310.5 ± 1.5	315.3 ± 1.4	317.5 ± 1.3
χ^2	0.997	0.670	0.372	1.986	0.18	0.731	1.564	0.955	1.144
a	-1843 ± 55	-1792 ± 65	-2062 ± 25	-1771 ± 123	-2274 ± 20	-2020 ± 71	-1863 ± 78	-2635 ± 150	-1854 ± 79
b	650 ± 23	646 ± 30	690.9 ± 8.9	582 ± 45	725.8 ± 6.6	687 ± 26	656 ± 32	879 ± 55	627 ± 32
c	14.3 ± 2.2	13.7 ± 3.2	13.10 ± 0.73	21.1 ± 3.9	12.02 ± 0.51	12.7 ± 2.3	14 ± 29	3.1 ± 4.8	17.4 ± 3.0
χ^2	0.311	0.510	0.380	0.393	0.00374	0.209	0.401	0.520	0.361

In these figures we observe that the frequency and damping times have a clear dependence on the EOS when represented against the central pressure. All the EOS with quark matter at the core present a characteristic behavior, with frequencies below those of the plain nuclear matter configurations, except the ALF4 EOS, which mimics the SLy EOS almost entirely.

In Fig. 19 we present the frequency of the fundamental mode scaled to the radius of each configuration. A linear fit can be made to each equation of state. We fit to the phenomenological relation presented in the previous subsection, equation (17). In Table IV we present the fit parameters A, B for each one of the equations of state studied.

In Fig. 20 we present the damping time of the fundamental mode scaled to the mass of each configuration. In this case, the results can be fitted to the empirical quadratic relation on M/R, as presented in Eq. (18). In Table IV we present the fit parameters a, b, and c.

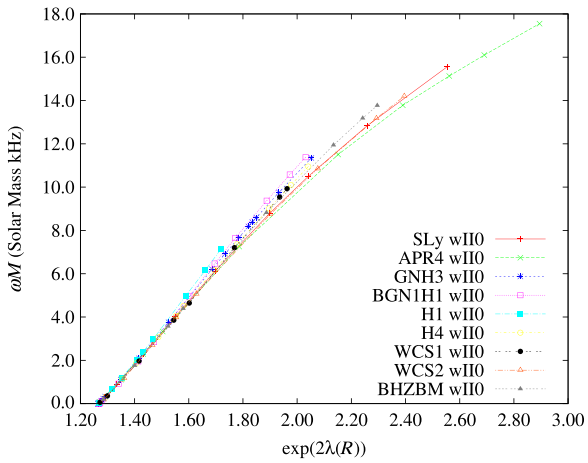

FIG. 12 (color online). Scaled frequency of the fundamental wII mode vs $e^{2\lambda(R)}$, for the EOS considered in Sec. VA. The frequency vanishes for compactness between $M/R = 0.1044$ and $M/R = 0.1066$. For low compactness, there are no or almost no hyperons in the core of the star, so at this point all the configurations are basically plain nuclear matter stars.

When we represent the scaled frequency and damping time vs M/R, all the wI0 modes have a similar behavior and the coincidence is greater for higher compactness. The only exceptions are WSPHS1-2 EOS (pure quark stars). Their behavior is clearly differentiated from the rest because of the different layer structure found at the exterior of the star.

First excited wI mode.—We present a similar study of the first excited wI mode. In Figs. 21 and 22 we plot the scaled frequency and damping time for the first excited wI mode. The empirical relations (17) and (18), with different parameters can be found in Table V. Note that the scaled frequency and damping time is quite similar for every EOS considered, and the only difference is found for the WSPHS1-2 EOS at low densities, for the same reasons than for the fundamental modes.

Fundamental wII mode.—Finally, in Fig. 23 we plot the frequency of the fundamental wII mode scaled with the mass vs the metric function $e^{2\lambda(R)}$. As in the previous subsection, it can be seen that there is, for all the equations of state studied, a minimal compactness below which the wII mode vanishes.

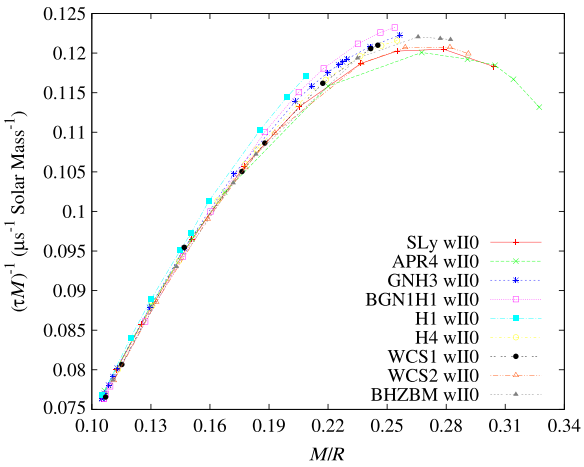

FIG. 13 (color online). Scaled damping time of the fundamental wII mode vs M/R, for the EOS considered in Sec. VA. The damping time does not vanish in the limit compactness as the frequency does.

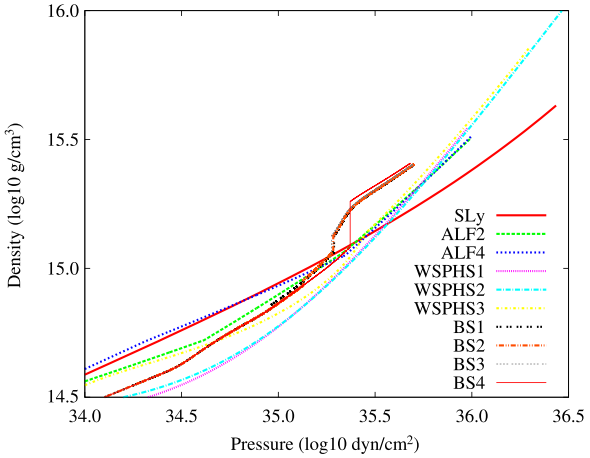

FIG. 14 (color online). Density vs pressure in logarithmic scale in the high density region, for the EOS considered in Sec. V B. Note that hybrid stars present important phase transitions at high pressures.

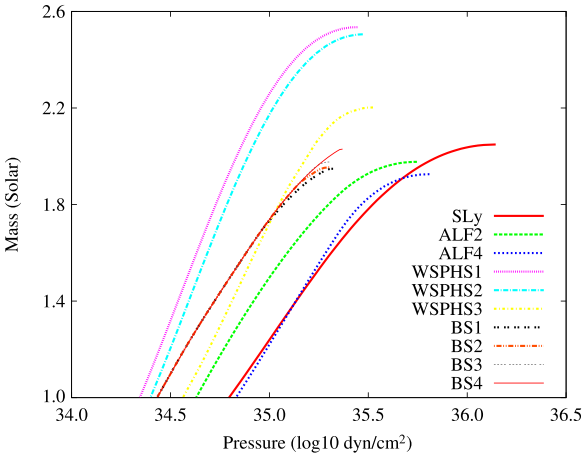

FIG. 16 (color online). Mass vs central pressure relation, for the EOS considered in Sec. V B. In this study we consider only stable configurations between $1M_\odot$ and the maximum mass of the particular EOS.

In Fig. 24 we show the damping time of the wII mode scaled with the mass, where it can be seen that for these limit configurations it tends to a limit τ dependent of the equation of state. Note that for the hybrid stars considered, the limit configuration is different depending on the matter composition of the outer layers. For hybrid stars ALF2, ALF4 and WSPHS3, the limit configurations have compactness between $M/R = 0.1046$ and $M/R = 0.1060$, similar to hyperon stars. For BS1-4, the limit configurations have compactness $M/R = 0.112$, and for quark stars WSPHS1 and WSPHS2, the limit configurations are quite different and have compactness $M/R = 0.126$. These differences are due to the behavior of the different equations of state of each configuration at the outer layers of the star. In fact, note that for quark stars WSPHS1 and WSPHS2 the pressure drops to zero with constant density around 2×10^{14} g/cm^3.

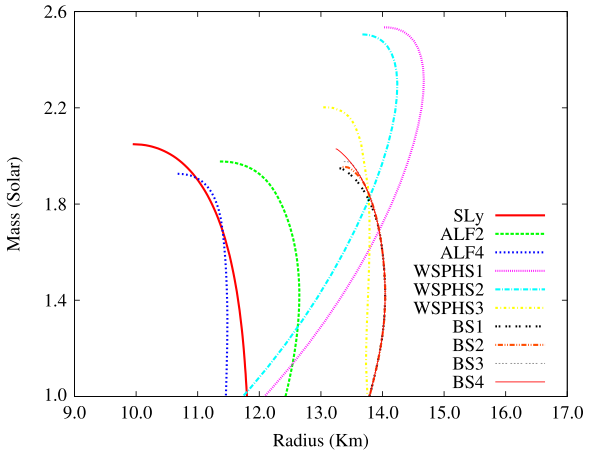

FIG. 15 (color online). Mass vs radius relation for the EOS considered in Sec. V B. All these EOS have maximum mass nearby or beyond $2M_\odot$ and radius beyond 10 Km.

1. BS equations of state

In order to study the influence of different phases in the compact star, we study four equations of state, considered by Bonanno and Sedrakian with the NL3 parametrization of the Walecka model [19]. These EOS correspond to hybrid stars with hyperons and quark color-superconductivity. They usually have four regions,

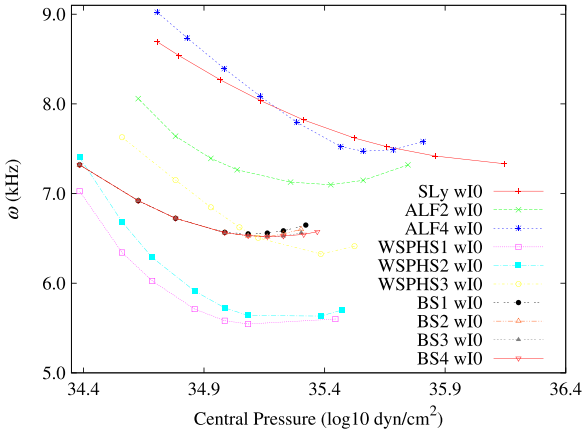

FIG. 17 (color online). Frequency of the fundamental wI mode vs central pressure in logarithmic scale. Hybrid stars tend to have lower frequencies than plain nuclear matter stars or hyperon matter. Pure quark stars have the smallest frequencies, below 6 kHz.

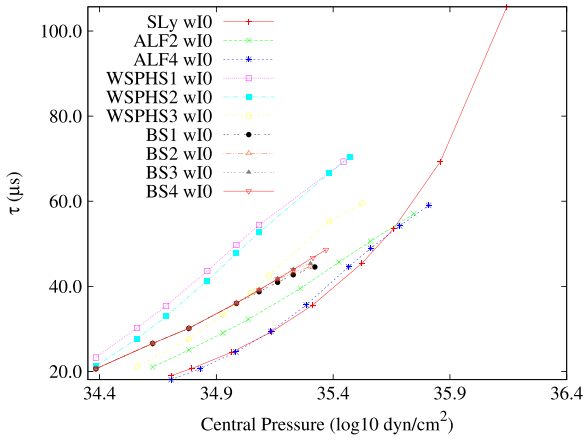

FIG. 18 (color online). Damping time of the fundamental wI mode vs central pressure in logarithmic scale, for the EOS considered in Sec. V B. Hybrid stars are found in between the pure quark matter configurations and the plain nuclear matter ones.

which are, from the inside to the outside: CFL (quark matter three-flavor color-flavor-locked), 2SC (quark matter two-superconducting colors phase), N + Hyp (nuclear and Hyper-nuclear matter), and N (nuclear matter). The extent of each region depends on the quark-hadron transition density $\rho_{\rm tr}$ and the vector coupling constant G_V. We study four equations of state with $G_V = 0.6G_S$ and $\rho_{\rm tr} = 2\rho_0$, $3\rho_0$, $3.5\rho_0$, $4\rho_0$ where ρ_0 is the density of nuclear saturation.

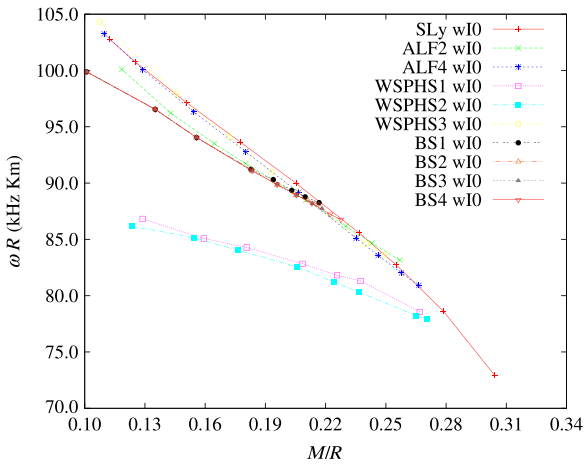

FIG. 19 (color online). Scaled frequency of the fundamental wI mode vs M/R, for the EOS considered in Sec. V B. All the scaled frequencies can be fitted to a linear relation with the compactness (17), even the ones for WSPHS1-2. The empirical parameters of hybrid stars are quite different from those of pure quark stars. The fits can be found in Table IV.

In Fig. 25 we plot the equations of state in the high density region. In Fig. 26 we plot the frequency of the fundamental wI mode as a function of the central pressure of the star in logarithmic scale. In Fig. 27 we make a similar plot for the damping time of these configurations.

We can see in Fig. 25 that the BS equations of the state have phase transitions, where for a given pressure, the density suffers a finite jump that increases its value (the EOS become softer). The effect of these phase transitions is reflected clearly in the frequency and damping time of the wI0 modes as it can be seen in Figs. 26 and 27.

VI. EMPIRICAL RELATIONS FOR W MODES

In Fig. 28 we present $\omega_I M$ vs $\omega_R M$ for wI0, wI1, and wII0 modes, for all the equations of state studied. This is a plot similar to Fig. 4 of [49] for constant density stars. It can be seen that for the fundamental modes, the scaling with the mass is quite independent of the equation of state.

Now let us define $\bar{\omega}_R$ and $\bar{\omega}_I$ (real and imaginary part of the w modes in units of the central pressure) by the following relations

$$\bar{\omega}_R = 2\pi \frac{1}{\sqrt{p_c(\mathrm{cm}^{-2})}} \frac{10^3}{c}\, \omega(\mathrm{Khz}),$$
$$\bar{\omega}_I = \frac{1}{\sqrt{p_c(\mathrm{cm}^{-2})}} \frac{10^6}{c} \frac{1}{\tau(\mu\mathrm{s})}, \tag{19}$$

where c is the speed of light in cm/s. If we plot $\bar{\omega}_R$ vs $\bar{\omega}_I$ of wI0, wI1, and wII0 modes for all the equations of state, we obtain Fig. 29 with three curves, one for each type of modes. A remarkable feature is that all the wI0 modes of Fig. 28 can be described by the curve marked wI0 in Fig. 29, almost independently of the equation of state. A similar behavior is obtained for wI1 and wII0 modes. One would expect all the wI0 modes of a given EOS to describe a curve depending on one parameter (for instance, the central pressure). And in principle, different equations of state should describe different curves. It is interesting to note that this is not the case, since the empirical relation between $\bar{\omega}_R$ and $\bar{\omega}_I$ is independent of the equation of state. Hence, all the modes of the same type are located in the same curve in Fig. 29, independently of the EOS. Nevertheless, the parametrization of the curve using the central pressure depends on the EOS. It is interesting to note that the only points that separate slightly from the corresponding line are those of modes for equations of state WSPHS1 and WSPHS2 of quark stars.

This result allows us to present an empirical relation between $\bar{\omega}_R$ and $\bar{\omega}_I$ that seems to be independent of the equation of the state. As far as we know this has not been obtained before.

For all the EOS except WSPHS1 and WSPHS2, we obtain the following:

For the fundamental wI modes, our results of $\bar{\omega}_I$ vs $\bar{\omega}_R$ can be fitted to a quadratic relation as follows:

TABLE IV. Fits for the wI0 modes. Parameters A and B correspond to the linear empirical relation for the frequency (17). Parameters a, b, and c correspond to the quadratic empirical relation for the damping time (18).

wI0	ALF2	ALF4	WSPHS1	WSPHS2	WSPHS3	BS1	BS2	BS3	BS4
A	-119.0 ± 3.0	-141.4 ± 1.2	-56.5 ± 3.7	-57.95 ± 3.1	-145.3 ± 3.4	-102.1 ± 1.8	-104.3 ± 1.7	-104.9 ± 1.4	-104.7 ± 1.1
B	113.51 ± 0.59	118.40 ± 0.25	94.31 ± 0.75	93.96 ± 0.65	119.98 ± 0.66	110.14 ± 0.32	110.42 ± 0.31	110.50 ± 0.25	110.46 ± 0.20
χ^2	0.151	0.039	0.182	0.182	0.178	0.0359	0.0343	0.0227	0.0174
a	-1290 ± 42	-1158 ± 26	-1319 ± 75	-295 ± 35	-1147 ± 24	-1275 ± 46	-1263 ± 46	-1266 ± 43	-1283 ± 34
b	395 ± 16	345.3 ± 9.8	455 ± 30	445 ± 14	340.4 ± 8.7	394 ± 15	390 ± 15	391 ± 14	397 ± 11
c	18.6 ± 1.4	23.06 ± 0.88	9.3 ± 2.3	10.4 ± 1.4	23.62 ± 0.76	18.4 ± 1.1	18.6 ± 1.1	18.5 ± 1.1	18.14 ± 0.90
χ^2	0.043	0.028	0.134	0.044	0.017	0.025	0.025	0.023	0.021

$$\bar{\omega}_I = (-2.30 \pm 0.13) + (0.58 \pm 0.16)\bar{\omega}_R + (0.0165 \pm 0.0004)\bar{\omega}_R^2, \quad (20)$$

with $\chi^2 = 0.107$.

For the first excited wI mode, we obtain the following fit:

$$\bar{\omega}_I = (-1.22 \pm 0.13) + (0.485 \pm 0.008)\bar{\omega}_R + (0.00163 \pm 0.00011)\bar{\omega}_R^2, \quad (21)$$

with $\chi^2 = 0.170$. It is almost linear with $\bar{\omega}_R$.

For the fundamental wII mode, $\bar{\omega}_R$ is quadratic with $\bar{\omega}_I$. We obtain the following fit:

$$\bar{\omega}_R = (4.21 \pm 0.14) + (0.173 \pm 0.012)\bar{\omega}_I + (-0.00524 \pm 0.00020)\bar{\omega}_I^2, \quad (22)$$

with $\chi^2 = 0.165$.

For quark stars (EOS WSPHS1 and WSPHS2) we obtain slightly different values for the parameters of the empirical relation:

For the fundamental wI modes, our results of $\bar{\omega}_I$ vs $\bar{\omega}_R$ can be fitted to a quadratic relation as follows:

$$\bar{\omega}_I = (-2.20 \pm 0.22) + (0.557 \pm 0.024)\bar{\omega}_R + (0.0148 \pm 0.0006)\bar{\omega}_R^2, \quad (23)$$

with $\chi^2 = 0.0220$.

For the first excited wI mode, we obtain the following fit:

$$\bar{\omega}_I = (-1.275 \pm 0.097) + (0.476 \pm 0.005)\bar{\omega}_R + (0.0010 \pm 0.00005)\bar{\omega}_R^2, \quad (24)$$

with $\chi^2 = 0.00902$. It is almost linear with $\bar{\omega}_R$.

For the fundamental wII mode, $\bar{\omega}_R$ is quadratic with $\bar{\omega}_I$. We obtain the following fit:

$$\bar{\omega}_R = (4.32 \pm 0.30) + (0.198 \pm 0.022)\bar{\omega}_I + (-0.0051 \pm 0.0004)\bar{\omega}_I^2, \quad (25)$$

with $\chi^2 = 0.061$.

These relations allow us to obtain $\bar{\omega}_I$ if $\bar{\omega}_R$ is known. From a practical point of view, these relations can be used to simplify the numerical calculations to obtain quasinormal modes for any equation of state, reducing, in our

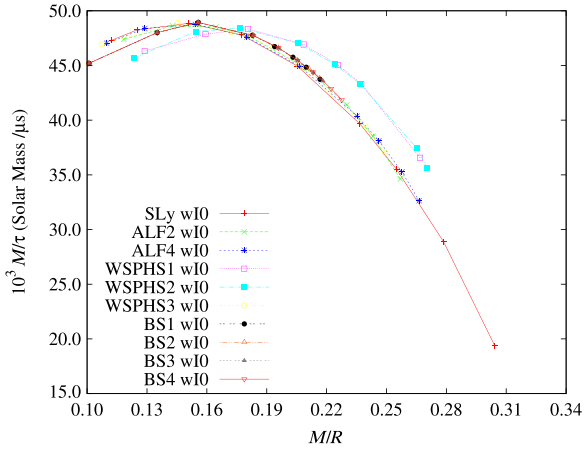

FIG. 20 (color online). Scaled damping time of the fundamental wI mode vs M/R, for the EOS considered in Sec. V B. The scaled damping times can be fitted to a quadratic relation with the compactness (18). Again, WSPHS1-2 present a different behavior from the hybrid stars. The fits can be found in Table IV.

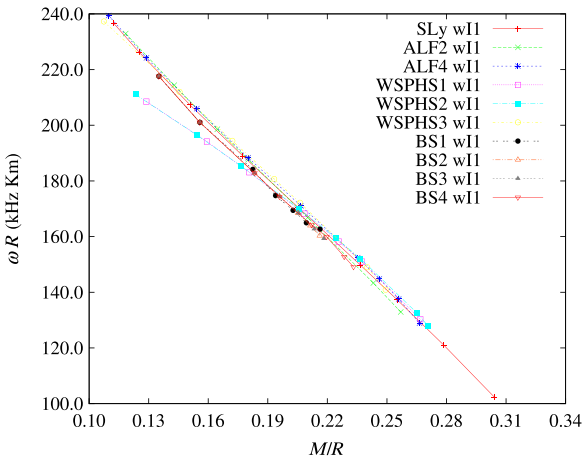

FIG. 21 (color online). Scaled frequency of the first excited wI mode vs M/R, for the EOS considered in Sec. V B. In this case, all these EOS fit perfectly the linear relation with the compactness (17). The fits can be found in Table V.

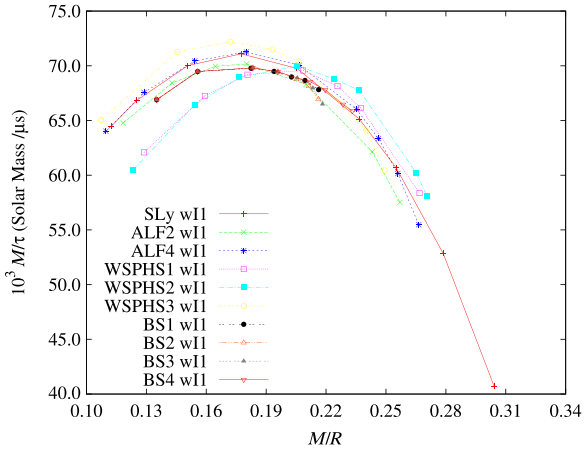

FIG. 22 (color online). Scaled damping time of the first excited wI mode vs M/R, for the EOS considered in Sec. V B. A quadratic relation with the compactness (18) can be found for all these EOS. For low compactness WSPHS1-2 configurations the scaled damping time can be a 10% smaller than for hybrid stars. The fits can be found in Table V.

method, the time necessary to find the zeros of the determinant.

Let us present a possible application of these empirical relations. Suppose that the frequency $\omega(Khz)$ and the damping time $\tau(\mu s)$ of the fundamental mode wI0 of a neutron star are detected. Then, using the Eq. (19) we can plot a line for $\bar{\omega}_I$ vs $\bar{\omega}_R$ in Fig. 29 with parameter of the line p_c. The crossing point of this line with the curve marked wI0, given by the empirical relation (20), gives us an estimation of the central pressure p_c independently of the equation of state. Now, we can check which equations of state are compatible with this p_c; i.e., which EOS have the measured wI0 mode near the crossing point for the estimated central pressure. Hence, this method allows us to estimate the central pressure p_c and, in some situations, discard certain equations of state. Let us mention that using this p_c, we can estimate the mass and the radius of the star using our calculations for the possible EOS. Note, that if these data (mass and radius) are measured by other methods, we would have another filter to impose to the EOS.

VII. OTHER RESULTS

Finally, we study the effect of core-crust transition pressure variations in the quasinormal mode spectrum using our model of crust as a surface energy density enveloping the core. We will consider the SLy equation of state, for which the core-crust transition is found at density 1.29×10^{14} g/cm^3. We construct a star of $1.4M_\odot$ with and without a surface energy density enveloping the core of the star at this core-crust transition region. We can compare the difference in the fundamental w modes between our approximation of crust as a thin shell enveloping the core, and the standard calculation. The result is the following: for the fundamental wI mode, the change in the frequency is 0.07% and the variation in the damping time is -0.02%. For the fundamental wII mode, the changes are bigger. For the frequency 0.3% and for the damping time -0.07%. This indicates that this approximation makes small changes in the w quasinormal spectrum.

Next, we consider this neutron star with $1.4M_\odot$ and surface energy density at the core-crust transition point: 4.8×10^{32} dyn/cm^2. Fixing the central pressure, we variate the core-*crust* transition pressure between 10^{32} dyn/cm^2 and 10^{33} dyn/cm^2, and compare with the modes for the initial configuration. The impact of transition pressure variations on the frequency is small, between -0.05% and 0.08% for the fundamental wI mode, and between -0.24% and 0.35% for the fundamental wII mode. Similarly, transition pressure variations have a small impact on the damping time, between 0.02% and -0.035% for the fundamental wI mode, and between 0.06% and -0.1% for the fundamental wII mode.

VIII. SUMMARY

In this paper we have studied the axial w quasinormal modes for 18 equations of state. In particular, we consider the influence of the presence of exotic matter in the core of the neutron star.

We have seen that the hyperon core changes the frequency and the damping time of the modes for configurations of high compactness. The frequency increases with the central pressure above $\sim 10^{35}$ dyn/cm^2, where the hyperon phases are more important due to the high density of the star core. This effect is related to the softening of the

TABLE V. Fits for the wI1 modes. Parameters A and B correspond to the linear empirical relation for the frequency (17). Parameters a, b, and c correspond to the quadratic empirical relation for the damping time (18).

wI1	ALF2	ALF4	WSPHS1	WSPHS2	WSPHS3	BS1	BS2	BS3	BS4
A	-715.8 ± 4.0	-688.7 ± 6.8	-560 ± 19	-562 ± 18	-672.6 ± 6.7	-685 ± 19	-694 ± 10	-689 ± 11	-681 ± 11
B	316.98 ± 0.78	313.5 ± 1.4	283.0 ± 4.0	283.3 ± 3.8	310.0 ± 1.3	308.9 ± 3.5	310.4 ± 2.0	309.7 ± 2.0	308.3 ± 2.0
χ^2	0.258	1.236	5.073	6.203	0.691	1.821	0.6037	0.662	0.921
a	-1828 ± 72	-1857 ± 110	-2026 ± 103	-2017 ± 117	-1870 ± 79	-1536 ± 142	-1874 ± 155	-1897 ± 205	-1458 ± 85
b	637 ± 27	654 ± 42	780 ± 40	785 ± 47	639 ± 29	549 ± 50	661 ± 55	670 ± 73	524 ± 32
c	14.7 ± 2.5	14.2 ± 3.8	-5.1 ± 3.9	6.3 ± 4.5	17.9 ± 2.5	20.9 ± 4.3	11.8 ± 4.7	11.0 ± 6.3	22.8 ± 2.9
χ^2	0.1242	0.510	0.252	0.486	0.187	0.0502	0.0584	0.1167	0.0457

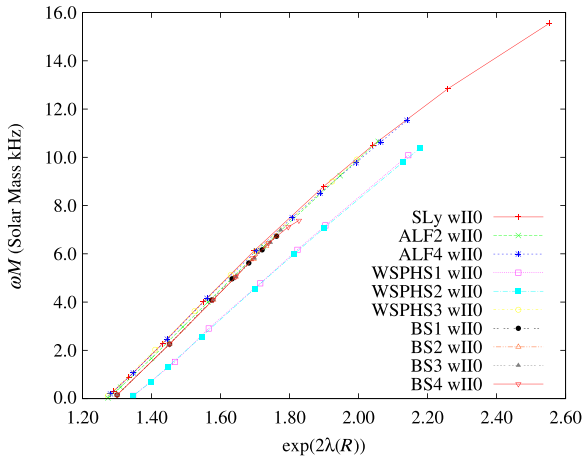

FIG. 23 (color online). Scaled frequency of the fundamental wII mode vs $e^{2\lambda(R)}$, for the EOS considered in Sec. V B. The frequency vanishes for a compactness that depends on the lower densities of the equation of state considered, around $M/R = 0.105$ and $M/R = 0.110$ for hybrid stars. The most different are the pure quark stars WSPHS1-2, which have the limit at $M/R = 0.126$.

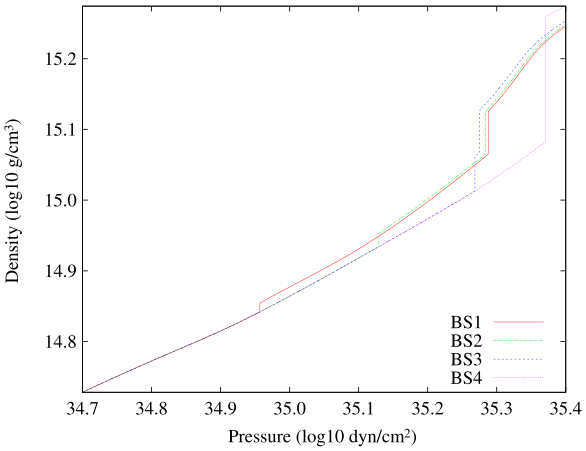

FIG. 25 (color online). Density vs pressure in logarithmic scale for the BS EOS for high densities. Note that at high pressures different phase transitions are taken into account, affecting the stiffness of the EOS.

equation of state at the inner regions of the star. For stars including quark matter in the core, we obtain a clear influence of the quark presence on the frequency and damping time when represented vs central pressure, with a characteristic behavior for all the EOS with quark matter in the core.

We have obtained phenomenological relations for the frequency and damping time with M/R for wI and wII modes. For some equations of state (for hyperon matter H1 and BGN1H1, and for pure quark stars WSPHS1-2) the scaling relations are quite different from the rest of the EOS. For the rest of the EOS considered, the scaled relations are quite similar, providing useful information that could be used to measure the radius of a neutron star.

A detailed analysis of four equations of state considered by Bonanno and Sedrakian allows us to study the influence of the presence of different phase transitions in the spectrum of a compact star.

Another interesting result is the new phenomenological relation between the real part $\bar{\omega}_R$ and the imaginary part $\bar{\omega}_I$ (scaled to the central pressure) of w quasinormal modes,

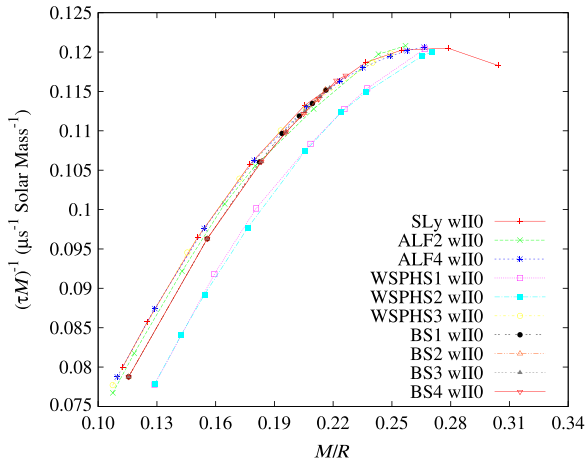

FIG. 24 (color online). Damping time of the fundamental wII mode vs M/R, for the EOS considered in Sec. V B. The damping time does not vanish in the limit compactness as the frequency does.

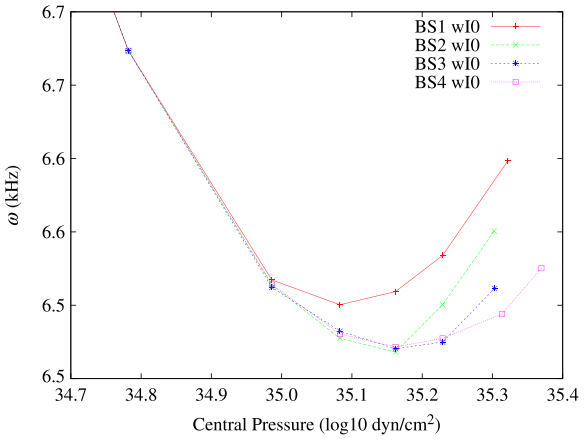

FIG. 26 (color online). Frequency of the fundamental wI mode vs central pressure for the BS equations of state. The phase transitions that can be seen in the previous figure affects the frequency curves. These curves branch once the EOS is affected by the phase transition.

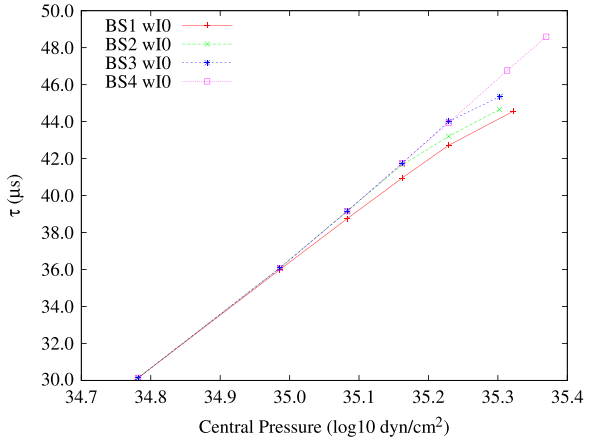

FIG. 27 (color online). Damping time of the fundamental wI mode vs central pressure for the BS equations of state. In a similar way to the frequency, the phase transitions in the equations of state are clearly reflected in the branching of the damping time curves.

valid for all the EOS, except, perhaps, for WSPHS1 and WSPHS2 EOS (quark stars).

The precision of our algorithm allows us to construct explicitly the universal low compactness limiting configuration around $M/R = 0.106$ for which the fundamental wII mode vanishes. The existence of this configuration was conjectured by [30].

Finally, we have studied the influence of changes in the core-crust transition pressure obtaining that the influence is very small.

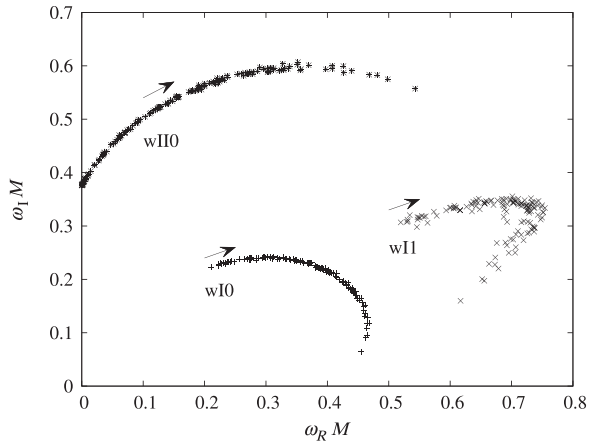

FIG. 28. Adimensional quantities $\omega_I M$ vs $\omega_R M$ for all w modes and EOS considered. Note that here we choose $c = G = 1$, so the products $\omega_R M$, $\omega_I M$ are adimensional. It can be seen that the scaling with the mass is quite independent of the equation of state, especially for the fundamental modes. The arrow indicates increasing compactness.

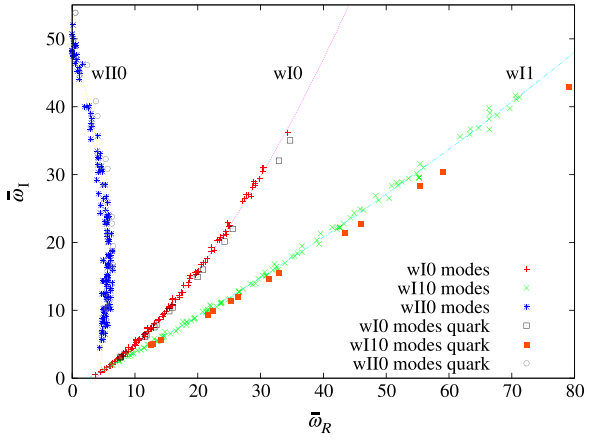

FIG. 29 (color online). $\bar{\omega}_I$ vs $\bar{\omega}_R$ as defined in Eqs. (19) for all the w modes and for every equation of state we considered in the study. Here it can be seen that the scaling with the central pressure is also quite independent of the equation of state. This universal relation could be used to estimate, for example, the central pressure of the star independently of the EOS. The compactness decreases when increasing $\bar{\omega}_I$.

In order to perform this analysis, we developed a new numerical method to calculate w-axial quasinormal modes. The use of the phase of the Regge-Wheeler function together with exterior complex scaling, allow us to impose the outgoing wave behavior with stringent conditions. We allow for variable angle in the complex scaling, which makes it possible to obtain new modes and enhances precision with respect to previous works.

We present a complete study of the junction conditions between the exterior and interior solution in a surface of constant pressure (also including the case $p = 0$, the border of the star). The matching conditions can be written in terms of a determinant whose zeros correspond to quasinormal modes for the particular integrated configuration.

ACKNOWLEDGMENTS

We would like to thank I. Bednarek for kindly providing us with the EOS BHZBM, I. Sagert for EOS WSPHS1-3, A. Sedrakian for EOS BS1-4, and S. Weissenborn for EOS WCS1-2. We thank Professor Kostas D. Kokkotas for very helpful discussions concerning quasinormal modes of neutron stars and for the hospitality to J. L. B. We are very grateful to Professor Gabriel A. Galindo for his help concerning the exterior complex scaling method. We also want to thank the referees for his/her very helpful comments and suggestions. This work was supported by the Spanish Ministerio de Ciencia e Innovacion, research Project No. FIS2011-28013. J. L. B. was supported by the Spanish Universidad Complutense de Madrid.

[1] M. Pitkin, S. Reid, S. Rowan, and J. Hough, Living Rev. Relativity **14**, 5 (2011).
[2] B. Sathyaprakash and B. F. Schutz, Living Rev. Relativity **12**, 2 (2009).
[3] N. Andersson, V. Ferrari, D. Jones, K. Kokkotas, B. Krishnan, J. Read, L. Rezzolla, and B. Zink, Gen. Relativ. Gravit. **43**, 409 (2011).
[4] N. Andersson and K. D. Kokkotas, Phys. Rev. Lett. **77**, 4134 (1996).
[5] M. Shibata, K. Taniguchi, and K. b. o. Uryū, Phys. Rev. D **71**, 084021 (2005).
[6] M. Shibata and K. Uryū, Prog. Theor. Phys. **107**, 265 (2002).
[7] R. Oechslin, H.-T. Janka, and A. Marek, Astron. Astrophys. **467**, 395 (2007).
[8] T. Hinderer, B. D. Lackey, R. N. Lang, and J. S. Read, Phys. Rev. D **81**, 123016 (2010).
[9] J. S. Read, C. Markakis, M. Shibata, K. b. o. Uryū, J. D. E. Creighton, and J. L. Friedman, Phys. Rev. D **79**, 124033 (2009).
[10] J. Abadie *et al.* (LIGO Scientific Collaboration), Phys. Rev. D **83**, 042001 (2011).
[11] K. D. Kokkotas and B. Schmidt, Living Rev. Relativity **2**, 2 (1999).
[12] H.-P. Nollert, Classical Quantum Gravity **16**, R159 (1999).
[13] L. Rezzolla, *Gravitational Waves from Perturbed Black Holes and Relativistic Stars* (ICTP, Trieste, 2003).
[14] A. Haensel, P. Potekhin, and D. Yakovlev, *Neutron Stars: Equation of State and Structure*, Astrophysics and Space Science Library (Springer, Berlin, 2007).
[15] N. Glendenning, *Compact Stars: Nuclear Physics, Particle Physics, and General Relativity*, Astronomy and Astrophysics Library (Springer, Berlin, 2000).
[16] H. Heiselberg and M. Hjorth-Jensen, Phys. Rep. **328**, 237 (2000).
[17] M. Prakash and J. M. Lattimer, in *From Nuclei to Stars*, edited by S. Lee (World Scientific, Singapore, 2011), Chap. 12, p. 275.
[18] I. Bednarek, P. Haensel, J. L. Zdunik, M. Bejger, and R. Mánka, Astron. Astrophys. **543**, A157 (2012).
[19] L. Bonanno and A. Sedrakian, Astron. Astrophys. **539**, A16 (2012).
[20] S. Weissenborn, D. Chatterjee, and J. Schaffner-Bielich, Phys. Rev. C **85**, 065802 (2012).
[21] S. Weissenborn, I. Sagert, G. Pagliara, M. Hempel, and J. Schaffner-Bielich, Astrophys. J. Lett. **740**, L14 (2011).
[22] J. S. Read, B. D. Lackey, B. J. Owen, and J. L. Friedman, Phys. Rev. D **79**, 124032 (2009).
[23] L. Lindblom, Phys. Rev. D **82**, 103011 (2010).
[24] O. Benhar, E. Berti, and V. Ferrari, Mon. Not. R. Astron. Soc. **310**, 797 (1999).
[25] K. D. Kokkotas, T. A. Apostolatos, and N. Andersson, Mon. Not. R. Astron. Soc. **320**, 307 (2001).
[26] O. Benhar, V. Ferrari, and L. Gualtieri, Phys. Rev. D **70**, 124015 (2004).
[27] O. Benhar, Mod. Phys. Lett. A **20**, 2335 (2005).
[28] V. Ferrari and L. Gualtieri, Gen. Relativ. Gravit. **40**, 945 (2008).
[29] D. Chatterjee and D. Bandyopadhyay, Phys. Rev. D **80**, 023011 (2009).
[30] D.-H. Wen, B.-A. Li, and P. G. Krastev, Phys. Rev. C **80**, 025801 (2009).
[31] T. Regge and J. A. Wheeler, Phys. Rev. **108**, 1063 (1957).
[32] F. J. Zerilli, Phys. Rev. Lett. **24**, 737 (1970).
[33] K. Thorne and A. Campolattaro, Astrophys. J. **149**, 591 (1967).
[34] R. Price and K. Thorne, Astrophys. J. **155**, 163 (1969).
[35] K. Thorne, Astrophys. J. **158**, 1 (1969).
[36] K. Thorne, Astrophys. J. **158**, 997 (1969).
[37] A. Campolattaro and K. Thorne, Astrophys. J. **159**, 847 (1970).
[38] L. Lindblom and S. L. Detweiler, Astrophys. J. Suppl. Ser. **53**, 73 (1983).
[39] S. Detweiler and L. Lindblom, Astrophys. J. **292**, 12 (1985).
[40] S. Chandrasekhar and V. Ferrari, Proc. R. Soc. A **432**, 247 (1991).
[41] S. Chandrasekhar, V. Ferrari, and R. Winston, Proc. R. Soc. A **434**, 635 (1991).
[42] S. Chandrasekhar and V. Ferrari, Proc. R. Soc. A **434**, 449 (1991).
[43] Y. Kojima, Phys. Rev. D **46**, 4289 (1992).
[44] N. Andersson, Y. Kojima, and K. D. Kokkotas, Astrophys. J. **462**, 855 (1996).
[45] K. D. Kokkotas, Mon. Not. R. Astron. Soc. **268**, 1015 (1994).
[46] K. D. Kokkotas and B. F. Schutz, Mon. Not. R. Astron. Soc. **255**, 119 (1992).
[47] N. Andersson, K. D. Kokkotas, and B. F. Schutz, Mon. Not. R. Astron. Soc. **274**, 9 (1995).
[48] S. Chandrasekhar and S. Detweiler, Proc. R. Soc. A **344**, 441 (1975).
[49] N. Andersson, Y. Kojima, and K. D. Kokkotas, Astrophys. J. **462**, 855 (1996).
[50] N. Andersson, Proc. R. Soc. A **439**, 47 (1992).
[51] L. Samuelsson, N. Andersson, and A. Maniopoulou, Classical Quantum Gravity **24**, 4147 (2007).
[52] E. W. Leaver, Proc. R. Soc. A **402**, 285 (1985).
[53] M. Leins, H. P. Nollert, and M. H. Soffel, Phys. Rev. D **48**, 3467 (1993).
[54] G. Darmois, *Mémorial des Sciences Mathématiques* (Gauthier-Villars, Paris, 1927), Vol. 25.
[55] A. Lichnerowicz, *Théories Relativistes de la Gravitation et de l'Electromagnétism* (Maison, Paris, 1955).
[56] S. O'Brien and J. L. Syngr, Comm. Dublin Inst. Adv. Stud. A **9**, 1 (1952).
[57] W. Israel, Nuovo Cimento B **44**, 1 (1966).
[58] M. Mars and J. M. Senovilla, Classical Quantum Gravity **10**, 1865 (1993).
[59] R. Vera, Classical Quantum Gravity **19**, 5249 (2002).
[60] M. Mars, Classical Quantum Gravity **22**, 3325 (2005).
[61] L. M. González-Romero, Phys. Rev. D **67**, 064011 (2003).
[62] M. A. H. MacCallum, M. Mars, and R. Vera, Phys. Rev. D **75**, 024017 (2007).
[63] H. Sotani, K. Tominaga, and K.-i. Maeda, Phys. Rev. D **65**, 024010 (2001).
[64] C. Misner, K. Thorne, and J. Wheeler, *Gravitation*, Physics Series (W. H. Freeman, New York, 1973).
[65] U. Ascher, J. Christiansen, and R. D. Russell, Math. Comput. **33**, 659 (1979).
[66] J. Aguilar and J. Combes, Commun. Math. Phys. **22**, 269 (1971).

[67] E. Balslev and J. Combes, Commun. Math. Phys. **22**, 280 (1971).
[68] B. Simon, Commun. Math. Phys. **27**, 1 (1972).
[69] G. Alvarez, R. Damburg, and H. Silverstone, Phys. Rev. A **44**, 3060 (1991).
[70] F. Fritsch and R. Carlson, SIAM J. Numer. Anal. **17**, 238 (1980).
[71] F. Douchin and P. Haensel, Astron. Astrophys. **380**, 151 (2001).
[72] A. Akmal, V. R. Pandharipande, and D. G. Ravenhall, Phys. Rev. C **58**, 1804 (1998).
[73] N. Glendenning, Astrophys. J. **293**, 470 (1985).
[74] B. D. Lackey, M. Nayyar, and B. J. Owen, Phys. Rev. D **73**, 024021 (2006).
[75] S. Balberg and A. Gal, Nucl. Phys. **A625**, 435 (1997).
[76] M. Alford, M. Braby, M. Paris, and S. Reddy, Astrophys. J. **629**, 969 (2005).
[77] N. Andersson and K. D. Kokkotas, Mon. Not. R. Astron. Soc. **299**, 1059 (1998).
[78] O. Benhar, E. Berti, and V. Ferrari, Mon. Not. R. Astron. Soc. **310**, 797 (1999).

2.3.3 Publication: Jose Luis Blázquez-Salcedo, Luis Manuel González-Romero, and Francisco Navarro-Lérida, *Polar quasi-normal modes of neutron stars with equations of state satisfying the 2 $M_\odot$ constraint*, Physical Review D 89 (2014) 044006

PHYSICAL REVIEW D **89,** 044006 (2014)

Polar quasi-normal modes of neutron stars with equations of state satisfying the 2 $M_\odot$ constraint

J. L. Blázquez-Salcedo,[1] L. M. González-Romero,[1] and F. Navarro-Lérida[2]

[1]*Departamento de Física Teórica II, Facultad de Ciencias Físicas, Universidad Complutense de Madrid, 28040 Madrid, Spain*

[2]*Departamento de Física Átomica, Molecular y Nuclear, Facultad de Ciencias Físicas, Universidad Complutense de Madrid, 28040 Madrid, Spain*

(Received 3 July 2013; published 6 February 2014)

In this paper, we analyze the quasinormal mode spectrum of realistic neutron stars by studying the polar modes. In particular, we calculate the fundamental mode (f mode), the fundamental pressure mode (p mode), and the fundamental curvature mode (wI mode) for 15 different equations of state satisfying the 2 $M_\odot$ constraint, most of them containing exotic matter. Since f and p modes couple to matter perturbations, the influence of the presence of hyperons and quarks in the core of the neutron stars is more significant than for the axial component. We present phenomenological relations, which are compatible with previous results, for the frequency and damping time with the compactness of the neutron star. We also consider new phenomenological relations between the frequency and damping time of the wI mode and the f mode. These new relations are independent of the equation of state and could be used to estimate the central pressure, mass, or radius and eventually constrain the equation-of-state of neutron stars. To obtain these results, we have developed a new method based on the exterior complex scaling technique with a variable angle.

DOI: 10.1103/PhysRevD.89.044006 PACS numbers: 04.40.Dg, 04.30.−w, 95.30.Sf, 97.60.Jd

I. INTRODUCTION

Neutron stars can be used as probes to gain insight into the structure of matter at high densities (10^{15} g/cm^3 at their core). Knowledge on mass, radius, and any other global properties of the neutron star can give us important information on the state and composition of matter at those extreme physical conditions. However, although the mass can be determined with quite good precision, a direct measurement of the radius is currently very difficult using astrophysical observations.

Nevertheless, the detection of gravitational waves originated in the neutron stars could be used to obtain estimations, or at least constraints, on the value of the gravitational radius of the star. With knowledge on the mass and radius, we would be able to have a better understanding of the behavior of matter at high density and pressure. Therefore, the study of these gravitational waves is crucial in the understanding of the physics of matter at extreme densities.

Neutron stars present a layer structure, which can be essentially described by two very different regions: a core (where exotic matter could be found) enveloped by a *crust* (with a solid crystalline structure similar to a metal). The relativistic fluid that composes the neutron star can be described as a perfect fluid, for which the equation of state is needed. Because not much information is available beyond the nuclear densities, the equation of state is very model dependent, since different particle populations may appear at those energies [1,2]. Another interesting feature is that along the core of the star and especially in the core-crust interface first-order phase transitions could be found in realistic equations of state. These phase transitions result in small discontinuities in the energy density of the star matter [1,3].

Very interesting information can be obtained from the recent measurement of the mass of PSR J1614-2230, of 1.97 $M_\odot$, which imposes constraints on equations of state for exotic matter that could be found in neutron stars [4]. Several equations of state that are able to produce neutron star configurations with 2 $M_\odot$ and exotic matter in their cores have been proposed [5–8]. If other global parameters could be measured, more important constraints could be imposed on the equation of state.

If an internal or external event perturbates a neutron star, it may oscillate nonradially, emitting gravitational waves to the space [9]. Large-scale interferometric gravitational wave detectors such as LIGO, GEO, TAMA, and VIRGO have reached the original design sensitivity, and the detection of the first gravitational waves could happen in the next few years [10]. These detections will provide useful information about the composition of the astrophysical objects that generate them, like neutron stars [9].

The gravitational waves emitted by a neutron star present dominant frequencies, which can be studied using the quasinormal mode formalism [11–13]. These eigenfrequencies are given by a complex number. The real part gives us the oscillation frequency of the mode, while the imaginary part gives us the inverse of the damping time. The quasinormal mode spectrum is quite dependent on the properties of the star, i.e., the equation of state.

Hence, the detection of gravitational radiation from neutron stars combined with a complete theoretical study of the possible spectra that can be obtained with different equations of state can be very useful in the determination of the matter behavior beyond nuclear matter [14–20].

The necessary formalism to study quasinormal modes was first developed for black holes by Regge and Wheeler [21]

and by Zerilli [22]. Quasinormal modes can be separated into polar and axial modes. The equation describing the quasinormal mode perturbation of the Schwarzschild metric is essentially a Schrödinger-like equation: the Regge–Wheeler equation for axial perturbations and the Zerilli equation for polar ones. For black holes, both types of modes are space-time modes. The formalism was first studied in the context of neutron stars by Thorne [23–27] and Lindblom [28,29] and then reformulated by Chandrasekhar and Ferrari [30–32], Ipser and Price [33], and Kojima [34]. In neutron stars, axial modes are purely space-time modes of oscillation (w modes), while polar modes can be coupled to fluid oscillations (fundamental f modes, pressure p modes, and also a branch of space-time w modes). In this paper, we will consider only polar modes of oscillation. The corresponding study of axial modes can be found in Ref. [35].

Although the perturbation equations for neutron stars can be simplified into a Regge–Wheeler equation or a Zerilli equation for the vacuum part of the problem, it is complicated to obtain the quasinormal mode spectrum of neutron stars. The equations must be solved numerically, and no analytical solution is known for physically acceptable configurations. The main difficulty is found on the diverging and oscillatory nature of the quasinormal modes. These functions are not handled well numerically.

Several methods have been developed to deal with these and other difficulties. For a complete review on the methods, see the review by Kokkotas and Schmidt [11].

The axial part of the spectrum has been extensively studied for simplified constant density models and polytropes [36–38]. Important results for the polar spectrum have been obtained using several methods, for example, the continued fraction method, which has been used to study realistic equations of state [14,16,20]. More recently, Samuelsson *et al.* [39] used a complex-radius approach for a constant density configuration to study axial quasinormal modes.

To use the results for future observations, Andersson and Kokkotas, first for polytropes [40] and later for some realistic equations of state [41], proposed some empirical relations between the modes and the mass and the radius of the neutron star that could be used together with observations to constrain the equation of state. In later works, Benhar, Ferrari, and Gualtieri [16,18,42] reexamined those relations for other realistic equations of state. Recently, the authors studied these relations for axial modes, using new equations of state satisfying the 2 $M_\odot$ condition [35].

In this work, we study similar relations for the polar modes that could be used to estimate global parameters of the star, constraining the equation of state of the core of the neutron star. We present a new approach to calculate quasinormal modes of realistic neutron stars. Essentially, it is the implementation to polar modes of the method used previously for axial modes in Ref. [35]. We make use of several well-known techniques, like the use of the phase for the exterior solution and the use of a complexified coordinate to deal with the divergence of the outgoing wave. We also introduce some new techniques not used before in this context: freedom in the angle of the exterior complex path of integration, the use of the Colsys package to integrate all the system of equations at once with proper boundary and junction conditions, and the possibility of the implementation of phase transition discontinuities. These new techniques allow us to enhance accuracy, to obtain more modes in shorter times, and also to study several realistic equations of state, comparing results for different compositions.

In Sec. II, we present a brief review on the quasinormal mode formalism in order to fix notation. In Sec. III, we present the numerical method, which has been implemented in Fortran-based double-precision programs. In Sec. IV, we present the numerical results obtained from the application of the method and use them to study the realistic equations of state. We finish in Sec. V by presenting a summary of the main points of the paper.

II. OVERVIEW OF THE FORMALISM

In this section, we will give a brief review of the formalism used to describe polar quasinormal modes and the method used to calculate them. Here and in the following section, we will use geometrized units ($c = 1$, $G = 1$).

We consider polar perturbations on the static spherical space-time describing the star: $ds^2 = e^{2\nu}dt^2 - e^{2\lambda}dr^2 - r^2(d\theta^2 + \sin^2\theta d\varphi^2)$. The matter is considered as a perfect fluid with a barotropic equation of state. As can be demonstrated, only polar modes do couple to the matter perturbations of the star [23–34], i.e., first-order perturbations of the energy density and pressure. Axial modes, which were studied in Ref. [35], are only coupled to the Lagrangian displacement of the matter. Therefore, the spectrum of polar modes is much more dependent on the matter content of the star than the axial modes.

Up to first order in perturbation theory, and once the gauge is fixed (Regge–Wheeler gauge [12]), the number of functions needed to describe the polar perturbations is 8, which are, following Lindblom notation [28,29], $(H^0_{lm}, H^1_{lm}, H^2_{lm}, K_{lm}, W_{lm}, X_{lm}, \Pi_{lm}, E_{lm})$. The Einstein equations, together with the conservation of energy and baryon number, can be reduced to four first-order differential equations for $(H^1_{lm}, K_{lm}, W_{lm}, X_{lm})$ and four algebraic relations for $(H^0_{lm}, H^2_{lm}, \Pi_{lm}, E_{lm})$.

The angular dependence of the functions is known from the tensor expansion, and we will only consider in this work the $l = 2$ case. We can extract the time dependence from the functions by making a Laplace transformation resulting in equations explicitly dependent on the eigenvalue ω.

Inside of the star, we will need to solve the well-known zeroth-order system of equations for the hydrostatic equilibrium of a spherical star (Tolman–Oppenheimer–Volkoff equations):

$$\frac{dm}{dr} = 4\pi r^2 \rho, \tag{1}$$

$$\frac{dp}{dr} = -(\rho + p)\frac{m + 4\pi r^3 p}{(r - 2m)r}, \tag{2}$$

$$\frac{d\nu}{dr} = -\frac{1}{\rho + p}\frac{dp}{dr}. \tag{3}$$

Note that $e^{-2\lambda(r)} = 1 - \frac{2m(r)}{r}$. The total mass of the static configuration is $M = \int_0^R dr 4\pi r^2 \rho$, and the radius R of the star is defined where the pressure is zero $p(R) = 0$.

We need to specify the equation of state for the matter. Once we have a static solution, we can solve the system of four differential equations for the perturbations.

Outside the star (no matter), it can be seen that the system of equations can be rewritten, and it is reduced to a single second-order differential equation (Zerilli equation),

$$\frac{d^2 Z_{\rm lm}}{dr_*^2} + [\omega^2 - V(r)]Z_{\rm lm} = 0, \tag{4}$$

where r_* is the tortoise coordinate,

$$r_* = \int_0^r e^{\lambda - \nu} dr, \tag{5}$$

and the eigenfrequency of the polar mode is a complex number $\omega = \omega_{\Re} + i\omega_{\Im}$. As usual for quasinormal modes, we will consider $\omega_{\Re} > 0$ and $\omega_{\Im} > 0$. The potential can be written as

$$V(r) = 2(r - 2M)\frac{n^2(n+1)r^3 + 3Mn^2r^2 + 9M^2nr + 9M^3}{r^4(nr + 3M)^2}, \tag{6}$$

where $n = (l + 2)(l - 1)/2$ and $l = 2$ in this work.

III. NUMERICAL METHOD

Note that, in general, the perturbation functions are complex functions. So, numerically, we will have to integrate eight real first-order differential equations for the perturbation functions inside the star. These also translate into a set of two real second-order differential equations outside the star.

The perturbation has to satisfy a set of boundary conditions that can be obtained from the following two requirements [30]: (i) the perturbation must be regular at the center of the star, and (ii) the resulting quasinormal mode must be a pure outgoing wave.

In general, a quasinormal mode will be a composition of incoming and outgoing waves, i.e.,

$$\lim_{r_* \to \infty} Z^{\rm in} \sim e^{i\omega r_*}, \qquad \lim_{r_* \to \infty} Z^{\rm out} \sim e^{-i\omega r_*}. \tag{7}$$

Note that, while the real part of ω determines the oscillation frequency of the wave, the imaginary part of the eigenvalue determines the asymptotic behavior of the quasinormal mode. Since $\omega_{\Re} > 0$ and $\omega_{\Im} > 0$, outgoing quasinormal modes are divergent at radial infinity, while ingoing ones tend exponentially to zero as the radius grows. We should impose the solution to behave as a purely outgoing quasinormal mode at a very distant point. This has the inconvenience that any small contamination of the outgoing signal gives rise to an important incoming wave component.

We have adapted a method based on the exterior complex scaling method, which we will describe briefly in the following paragraphs. It is an adaptation to polar modes of the method previously employed for axial quasinormal modes [35].

Outside the star, and following Refs. [39,43], we study the phase function (logarithmic derivative of the Z function),

$$g = \frac{1}{Z}\frac{dZ}{dr}, \tag{8}$$

which does not oscillate toward asymptotic infinity. The differential equation we need to solve for the phase reads

$$\frac{dg}{dr} = -g^2 - \frac{2M}{r(r - 2M)}g + \frac{r^2}{(r - 2M)^2}(\omega^2 - V(r)). \tag{9}$$

Although the phase allows us to eliminate the oscillation, we cannot distinguish between the mixed incoming and outgoing waves and the purely outgoing ones. To do so, we can study an analytical extension of the phase function, rotating the radial coordinate into the complex plane,

$$r = R + ye^{-i\alpha}, \tag{10}$$

with $y \in [0, \infty)$. This technique of complexification of the integration variable is called exterior complex scaling [44–46].

Once a configuration is chosen, and a couple of values $\omega_{\Re}$ and $\omega_{\Im}$ are also chosen, then we take α so that

$$\omega_{\Re} \sin\alpha + \omega_{\Im} \cos\alpha < 0. \tag{11}$$

If α satisfies this relation, then it can be demonstrated [35] that for pure outgoing waves the boundary condition $g(y = \infty) = -i\omega$ is satisfied. Instead, any solution containing any ingoing wave contribution will satisfy $g(y = \infty) = i\omega$. Hence, if the boundary condition $g(y = \infty) = -i\omega$ is imposed on a particular solution outside the star, it must be a purely outgoing wave.

In our method, the angle α is constrained by relation (11). Nevertheless, we can choose this angle freely satisfying $\alpha > \arctan\frac{\omega_{\Im}}{\omega_{\Re}} \equiv \alpha_0$. Typically, the accuracy can be increased and the integration time reduced if $1 < \alpha/\alpha_0 < 1.5$. Usually, for a particular family of modes, the optimum value of α can be estimated at once for the maximum mass configuration.

The use of the phase and exterior complex scaling with variable angle allows us to compactify the radial coordinate

$$\bar{y} = \frac{y}{1+y}, \tag{12}$$

where $\bar{y} \in [0, 1]$. Hence, we can impose the outgoing quasinormal mode behavior as a boundary condition at infinity ($g(\bar{y} = 1) = -i\omega$), without using any cutoffs for the radial coordinate.

The interior part is integrated satisfying the regularity condition at the origin. We integrate together the zeroth order and the Zerilli equation. In this way, we can automatically generate more points in the zeroth-order functions if we require a more accurate result in our quasinormal modes.

As we are interested in realistic equations of state, the implementation of the equation of state is a fundamental step of the procedure. We use two possibilities. The first one is a piecewise polytrope approximation, done by Read *et al.* [47] for 34 different equations of state, where each equation of state is approximated by a polytrope in different density-pressure intervals. For densities below the nuclear density, the Douching and Haensel [48] equation of state (SLy) is considered. The second kind of implementation for the equation of state, more general, is a piecewise monotonic cubic Hermite interpolation. We use this method to interpolate the density ρ as a function of the pressure satisfying local thermodynamic conditions [49]. The interpolation is made on several tabulated equations of state that we will present later.

We implement this method into different Fortran programs and routines, making use of the Colsys package [50] to solve numerically the differential equations. The advantage of this package is that it allows the use of quite flexible multiboundary conditions and an adaptive mesh that increases accuracy.

The matching of the interior and exterior solutions is performed on a surface S, defined by the points at which the pressure is null, or, more generally, constant. As we have mentioned previously, the polar oscillations modify the pressure and the density, so the surfaces of constant pressure of the perturbed star are given by the surfaces S of

$$p_{\text{total}} = p(r) + \Pi_{\text{lm}}(r, t)Y_{\text{lm}} = \text{const}, \tag{13}$$

where Π_{lm} is the perturbation of the pressure. In particular, the surface of the star is located where $p_{\text{total}} = 0$.

We calculate a vector normal to these surfaces, n^μ, and from it the projector $h_{\mu\nu} = g_{\mu\nu} + n_\mu n_\nu$ and the projected covariant derivative of the normal vector $\chi_{\mu\nu} = h^\alpha_\mu h^\beta_\nu n_{\alpha;\beta}$. Evaluating these tensors at a surface of constant pressure, from inside and from outside S, we obtain the first fundamental form and the second fundamental form inside and outside S [51]. We must make a series expansion of these conditions in order to obtain matching relations for each one of the metric functions. We also must expand in spherical harmonics and make a Laplace transformation, in order to obtain the junction of the radial component of the functions.

Let us consider a surface layer on top of S described by a surface stress-energy tensor of a perfect fluid of the form

$$T^{\mu\nu}_S(R) = \rho_c u^\mu_S(R) u^\nu_S(R), \tag{14}$$

where $\rho_c = \varepsilon + \delta\varepsilon_{\text{lm}}Y_{\text{lm}}$ is the surface energy density of the fluid moving in S and $u^\mu_S(R)$ is its velocity.

The second fundamental form conditions impose a jump in the pressure if $\varepsilon \neq 0$. Let the pressure in the inner part of the surface S be p_{int} and in the outer part be p_{ext} with $p_{\text{ext}} < p_{\text{int}}$.

At zeroth order, we obtain the following conditions:

$$\nu(R)|_{\text{int}} = \nu(R)|_{\text{ext}} \equiv \nu(R), \tag{15}$$

$$M_{\text{ext}} = M_{\text{int}} + 4\pi R^2\sqrt{1 - \frac{2M_{\text{int}}}{R}}\varepsilon - 8\pi^2 R^3\varepsilon^2, \tag{16}$$

$$\frac{M_{\text{ext}} + 4\pi R^3 p_{\text{ext}}}{R^2\sqrt{1 - \frac{2M_{\text{ext}}}{R}}} - \frac{M_{\text{int}} + 4\pi R^3 p_{\text{int}}}{R^2\sqrt{1 - \frac{2M_{\text{int}}}{R}}} = 4\pi\varepsilon. \tag{17}$$

The first-order perturbation functions must satisfy the following matching condition:

$$V_{\text{lm}}(R)|_{\text{ext}} = V_{\text{lm}}(R)|_{\text{int}} \equiv V_{\text{lm}}(R), \tag{18}$$

$$\Delta[K_{\text{lm}}(R)] - \frac{2}{R}\Delta\left[\frac{W_{\text{lm}}(R)}{e^\lambda}\right] + \frac{4}{e^{\nu(R)}}\Delta\left[\frac{X_{\text{lm}}(R)}{(1 + 8\pi R^2 p)e^{2\lambda} - 1}\right] = 0, \tag{19}$$

$$\Delta[W_{\text{lm}}(R)] = 2a^2 e^{-\nu(R)}\Delta\left[\frac{e^\lambda X_{\text{lm}}(R)}{(\rho + p)(8\pi R^2 p e^{2\lambda} + e^{2\lambda} - 1)}\right], \tag{20}$$

$$\Delta[e^{-\lambda}H^1_{\text{lm}}(R)] + 16\pi R^{-1}\epsilon V_{\text{lm}}(R) = 0, \tag{21}$$

where $\Delta[F(R)] = F(R)|_{\text{ext}} - F(R)|_{\text{int}}$. Note that since we are matching with the exterior, $X_{\text{lm}}(R)|_{\text{ext}} = 0$ [28,29]. Recall that in the previous expressions we allow for the possibility of surface energy density ε and jumps in pressure and density [35]. The standard matching conditions are reobtained when $\varepsilon = 0$.

The full solution is generated using two independent solutions of the perturbation equations for the same static configuration and value of ω. Let us index each one of the independent solutions with a label $i = \{A, B\}$. If a linear combination of these two independent interior solutions matches the exterior phase, then we will have an outgoing quasinormal mode for the full solution.

We can always impose conditions (18), (20), and (21) on the two independent solutions. Then, it can be demonstrated that the junction can be written in terms of a determinant of a 2×2 matrix,

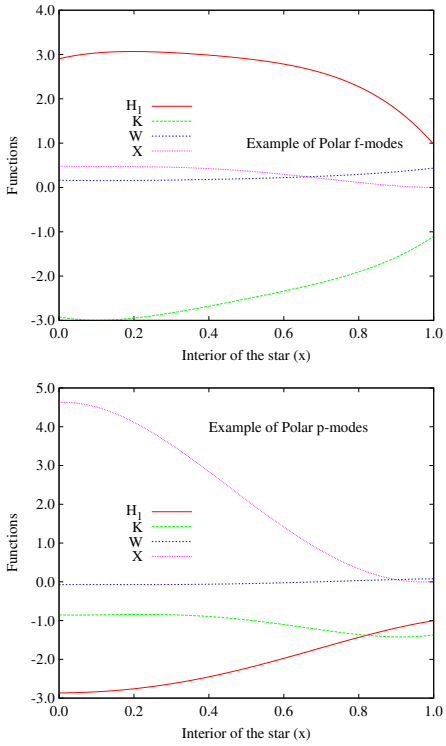

FIG. 1 (color online). Typical form of the functions integrated inside of the star for f modes and p modes ($x = r/R$).

$$M^i_j = K|^{(i)}_{\mathrm{ext},(j)} - K|^{(i)}_{\mathrm{int},(j)} + \frac{2}{R^2}(e^{-\lambda_{\mathrm{int}}} - e^{-\lambda_{\mathrm{ext}}})W|^{(i)}_{\mathrm{int},(j)} + \frac{4[e^{2(\lambda_{\mathrm{int}}-\lambda_{\mathrm{ext}})} - 1]X|^{(i)}_{\mathrm{int},(j)}}{(8\pi R p_{\mathrm{int}} e^{2\lambda_{\mathrm{int}}} + e^{2\lambda_{\mathrm{int}}} - 1)(\rho_{\mathrm{int}} + p_{\mathrm{int}})e^{\nu(R)}}, \quad (22)$$

where $i = \{A, B\}$ and $j = \{\Re, \Im\}$. The determinant is zero only if the junction conditions are satisfied: a combination of the interior solutions can be matched to the exterior phase (an outgoing wave). The determinant of this matrix, once the static configuration is fixed, only depends on the values $(\omega_\Re, \omega_\Im)$. Therefore, if for a fixed configuration a value of the eigenfrequency makes the determinant null, that couple of values $(\omega_\Re, \omega_\Im)$ corresponds to a quasinormal mode of the static configuration. Then, the behavior of the perturbation functions can be analyzed to deduce if the quasinormal mode is a wI mode, a p mode, or an f mode.

In Fig. 1, we show a particular solution for the interior of a neutron star of 1.4 $M_\odot$, equation of state GNH3. They correspond to the f mode and the fundamental p mode.

IV. RESULTS

In this section, we present our results for the polar quasinormal modes of neutron stars with realistic equations of state. We consider a wide range of equations of state in order to study the influence of exotic matter on the polar quasinormal modes. For a similar study performed on the axial component of the spectra, see Ref. [35].

We have tested our method for the constant density model, reproducing the results from Ref. [52]. We have also tested our results for the APR2 equation of state. Our calculations for the real part are in perfect agreement with the results presented in Ref. [16]. The imaginary part is reproduced with a 1% difference for the maximum mass configurations, up to 10%–20% for the softer configurations. This is also expected due to the different methods used in the parametrization of the equation of state, determination of the radius, and quasinormal modes calculation.

As we will see, another test of our method is in the parameters of the empirical relations of the quasinormal modes we calculate. For the equations of state we consider, the parameters of the empirical relations are compatible with the ones obtained by Benhar *et al.* [14,16] for different equations of state.

We start presenting the equations of state used in the study. Using the parametrization presented by Read *et al.* [47], we have considered SLy, GNH3, H4, ALF2, ALF4.

After the recent measurement of 1.97 $M_\odot$ for the pulsar PSR J164-2230, several new equations of state have been proposed. These equations of state take into account the presence of exotic matter in the core of the neutron star, and they have a maximum mass stable configuration over 1.97 $M_\odot$. We have considered the following ones: two equations of state presented by Weissenborn *et al.* with hyperons in Ref. [7], which we call WCS1 and WCS2; three equations of state presented by Weissenborn *et al.* with quark matter in Ref. [8], which we call WSPHS1, WSPHS2, and WSPHS3; four equations of state presented by Bonanno and Sedrakian in Ref. [6], which we call BS1, BS2, BS3, and BS4; and one equation of state presented by Bednarek *et al.* in Ref. [5], which we call BHZBM.

In Fig. 2, we plot all 15 equations of state we have studied in order to give an idea of the range considered.

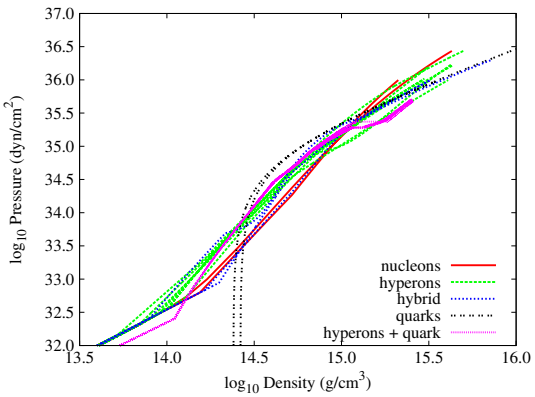

FIG. 2 (color online). Pressure vs density in logarithmic scale for the 15 equations of state considered, in the high density region.

We follow the notation previously used in Ref. [35]. We discuss their characteristics in the following paragraph.

For plain $npe\mu$ nuclear matter, we use:

(i) SLy [48] with $npe\mu$ using a potential method to obtain the equation of state.

For mixed hyperon-nuclear matter, we use:

(i) GNH3 [53], a relativistic mean-field theory equation of state containing hyperons;

(ii) H4 [54], a variant of the GNH3 equation of state;

(iii) WCS1 and WCS2 [7], two equations of state with hyperon matter, using "model $\sigma\omega\rho\phi$," and considering ideal mixing, the SU(6) quark model, and the symmetric-antisymmetric couplings ratios $\alpha_v = 1$ and $\alpha_v = 0.2$, respectively.

(iv) BHZBM [5], a nonlinear relativistic mean-field model involving a baryon octet coupled to meson fields.

For hybrid stars, we use:

(i) ALF2 and ALF4 [55], two hybrid equations of state with mixed nuclear matter and color-flavor-locked quark matter;

(ii) WSPHS3 [8], a hybrid star calculated using a bag model, mixed with NL3 RMF hadronic equations of state, and the parameters employed are $B_{\rm eff}^{1/4} = 140$ MeV, $a_4 = 0.5$, and a Gibbs phase transition.

For Hybrid stars with hyperons and quark color superconductivity, we use:

(i) BS1, BS2, BS3, and BS4, [6], four equations of state calculated using a combination of a phenomenological relativistic hypernuclear density functional and an effective Nambu-Jona-Lasinio model of quantum chromodynamics, and the parameters considered are vector coupling $G_V/G_S = 0.6$ and quark-hadron transition density ρ_{tr}/ρ_0 equal to 2, 3, 3.5, and 4, respectively, where ρ_0 is the density of nuclear saturation.

For quark stars, we use:

(i) WSPHS1 and WSPHS2 [8], and the first equation of state is for unpaired quark matter, and we have considered the parameters $B_{\rm eff}^{1/4} = 123.7$ MeV, $a_4 = 0.53$; the second equation of state considers quark matter in the color-flavor-locked phase (paired), and the parameters considered are $B_{\rm eff}^{1/4} = 130.5$ MeV, $a_4 = 0.66$, and $\Delta = 50$ MeV.

In Fig. 3, we plot the frequencies of all the f modes, p modes, and wI0 modes we have calculated using our method, for the 15 equations of state considered, in order to present the range in which each mode is found. In the next subsections, we will explain the features of each class of modes depending on the equation of state composition: hyperon matter or quark matter.

A. Hyperon matter

1. Fundamental wI mode

At the maximum mass configuration of each equation of state (around 2 $M_\odot$), all the equations of state yield frequencies near 8.5 kHz. This is found for stars containing hyperon matter or only nuclear matter. The only exception is the interesting case of the WCS2 (maximum mass of 2.4 $M_\odot$) with the smallest frequency (7.5 kHz). In general, for configurations with one solar mass, the frequency of stars containing hyperon matter is much smaller (11 kHz) than the frequencies for plain nuclear matter stars (14 kHz).

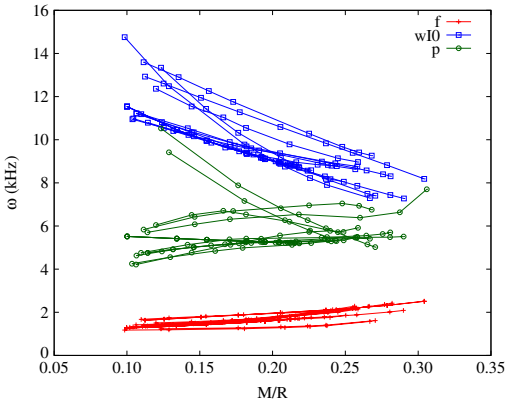

FIG. 3 (color online). Frequency vs compactness for all the modes calculated in this work.

To use future observations of gravitational waves to estimate the mass and the gravitational radius of the neutron star, as well as to discriminate between different families of equations of state, we obtain empirical relations between the frequency and damping time of quasinormal modes and the compactness of the star, following Refs. [14–16,40,41]. In Fig. 4, we present the frequency of the fundamental mode scaled to the radius of each configuration. The range of the plot is between 1 $M_\odot$ and the maximum mass configuration, so we consider only stable stars. It is interesting to note that even for the softest

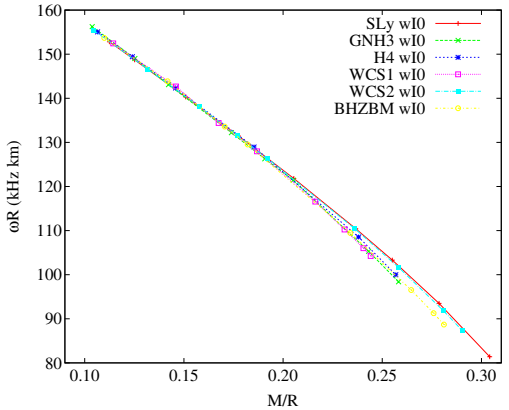

FIG. 4 (color online). Scaled frequency of the fundamental wI mode vs M/R for hyperon matter equations of state. The phenomenological relation is quite independent of the matter composition, as expected from spatial modes.

TABLE I. Fits for the wI0 modes for hyperon equations of state. Parameters A and B (kHz $\times$ km) correspond to the linear empirical relation for the frequency (23). Parameters a, b, and d (kHz $\times$ $(\mu s)^{-1}$) correspond to the quadratic empirical relation for the damping time (24). Pure nucleonic matter equation of state SLy is included for comparison.

wI0	SLy	GNH3	H4	WCS1	WCS2	BHZBM
A	-365.3 ± 8.2	-371.0 ± 8.6	-364.4 ± 1.6	-374.4 ± 8.2	-365.2 ± 7.2	-384.2 ± 8.2
B	195.3 ± 1.8	195.9 ± 1.6	194.9 ± 1.6	196.7 ± 1.6	195.3 ± 1.5	198.0 ± 1.8
χ^2	2.523	1.547	1.479	1.06	1.84	2.03
a	-155 ± 31	-339 ± 31	-330 ± 35	-401 ± 16	-217 ± 30	-253 ± 41
b	-11 ± 13	49 ± 11	48 ± 13	70 ± 6	13 ± 12	21 ± 17
d	19.7 ± 1.3	15.1 ± 1.0	15.1 ± 1.1	13.34 ± 0.51	17.6 ± 1.2	17.2 ± 1.6
χ^2	0.10	0.041	0.0308	0.005	0.0827	0.0968

equations of state with hyperon matter the scaling relation is very well satisfied. Since the wI modes do not couple to matter oscillations, it is not a surprise that these scaled relations are universal.

A linear fit can be made for each equation of state. We fit to the phenomenological relation

$$\omega(\mathrm{kHz}) = \frac{1}{R(\mathrm{km})}\left(A\frac{M}{R} + B\right), \tag{23}$$

where A and B are given in kHz $\times$ km. Note $\frac{M}{R}$ is dimensionless. We are choosing the units so that we can compare our fits with the results from Ref. [16]. In this section, we will express the fit parameters of the phenomenological relations following the units from Ref. [16], which are appropriate in an astrophysical context.

In Table I, we present the fit parameters A, B for each one of the equations of state studied. For all the equations of state, very similar results are obtained. The empirical parameters are compatible with the empirical relation obtained by Benhar *et al.* [16] for six different equations of state.

A similar study can be done to the damping time of the wI0 modes. In Fig. 5 we present the damping time of the fundamental mode scaled to the mass of each configuration. In this case, the results can be fitted to a empirical quadratic relation on M/R as

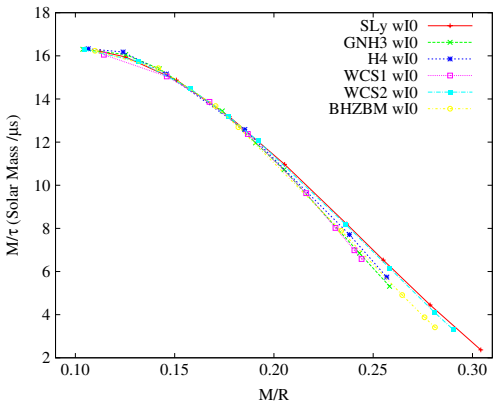

FIG. 5 (color online). Scaled damping time of the fundamental wI mode vs M/R for hyperon matter equations of state.

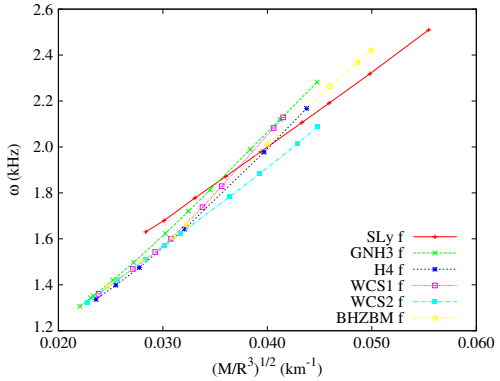

FIG. 6 (color online). Scaled frequency of the fundamental f mode vs $\sqrt{M/R^3}$ for hyperon matter. Although the frequency is linear with the square root of the mean density, each equation of state has its own particular phenomenological parameters, and so the empirical relation is less useful in asteroseismology.

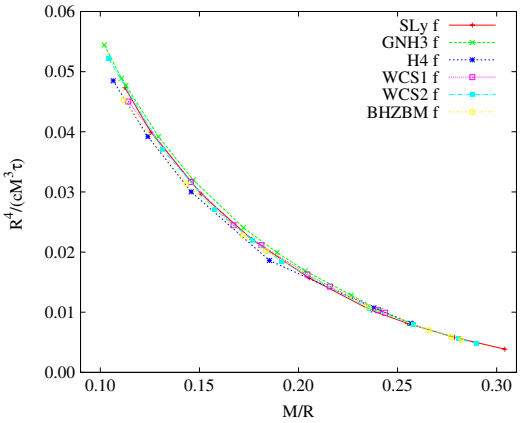

FIG. 7 (color online). Scaled damping time of the fundamental f mode vs M/R for hyperon matter. In this case, the scaled damping time is quite independent of the equation of state.

TABLE II. Fits for the f modes for hyperon equations of state. Parameters U (in kHz) and V (in kHz $\times$ km) correspond to the linear empirical relation for the frequency (25). Parameters u and v (dimensionless) correspond to the linear empirical relation for the damping time (26). Pure nucleonic matter equation of state SLy is included for comparison.

f	SLy	GNH3	H4	WCS1	WCS2	BHZBM
U	0.7041 ± 0.0063	0.338 ± 0.018	0.337 ± 0.055	0.257 ± 0.055	0.5330 ± 0.0083	0.328 ± 0.026
V	32.44 ± 0.15	43.07 ± 0.55	41.5 ± 1.1	44.5 ± 1.6	34.52 ± 0.24	41.93 ± 0.68
χ^2	1.58×10^{-5}	1.82×10^{-4}	3.75×10^{-4}	7.41×10^{-4}	2.77×10^{-5}	3.14×10^{-4}
u	0.065 ± 0.005	0.079 ± 0.004	0.071 ± 0.006	0.070 ± 0.004	0.067 ± 0.006	0.063 ± 0.005
v	-0.221 ± 0.023	-0.295 ± 0.021	-0.255 ± 0.030	-0.251 ± 0.022	-0.231 ± 0.021	-0.213 ± 0.021
χ^2	1.98×10^{-5}	1.32×10^{-5}	1.72×10^{-5}	7.18×10^{-6}	2.42×10^{-5}	1.33×10^{-5}

$$\frac{1}{\tau(\mu s)} = \frac{1}{M(M_\odot)}\left[a\left(\frac{M}{R}\right)^2 + b\frac{M}{R} + d\right], \tag{24}$$

where a, b, and d are given in $M_\odot \times (\mu s)^{-1}$. Here, again, we are choosing the units like in Ref. [16]. In Table I, we present the fit parameters a, b, and d. Note that they are quite similar for all the equations of state and also in accordance with the results obtained in Ref. [16].

For a similar study of the axial wI modes using these equations of state, see Ref. [35].

2. f mode

Now, we will present the results for the f modes of these configurations. For these modes, the frequency of the SLy stars is always above the hyperon stars considered. The SLy configurations range from 1.6 kHz for 1 $M_\odot$ to 2.5 kHz for the maximum mass configuration. Hyperon stars range from 1.3 kHz for 1 $M_\odot$ to 2.2 kHz, with again the exception of WCS2, which reaches only 2.1 kHz.

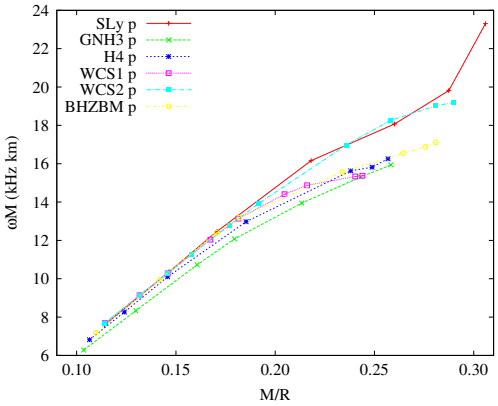

FIG. 8 (color online). Scaled frequency of the fundamental p mode vs M/R. At high compactness the scaled frequency is more sensible to the presence of hyperon matter, with the exception of WCS2.

In this case, one can also study some empirical relations. It is interesting to study the dependence of the frequency with the square root of the mean density. The empirical relations considered for the f modes are the following. For the frequency,

$$\omega(\text{kHz}) = U + V\sqrt{\frac{M}{R^3}}, \tag{25}$$

where U is given in kHz and V in kHz $\times$ km. Note that the mean density $\frac{M}{R^3}$ is given in $(\text{km})^{-2}$. For the damping time,

$$\tau(\text{s}) = \frac{R^4}{cM^3}\left[u + v\frac{M}{R}\right]^{-1}, \tag{26}$$

where u and v are dimensionless parameters, M and R are given in km, and $c = 2.99792458 \times 10^5$ km/s is the speed of light. For these formulas, we have chosen dimensions like in Benhar *et al.* [16]. In Figs. 6 and 7, we plot these relations. In Fig. 6, it can be seen that Eq. (25) is quite different depending on the equation of state. Again, WCS2 presents a very different behavior close to the maximum mass configurations. For the damping time, relation (26) is very well satisfied for every equation of state along all the range.

In Table II, we present the fit parameters U and V for the frequency and u and v for the damping time. These empirical parameters are compatible with those obtained by Benhar *et al.* [16] for six different equations of state.

TABLE III. Fits for the p modes for hyperon equations of state. Parameters K and K_0 (kHz $\times$ km) correspond to the linear empirical relation for the frequency (27). Pure nucleonic matter equation of state SLy is included for comparison.

p	SLy	GNH3	H4	WCS1	WCS2	BHZBM
K	74.9 ± 4.5	62.2 ± 3.3	61.8 ± 3.3	59.8 ± 4.8	66.8 ± 2.7	54.4 ± 4.5
K_0	-0.68 ± 1.0	0.368 ± 0.634	0.74 ± 0.64	1.54 ± 0.90	0.616 ± 0.553	2.33 ± 0.96
χ^2	0.65	0.218	0.249	0.401	0.260	0.590

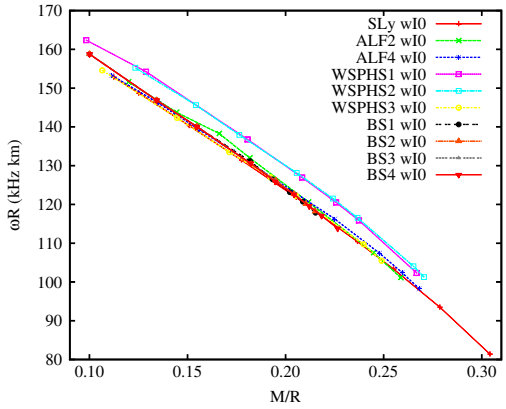

FIG. 9 (color online). Scaled frequency of the fundamental wI mode vs M/R for equations of state containing quarks. Note that the pure quark configurations of equations of state WSPHS1–WSPHS2 present a different set of phenomenological parameters.

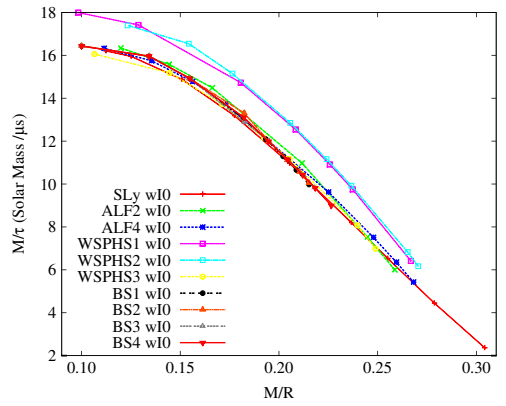

FIG. 10 (color online). Scaled damping time of the fundamental wI mode vs $M/R$for equations of state containing quarks. Hybrid and quark stars have different parameters in the empirical relations.

3. Fundamental p mode

The frequency of the fundamental p mode is the most sensitive to the equations of state of the configuration. For the SLy equation of state, the frequency ranges from 5.7 kHz for 1 $M_\odot$ to 7.8 kHz for the maximum mass configuration. In the presence of hyperon matter, the range of frequencies is much shorter, varying from 4.6 kHz for 1 $M_\odot$ to 5.5 kHz for the maximum mass configuration.

In principle, selecting the units like in Ref. [16], an interesting empirical relation is

$$\omega(\mathrm{kHz}) = \frac{1}{M(\mathrm{km})}\left(K\frac{M}{R} + K_0\right), \tag{27}$$

where K and K_0 are given in kHz × km. In Fig. 8, we present the frequency scaled to the mass vs the compactness. There is an important resemblance between the SLy equation of state and the WCS2, which presents a similar behavior for high compact stars. The relation is quite different from the rest of hyperon matter equations of state. This effect could be used to constrain the value of α_v for compact enough stars.

In Table III, we present the fit parameters K and K0 for the frequency. The results are compatible with Ref. [16].

B. Quark matter

1. Fundamental wI mode

The frequencies for the hybrid equation of state ALF4 give almost the same results as the SLy equation of state. The four BS1–BS4 equations of state are essentially similar, with quite a low frequency: 8.8 kHz for the maximum mass configuration (2 $M_\odot$). Nevertheless, the WSPHS3 is the equation of state with the lowest frequency: 8 kHz for the maximum mass configuration (2.2 $M_\odot$). For pure quark stars WSPHS1–WSPHS2, even lower frequencies (7.2 kHz) are obtained at the maximum mass configuration (2.5 $M_\odot$).

We study the empirical relations (23) and (24) for these equations of state. We present them in Figs. 9 and 10 for frequency and damping time, respectively. It can be seen

TABLE IV. Fits for the wI0 modes for quark and hybrid equations of state. Parameters A and B (kHz × km) correspond to the linear empirical relation for the frequency (23). Parameters a, b, and d (kHz × $(\mu s)^{-1}$) correspond to the quadratic empirical relation for the damping time (24).

wI0	ALF2	ALF4	WSPHS1	WSPHS2	WSPHS3	BS1	BS2	BS3	BS4
A	-365.3 ± 11.9	-368.9 ± 6.7	-351.9 ± 12.3	-365.5 ± 10.3	-342.1 ± 6.7	-351.4 ± 4.7	-350.0 ± 0.30	349.6 ± 2.7	353.2 ± 3.2
B	197.1 ± 2.3	193.3 ± 1.4	199.0 ± 2.5	202.0 ± 2.2	191.8 ± 1.3	194.2 ± 0.8	193.9 ± 0.5	194.4 ± 0.6	
χ^2	2.227	1.164	3.326	2.039	0.687	0.251	0.11	0.086	0.149
a	-347 ± 18	-281 ± 19	-333.9 ± 8.7	-332 ± 24	-339 ± 21	-339 ± 21	-473 ± 21	-492 ± 29	-432 ± 34
b	56.1 ± 6.9	35.9 ± 7.4	52.6 ± 3.2	53.1 ± 9.6	56.3 ± 7.6	92.3 ± 6.6	99.0 ± 9.2	80 ± 11	79.9 ± 8.0
d	14.66 ± 0.63	15.93 ± 0.67	16.10 ± 0.27	16.03 ± 0.92	13.97 ± 0.65	11.98 ± 0.51	11.46 ± 0.71	12.79 ± 0.85	12.82 ± 0.63
χ^2	0.0079	0.013	0.0037	0.0204	0.0133	0.0049	0.0096	0.0148	0.0102

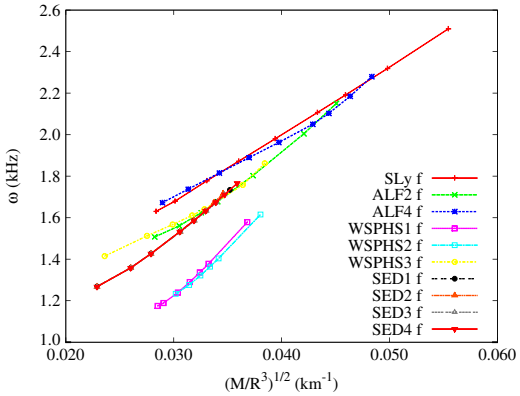

FIG. 11 (color online). Scaled frequency of the fundamental f mode vs $\sqrt{M/R^3}$ for equations of state containing quarks. In this case, the empirical relation is dependent of the equation of state considered, and so it is less useful in asteroseismology.

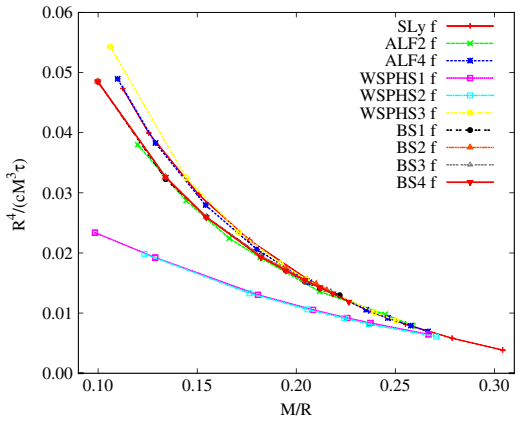

FIG. 12 (color online). Scaled damping time of the fundamental f mode vs M/R for hybrid and quark stars. The empirical relation is almost insensitive of the equation of state, except for the pure quark stars.

that the empirical relation is again very well satisfied for all the hybrid equations of state. For the pure quark stars, a similar relation with different parameters is found. The fits can be found in Table IV (compatible with Ref. [16]).

Note that, although the empirical relation is also satisfied for pure quark stars, it is slightly different. This is due to the different layer structure of these pure quark stars. These stars are essentially naked quark cores, where the pressure quickly drops to zero in the outer layers, although the density is almost constant.

The study of the axial wI modes using these equations of state can be found in Ref. [35].

2. f mode

The lowest frequency is around 1.2 kHz for 1 $M_\odot$ stars composed only of quark matter (WSPHS1–WSPHS2). The higher frequencies are reached at 2.2 kHz for hybrid stars beyond 2 $M_\odot$. For ALF2–ALF4, frequencies approach those of pure nuclear matter. The configurations with equations of state WSPH3 and BS1–BS4 always have lower frequencies than the rest of hybrid stars but are larger than the pure quark stars. Concerning the damping time, there is essentially no difference among the equations of state (0.3 s for maximum mass configurations), except for WSPHS1–WSPHS2, which have slightly larger damping times for the most compact ones (0.4 s for maximum mass configurations).

We study the dependence of the frequency with the square root of the mean density as we did before for hyperon matter. The empirical relations to consider are again Eqs. (25) and (26). In Figs. 11 and 12, we plot these relations. In Fig. 11, it can be seen that Eq. (25) is quite different, depending on the equation of state. ALF4 is almost identical to SLy, while the other hybrid equations are in between these ones and the pure quark equations of state. Regarding the damping time (Fig. 12), relation (26) is very well satisfied for every hybrid equation of state considered along all the range. These relations are compatible with Ref. [16]. In Table V, we present the fits to Eqs. (25) and (26) of these results.

3. Fundamental p mode

At high compactness, ALF4 has higher frequencies (near 7 kHz) than the rest of hybrid equations of state (for example, BS1–BS4 and WSPHS1–WSPHS2 have similar frequencies around 5.2 kHz). The highest frequencies are reached for pure quark stars at 1 $M_\odot$, with 10 kHz.

TABLE V. Fits for the f modes for quark and hybrid equations of state. Parameters U (in kHz) and V (in kHz × km) correspond to the linear empirical relation for the frequency (25). Parameters u and v (dimensionless) correspond to the linear empirical relation for the damping time (26).

f	ALF2	ALF4	WSPHS1	WSPHS2	WSPHS3	BS1	BS2	BS3	BS4
U	0.38 ± 0.06	0.79 ± 0.04	-0.24 ± 0.07	-0.28 ± 0.07	0.71 ± 0.06	0.37 ± 0.04	0.36 ± 0.04	0.38 ± 0.04	0.36 ± 0.03
V	38.7 ± 1.6	30.0 ± 1.1	48.9 ± 2.1	49.4 ± 2.1	29.2 ± 1.9	98.3 ± 1.2	38.6 ± 1.3	37.9 ± 1.1	38.8 ± 1.1
χ^2	6.03×10^{-4}	4.66×10^{-4}	2.15×10^{-4}	1.67×10^{-4}	5.58×10^{-4}	1.69×10^{-4}	2.04×10^{-4}	1.58×10^{-4}	1.77×10^{-5}
$10u$	0.59 ± 0.04	0.70 ± 0.05	0.32 ± 0.01	0.31 ± 0.02	0.79 ± 0.08	0.72 ± 0.04	0.73 ± 0.04	0.73 ± 0.04	0.71 ± 0.04
v	0.21 ± 0.02	0.25 ± 0.02	0.10 ± 0.01	0.09 ± 0.01	0.30 ± 0.04	0.28 ± 0.03	0.29 ± 0.02	0.28 ± 0.02	0.27 ± 0.02
χ^2	6.91×10^{-6}	1.45×10^{-5}	7.74×10^{-7}	6.69×10^{-7}	2.48×10^{-5}	7.55×10^{-6}	6.58×10^{-6}	6.84×10^{-6}	7.03×10^{-6}

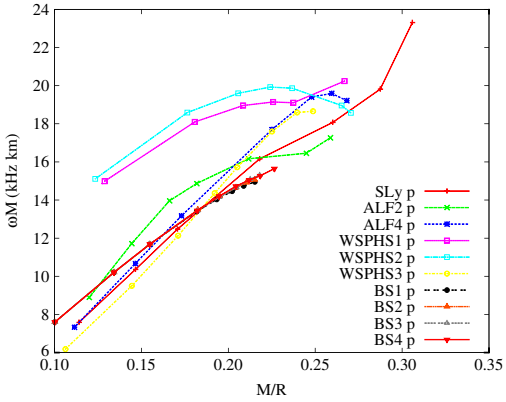

FIG. 13 (color online). Scaled frequency of the fundamental p mode vs M/R. Once again, a general tendency is seen, but the particular phenomenological relation of each equation of state is different from the rest. As expected, the p mode is very sensitive to the equation of state.

In Fig. 13 we present the empirical relations (27). It can be seen that all hybrid equations lie on the same range, although the linear relation is not very well satisfied for higher compactness. In the case of pure quark stars, the situation is much worse. In Table VI, we present the fits to Eq. (27) for each equation of state. These results are also compatible with Ref. [16].

C. Universal phenomenological relations

To use wave detections coming from neutron stars to estimate global properties like radius or mass, we would like to have empirical relations as much independent from the matter content of the configuration as possible. The empirical relations for the wI modes are quite universal and hence are useful for asteroseismology. On the other hand, the scaled relations for the f mode are still equation of state dependent, especially for the frequency. Here we propose some new phenomenological relations that we think could be useful for asteroseismology.

First, we present a new empirical relation for the wI fundamental mode. A similar empirical relation for the axial wI modes was first studied in Ref. [35].

As seen in Fig. 14, if the real and the imaginary parts are scaled as

$$\bar{\omega}_R = \frac{1}{\sqrt{p_c}}\omega_R, \qquad \bar{\omega}_I = \frac{1}{\sqrt{p_c}}\omega_I, \tag{28}$$

that is, normalized in units of the central pressure, then we obtain the following relation between real and imaginary parts of the eigenvalue for all the equations of state (except for WCSHS1–WCSHS2),

$$\bar{\omega}_I = (6.146 \pm 0.039)10^{-3}\bar{\omega}_R^2 + (-5.57 \pm 0.18)10^{-7}\bar{\omega}_R^4, \tag{29}$$

with $\chi^2 = 0.0214$. The relation is very well satisfied independently of the equation of state, in particular, for high-density stars. This could be used to estimate the central pressure of the star.

Note that although the empirical relation between $\bar{\omega}_R$ and $\bar{\omega}_I$ is quite independent of the equation of state, the parametrization of the curve in terms of the central pressure is equation of state dependent. If the frequency ω and the damping time τ are known (detected), we can parametrize a line defining $\bar{\omega}_R$ and $\bar{\omega}_I$, with parameter p_c, using the observed frequency and damping time. The observed values will give us the slope of the line. The crossing point of this line with the empirical relation presented in Fig. 14 gives us an estimation of the central pressure p_c independent of the equation of state. Now, we can check which equation of state is compatible with this p_c, i.e., which one has the measured wI0 mode near the crossing point for the estimated central pressure. Hence, this method could be used to constrain the equation of state. Note that if mass and radius are already measured, we would have another filter to impose on the equation of state.

As a practical test of this method, we have included in Fig. 14 the line that a measurement of a fundamental wI0 mode of $\omega = 11$ kHz and $\tau = 118.4$ μs will trace. The crossing point between this line and the empirical relation for the wI0 modes (29) determines the central pressure, yielding $p_c = 1.312 \times 10^{35}$ dyn/cm^2.

Concerning the f mode, an analogous relation can be obtained if we divide the real part and the imaginary part by the radius and mass, respectively. The empirical relation obtained is equation of state independent (excluding again WSPHS1–WSPHS2). It is

TABLE VI. Fits for the p modes for quark and hybrid equations of state. Parameters K and K_0 (kHz $\times$ km) correspond to the linear empirical relation for the frequency (27).

p	ALF2	ALF4	WSPHS1	WSPHS2	WSPHS3	BS1	BS2	BS3	BS4
K	54.5 ± 8.9	79.9 ± 5.0	36.1 ± 5.3	22.8 ± 10.1	92.1 ± 3.0	64.1 ± 2.4	65.0 ± 2.2	65.1 ± 2.0	63.7 ± 2.2
K_0	3.86 ± 1.73	−1.0 ± 1.1	10.9 ± 1.1	13.8 ± 2.2	−3.56 ± 0.60	1.5 ± 0.4	1.38 ± 0.40	1.36 ± 0.35	1.58 ± 0.41
χ^2	1.24	0.556	0.322	1.66	0.153	0.067	0.059	0.047	0.072

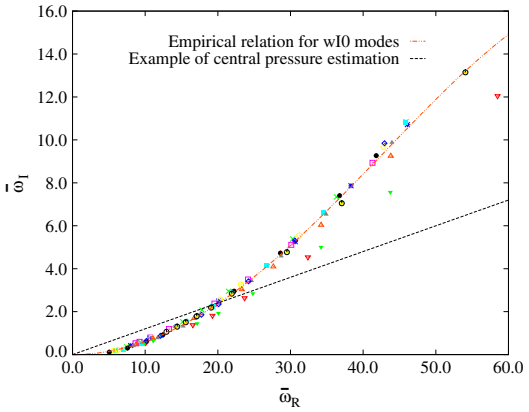

FIG. 14 (color online). All fundamental wI modes normalized to the square root of the central pressure [Eq. (28)]. This scaling makes all the wI0 modes lie on the same curve and could be used to estimate the central pressure as explained in the text.

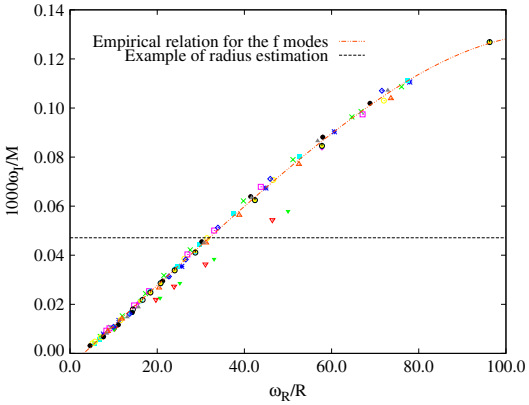

FIG. 15 (color online). All fundamental f modes. The real part of the eigenvalue is divided by the radius and the imaginary part by the mass. This universal relation can be very useful to estimate the radius or mass of a neutron star. Note that all the equations of state, with the exception of the pure quark stars, are found to satisfy the empirical relation (30).

$$(\omega_I/M) = (-5.16 \pm 0.24)10^{-3} + (164.63 \pm 0.83)10^{-5} \times (\omega_R/R) + (-3.14 \pm 0.12)10^{-10}(\omega_R/R)^4, \tag{30}$$

with $\chi^2 = 1.42 \times 10^{-6}$. It is an almost linear relation, although the $(\omega_R/R)^4$ plays an important role at low compactness configurations. This relation is very well satisfied for every configuration independently of the equation of state, as seen in Fig. 15. For pure quark stars, the relation is similar but with different parameters, due to the different density-pressure distribution at lower densities. But if only nuclear, hyperon matter, and hybrid stars are considered, the empirical relation is universal for these families of equations of state. If the mass of the star emitting the gravitational wave is known by other measurements, this relation could be used to obtain the radius of the star emitting the gravitational wave. Following a procedure similar to the one explained previously for the wI modes, a detection of frequency and damping time of a neutron star emission, for which the mass is already known by other measurements, would draw a horizontal line in Fig. 15. The intersection of this line with the empirical relation (30) would provide an estimation of the radius of the star.

Suppose that for the previous measurement of the wI0 mode we also have a measurement of the f mode, with $\omega = 1.9$ kHz and $\tau = 0.3$ s. If the correponding mass of the star is $M = 1.479\ M_\odot$, we can trace the horizontal line of Fig. 15. The intersection of this line with empirical relation (30) determines the radius of the star, $R = 11.53$ km.

The previous values of wI0 modes, f modes, and mass we have used for these estimation examples correspond to a real configuration of the SLy equation of state. This configuration has central pressure $p_c = 1.58 \times 10^{35}$ dyn/cm^2 and radius $R = 11.6$ km. Note that the error in the determination of the central pressure has been 17%, but, nevertheless, in the determination of the radius of the star, the error is 0.5%.

Combining the two empirical relations (29) and (30), the particular equation of state of the source of the detected emission could be constrained.

V. CONCLUSIONS

In this paper, we have considered the polar quasinormal modes for realistic neutron stars. In particular, we have calculated the fundamental wI mode, the f mode, and the fundamental p mode. The study has been realized for 15 realistic equations of state, all of them satisfying the 2 $M_\odot$ condition, and various compositions: hyperon, hybrid, and pure quark matter. We have calculated the quasinormal modes also for the SLy equation of state in order to compare it to a standard nucleonic equation of state. The numerical procedure developed to obtain the quasinormal modes is based on exterior complex scaling. A similar study for the axial part of the spectrum can be found in Ref. [35].

We have considered empirical relations between the scaled frequencies and damping times of the modes with the compactness and mean density. The results are in accordance with previous works [16]. We have studied in which cases the obtained relations are more independent of the equation of state and, hence, more useful for asteroseismology. We have found that the frequencies of the fundamental p mode and f mode are quite sensitive to the matter composition of the star, so these empirical relations are less useful.

New phenomenological relations have been studied, for the fundamental wI mode and f mode, between the real part

and the imaginary part of the fundamental modes. We have found universal empirical relations, independent of the particular equation of state. These relations can be useful in neutron star asteroseismology, allowing us to constrain the equation of state and so providing insight into the state of matter at high densities.

ACKNOWLEDGMENTS

We would like to thank I. Bednarek for kindly providing us with the equation of state BHZBM, I. Sagert for equations of state WSPHS1–WSPHS3, A. Sedrakian for equations of state BS1–BS4, and S. Weissenborn for equations of state WCS1–WCS2. We thank Daniela Doneva for valuable comments on our work and Gabriel A. Galindo for his help concerning the exterior complex scaling method. We would also like to thank the referee for his/her suggestions. This work was supported by the Spanish Ministerio de Ciencia e Innovacion, research Project No. FIS2011-28013. J. L. B. was supported by the Spanish Universidad Complutense de Madrid.

[1] A. Haensel, P. Potekhin, and D. Yakovlev, *Neutron Stars: Equation of State and Structure*, Astrophysics and Space Science Library (Springer, New York, 2007).
[2] N. Glendenning, *Compact Stars: Nuclear Physics, Particle Physics, and General Relativity*, Astronomy and Astrophysics Library (Springer, New York, 2000).
[3] H. Heiselberg and M. Hjorth-Jensen, Phys. Rep. **328**, 237 (2000).
[4] M. Prakash and J. M. Lattimer, *From Nuclei to Stars*, edited by S. Lee (World Scientific, Singapore, 2011), Chap. 12, p. 275–304.
[5] I. Bednarek, P. Haensel, J. L. Zdunik, M. Bejger, and R. Mańka, Astron. Astrophys. **543**, A157 (2012).
[6] L. Bonanno and A. Sedrakian, Astron. Astrophys. **539**, A16 (2012).
[7] S. Weissenborn, D. Chatterjee, and J. Schaffner-Bielich, Phys. Rev. C **85**, 065802 (2012).
[8] S. Weissenborn, I. Sagert, G. Pagliara, M. Hempel, and J. Schaffner-Bielich, Astrophys. J. Lett. **740**, L14 (2011).
[9] B. Sathyaprakash and B. F. Schutz, Living Rev. Relativity **12**, 1 (2009).
[10] M. Pitkin, S. Reid, S. Rowan, and J. Hough, Living Rev. Relativity **14**, 1 (2011).
[11] K. D. Kokkotas and B. Schmidt, Living Rev. Relativity **2**, 1 (1999).
[12] H.-P. Nollert, Classical Quantum Gravity **16**, R159 (1999).
[13] L. Rezzolla, *Gravitational Waves from Perturbed Black Holes and Relativistic Stars* (ICTP, Trieste, 2003).
[14] O. Benhar, E. Berti, and V. Ferrari, Mon. Not. R. Astron. Soc. **310**, 797 (1999).
[15] K. D. Kokkotas, T. A. Apostolatos, and N. Andersson, Mon. Not. R. Astron. Soc. **320**, 307 (2001).
[16] O. Benhar, V. Ferrari, and L. Gualtieri, Phys. Rev. D **70**, 124015 (2004).
[17] O. Benhar, Mod. Phys. Lett. A **20**, 2335 (2005).
[18] V. Ferrari and L. Gualtieri, Gen. Relativ. Gravit. **40**, 945 (2008).
[19] D. Chatterjee and D. Bandyopadhyay, Phys. Rev. D **80**, 023011 (2009).
[20] D.-H. Wen, B.-A. Li, and P. G. Krastev, Phys. Rev. C **80**, 025801 (2009).
[21] T. Regge and J. A. Wheeler, Phys. Rev. **108**, 1063 (1957).
[22] F. J. Zerilli, Phys. Rev. Lett. **24**, 737 (1970).
[23] K. Thorne and A. Campolattaro, Astrophys. J. **149**, 591 (1967).
[24] R. Price and K. Thorne, Astrophys. J. **155**, 163 (1969).
[25] K. Thorne, Astrophys. J. **158**, 1 (1969).
[26] K. Thorne, Astrophys. J. **158**, 997 (1969).
[27] A. Campolattaro and K. Thorne, Astrophys. J. **159**, 847 (1970).
[28] L. Lindblom and S. Detweiler, Astrophys. J. Suppl. Ser. **53**, 73 (1983).
[29] S. Detweiler and L. Lindblom, Astrophys. J. **292**, 12 (1985).
[30] S. Chandrasekhar and V. Ferrari, Proc. R. Soc. A **432**, 247 (1991).
[31] S. Chandrasekhar, V. Ferrari, and R. Winston, Proc. R. Soc. A **434**, 635 (1991).
[32] S. Chandrasekhar and V. Ferrari, Proc. R. Soc. A **434**, 449 (1991).
[33] J. R. Ipser and R. H. Price, Phys. Rev. D **43**, 1768 (1991).
[34] Y. Kojima, Phys. Rev. D **46**, 4289 (1992).
[35] J. L. Blázquez-Salcedo, L. M. González-Romero, and F. Navarro-Lérida, Phys. Rev. D **87**, 104042 (2013).
[36] K. D. Kokkotas and B. F. Schutz, Mon. Not. R. Astron. Soc. **255**, 119 (1992).
[37] N. Andersson, K. D. Kokkotas, and B. F. Schutz, Mon. Not. R. Astron. Soc. **274**, 9 (1995).
[38] K. D. Kokkotas, Mon. Not. R. Astron. Soc. **268**, 1015 (1994).
[39] L. Samuelsson, N. Andersson, and A. Maniopoulou, Classical Quantum Gravity **24**, 4147 (2007).
[40] N. Andersson and K. D. Kokkotas, Phys. Rev. Lett. **77**, 4134 (1996).
[41] N. Andersson and K. D. Kokkotas, Mon. Not. R. Astron. Soc. **299**, 1059 (1998).
[42] O. Benhar, V. Ferrari, L. Gualtieri, and S. Marassi, Gen. Relativ. Gravit. **39**, 1323 (2007).
[43] N. Andersson, Proc. R. Soc. A **439**, 47 (1992).
[44] J. Aguilar and J. Combes, Commun. Math. Phys. **22**, 269 (1971).
[45] E. Balslev and J. Combes, Commun. Math. Phys. **22**, 280 (1971).
[46] B. Simon, Commun. Math. Phys. **27**, 1 (1972).
[47] J. S. Read, B. D. Lackey, B. J. Owen, and J. L. Friedman, Phys. Rev. D **79**, 124032 (2009).

[48] F. Douchin and P. Haensel, Astron. Astrophys. **380**, 151 (2001).
[49] F. Fritsch and R. Carlson, SIAM J. Numer. Anal. **17**, 238 (1980).
[50] U. Ascher, J. Christiansen, and R. D. Russell, Math. Comput. **33**, 659 (1979).
[51] C. Misner, K. Thorne, and J. Wheeler, *Gravitation*, Physics Series (Freeman, San Francisco, 1973).
[52] Y. Kojima, N. Andersson, and K. D. Kokkotas, Proc. R. Soc. A **451**, 341 (1995).
[53] N. Glendenning, Astrophys. J.**293**, 470 (1985).
[54] B. D. Lackey, M. Nayyar, and B. J. Owen, Phys. Rev. D **73**, 024021 (2006).
[55] M. Alford, M. Braby, M. Paris, and S. Reddy, Astrophys. J. **629**, 969 (2005).

2.4 Slow rotation

Since neutron stars are supposed to be realized in nature as pulsars, it is important to consider the case of a compact star in rotation. Neutron stars must be described using General Relativity, so the rotation of the star will have an effect on the space-time which is not observed in Newtonian gravity.

Let us enumerate the properties of an asymptotically flat, stationary and axisymmetric space-time [24].

Asymptotically flat. In a region sufficiently distant from the star, spherical coordinate system $(t,\ r,\ \theta,\ \phi)$ can be introduced so that

$$ds^2 = -dt^2 + dr^2 + r^2\left[d\theta^2 + \sin^2(\theta)d\phi^2\right] \ . \tag{2.19}$$

Stationary. We can define a Killing vector ξ that asymptotically approaches a time-like vector

$$\lim_{r\to\infty} \xi\cdot\xi = -1 \ . \tag{2.20}$$

Axisymmetric. We can define a Killing vector η, which is space-like at every point and asymptotically approaches

$$\lim_{r\to\infty} \eta\cdot\eta = r^2\sin^2(\theta) \ , \tag{2.21}$$

and is orthogonal to ξ

$$\lim_{r\to\infty} \eta\cdot\xi = 0 \ . \tag{2.22}$$

With the properties we have enumerated, the most general metric for an asymptotically flat, stationary and axisymmetric space-time can be written as

$$ds^2 = -H^2(r,\theta)dt^2 + Q^2(r,\theta)dr^2 + r^2K^2(r,\theta)\left[d\theta^2 + \sin^2(\theta)(d\phi - L(r,\theta)dt)^2\right] \ , \tag{2.23}$$

where H, Q, K y L are in general functions of r, θ, and the angular velocity of the star Ω.

The function $L(r,\theta)$ is called the inertial dragging: a free falling observer from spatial infinity will acquire a velocity $\frac{d\phi}{dt} = L(r,\theta)$ at position (t,θ), if he is initially at rest.

We will consider that the matter content of the star can be described by a perfect

fluid. The stress-energy tensor must satisfy the symmetries of the space-time, hence $\pounds_\xi T = \pounds_\eta T = 0$, where $\pounds$ denotes the Lie derivative. An observer, situated at spatial infinity, will observe each fluid element rotating with an angular velocity Ω. Since we are considering rigid rotation, the observer will measure this velocity for every fluid element of the star $\frac{d\varphi}{dt} = \Omega$, so we have $\frac{d\varphi}{d\tau} = \frac{d\varphi}{dt}\frac{dt}{d\tau} = \Omega\frac{dt}{d\tau}$. Hence the four-velocity of each fluid element can be written

$$u^\mu = (u^t, 0, 0, u^\varphi) = u^t(1, 0, 0, \Omega) \ . \tag{2.24}$$

We have not made any approximation on the functions describing the configurations. Let us now suppose that the rotation of the star is sufficiently slow so that we can make use of perturbation theory. First we have to bound the value of Ω. In general, perturbation theory will be appropriate when the contribution of the rotation to the total energy of the configuration is smaller than the total energy of the limit static configuration. A good way to establish this bound is to consider that the angular velocity of the star is much smaller than the Newtonian mass shedding velocity [17]

$$\Omega^2 << \frac{2GM}{R^3c^2} \ , \tag{2.25}$$

where M is the mass and R is the radius of the static configuration. Pulsars with periods of seconds, and even some millisecond pulsars can be studied under the slow rotation approximation.

We will follow Hartle [9] and consider first and second order in perturbation theory, using as parameter of the expansion Ω. Hence, we can expand the metric functions, and the stress-energy tensor up to second order in Ω, leaving out $o(\Omega^3)$ terms. In this case the metric can be written like

$$\begin{aligned} ds^2 = &-e^{2\psi(r)}(1 + 2h(r,\theta))dt^2 + e^{2\lambda(r)}(1 + \frac{2m(r,\theta)}{r - 2M(r)})dr^2 \\ &+r^2(1 + 2k(r,\theta))\left[d\theta^2 + \sin^2(\theta)(d\phi - \omega(r)dt)^2\right] \ . \end{aligned} \tag{2.26}$$

Under a reflection on the rotating plane, that is, $\Omega \to -\Omega$, first order perturbations do transform with a change of sign, while second order perturbations are not changed. Hence it can be seen that the only first order perturbation function is ω, while h, m and k are second order perturbation functions.

2.4.1 Results

In the following papers we apply the slow rotation model of neutron stars to the study of glitches. In order to do so, we will study the junction conditions between the solution inside the star and the solution outside it.

- The junction conditions are formulated intrinsically, using the fundamental forms. This provides the junction conditions that the metric and matter functions must satisfy between the interior and the exterior solutions. We will also consider the introduction of a surface energy density. The resulting model can be interpreted as an approximation of the outer layers of the star, assuming that the mass of the outer layers and its size are small.

- The essential parameters of this model of neutron star, enveloped by a surface energy density, are the core-crust transition pressure, the central pressure and the angular velocity of the star.

- Variations in the transition pressure are related to jumps in the angular velocity of the configuration. Hence we can apply this simple model to the description of giant glitches of pulsars (in particular to the Vela pulsar glitches). Since glitches are probably related to thermal variations in the outer layers of the neutron stars, we can relate the jump in the angular velocity to a variation of the core-crust transition pressure, assuming that the inner core is not changed. This change in the transition pressure would probably be related to a phase transition. The variations of the transition pressure are compatible with the expected temperature variations of the inner crust during the glitch.

2.4.2 Publication: Luis Manuel González-Romero and Jose Luis Blázquez-Salcedo, *Core-crust transition pressure for relativistic slowly rotating neutron stars*, AIP Conf. Proc. 1458 (2012) 419-422

Core-crust transition pressure for relativistic slowly rotating neutron stars

L. M. González-Romero and J. L. Blázquez-Salcedo

Depto. Física Teórica II, Facultad de Ciencias Físicas, Universidad Complutense de Madrid, 28040-Madrid.

Abstract. We study the influence of core-*crust* transition pressure changes on the general dynamical properties of neutron star configurations. First we study the matching conditions in core-*crust* transition pressure region, where phase transitions in the equation of state causes energy density jumps. Then using a surface *crust* approximation, we can construct configurations where the matter is described by the equation of state of the core of the star and the core-*crust* transition pressure. We will consider neutron stars in the slow rotation limit, considering perturbation theory up to second order in the angular velocity so that the deformation of the star is also taken into account. The junction determines the parameters of the star such as total mass, angular and quadrupolar momentum.

Keywords: Neutron Stars, Junction Conditions, Core-*crust* transition pressure, Slow Rotation
PACS: 04.40.Dg,97.60.Jd, 04.25.Nx

INTRODUCTION

The interior of the neutron stars is composed of matter in a highly compact state. Most of the theories that describe the matter composition of these stars predicts a layer structure, resulting from the different matter species that emerge as a result of the extreme densities reached [1]. Neutron stars are composed by the core and the *crust*, whose properties are very different. In the core of the star (around 10 Km of radius), matter is found at densities well beyond nuclear density. The equation of state for matter in this state is not well known, and different hypothesis exist, essentially differing on which particle populations could be found and which ones dominates over the others. The outer regions of the core is composed by neutrons, protons, electrons and possibly muons while in the interior regions more exotic matter states are thought to be found (pions, hyperons, quark matter...). The *crust* of neutron stars is reached at nuclear densities, and a mix of neutrons, free electrons, and neutron-rich atomic nuclei is thought to give a metallic structure to this region [2].

Along the core of the star and specially in the core-*crust* interface, first order phase transitions are expected to be found in realistic equations of state. These phase transitions result in small discontinuities in the energy density of the star matter [2, 3]. The appropriate way of treating these discontinuities is by analyzing the junction between every region in the interior of the star, i.e., the matching conditions in the core-*crust* transition region. This junction must satisfy some basic conditions so that the resulting metric is continuous and the Einstein equation is satisfied. We use the intrinsic formulation of these conditions that can be written in terms of the first and second fundamental forms [4, 5, 6]. We will make an interpretation of this matching in terms of physical

Towards New Paradigms: Proceeding of the Spanish Relativity Meeting 2011
AIP Conf. Proc. 1458, 419-422 (2012); doi: 10.1063/1.4734449

quantities like the transition pressure.

MATCHING THE TRANSITION PRESSURE REGION

In nature neutron stars are found rotating in the form of pulsars. Although the angular velocity of these objects is very high (with periods from seconds to milliseconds), when compared with the gravitational energy of the compact star, the rotational energy of the star is in most cases smaller. So that for modeling a realistic neutron star we can use the slow rotation Hartle-Thorne perturbative theory for rigid rotating axi-symmetric stars. We will consider the slow rigid rotation approximation up to second order in the angular velocity, so that the deformation of the star due to its rotation is also considered. We will follow the notation of the original papers by Hartle and Thorne [7, 8], with the perturbed metric given by $ds^2 = -e^{2\psi}[1+2h]dt^2 + e^{2\lambda}[1+2m]dr^2 + r^2[1+2k]\left[d\theta^2 - \sin^2\theta(d\phi - \omega dt)^2\right]$.

We will consider the case in which a interior region with perfect fluid with a given equation of state is being matched to an exterior perfect fluid with another equation of state. The matching will be done on a surface of constant pressure (up to second order in the angular velocity). The inner face of the surface will have in general some values (p_-, ρ_-), and the exterior region (p_+, ρ_+) [9].

We must grant that the general solution satisfy the continuity of the first fundamental form in order to have a well defined metric on the surface. The Einstein equations tell us that the discontinuity resulting from the jump of the second fundamental form can be written as a surface stress-energy tensor in the core-*crust* interface. So introducing a surface energy density on the interface surface causes a discontinuity of the pressure on this surface. We will write this superficial stress-energy tensor as a perfect fluid tensor with surface density $\rho_c(\theta) = \varepsilon + \delta\varepsilon(\theta) = \varepsilon + \delta\varepsilon_0 + \delta\varepsilon_2 P_2(\theta)$ where ε is the zero order surface density and $\delta\varepsilon_0, \delta\varepsilon_2$ are the second order spherical and quadrupolar surface densities. They are all constant on the junction interface.

Some of the matching conditions for the functions of the metric are the following:

$$\Delta[e^{-\lambda(a)}] = -4\pi a\varepsilon \tag{1}$$

$$\Delta\left[\frac{M(a) + 4\pi a^3 p(a)}{\sqrt{1 - \frac{2M(a)}{a}}}\right] = 4\pi a^2 \varepsilon \tag{2}$$

$$\Delta[\omega(a)] = 0 \tag{3}$$

$$\Delta\left[e^{-\lambda(a)}\partial_R \overline{\omega}(a)\right] = \frac{16\pi\varepsilon}{a}(\Omega_c - \omega(a)) \tag{4}$$

Where $\Delta[f(a)] = f_+ - f_-$. These equations provides the matching for the zero and first order functions. Essentially the introduction of a discontinuity in density and pressure inside of the star implies the apparition of a surface energy density that also modifies the mass. The inertial dragging must be continuous across the surface, while the derivative of the inertial dragging presents a discontinuity given by the angular velocity of the surface density (which modifies the total angular momentum of the star). If the angular

velocity of the two regions is the same, then the surface density must rotate with the same angular velocity.

Studying the matching up two second order reveals matching conditions for the remaining metric functions, providing the jump in the mass perturbation, quadrupolar moment and second order terms of the surface energy density. These equations will be presented elsewhere.

SURFACE *CRUST* APPROXIMATION

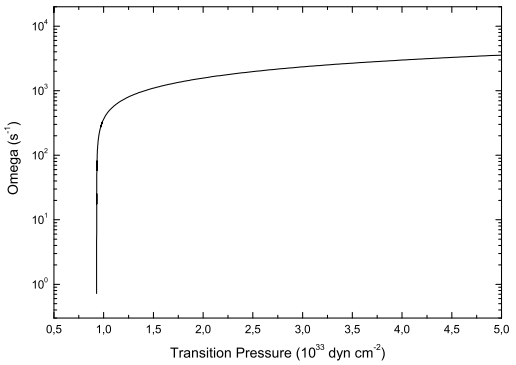

FIGURE 1. Angular velocity vs transition pressure for central density $1.279 \cdot 10^{15} gcm^{-3}$ and $1.44 M_{\odot}$

In general we will need to integrate, inside the star, the metric functions in different regions separated by the different phase transitions. If we just consider the phase transition at the core-*crust* interface, we will need to integrate in two regions, inside the core of the star and along the *crust*. We will need to impose the previous boundary conditions that grant the appropriate continuity of the metric across the regions. In order to simplify the situation so that only one region needs to be integrated, we can construct a simplified model of *crust* using the obtained matching conditions:

It can be proved that in the *crust* the density falls down to zero very quickly, and every contribution from the *crust* to integral properties of the star like the mass or the angular momentum can be neglected. The outer *crust* extends only over a region of some hundreds of meters with the density rapidly falling to zero. So approximating the *crust* of the star to a surface density enveloping the core of the neutron star is a well justified model of *crust* where the obtained radius can be interpreted as an effective radius of integration for the star. It can be seen that this approximation can be achieved in the following way.

We can integrate the core of the star with an appropriate equation of state, and match directly to the exterior vacuum solution. Then the exterior pressure and density becomes zero in the expressions for the matching, and the outer mass function becomes the mass outside the star. The interior pressure can be taken at the inner *crust*. The surface density obtained from the matching conditions can be interpreted as the approximated *crust*: the *crust* becomes a surface energy density enveloping the core of the star.

This simplified *crust* model can tell us a lot of information about the dependence of the properties of the star with the core-*crust* transition pressure. In Figure 1 we present

the relation of the angular velocity of the neutron star with the transition pressure. These results are for configurations with total second order mass $1.44 M_{\odot}$ and central density $1.279 \cdot 10^{15} g \cdot cm^{-3}$. The equation of state used for these results is the Glendenning 240 for high densities together with the BPS equation of state for lower densities [1].

In the figure it can be seen two different regions, one where the angular velocity is quite sensitive to core-*crust* transition pressure variations, and another where it is less important. Around core-*crust* transition pressure other properties of the star like the angular momentum and the quadrupolar momentum are also heavily modified with small perturbations of the core-*crust* transition pressure variation. The specific value for which this variations can affect the global properties of the star is different for other central densities and equations of state. In this case, small variations of the order of $10^{23} dyn \cdot cm^{-2}$ causes relative variations order 10^{-6} in the period, angular momentum and eccentricity.

The configurations have been generated integrating the differential equations for using a Fortran code based in the Colsys routine [10]. The equation of state has been interpolated numerically from the tables. The interpolation is based on a natural spline that makes the adiabatic index continuous (necessary to obtain a good precision in the second order perturbation functions).

Colsys is the appropriated way of resolving the problem, because Colsys allows to resolve differential equations with quite general boundary conditions. We impose the usual regularity conditions together with the boundary conditions at the border of the star that grants the solution outside the star to be asymptotically flat with the matching previously explained. Also Colsys allows to introduce fixed points of the mess where certain junction conditions could be imposed. This feature will be used in future works to integrate multiple regions with different equations of state.

The angular velocity of the star is quite dependent of the transition pressure, specially in the region nearby the core-*crust* transition. This means that small changes in the core-*crust* transition pressure could give rise to important changes in the dynamical properties of the star like angular momentum and quadrupolar moment. Energy depositions on the outer layers of the star could affect the phase transition, causing variations in the angular velocity of the star. These processes could explain pulsar *glitches*.

REFERENCES

1. N. Glendenning, *Compact stars: nuclear physics, particle physics, and general relativity*, Astronomy and astrophysics library, Springer, 2000, ISBN 9780387989778.
2. P. Haensel, P. Haensel, A. Potekhin, and D. Yakovlev, *Neutron stars: Equation of state and structure*, Astrophysics and space science library, Springer, 2007, ISBN 9780387335438.
3. H. Heiselberg, and M. Hjorth-Jensen, *Physics Reports* **328**, 237 (2000).
4. G. Darmois, *Les équations de la gravitation einsteinienne*, Mémorial des sciences mathématiques 25, Gauthier-Villars et cie, 1927.
5. A. Lichnerowicz, *Théories relativistes de la gravitation et de l'électromagnétisme:*, Collection d'ouvrages de mathématiques à l'usage des physiciens, Paris, 1955.
6. C. Misner, K. Thorne, and J. Wheeler, *Gravitation*, W. H. Freeman, 1973, ISBN 9780716703440.
7. J. B. Hartle, *Astrophys. J.* **150**, 1005 (1967).
8. J. B. Hartle, and K. S. Thorne, *Astrophys. J.* **153**, 807 (1968).
9. L. M. González-Romero, *Phys. Rev. D* **67**, 064011 (2003).
10. U. Ascher, J. Christiansen, and R. D. Russell, *ACM Trans. Math. Softw.* **7**, 209–222 (1981).

2.4.3 Publication: Luis Manuel González-Romero and Jose Luis Blázquez-Salcedo, *New model of relativistic slowly rotating neutron stars with surface layer crust: application to giant glitches of Vela Pulsar*, Journal of Physics: Conference Series 314 (2011) 012088

Journal of Physics: Conference Series **314** (2011) 012088 doi:10.1088/1742-6596/314/1/012088

New model of relativistic slowly rotating neutron stars with surface layer *crust*: application to giant *glitches* of Vela Pulsar

L. M. González-Romero and J. L. Blázquez-Salcedo

Depto. Física Teórica II, Facultad de Ciencias Físicas, Universidad Complutense de Madrid, 28040-Madrid, Spain.

E-mail: mgromero@fis.ucm.es, joseluis.blazquez@fis.ucm.es

Abstract.

Introducing a surface layer of matter on the edge of a neutron star in slow rigid rotation, we analyze, from an intrinsic point of view, the junction conditions that must be satisfied between the interior and exterior solutions of the Einstein equations. In our model the core-*crust* transition pressure arise as an essential parameter in the description of a configuration. As an application of this formalism, we describe giant *glitches* of the Vela pulsar as a result of variations in the transition pressure, finding that these small changes are compatible with the expected temperature variations of the inner crust during *glitch* time

1. Introduction

Many pulsars show sudden spin jumps, *glitches*, superimposed to the gradual spin down due to the continued loss of angular momentum suffered by the star. The study of the properties of the star during the *glitch* time is essential to understand the structure of the neutron star that models the pulsar [1, 2]. In Vela pulsar, giant *glitches* with relative period variation of the order of 10^{-6} have been observed. Many mechanisms have been proposed to explain *glitches*.

The models that deal with *glitches* are associated with the layer structure of neutron stars. Two regions of the star can be differentiated: the core and the *crust*. It is thought that the *crust* region has a solid crystalline structure similar to a metal [3]. Some theories propose that the *glitch* is triggered by the rupture of the *crust* as a consequence of the tensions on the *crust* that try to adequate the ellipticity of the *crust* to the changing angular velocity of the star.

Because of the large density gradient close to the transition between the core and the *crust*, most of the crustal matter resides in the shells in the inner part of the *crust* [4]. Furthermore, it is noteworthy that the dynamical properties of the neutron star depend strongly on the transition pressure between the star's core and the *crust* as have been pointed up by [5] and [6]. Because most of the matter of the *crust* is found in the shells near the transition region between the core of the star and the inner *crust*, this is the region where the properties of the *crust* are relevant [4]. Hence, we will treat the *crust* as a surface layer that envelops the star's core. In the next section we will describe how our model of slowly rotating neutron star with a surface layer *crust* is constructed.

2. Construction of models of slowly rotating neutron stars with surface *crust*.

We assume that the neutron star is in permanent rigid rotation. The star rotates with constant angular velocity Ω around an axis, so the resulting space-time is axisymmetric and stationary. We assume that the rotation of the star is sufficiently slow and, hence, the Hartle-Thorne perturbative solution can be used [7, 8]. To second order in the angular velocity of the star Ω, appropriate coordinates can be chosen so that the metric can be written as follows $ds^2 = -e^{2\psi(r)}[1+2h(r,\theta)]dt^2+e^{2\lambda(r)}[1+2m(r,\theta)]dr^2+r^2[1+2k(r,\theta)]\left[d\theta^2-\sin^2\theta(d\phi-\omega(r)dt)^2\right]$.

We have to solve the Einstein equations in the interior of the star, where the matter is described by a perfect fluid tensor with equation of state $\rho = \rho(p)$ and in the outer region, where space is empty. Also, we have to impose appropriate boundary conditions in the surface of the star. It is very desirable to introduce a new radial coordinate R adapted to the surface of the star [7, 8].

We assume that the core of the star is surrounded by a thin surface layer (simplified *crust* model). Then we find that in the surface of the star $R = a$, the stress-energy tensor is non null and it can be written as $T_c^{\mu\nu}(R) = \rho_c(\theta)u_c^\mu u_c^\nu(a)$, i.e. the surface layer can be described as a perfect fluid with its own angular velocity Ω_c. The surface energy density can be written up to second order as $\rho_c(\theta) = \varepsilon + \delta\varepsilon(\theta)$. We must impose the usual junction conditions on the interior and exterior solutions, but taking into account the introduction of a surface layer of matter on the border of the star. We use the intrinsic formulation of these conditions [9] [10]: the first fundamental form must be continuous across the surface of the star, and the second fundamental form presents a discontinuity given by the stress-energy tensor in the surface of the star. In order to use these junction conditions in the slow rotation approximation, we expand them in terms of Ω, finding the following results for each one of the metric functions:

Order zero: we obtain important conditions for the mass function and for the pressure of transition between core and *crust*

$$M_{ext} = M_{int} + 4\pi a^2\sqrt{1-\frac{2M_{int}}{a}}\varepsilon - 8\pi^2a^2\varepsilon^2 \tag{1}$$

$$\frac{M_{ext}}{a^2\sqrt{1-2M_{ext}/a}} - \frac{M_{int}+4\pi a^3 p_{int}}{a^2\sqrt{1-2M_{int}/a}} = 4\pi\varepsilon \tag{2}$$

The equation (1) gives the total mass of the star to zero order (M_{ext}) as the addition of three terms: the core mass ($M_{int} \equiv 4\pi\int_0^a \rho R^2 dR$), the *crust* mass, and a negative bounding energy term. We interpret (2) as an equation giving the surface density of energy ε in terms of the total mass of the star, the interior mass, and the core-*crust* transition pressure p_{int}. This condition is used to obtain the radius of the star.

First order: we obtain continuity of the rate of rotation of the inertial frames $\omega(a)_{ext} = \omega(a)_{int} \equiv \omega(a)$, and an expression for the total angular momentum:

$$J = a^6 e^{\lambda(a)_{ext}}(e^{-\lambda(a)_{int}}\left[\partial_R\overline{\omega}(a)\right]_{int} + 16\pi\varepsilon\overline{\omega_c})/6 \tag{3}$$

where $\overline{\omega_c} = \Omega_c - \omega(a)$. It can be seen [7, 8] that the first term of expression (3) has the same sign as Ω (in our case always positive). However, the second term depends on the sign of Ω_c. Hence, contra-rotating configuration are possible (the core and the *crust* contra-rotate), and even, we could find certain critical configuration in which the total angular momentum is null.

Second order: we obtain $\Delta[r^*(a,\theta)] = 0$ where r^* is defined as in [7, 8], so both the mean radius and the eccentricity are continuous. Also, conditions for the second order perturbation of the mass function and surface density ($\delta\varepsilon$) are obtained.

Finally the last of the second order conditions fixes the value of the angular velocity of the *crust* $\Omega_c = \omega(a) \pm (\Omega - \omega(a))$. We obtain two possible configurations for the same star core and transition pressure: one with the *crust* co-rotating with the interior fluid and with identical velocity, and a special configuration with contra-rotating *crust*.

3. Some properties of the model using realistic equations of state for the core

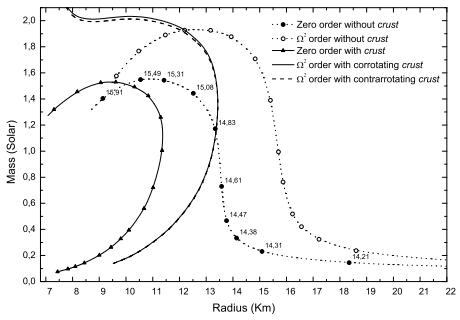

Figure 1. Mass vs radius for static/rotating configurations with a 10% *crust* (BPS)

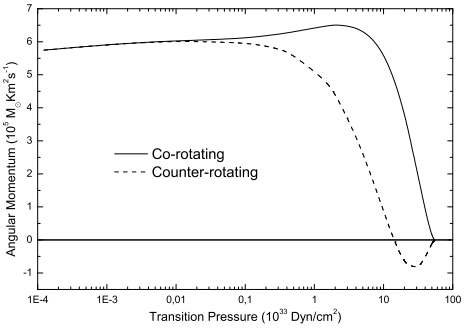

Figure 2. Angular momentum vs transition pressure for fixed ρ_c (BPS).

To obtain a model of a neutron star with a surface layer *crust* in permanent slow rotation, for a given equation of state of the core, we have to fix three parameters. We choose the total mass of the star, the central density, and the core-*crust* transition pressure. Then, we integrate the Einstein equations inside the star (using a realistic equation of state for the core) and we match this solution with the exterior solution found in [7, 8] using the junction conditions explained above. We have performed our simulations using an equation of state for high pressures from [11, K=240 MeV, $\frac{m^*}{m} = 0.78$ and $x_\sigma = 0.6$] and the BPS equation of state for the lower pressures. Similar results have been obtained for the analytical fit of the Sly equation presented in [3].

We present some of our results in figures 1 and 2. In fig. 1, we show multiple configurations for both static stars and rotating stars, with a *crust* of approximately 10% of the total mass and mass shedding angular velocity. On the static configurations without *crust* we write the value $\log 10(\rho_c)$. Note that the mass-radius behavior of the configurations with surface *crust* resembles those of the quark stars [11]. In fig. 2 we show the angular momentum for mass shedding angular velocity as a function of the core-*crust* transition pressure. In the counter rotating configuration we find that if the core-*crust* transition pressure is large enough, the angular momentum of the inner *crust* region could be equal or even higher than the angular momentum of the star core, resulting in a null or negative total angular momentum.

4. Core-*crust* transition pressure evolution in giant *glitches* of the Vela pulsar

On a typical pulsar, the rupture of the solid *crust* produces a release of energy 10^{41}-10^{43} ergs to the inner part of the *crust*. Several works study the thermal response of a neutron star after a *glitch* [12, 13], obtaining that increases in the temperature of the transition region of the order of $10^6 K$. This small rise of the temperature will produce an small but sensitive increase in the transition pressure [14]. We propose that the *glitch* can be explained by changes in the equation of the state of the star in the transition region between the *crust* and the core. In our model, these changes are represented by variations of the transition pressure due to the increase of the temperature produced by the deposition of the energy, coming from the rupture of the *crust*.

Using the observational data from the ATNF Pulsar Catalogue [15] we can study the giant glitches of Vela pulsar using our model. We assume that during the *glitch* neither the total mass nor the central density of the star are changed. Hence, in our description, the changes in the pulsar during this epoch are due to readjustment of the core-*crust* transition pressure, i.e., a variation of the equation of state in transition region between the core and the *crust*. Assuming this, we can give a description of the effects of these *glitches* over the neutron star using our model of slowly rotating neutron star with superficial *crust*. We assume that the star has a total

Date (MJD)	$\delta\Omega(10^{-6})$	$\delta p_{int}(10^{-10})$	$\delta ecc(10^{-6})$	$\delta Q(10^{-6})$
40289	2.34	0.70	2.36	4.73
41192	2.05	0.58	1.97	3.94
43693	3.06	0.93	3.15	6.31
45192	2.05	0.58	1.96	3.93
48457	2.72	0.81	2.76	5.51
51559	3.09	0.93	3.14	6.28
53959	2.62	0.82	2.74	5.48

Table 1. Date of each giant *glitch* of the Vela pulsar in modified Julian days and relative increases of angular velocity, transition pressure, eccentricity and quadrupolar moment

mass of $1.44M_{\odot}$, a central density of $1.279 \cdot 10^{15} gcm^{-3}$, and a transition pressure before the *glitch* of $3.751 \cdot 10^{33} dyn/cm^2$. We calculate the resulting configuration after the *glitch* varying the core-*crust* transition pressure until we reach an equivalent configuration (same mass and central density) with the resulting angular velocity just after the *glitch*. As it can be seen in table 1, our model predicts a relative transition pressure increase of the order of 10^{-10} for the considered *glitches*. This small variation in the equation of state on the surface of the star causes a redistribution of other properties of the star. The eccentricity of the star increases order 10^{-6}. Also, a movement of matter on the surface of the star, from the poles to the equator, produce an increase of the quadrupolar momentum (10^{-6}) which may cause gravitational radiation.

Using a estimation for the thermal pressure variations it can be seen that the corresponding increase of the inner *crust* temperature is order $10^6 K$ [14], which agree with the results obtained in the works previously commented. So the relative core-*crust* transition pressure changes we obtain in our model can be understood as variations in the equation of state of the transition region between the core and the *crust* of the neutron star, resulting from the deposition of energy of 10^{41}-$10^{43} erg$ in the outer layers of the neutron star during the *glitch* time.

In conclusion, we propose a new model for the giant *glitches* of the Vela pulsar: The tensions on the *crust* trying to adequate the ellipticity of the *crust* to the changed angular velocity produce the rupture of the *crust*. Then, there is a sudden energy deposition in the inner *crust* layers, which causes a rise of its temperature, resulting in an increase of the core-*crust* transition pressure of the neutron star (a change in the equation of the state in the core-*crust* transition region is produced). Hence, the properties of the neutron star (angular velocity, eccentricity, surface matter distribution and quadrupolar moment) change and a *glitch* is generated/observed.

The present work has been supported by Spanish Ministry of Science Project FIS2009-10614. The authors wish to thank F. Navarro-Lérida for valuable discussions.

References

[1] Lorenz C. P., Ravenhall D. G., Pethick C. J., 1993, *Phys. Rev. Lett.* **70**, 379
[2] Link B., Epstein R. I., Lattimer J. M., 1999, *Phys. Rev. Lett.* **83** 3362
[3] Haensel P., Potekhin A. Y., 2004, *Astron. Astrophys.* **428** 191 [arXiv:astro-ph/0408324]
[4] Pethick C. J., Lorenz C. P., Ravenhall D. G., 1995, *Nucl. Phys. A* **584** 675
[5] Lattimer J. M., Prakash M., 2001, *Astrophys. Journal* **550** 426
[6] Cheng K. S., Yuan Y. F., Zhang J. L., 2002, *Astrophys. Journal* **564** 909
[7] Hartle J. B., 1967, *Astrophys. Journal* **150** 1005
[8] Hartle J. B., Thorne K. S., 1968, *Astrophys. Journal* **153**, 807
[9] Misner C. W., Thorne K. S., Wheeler J. A., 1973, *Gravitation*, Freeman, San Francisco
[10] González-Romero L. M., 2003, *Phys. Rev. D* **67**, 064011
[11] Glendening N. K., 2000, *Compact stars* Astronomy & Astrophysics library, Springer, New York
[12] Hirano S. *et al* , 1997, *Astrophys. Journal* **491**, 286
[13] Van Riper K. A., Epstein I., Miller, G. S., 1991, *Astrophys. Journal* **381** L47
[14] Prakash M. *et al* , 1997, *Phys. Rep.* **280** 1
[15] Manchester, R. N. *et al* , 2005, *Astrophys. Journal* **129**, 1993

CHAPTER 3

HIGHER DIMENSIONAL BLACK HOLES

3.1 Outline and objectives

In this chapter we will study higher dimensional black holes in two different theories: Eintein-Maxwell-dilaton (EMd) and Einstein-Maxwell-Chern-Simons (EMCS). We have performed a numerical analysis together with the study of the near-horizon formalism.

We will consider odd-dimensional black holes in Einstein-Maxwell-dilaton theory. We are interested in solutions with spherical topology of the horizon. We will assume all the angular momenta have the same magnitude. We will be particularly interested in the extremal case. When the dilaton field is turned off, two different branches of extremal black holes are found. The branch emerging from the uncharged rotating solution (Myers-Perry solution [52]) has angular momentum proportional to the horizon area, while the branch emerging from the static, electrically charged solution (Tangherlini solution [53]) has the angular momentum proportional to the horizon angular momentum. In the case of a dilaton included, only the branch emerging from the Myers-Perry solution is found, and the angular momentum is always proportional to the horizon area. This study has been published in Physics Letters B **727** (2013) 340-344 [5] (included in section 3.5.1) and in Physical Review D **89** (2014) 024038 [6] (included in section 3.5.2).

We have considered the same type of black holes in Einstein-Maxwell-Chern-Simons theory. The standard Chern-Simons term can be added to Einstein-Maxwell theory in odd dimensions. In this work nonetheless, we have restricted to 5 dimensions. In this case we find non-static $J = 0$ extremal black holes, with lower mass than that of the

extremal Reissner-Nordström solution. Uniqueness of the solutions with respect the global charges no longer holds. These results have been presented in Physical Review Letters **112** (2014) 011101 [7] (included in section 3.6.1).

Let us begin with a brief review of higher dimensional black holes and their general properties.

3.2 Brief introduction to higher dimensional black holes

One of the most striking predictions in General Relativity are black holes, special regions of space where not even light can classically scape from. The space-time metric describing the static uncharged black hole in 3+1 dimensions was discovered by Schwarzschild in 1915, and a couple of years later it was generalized to include a Maxwell electric field (Reissner-Nordström solution). In the beginnings these solutions of Einstein equations were considered as singular solutions with only academic interest. It was not until the sixties that the nature of the black hole horizon was fully understood (coordinate singularity). In 1963 Kerr makes the very important discovery of the rotating uncharged black hole, and a couple of years later the Kerr solution is generalized to include a Maxwell electromagnetic field (Kerr-Newmann solution) [54].

There is strong astrophysical evidence for the presence of massive black holes at the core of spiral galaxies. Other astrophysical objects within our galaxy, with strong X-ray emission and a few times the mass of the Sun, are very strong candidates to astrophysical black holes, resulting probably from supernova explosions of very massive stars [17].

Asymptotically flat stationary black holes of Einstein-Maxwell theory in 4 dimensions have very special properties. They must be spherical, with no other topologies allowed for stable solutions, if the dominant energy condition is satisfied. Then a black hole solution is uniquely characterized by a set of global charges, i.e., the mass M, the angular momentum J, and the electric charge Q. Given these three parameters, there is only one black hole solution of Einstein-Maxwell equations in 4 dimensions [55].

In more than 4 dimensions, or when more general fields are coupled to gravity (Yang-Mills fields, dilaton fields), black holes do not posses these special features [56]. In higher dimensions there are two main differences: the black hole horizon can have topologies different from spherical, or even be an extended object; and there is more than one independent plane of rotation.

Concerning the first feature, it is easy to see that given a black hole in D dimensions with a certain horizon Σ_H, a perfectly valid black hole solution in $D+1$ dimensions can be constructed just by adding an additional space dimension [57]. The new black hole has horizon $\Sigma_H \times \Re$. Note that now the black hole horizon is an extended object, with a topology different from spherical. Black strings, and in general, extended black p-branes, can be found for arbitrary higher than 4 dimensions.

Nevertheless, these black holes are not asymptotically flat. But we can think about taking the $D+1$ dimensions black string of horizon $\Sigma_H \times \Re$ and bending it so that the horizon becomes $\Sigma_H \times S^1$ [57]. The resulting black ring is unstable and tends to contract. But appropriately choosing the angular momentum of each rotation plane, we can re-equilibrate the black ring, obtaining a stable solution. Stable black holes solutions with ring-like topologies can be found for arbitrary higher than 4 dimensions [56].

Even more, black p-branes with compact horizon can in principle be constructed in a similar way. The topology of the resulting p-branes can become very complicated [56].

Black holes in higher dimensions have more than one independent plane of rotation. In general, for $D-1$ space-like dimensions, the rotation group $SO(D-1)$ has $N = [(D-1)/2]$ independent planes of rotation, where N is the integer part of $(D-1)/2$. An angular momentum can be associated with each plane of rotation.

There is a number of reasons why gravity models with more than 3 space dimensions, and specially black hole solutions of these theories, are interesting. Let us briefly enumerate some of them.

After the General Theory of Relativity was formulated by Einstein, Kaluza in 1921 [58] and Klein in 1926 [59] noticed that if one extra space dimension was added to Einstein's gravity, in a four dimensional slice of this extended theory, gravity on this slice was naturally coupled to an extra electro-magnetic field [56]. Hence one could interpret Einstein-Maxwell theory in four dimensions as Einstein theory in five dimensions. This was the first hint towards the idea that natural interactions (in this case electro-magnetism and gravity) could be unified to one unique force (in this case Einstein gravity) acting in a higher dimensional space-time.

More lately, string theory, a very successful approach to quantum gravity, predicts the existence of more than 4 space-time dimensions (M-theory has 11 dimensions). The extra space dimensions are compact and much smaller in scale than our usual 3 space dimensions. These extra space dimensions are curled up into small volumes (compactification).

Other theories, like the brane-world idea, suggest that our 3-dimensional space is just a slice of a higher dimensional space-time. In these theories, space could have extended extra dimensions, as well as compact extra dimensions.

Some of these theories present as a possible scenario the production of higher dimensional black holes in the LHC and future TeV colliders, so falsifiability of some of these theories could be made.

Another interesting application of higher dimensional black holes can be found, in the context of string theory, in the gauge-gravity duality [56]. This conjecture proposed by Maldacena in 1997 [60] as a correspondence between Anti-de Sitter space-time and two conformal field theories, tells us that quantum field theories could be related to higher dimensional theories of gravity. Thermal equilibrium in 3+1-dimensional non-gravitational systems could be dual to higher dimensional black holes. Strongly interacting systems could be studied using their duals as black hole solutions.

Since the properties of higher dimensional black holes are very different to those of $3+1$-dimensional black holes, their study has a lot of interest. Insight on why the topology, uniqueness and stability of 4-dimensional black holes is so special can be gained by the dependence of these properties with the space-time dimension [57].

The first generalization of a black hole solution to higher dimensions, the static black hole in Einstein gravity (generalization of the Schwarzschild metric), was pioneered by Tangherlini [53], who also generalized the Reissner-Nordström solution. The corresponding generalization of the Kerr black hole to higher dimensions was found by Myers and Perry [52]. Other stationary non-vacuum solutions have been obtained in effective theories whose low energy actions are related to string theory [61, 62, 63]. See [57] for a complete review on known higher dimensional black hole solutions.

Let us start by presenting some of the most important properties of black holes, introducing the Ansatz we will be using throughout this chapter in order to generate the black holes. Finally, we will end by introducing the near-horizon formalism, a very useful tool that will allow us to obtain analytical expressions that will complement our numerical analysis.

3.3 Some properties of the stationary black holes

Here we will make a brief exposition of the main features of the higher dimensional black holes we will consider. In the following we will consider that D-dimensional Newton constant is fixed such that $16\pi G_D = 1$.

3.3.1 The Action

We will be interested in Einstein theory coupled to different fields coming from string theory. We will restrict to odd D-dimensional space-times. All these theories can be formulated using the variational principle of a certain action. If we consider the D-dimensional action of gravity coupled to some fields

$$I = \int d^D x \sqrt{-g} \Big[R + \mathcal{L}_M \Big] \ , \tag{3.1}$$

with curvature scalar R, and $\mathcal{L}_M$ is the Lagrangian including the fields that couple to the space-time. As we said, we will be interested in two different theories. In one of them, a Maxwell electromagnetic potential is also coupled to a dilaton field, with $\mathcal{L}_M = -\frac{1}{2}\partial_\mu \Phi \partial^\mu \Phi - \frac{1}{4} F^2 e^{-2h\Phi}$, and $D = 2N+1$. Note that we have the dilaton field Φ, the dilaton coupling constant h, and the field strength tensor $F_{\mu\nu} = \partial_\mu A_\nu - \partial_\nu A_\mu$, where A_μ denotes the gauge potential. Another case we will consider is 5-dimensional black holes, with a Maxwell electromagnetic potential and a Chern-Simons term coupled to gravity, where $\mathcal{L}_M = -F^2 - \frac{2\lambda}{3\sqrt{3}} \epsilon^{\alpha\beta\mu\nu\rho} A_\alpha F_{\beta\mu} F_{\nu\rho}$. The parameter λ is the Chern-Simons coupling constant.

Variation of the action with respect to the metric leads to the Einstein equations

$$R_{\mu\nu} - \frac{1}{2} g_{\mu\nu} R = \frac{1}{2} T_{\mu\nu} \ , \tag{3.2}$$

with stress-energy tensor

$$T_{\mu\nu} = g_{\mu\nu} \mathcal{L}_M - 2 \frac{\delta \mathcal{L}_M}{\delta g^{\mu\nu}} \ , \tag{3.3}$$

whereas variations with respect to the other fields yield the matter field equations.

These differential equations are highly non-linear, and the metric components are in principle strongly coupled to the field components and viceversa. These equations form a second-order differential equation system. It is very difficult to obtain general solutions to these differential equations. We will be interested in a certain subset of the solutions with more symmetries, which will reduce considerably the difficulty.

3.3.2 Ansatz for stationary axisymmetric black holes with equal-magnitude angular momenta

In this work we will consider axisymmetric and stationary configurations. The proper way of imposing these two conditions is by defining a set of $N+1$ vector fields ξ and

$\eta_{(k)}$ with $k = 1, \ldots, N$. The vector field ξ approaches asymptotically a time-like vector field of unitary norm, whereas each $\eta_{(k)}$ approach asymptotically a space-like vector field. Even more, we impose that $\eta_{(k)}$ are cyclic vector fields. These $N+1$ vector fields commute [55].

The space-time will be invariant under local flow diffeomorphisms defined by these vector fields (Killing vector fields). The precise way of imposing these symmetries on the space-time metric is with the Lie derivative

$$\pounds_\xi g = \pounds_{\eta_{(k)}} g = 0 \ . \tag{3.4}$$

The same symmetries should be found on the electromagnetic field (up to a gauge factor) and in the dilaton field when included

$$\pounds_\xi A = \pounds_{\eta_{(k)}} A = \delta f \ , \tag{3.5}$$

$$\pounds_\xi \Phi = \pounds_{\eta_{(k)}} \Phi = 0 \ . \tag{3.6}$$

Since the Killing vector commute, we can always find a system of coordinates adapted to these Killing symmetries so that

$$\xi = \partial_t \ , \tag{3.7}$$

$$\eta_{(k)} = \partial_{\varphi_k} \ . \tag{3.8}$$

In this system of coordinates, the metric and the fields components will not depend on the (t, φ_k) coordinates, which is a very important simplification to the problem. In this coordinates, the gauge of the Maxwell field will be chosen so that

$$\pounds_\xi A = \pounds_{\eta_{(k)}} A = 0 \ . \tag{3.9}$$

In addition, we will be considering black holes with spherical horizon topology.

While in general, there is an independent angular momentum associated with each rotational Killing vector $\eta_{(k)}$, we will also restrict to the case in which all the independent angular momenta have the same magnitude, $|J_i| = |J_k|$. In odd dimensions the problem is reduced to cohomogeneity-1. In other words, the symmetry group associated to the axial rotation increases from $U(1)^N$ to $U(N)$. It can be seen that in this case the dependence of the metric functions on the angular coordinates can be explicitly written, but the dependence on the radial-like coordinate is not known in general. Lewis-Papapetrou coordinates can be found, so that our Ansatz for axially

symmetric, stationary black holes, with horizon of spherical topology and all angular momenta of equal magnitude is [64, 65]

$$\begin{aligned} ds^2 &= -f dt^2 + \frac{m}{f}\left[dr^2 + r^2 \sum_{i=1}^{N-1}\left(\prod_{j=0}^{i-1}\cos^2\theta_j\right) d\theta_i^2\right] \\ &+ \frac{n}{f} r^2 \sum_{i=1}^{N}\left(\prod_{j=0}^{i-1}\cos^2\theta_j\right)\sin^2\theta_i\left(\varepsilon_i d\varphi_i - \frac{\omega}{r}dt\right)^2 \\ &+ \frac{m-n}{f} r^2 \left\{\sum_{i=1}^{N}\left(\prod_{j=0}^{i-1}\cos^2\theta_j\right)\sin^2\theta_i d\varphi_i^2 \right. \\ &\left. - \left[\sum_{i=1}^{N}\left(\prod_{j=0}^{i-1}\cos^2\theta_j\right)\sin^2\theta_i\varepsilon_i d\varphi_i\right]^2\right\} , \end{aligned} \tag{3.10}$$

where $\theta_0 \equiv 0$, $\theta_i \in [0, \pi/2]$ for $i = 1, \ldots, N-1$, $\theta_N \equiv \pi/2$, $\varphi_k \in [0, 2\pi]$ for $k = 1, \ldots, N$, and $\varepsilon_k = \pm 1$ denotes the sense of rotation in the k-th orthogonal plane of rotation. Note that we have chosen isotropic coordinates.

An adequate parametrization for the gauge potential is given by

$$A_\mu dx^\mu = a_0 dt + a_\varphi \sum_{i=1}^{N}\left(\prod_{j=0}^{i-1}\cos^2\theta_j\right)\sin^2\theta_i\varepsilon_i d\varphi_i \ . \tag{3.11}$$

Independent of the number of dimensions D, this parametrization involves four functions for the metric, f, m, n, ω, two functions for the gauge field, a_0, a_φ, and one function for the dilaton field, ϕ, all of which depend only on the radial coordinate r.

3.3.3 Event horizons and ergoregions

The most intriguing characteristic of a black hole is its event horizon. The event horizon is a region of the space-time (a space-like hypersurface) which can only be crossed inwards towards the singularity of the black-hole. No matter or light can scape classically from the region delimited by the event horizon [54]. Although the event horizon for higher dimensional axisymmetric stationary black holes can present very diverse topologies (spherical, toroidal, disc-like...) or with more than one connected component of the horizon (black Saturn, di-ring) [56, 57], there is actually a lot of discussion on the limitations on the possible horizon topologies [66]. The Ansatz we have presented in the previous section constrains to single horizons with spherical topology.

We will assume that these stationary and axisymmetric black holes satisfy the rigidity theorem [67, 68, 69]. Hence we will consider that the event horizon is a Killing horizon.

A Killing horizon is a null hypersurface to which a Killing field is normal (and tangent, since it is a null surface). The Killing vector field that characterizes the horizon can be defined at every point of the space-time, and it coincides with the temporal Killing vector field in the static case. In the stationary case, assuming equal-magnitude angular momenta and making use of the adapted coordinates we have introduced, the Killing vector field can be written like [55]

$$\chi = \xi + \Omega \sum_{k=1}^{N} \varepsilon_k \eta_{(k)} \ . \tag{3.12}$$

Ω represents the horizon angular velocity, i.e, the angular velocity that an observer at infinity will observe for a particular point of the event horizon. Since we are considering the case of equal angular momenta, there is only one angular velocity Ω. Without loss of generality, this Ω is assumed to be non-negative, any negative sign being included in ε_k. A static configuration will have both vanishing angular momenta and angular velocity. But we will find that there are non-static configurations with vanishing angular momenta but non-vanishing angular velocity, and viceversa. Note that the angular velocity is constant, meaning that the event horizon rotates rigidly.

Rotating black holes present another interesting feature, the ergo-region. Asymptotically, the Killing vector field ξ will become a time-like vector field. But in a rotating black hole, there could be a region of space-time (outside the horizon) where this Killing vector field may become space-like. This region is called the ergo-region, and its boundary is the ergo-sphere. The ergo-sphere is really an ellipsoid whose poles touch the event horizon of the black hole. Inside the ergo-region, it is impossible to any particle to be at rest with respect an observer at infinity. A very interesting property of this region is that it could be used to extract energy from a black hole by virtue of the Penrose mechanism [70].

In the Lewis-Papapetrou coordinate system we are using, the event horizon is found when the metric component g^{rr} vanishes, resulting in $f = 0$. This equation has several roots which define different horizons of the space-time. The largest of these roots, r_H satisfying $f(r_H) = 0$, is what we will call the event horizon.

The ergo-sphere is determined by the vanishing of the g_{tt} component. This results in the equation $\frac{n}{f}\omega^2 - f = 0$. This equation has in general several roots, defining different ergo-spheres. The ergo-sphere of interest to us is the one localized outside

the event horizon.

3.3.4 Extremality

We will be interested in extremal and non-extremal black holes. There are different definitions for extremal black holes. One way to define them is the following: a black hole is said to be extremal when, for a given electric charge and angular momentum, its mass is minimal whereas the event horizon is preserved. If for the same electric charge and angular momenta, an even smaller mass is considered, then the black hole does not develop an event horizon, giving rise to a naked singularity. These naked singularities are considered to be non-physical solutions, and hence prevented in the natural world (cosmic censorship hypothesis [54]).

Nevertheless, this definition of extremal black hole may not be useful if there is not non-uniqueness of the solutions with respect the global charges (as we will find for example in our results in EMCS theory in section 3.6.1).

Extremal black holes can also be characterized by the vanishing of the surface gravity κ. The surface gravity can also be interpreted as the temperature of the black hole, and hence extremal black holes would be those with zero temperature. Nevertheless, there are examples of extremal black holes with non-vanishing surface gravity [71].

Extremal black holes can be also characterized by the structure of their g^{rr} roots. In the extremal case, the roots degenerate into a double root. In some cases, the ergo-spheres also coincide with the event horizon, giving rise to special ergo-free black holes.

Typically, extremal black holes are of interest because the space-time symmetries are very much enhanced. Supersymmetric black holes, like the BMPV solution [61], are extremal. In fact, the first counting of black hole entropy microstates was achieved for these supersymmetric extremal black holes [72].

Extremal black holes are also of interest in order to study the domain of existence of black holes. Note that extremal black holes have minimal mass for fixed charges. Extremal black holes are expected to form the boundary of the domain of existence, but this is only true if there is uniqueness with respect the global charges. If uniqueness is violated, then very interesting phenomena can happen, as we will see in EMCS theory.

If there is uniqueness, then black holes are characterized by their global charges, which are mainly the mass, the electromagnetic charges, and the angular momenta. Extremal black holes on the other hand, are characterized by one less global parameter. In an extremal black hole, we can always obtain a relation (probably implicit) between

the mass and the rest of charges. If there is non-uniqueness, then an additional parameter must be supplemented in order to characterize the configuration (typically a horizon charge).

3.3.5 Global charges

In this section we will see how to calculate the global charges of the black holes (mass, electro-magnetic charges, angular momenta). In the next section we will consider the horizon charges.

Since we are looking for asymptotically flat solutions, the metric should approach the Minkowski metric far enough from the black hole.

The mass M of a stationary, asymptotically flat solution can be calculated by means of the Komar integral [73]

$$M = -\frac{D-2}{D-3}\int_{S^{D-2}_{\infty}} \alpha \ , \tag{3.13}$$

where α is a $D-2$ form with components $\alpha_{\mu_1\ldots\mu_{D-2}} \equiv \epsilon_{\mu_1\ldots\mu_{D-2}\rho\sigma}\nabla^{\rho}\xi^{\sigma}$, the form associated to the temporal Killing field ξ.

The angular momentum can be calculated in a similar way, assuming that the metric is axisymmetric (as it happens in the Ansatz we are considering). Hence the Komar expression for the angular momentum associated to the (k)-th Killing vector fields is [55]

$$J_{(k)} = \int_{S^{D-2}_{\infty}} \beta_{(k)} \ , \tag{3.14}$$

where β is a $D-2$ form with components $\beta_{(k)\mu_1\ldots\mu_{D-2}} \equiv \epsilon_{\mu_1\ldots\mu_{D-2}\rho\sigma}\nabla^{\rho}\eta^{\sigma}_{(k)}$. Since in our case we have equal-magnitude angular momenta, it can be seen that $|J_{(k)}| = J$, $k = 1, \ldots, N$.

The electric charge Q is obtained from the conservation of the electro-magnetic flux. Asymptotically, the Chern-Simons terms of the action vanish, and hence we can calculate it with the integral [55]

$$Q = -\frac{1}{2}\int_{S^{D-2}_{\infty}} e^{-2h\phi}\ {}^{*}F \ , \tag{3.15}$$

with ${}^{*}F_{\mu_1\ldots\mu_{D-2}} \equiv \epsilon_{\mu_1\ldots\mu_{D-2}\rho\sigma}F^{\rho\sigma}$.

3.3.6 Horizon properties

If the event horizon is located at $r = r_{\rm H}$, then the area of the horizon $A_{\rm H}$ can be calculated using the embedded metric of the horizon

$$A_{\rm H} = \int_{\mathcal{H}} \sqrt{|g^{(D-2)}|} = r_{\rm H}^{D-2} A(S^{D-2}) \lim_{r\to r_{\rm H}} \sqrt{\frac{m^{D-3}n}{f^{D-2}}} \ . \tag{3.16}$$

The entropy of the black hole is directly related to its area by the Bekenstein-Hawking formula

$$S = A_{\rm H}/4. \tag{3.17}$$

We can also give some definitions for the horizon charges. Following the definitions for the global charges using the Komar expressions, we define the horizon mass $M_{\rm H}$ and horizon angular momenta $J_{{\rm H}(k)}$ are given by

$$M_{\rm H} = -\frac{D-2}{D-3} \int_{\mathcal{H}} \alpha \ , \tag{3.18}$$

$$J_{{\rm H}(k)} = \int_{\mathcal{H}} \beta_{(k)} \quad , \tag{3.19}$$

where $\mathcal{H}$ represents the surface of the horizon. Note that for equal-magnitude angular momenta $|J_{{\rm H}(k)}| = J_{\rm H}$, $k = 1, \ldots, N$.

The horizon electrostatic potential $\Phi_{\rm H}$ is defined by

$$\Phi_{\rm H} = \chi^{\mu} A_{\mu}|_{r=r_{\rm H}} \ . \tag{3.20}$$

$\Phi_{\rm H}$ is constant at the horizon.

The surface gravity κ can be defined like

$$\kappa^2 = -\frac{1}{2} (\nabla_{\mu}\chi_{\nu})(\nabla^{\mu}\chi^{\nu}) \Big|_{\mathcal{H}} \ . \tag{3.21}$$

As we have said, black hole thermodynamics relates the surface gravity of a black hole with its temperature $T = \kappa/2\pi$.

3.3.7 Mass formula

The Smarr mass formula for Einstein-Maxwell black holes with N equal-magnitude angular momenta reads [64, 74]

$$\frac{D-3}{D-2}M = 2\kappa A_{\rm H} + N\Omega J + \frac{D-3}{D-2}\Phi_{\rm H} Q \ . \tag{3.22}$$

This mass formula holds also in the presence of a dilaton field [75].

3.4 Near-horizon formalism

Although we have limited ourselves to certain types of black holes which present an important amount of simplification due to their symmetries, in general we will not be able to solve the field equations explicitly. In fact, for 5D EMCS we will only have the solution in the special uncharged case (Myers-Perry solution), and the static black hole (Reissner-Nordström). In addition, for a specific value of the Chern-Simons (CS) coupling constant $\lambda = 1$ (supergravity), we will have another analytic solution (the Cvetič-Youm solution [76] for the non-extremal case, and the BMPV solution [61] for the extremal cases). For the odd-dimensional EMd case, we will have a similar situation, with the Myers-Perry solution, the Reissner-Nordström solution, and in addition a special solution obtained from Kaluza-Klein compactification, where the dilaton coupling constant adquires the special value $h_{KK} = \sqrt{\frac{D-1}{2(D-2)}}$. But in both EMCS and EMd cases, for arbitrary values of the charges and coupling constants, we will resort to numerical analysis.

Hence we will be interested in applying some techniques which allow us to obtain some analytical or partially analytical expressions, which could allow us to compare with the numerical results (in addition to comparing the explicitly known solutions we have enumerated).

One technique we will use is the near-horizon formalism. This formalism allows us to consider the geometry in a region close enough to the event horizon. In this region, the symmetries of the black hole space-time increase, and some information can be obtained concerning the black hole charges, entropy, and branch structure of the parameter space.

3.4.1 Near-horizon limit

Let us suppose that the space-time outside of a black hole event horizon can be divided in two distinct regions [77]. One region is close to its event horizon (near-horizon geometry), and the other one corresponds to the region which reaches, in our case, the asymptotically flat space-time (usually called the bulk geometry). The geometry close to a black hole event horizon can be obtained by a certain limit of a coordinate transformation, which eliminates the bulk geometry. In general, the coordinate transformation selects a frame comoving with the event horizon, and centers the radial coordinate in the horizon. The transformation depends on one scale parameter, Λ, which in the limit $\Lambda \to 0$ suppresses the bulk geometry of the black hole, and keeps the region of space-time close to the horizon. In order to remove possible coordinate singularities, a certain gauge must be taken for the gauge fields.

Let us enumerate some general properties of the near-horizon geometry [78]:

Since we will be considering black holes with event horizons with spherical topology, the limiting space-time of the near-horizon region can be described as the product of two independent spaces. One of them can be mapped with angular coordinates (θ_i, ϕ_j) (depending on the dimension we are considering) and describes an ordinary (squashed) $D-2$ dimensional sphere S^{D-2}. The other factor of the space-time can be labelled by a temporal and a radial coordinate (t, r), and describes a two dimensional anti-de-Sitter space-time, AdS_2 (two dimensional Einstein gravity with a negative cosmological constant). Let us make it clear that this factorized space-time is an exact solution of the Einstein equations. But note that this factorization of the space-time manifold will not hold in the bulk geometry of asymptotically flat black holes, and hence this analytic solution cannot describe the full global solution.

Now it should be clear to us that the space-time near the event horizon of a black hole has a very high amount of symmetry. The near-horizon geometry has $SO(D-1)$ isometry acting on the S^{D-2} sphere in the case of a static black hole, and $U(1)^N$ isometry group acting on a squashed sphere in the case of a rotating black hole, with independent rotation in each one of its N axial planes [79]. This symmetry is inherited from the global solution, which has spherical horizon topology. In the near-horizon limit, the coordinates are adapted to the event horizon squashed sphere geometry. If the angular momenta have equal magnitude, the symmetry increases into a cohomogeneity-1 group, and we have a factorized squashed sphere with $U(N)$ isometry. The other space-time factor, the anti-de-Sitter component, has a $SO(2,1)$ isometry generated by three independent Killing vectors. Note that the gauge and

scalar fields are also invariant under the isometries acting on the $AdS_2 \times S^{D-2}$ metric.

All the known examples of extremal black holes, with spherical topology and non-singular horizons, have near-horizon geometry factorized as $AdS_2 \times S^{D-2}$ and associated $SO(2,1) \times SO(D-1)$ isometry for the spherically symmetric case, and $SO(2,1) \times U(1)^N$ if rotation is considered [78]. AdS_2 factorization is also found in the near-horizon geometry of black holes with different topologies, like black rings. A classification of near-horizon geometries can be found in [77].

Although all the information from the bulk space-time, and in particular its asymptotical structure, is lost when considering the near-horizon limit, there is still a lot of information from the global solution encoded in the near-horizon geometry [80].

In particular, since the near-horizon geometry is obtained in a comoving frame with the horizon, and the connection with the asymptotically flat coordinate frame is lost, the horizon angular velocity cannot be calculated with the near-horizon geometry alone. Also because of this fact, since the time-like Killing field of the near-horizon geometry cannot be related to the global Killing field ξ, the total mass of the configuration cannot be calculated with the near-horizon geometry alone. For these two parameters, some relation between the global solution and the near-horizon solution must be supplemented. For example, if an analytical global solution is known, of course its near-horizon geometry will be parametrized in terms of the total mass and/or angular velocity. Otherwise, no Komar integral can be defined in the near-horizon geometry to obtain the total mass. The same can be said for the horizon mass.

The conserved charges related to the gauge fields and rotation symmetry can be calculated without problem [81, 82]. In fact, the angular momentum and the gauge field charges can be obtained from the conservation of their respective Noether charges. Let us consider explicitly the 5 dimensional EMCS case (this discussion is easily generalized to odd-dimensional EMd black holes). Here the Komar integral can be generalized, making use of the Noether charge, to any surface Σ enclosing the black hole

$$Q = -\frac{1}{2}\int_{\Sigma}\left[*F + \frac{\lambda}{\sqrt{3}}A \wedge F\right]. \tag{3.23}$$

In particular, when Σ is taken as asymptotical infinity, this integral is equivalent to the Maxwell charge integral. Since we are eliminating the bulk geometry in the near-horizon limit, we can use this expression for a Σ close enough to the horizon in order to calculate the conserved charge. Note that this conserved charge (also called the Page charge) is not invariant under global gauge transformations because of the Chern-Simons term [83]. But this should not be a problem since we are deploying the

bulk of the space-time, and hence, in order for the calculation to be consistent, we only need the conserved charge of the near-horizon geometry to be locally gauge-invariant. A global gauge transformation should only be considered if the bulk geometry is also considered, and in the near-horizon formalism we are deploying it. With the Chern-Simons term we are considering, only the Maxwell charge calculated at asymptotical infinity of the global solution is conserved and globally gauge invariant [84].

A similar calculation can be done for the angular momentum in our 5D EMCS black holes. Here the associated Noether charge can be written at any surface Σ enclosing the black hole

$$J_{(k)} = -\int_{\Sigma}\left[*\nabla\eta_k + 4(\eta_k A)F + \frac{2\lambda}{3\sqrt{3}}(\eta_k A)A\wedge F\right], \tag{3.24}$$

When Σ is taken as asymptotical infinity, this integral is equivalent to the Komar integral.

Of course, in the EMd black holes we will consider, since no Chern-Simons term is present in the Lagrangian density, there will be no broken global gauge invariance of charges calculated at intermediate surfaces enclosing the black hole. In this case, the discussion concerning the charges calculation simplifies, and we can safely calculate the Maxwell charge in the near-horizon geometry.

Finally, the horizon charges of the black hole can be safely calculated with the near-horizon geometry. In particular, the horizon angular momentum and the area of the event horizon can be calculated using (3.16) and (3.19).

3.4.2 Ansatz for the near-horizon formalism

We know the symmetries of the resulting near-horizon geometry of the extremal black holes we will consider, but since we have no global analytic expression for their metric or fields, we cannot explicitly calculate the near-horizon limit. We need to obtain the near-horizon geometry in another way, and then compare with the numerical results for the global solutions. An appropriate Ansatz for the near-horizon geometry $SO(2,1)\times U(N)$ can be written like [85]

$$\begin{aligned} ds^2 &= v_1\left(\frac{dr^2}{r^2} - r^2dt^2\right) + v_2\sum_{i=1}^{N-1}\left(\prod_{j=0}^{i-1}\cos^2\theta_j\right)d\theta_i^2 \\ &\quad + v_2v_3\sum_{i=1}^{N}\left(\prod_{j=0}^{i-1}\cos^2\theta_j\right)\sin^2\theta_i\left(\varepsilon_i d\varphi_i - krdt\right)^2 \end{aligned}$$

$$+v_2(1-v_3)\left\{\sum_{i=1}^{N}\left(\prod_{j=0}^{i-1}\cos^2\theta_j\right)\sin^2\theta_i d\varphi_i^2 - \left[\sum_{i=1}^{N}\left(\prod_{j=0}^{i-1}\cos^2\theta_j\right)\sin^2\theta_i\varepsilon_i d\varphi_i\right]^2\right\} . \tag{3.25}$$

And for the electromagnetic vector

$$A_\mu dx^\mu = (q_1 - q_2 k) r dt + q_2 \sum_{i=1}^{N}\left(\prod_{j=0}^{i-1}\cos^2\theta_j\right)\sin^2\theta_i\varepsilon_i d\varphi_i . \tag{3.26}$$

We parametrize the dilaton near the horizon with the parameter u.

The advantage of the cohomogeneity-1 isometry is that the enhanced symmetry allows us to factorize the angular dependence. Hence the metric and the gauge fields can be parametrized with just a set of constant parameters. Since we are dealing with extremal black holes, in principle we should be able to obtain expressions for each parametrization in terms of the total angular momentum J and the electric charge Q. We can obtain these expressions by solving the algebraic relations obtained from substituting our Ansatz in the Einstein and field equations. Then with these relations we can calculate the angular momentum and electric charge using (3.23) and (3.24). Sometimes this dependence of the field parameters on J and Q can only be written implicitly in terms of transcendental algebraic equations.

Note we are solving the Einstein equations for this near-horizon Ansatz without further assumptions. Hence note that there can be near-horizon solutions which do not describe the near-horizon geometry of a asymptotically flat global solution. On the other hand, one near-horizon solution can describe the near-horizon region of several global solutions whose global charges are different. We will find both situations in the following papers.

Another way to obtain the algebraic relations of the parameters k, v_i, q_i, and u is by using the entropy function formalism proposed in [79, 86].

To introduce this formalism, first we must define the function $f(k, v_1, v_2, v_3, q_1, q_2, u)$, which is the Lagrangian density $\sqrt{-g}\mathcal{L}$ evaluated for the near-horizon geometry (3.25) and potential (3.26) and integrated over the angular coordinates,

$$f(k, v_1, v_2, v_3, q_1, q_2, u) = \int d\theta_1 \dots d\theta_{N-1} d\varphi_1 \dots d\varphi_N \sqrt{-g}\mathcal{L} . \tag{3.27}$$

Note that f is a function of the near-horizon geometry parameters. Variations with

respect these parameters should give us constraints equivalent to those from field equations

$$\frac{\partial f}{\partial v_i} = 0,\ i = 1, 2, 3\ , \quad \frac{\partial f}{\partial q_2} = 0\ , \quad \frac{\partial f}{\partial u} = 0\ . \tag{3.28}$$

Variations with respect the other parameters do not vanish

$$\frac{\partial f}{\partial k} = 2\bar{J}\ , \quad \frac{\partial f}{\partial q_1} = \bar{Q}\ . \tag{3.29}$$

Variations with respect to these parameters are related to the conservation of the angular momentum and electric charge respectively. In fact, in most of the near-horizon calculations, the parameters $\bar{J}$ and $\bar{Q}$ are precisely J and Q. But this is not true in the presence of Chern-Simons terms, where the invariance of the Lagrangian under global gauge transformations is broken. In this case, it is not safe to use these variation equations to calculate the conserved charges. Use of the Noether charges will give the correct result [81].

The entropy function is obtained by taking the Legendre transform of the above integral with respect to the parameter k and with respect to the parameter q_1

$$\begin{aligned} &\mathcal{E}(j, k, q, q_1, q_2, v_1, v_2, v_3, u) = \\ &2\pi \left[N\bar{J}k + \bar{Q}q_1 - f(k, v_1, v_2, v_3, q_1, q_2, u) \right]\ . \end{aligned} \tag{3.30}$$

Then the entropy associated with the black holes can be calculated by evaluating this function at the extremum, $S = \mathcal{E}_{extremum}$.

3.4.3 Example: Kaluza-Klein EMd solution in 5D ($J_1 = J_2$)

Here we will present an example of near-horizon solutions in the Einstein-Maxwell-dilaton theory. In [75] exact solutions of rotating black holes in D dimensions are constructed. One starts with Myers-Perry in $D + 1$ dimensions, where a boost to the time and the additional coordinate is performed. Then, reducing to D dimensions by a Kaluza-Klein compactification, a full family of Einstein-Maxwell-dilaton black holes can be obtained. Let us consider the $D = 5$ case. The action of these solutions can be written as:

$$I = \int d^5x\sqrt{-g}\Big[R - \frac{1}{2}\partial_\mu\Phi\,\partial^\mu\Phi - \frac{1}{4}e^{-2h\Phi}F_{\mu\nu}F^{\mu\nu}\Big], \tag{3.31}$$

with $h = \sqrt{\frac{2}{3}}$.

We consider the case in which $J_1 = J_2$. The metric components of the Kaluza-Klein black hole are, after reducing to 5 dimensions

$$g_{tt} = \kappa^{2/3}(-1 + \frac{m\cosh(\alpha)^2}{\Sigma} - \kappa^2 A_t^2) \ , \tag{3.32}$$

$$g_{t\varphi_1} = \kappa^{2/3}(-\frac{ma\cosh(\alpha)^2\sin(\theta)^2}{\Sigma} - \kappa^2 A_t A_{\varphi_1}) \ , \tag{3.33}$$

$$g_{t\varphi_2} = \kappa^{2/3}(-\frac{ma\cosh(\alpha)^2\cos(\theta)^2}{\Sigma} - \kappa^2 A_t A_{\varphi_2}) \ , \tag{3.34}$$

$$g_{rr} = \kappa^{2/3}\frac{\Sigma r^2}{\Delta} \ , \tag{3.35}$$

$$g_{\theta\theta} = \kappa^{2/3}\Sigma \ , \tag{3.36}$$

$$g_{\varphi_1\varphi_1} = \kappa^{2/3}(\frac{ma^2\sin(\theta)^4}{\Sigma} + \Sigma\sin(\theta)^2 - \kappa^2 A_{\varphi_1}^2) \ , \tag{3.37}$$

$$g_{\varphi_1\varphi_2} = \kappa^{2/3}(\frac{ma^2\sin(\theta)^2\cos(\theta)^2}{\Sigma} - \kappa^2 A_{\varphi_1} A_{\varphi_2}) \ , \tag{3.38}$$

$$g_{\varphi_2\varphi_2} = \kappa^{2/3}(\frac{ma^2\cos(\theta)^4}{\Sigma} + \Sigma\cos(\theta)^2 - \kappa^2 A_{\varphi_2}^2) \ , \tag{3.39}$$

$$\tag{3.40}$$

where

$$\Sigma = r^2 + a^2 \ , \tag{3.41}$$

$$\kappa = \sqrt{1 + \frac{m\sinh(\alpha)^2}{r^2+a^2}} \ , \tag{3.42}$$

$$\Delta = (r^2+a^2)^2 - mr^2 \ , \tag{3.43}$$

$$A_t = \frac{m\cosh(\alpha)\sinh(\alpha)}{(1+\frac{m\sinh(\alpha)}{r^2+a^2})(r^2+a^2)} \ , \tag{3.44}$$

$$A_{\varphi_1} = -\frac{ma\sinh(\alpha)\sin(\theta)^2}{(1+\frac{m\sinh(\alpha)}{r^2+a^2})(r^2+a^2)} \ , \tag{3.45}$$

$$A_{\varphi_2} = -\frac{ma\sinh(\alpha)\cos(\theta)^2}{(1+\frac{m\sinh(\alpha)}{r^2+a^2})(r^2+a^2)} \ . \tag{3.46}$$

$$\tag{3.47}$$

The gauge vector is given by

$$A = A_t dt + A_{\varphi_1} d\varphi_1 + A_{\varphi_2} d\varphi_2 \ . \tag{3.48}$$

The dilaton is

$$\Phi = -\frac{2}{3}\sqrt{6}\ln(\sqrt{1 + \frac{m\sinh(\alpha)}{r^2+a^2}}) \ . \tag{3.49}$$

We have three free parameters m, α, and a, related to the mass, angular momentum, and charge. The radius of the horizon is found at

$$\frac{1}{g_{rr}} = 0 \to (r_h^2 + a^2)^2 - m r_h^2 = 0 \ . \tag{3.50}$$

The extremal case is obtained when $m = 4a^2$. The radius of the horizon in the extremal case is $r_h = a$. In the following we will consider only the extremal case.

The near-horizon limit is obtained first by moving to a corrotating frame, where the appropriate coordinates for the near-horizon geometry can be defined.

If the Killing horizon generator is the vector $\chi = \partial_t + \Omega(\partial_{\varphi_1} + \partial_{\varphi_2})$, then at $r = a$ we have $\chi^2 = 0$, and $\Omega = \frac{e^\alpha}{a(e^{2\alpha}+1)}$.

To move into the corrotating frame we shift the angular coordinates some multiple of the time coordinate: $d\varphi_1 \to d\varphi_1 - \Omega dt$, $d\varphi_2 \to d\varphi_2 - \Omega dt$. In the corrotating frame, the temporal Killing is the generator of the Killing horizon, $\chi = \partial_t$ with $\chi^2|_{r=a} = 0$. Once on the corrotating frame, we apply another change of coordinates:

$$r = (\Lambda y + a) \ , \tag{3.51}$$

$$dt = \frac{a_0}{\Lambda} dT + (a_2/r^2 + a_1/r) dr \ , \tag{3.52}$$

$$d\varphi_1 = d\bar{\varphi}_1 + b/r dr \ , \tag{3.53}$$

$$d\varphi_1 = d\bar{\varphi}_1 + c/r dr \ . \tag{3.54}$$

$$\tag{3.55}$$

Coefficients a_1, a_2, b, and c can be chosen in order to avoid undesired divergences in the metric functions once the near-horizon limit is approached. In our particular case, we can choose $a_1 = a_2 = b = c = 0$. The parameter a_0 is some scaling that we can choose conveniently to simplify some expressions.

Once we have the metric, gauge potential, and dilaton transformed, we make a series expansion in Λ, keeping always up to first order in the expansion. The result for the metric components is the following:

$$g_{TT} = a_0^2 \frac{2^{5/3} e^{10\alpha/3}}{a^2 (e^{4\alpha}+1)(e^{2\alpha}+1)^2} y^2 + O(\Lambda) \ , \tag{3.56}$$

$$g_{T\bar{\varphi}_1} = a_0 \frac{2^{2/3} e^{\alpha/3}(e^{2\alpha}+1)}{(e^{4\alpha}+1)^{2/3}} \sin(\theta)^2 y + O(\Lambda) \ , \tag{3.57}$$

$$g_{T\bar{\varphi}_2} = a_0 \frac{2^{2/3} e^{\alpha/3}(e^{2\alpha}+1)}{(e^{4\alpha}+1)^{2/3}} \cos(\theta)^2 y + O(\Lambda) \ , \tag{3.58}$$

$$g_{yy} = \frac{1}{4}2^{2/3}a^2e^{-2\alpha/3}(e^{4\alpha}+1)^{1/3}y^{-2} + O(\Lambda)\ , \tag{3.59}$$

$$g_{\theta\theta} = a^2 2^{2/3}(\frac{e^{4\alpha}+1}{e^{2\alpha}})^{2/3} + O(\Lambda)\ , \tag{3.60}$$

$$g_{\bar{\varphi}_1\bar{\varphi}_1} = a^2 2^{2/3}(e^{4\alpha}+2\sin(\theta)^2e^{2\alpha}+1)\frac{e^{-2\alpha/3}}{(e^{4\alpha}+1)^{2/3}}\sin(\theta)^2 + O(\Lambda)\ , \tag{3.61}$$

$$g_{\bar{\varphi}_1\bar{\varphi}_2} = a^2 2^{5/3}\frac{e^{4\alpha/3}}{(e^{4\alpha}+1)^{2/3}}\sin(\theta)^2\cos(\theta)^2 + O(\Lambda)\ , \tag{3.62}$$

$$g_{\bar{\varphi}_2\bar{\varphi}_2} = a^2 2^{2/3}(e^{4\alpha}+2\cos(\theta)^2e^{2\alpha}+1)\frac{e^{-2\alpha/3}}{(e^{4\alpha}+1)^{2/3}}\cos(\theta)^2 + O(\Lambda)\ . \tag{3.63}$$

For the gauge potential we have:

$$\begin{aligned} A = a_0\left(\frac{2\sinh(\alpha)e^{\alpha}}{e^{2\alpha}+1}\frac{1}{\Lambda} - \frac{4\sinh(\alpha)e^{3\alpha}}{a(e^{4\alpha}+1)(e^{2\alpha}+1)}y\right)dT \\ -\frac{2a\sinh(\alpha)}{1+2\sinh(\alpha)^2}\left(\sin(\theta)^2d\bar{\varphi}_1+\cos(\theta)^2d\bar{\varphi}_2\right) + O(\Lambda)\ . \end{aligned} \tag{3.64}$$

For the dilaton we simply have:

$$\Phi = -\frac{2}{3}\sqrt{6}\ln(\sqrt{1+2\sinh(\alpha)^2})\ . \tag{3.65}$$

Note that there is a divergent term in the A_T component. We can eliminate this divergence by an appropriate gauge transformation $A \to A + \partial_\mu f dx^\mu$.

$$\partial_\mu f = -a_0(\frac{2\sinh(\alpha)e^{\alpha}}{e^{2\alpha}+1}\frac{1}{\Lambda})\ . \tag{3.66}$$

We can always parametrize the near-horizon geometry with the Ansatz

$$ds^2 = v_1(\frac{dr^2}{r^2} - r^2dt^2) + \frac{v_2}{4}(\sigma_1^2+\sigma_2^2) + \frac{v_2v_3}{4}(\sigma_3+2krdt)^2\ , \tag{3.67}$$

where $\sigma_1 = \cos\psi d\bar{\theta} + \sin\psi\sin\bar{\theta}d\phi$, $\sigma_2 = -\sin\psi d\bar{\theta} + \cos\psi\sin\bar{\theta}d\phi$, $\sigma_3 = d\psi + \cos\bar{\theta}d\phi$ and $2\theta = \bar{\theta}$, $\varphi_2 - \varphi_1 = \phi$, $\varphi_1 + \varphi_2 = \psi$. And for the electromagnetic potential we have

$$A_\mu dx^\mu = q_1 r dt + q_2\sin^2\theta\,(d\varphi_1 - krdt) + q_2\cos^2\theta\,(d\varphi_2 - krdt)\,. \tag{3.68}$$

Now let us identify the coordinates of this Ansatz with the near-horizon coordinates we have used $T = t$, $y = r$, $\theta = \theta$, $\varphi_1 = \bar{\varphi}_1$, $\varphi_2 = \bar{\varphi}_2$. We fix the coefficient $a_0 = \frac{1}{2}a^2(e^{\alpha}+e^{-\alpha})$. Then we can write identify the Ansatz parametrization with the

near-horizon limit of the Kaluza-Klein black hole

$$v_1 = \frac{1}{4} 2^{2/3} a^2 (e^{2\alpha} + e^{-2\alpha})^{1/3} \ , \tag{3.69}$$

$$v_2 = 4 v_1 \ , \tag{3.70}$$

$$v_3 = \frac{(e^{2\alpha}+1)^2}{e^{4\alpha}+1} \ , \tag{3.71}$$

$$k = 1/2 \ , \tag{3.72}$$

$$q_1 = 0 \ , \tag{3.73}$$

$$q_2 = \frac{2a \sinh(\alpha)}{1 + 2\sinh(\alpha)^2} \ , \tag{3.74}$$

$$u = -\frac{2}{3}\sqrt{6} \ln(\sqrt{1 + 2\sinh(\alpha)^2}) \ . \tag{3.75}$$

The angular momentum and electric charge can be calculated and yield

$$J = 16\pi^2 a^3 \cosh(\alpha) \ , \tag{3.76}$$

$$Q = 16\pi^2 a^2 \cosh(\alpha)\sinh(\alpha) \ . \tag{3.77}$$

The area of the black hole horizon satisfies the interesting relation $A_{\rm H} = J/2$.

3.5 Results on Einstein-Maxwell-dilaton black holes

Here we will present the results on Einstein-Maxwell-dilaton black holes. This is the topic of the papers Physics Letters B **727** (2013) 340-344 [5] (included in the following section 3.5.1) and Physical Review D **89** (2014) 024038 [6] (included in the following section 3.5.2). The main results can be summarized as follows:

- We study odd-dimensional black holes, with event horizon of spherical topology, and consider equal magnitude angular momenta. These black holes are generalizations of the Reissner-Nordström and Myers-Perry solutions, meaning that in principle they can have arbitrary values of the electric charge and angular momentum. The value of the Higgs coupling parameter is also free.

- In the Einstein-Maxwell case, that is, when there is no dilaton field, two distinct branches appear when extremal black holes are considered. One of them emerges from the Myers-Perry solution (MP branch). This branch is composed of charged generalizations of the Myers-Perry solution. The second branch is composed by rotating generalizations of the Reissner-Nordström solution (RN branch). Both branches meet at a certain non-singular configuration.

- In the MP branch, the area is proportional to the angular momentum. The charge does not enter into the relation. Hence the entropy is independent of the charge. On the other hand, the horizon angular momentum is dependent on both the angular momentum and the charge.

- In the RN branch, the area depends on the angular momentum and the charge. But the horizon angular velocity is proportional to the angular momentum. Hence, there is a switch in the behavior of the area with the horizon angular momentum between the MP branch and the RN branch.

- These results have been obtained both using numerical methods (for the full solution), and using the near-horizon formalism (where only the near-horizon geometry can be studied). Nevertheless, in the near-horizon formalism, there are solutions to the equations that are not found globally. Hence we conclude that not all the near-horizon solutions correspond to global solutions. The branch of non-physical near-horizon solutions is connected to the branch of physical ones.

- When a dilaton field is included, for arbitrary values of the dilaton coupling, the two branch structure is lost. There is only one branch of solutions that

corresponds to the MP branch. These solutions have entropy proportional to the angular momentum, with independence of the charge.

- The boundary of the domain of existence of these black holes is composed by extremal black holes. We plot this boundary by scaling the different parameters of the black holes to the mass. There is a certain duality between the scaled angular velocity for extremal black holes, and the surface gravity for the static black holes, when these quantities are plotted as a function of the scaled charge of the black holes. A similar relation is found between the scaled area of static configurations and the scaled angular momentum of extremal black holes. The approximate similarity of these relations becomes an equality in the case of Kaluza-Klein black holes (when the value of the dilaton coupling becomes $h_{KK} = \sqrt{\frac{D-1}{2(D-2)}}$). Note that these Kaluza-Klein black holes are known analytically, and we have used them to test our numerical results.

3.5.1 Publication: Jose Luis Blázquez-Salcedo, Jutta Kunz, and Francisco Navarro-Lérida, *Angular momentum – area – proportionality of extremal charged black holes in odd dimensions*, Physics Letters B 727 (2013) 340–344

Physics Letters B 727 (2013) 340–344

Contents lists available at ScienceDirect

Physics Letters B

www.elsevier.com/locate/physletb

Angular momentum – area – proportionality of extremal charged black holes in odd dimensions

Jose Luis Blázquez-Salcedo [a], Jutta Kunz [b], Francisco Navarro-Lérida [c,*]

[a] Dept. de Física Teórica II, Ciencias Físicas, Universidad Complutense de Madrid, E-28040 Madrid, Spain
[b] Institut für Physik, Universität Oldenburg, Postfach 2503, D-26111 Oldenburg, Germany
[c] Dept. de Física Atómica, Molecular y Nuclear, Ciencias Físicas, Universidad Complutense de Madrid, E-28040 Madrid, Spain

ARTICLE INFO

Article history:
Received 6 September 2013
Received in revised form 16 October 2013
Accepted 18 October 2013
Available online 23 October 2013
Editor: M. Cvetič

ABSTRACT

Extremal rotating cohomogeneity-1 black holes in Einstein–Maxwell theory feature two branches. On the branch emerging from the Myers–Perry solutions their angular momentum is proportional to their horizon area, while on the branch emerging from the Tangherlini solutions their angular momentum is proportional to their horizon angular momentum. The transition between these branches occurs at a critical value of the charge, which depends on the value of the angular momentum. However, when a dilaton is included, the angular momentum is always proportional to the horizon area.

1. Introduction

Although in $D = 4$ dimensions the Kerr–Newman solution represents the unique family of stationary asymptotically flat black holes of Einstein–Maxwell (EM) theory, the corresponding $D > 4$ charged rotating black holes have not been obtained in closed form yet. Only certain subsets are known: the generalization of the static black hole to higher dimensions pioneered by Tangherlini [1], and the rotating vacuum black holes, obtained by Myers and Perry (MP) [2]. Other subsets could be constructed perturbatively [3–7] and numerically [8,9].[1]

Nevertheless, if additional fields and/or interactions are allowed into the theory, exact higher dimensional charged rotating black holes can be obtained by solution generating techniques. For example, in the simplest Kaluza–Klein (KK) case, a boost is done to the $D+1$ embedding of the uncharged D-dimensional MP black holes along the extra dimension. After dimensional reduction the result is a charged D-dimensional black hole in Einstein–Maxwell-dilaton (EMd) theory. The dilaton coupling constant h for this solution has a particular value, which we denote $h_{\rm KK}$, that depends on the dimension D [10]. To generate rotating EMd black hole solutions with other values of the coupling constant h, currently perturbative or numerical techniques must be used.

D-dimensional stationary black holes possess, in general, N independent angular momentum J_i associated with N orthogonal planes of rotation [2], where N is the integer part of $(D-1)/2$, corresponding to the rank of the rotation group $SO(D-1)$. As a result, we can distinguish between odd-D and even-D black holes, where the latter have an unpaired spatial coordinate [2]. In the particular case in which all N angular momenta are equal in magnitude, the EMd equations simplify considerably, yielding, for odd dimensions, cohomogeneity-1 equations from which the angular dependence can be extracted analytically. Hence, the equations reduce to a more tractable system of ordinary differential equations.

When the N angular momenta are of equal magnitude, $J = |J_i|$, it is interesting to note that, for extremal MP black holes, the angular momentum J and the horizon area $A_{\rm H}$ are proportional: $J = \sqrt{2(D-3)}A_{\rm H}$. This is a special case of a more general type of relations for MP black holes in terms of the non-degenerate inner and outer horizon areas of non-extremal black holes [11], and was pointed out in 4 dimensions before [12–18]. In the case of charged black holes, the relation for the product of the horizon areas can be typically written as a sum between the squares of the angular momentum and some power of the charge [11–19]. In this context, several inequalities between angular momenta, area, electric charge and magnetic fluxes were studied for axisymmetric stably outer marginally trapped surfaces, for EMd theory in 4 dimensions [20], and in 5 dimensions [21].

In this Letter we study relations between area, angular momentum and charge for extremal EM and EMd black holes with equal angular momenta. We construct the global solutions numerically and local solutions in the near horizon formalism. The EM case is special since two different branches of charged extremal solutions exist. One branch emerges from the uncharged MP black holes, and the other branch emerges from the static Tangherlini black holes. The area relations are different on each branch: the first branch

* Corresponding author.
E-mail address: fnavarro@fis.ucm.es (F. Navarro-Lérida).

[1] In this Letter we will consider only asymptotically flat black holes with spherical horizon topology.

0370-2693/$ – see front matter
http://dx.doi.org/10.1016/j.physletb.2013.10.046

retains the proportionality between the angular momentum and the area of the MP solutions. Thus the area of these charged black holes is independent of the charge. In contrast, the second branch exhibits a proportionality between the angular momentum and the horizon angular momentum, while the charge enters into the area relation yielding $A_H^2 = C_1 J^2 Q^{-3/2} + C_2 Q^{3/2}$, where C_1 and C_2 are some constants and Q is the electric charge. However, as soon as the dilaton is coupled, the branch structure changes, and only a single branch – similar to the first branch of the EM case – is found. Again along this branch the proportionality between the angular momentum and the area persists for all extremal solutions. We will proceed by first presenting the $D = 5$ results and then discussing their generalization to odd $D > 5$ dimensions.

2. 5D EMd near horizon solutions

In 5 dimensions, the EMd action can be written as

$$I = \int d^5x \sqrt{-g}\mathcal{L} = \int d^5x \sqrt{-g}\left[R - \frac{1}{2}\partial_\mu\phi\partial^\mu\phi - \frac{1}{4}e^{-2h\phi}F_{\mu\nu}F^{\mu\nu}\right], \quad (1)$$

where R is the curvature scalar, ϕ the scalar dilaton field, h the dilaton coupling constant and $F_{\mu\nu} = \partial_\mu A_\nu - \partial_\nu A_\mu$ the field strength tensor, where A_μ denotes the gauge vector potential. The units have been chosen so that $16\pi G = 1$, G being Newton's constant. If we set $h = 0$, the pure EM action is recovered, while $h_{KK} = \sqrt{\frac{2}{3}}$ is the KK value.

For cohomogeneity-1 solutions the isometry group is enhanced from $\mathcal{R} \times U(1)^2$ to $\mathcal{R} \times U(2)$, where $\mathcal{R}$ represents time translations. This symmetry enhancement allows to factorize the angular dependence and thus leads to ordinary differential equations.

Following the near horizon formalism [22,23], we now obtain exact near horizon solutions for these extremal EM and EMd black holes. In terms of the left-invariant 1-forms $\sigma_1 = \cos\psi\, d\bar\theta + \sin\psi\sin\bar\theta\, d\varphi$, $\sigma_2 = -\sin\psi\, d\bar\theta + \cos\psi\sin\bar\theta\, d\varphi$, and $\sigma_3 = d\psi + \cos\bar\theta\, d\varphi$, the near horizon metric can be written as

$$ds^2 = v_1\left(\frac{dr^2}{r^2} - r^2 dt^2\right) + \frac{v_2}{4}(\sigma_1^2 + \sigma_2^2) + \frac{v_2 v_3}{4}(\sigma_3 + 2kr\, dt)^2, \quad (2)$$

where we have defined $2\theta = \bar\theta$, $\varphi_2 - \varphi_1 = \varphi$, $\varphi_1 + \varphi_2 = \psi$, $\theta \in [0, \pi/2]$, $(\varphi_1, \varphi_2) \in [0, 2\pi]$. The horizon is located at $r = 0$, which can always be achieved via a transformation $r \to r - r_H$. Note, that the metric is written in a co-rotating frame.

The metric corresponds to a rotating squashed $AdS_2 \times S^3$ spacetime, describing the neighborhood of the event horizon of an extremal black hole. The corresponding Ansatz for the gauge potential in the co-rotating frame reads

$$A_\mu\, dx^\mu = q_1 r\, dt + q_2 \sin^2\theta(d\varphi_1 - kr\, dt) + q_2\cos^2\theta(d\varphi_2 - kr\, dt). \quad (3)$$

The dilaton field is simply given by $\phi = u$. The parameters k, v_i, q_i and u are constants, and satisfy a set of algebraic relations, which can be obtained, according to [22,23], in the following way.

Evaluating the Lagrangian density $\sqrt{-g}\mathcal{L}$ for the near horizon geometry (2) and integrating over the angular coordinates yields the function f,

$$f(k, v_1, v_2, v_3, q_1, q_2, u) = \int d\theta\, d\varphi_1\, d\varphi_2\, \sqrt{-g}\mathcal{L}, \quad (4)$$

from which the field equations follow. In particular, the derivatives of f with respect to the parameters vanish except for

$$\frac{\partial f}{\partial k} = 2J, \qquad \frac{\partial f}{\partial q_1} = Q, \quad (5)$$

where J is the total angular momentum and Q is the charge. From these equations a set of algebraic relations for the near horizon expressions (2), (3) is obtained.

The entropy function is obtained by taking the Legendre transform of the above integral with respect to the parameter k, associated with both angular momenta, $J_1 = J_2 = J$, and with respect to the parameter q_1, associated with the charge Q,

$$\mathcal{E}(J, k, Q, q_1, q_2, v_1, v_2, v_3, u) = 2\pi\big(2Jk + Q q_1 - f(k, v_1, v_2, v_3, q_1, q_2, u)\big). \quad (6)$$

Then the entropy associated with the black holes can be calculated by evaluating this function at the extremum, $S = \mathcal{E}_{extremal}$.

The horizon angular momenta $J_{H(k)}$ of the black holes are obtained from the Komar expressions associated with the corresponding Killing vector fields $\eta_{(k)} \equiv \partial_{\varphi_k}$

$$J_{H(k)} = \int_{\mathcal{H}} \beta_{(k)}, \quad (7)$$

where $\mathcal{H}$ represents the surface of the horizon and $\beta_{(k)\mu_1\mu_2\mu_3} \equiv \epsilon_{\mu_1\mu_2\mu_3\rho\sigma}\nabla^\rho\eta^\sigma_{(k)}$. Note that $J_{H(1)} = J_{H(2)} \equiv J_H$, since we are considering solutions with equal angular momenta.

For the discussion of the solutions we need to consider the EM and the EMd case separately. In the EM case, i.e. for $h = 0$, the system of equations yields two distinct solutions, depending on two parameters. These two solutions of the near horizon geometry have been found independently by Kunduri and Lucietti in [24].[2] Here we now calculate the charges and entropies associated with these two branches. The solution containing the MP limit, and thus the first branch, has $v_2 = 4v_1$, $v_3 = 2 - \frac{q_2^2}{v_1}$, $q_1 = 0$, $k = \frac{1}{2}$ and

$$J = 32\pi^2 v_1\sqrt{2v_1 - q_2^2}, \qquad Q = -32\pi^2 q_2\sqrt{2v_1 - q_2^2},$$
$$S = 2\pi J, \qquad J_H = 16\pi^2(2v_1 - q_2^2)^{3/2}, \quad (8)$$

while the solution containing the Tangherlini limit, and thus the second branch, has $v_2 = 4v_1$, $v_3 = \frac{1}{4k^2+1}$, $q_1 = -\frac{(2k+1)(2k-1)\sqrt{3}}{2} \times \sqrt{\frac{|v_1|}{4k^2+1}}$, $q_2 = -2\sqrt{3}k\sqrt{\frac{|v_1|}{4k^2+1}}$ and

$$J = 128\pi^2 k\left(\frac{|v_1|}{4k^2+1}\right)^{3/2}, \qquad Q = 32\sqrt{3}\pi^2\frac{v_1}{4k^2+1},$$
$$S = 64\pi^3\frac{|v_1|^{3/2}}{\sqrt{4k^2+1}}, \qquad J_H = J/4, \quad (9)$$

where J_H is the horizon angular momentum. The two solutions match at $k = 1/2$, where $q_1 = 0$. At this critical point the angular momentum can be written as

$$J = \frac{1}{2\sqrt{2}\pi}\frac{1}{3^{3/4}}Q^{3/2}. \quad (10)$$

Thus we have the surprising result that along the first branch, the proportionality of the angular momentum and the area known for the MP black holes, continues to hold in the presence of charge until the critical point is reached. In contrast, on the second branch we have proportionality of the angular momentum and the horizon angular momentum.

[2] We thank Hari Kunduri for pointing this out to us.

In the case of the EMd black holes, only one solution is found. It can be obtained by replacing $q_2 \to q_2 e^{-hu}$, $\bar{Q} = Q\, e^{hu}$ in the first branch solution of the EM case. Hence, as long as $h \neq 0$, the angular momentum and the area are always proportional, independent of h and Q. In particular, this includes the KK case, where the full solution is known analytically.

3. 5*D* EMd black hole solutions

We now need to consider the full solutions, which we obtain by numerical integration. For the metric we employ the parametrization

$$\begin{aligned} ds^2 = &-f\,dt^2 + \frac{m}{f}\left(dr^2 + r^2\,d\theta^2\right) + \frac{n}{f} r^2 \sin^2\theta \left(d\varphi - \frac{w}{r}\,dt\right)^2 \\ &+ \frac{n}{f} r^2 \cos^2\theta \left(d\psi - \frac{w}{r}\,dt\right)^2 \\ &+ \frac{m-n}{f} r^2 \sin^2\theta \cos^2\theta (d\varphi - d\psi)^2, \end{aligned} \tag{11}$$

for the gauge potential we use

$$A_\mu\,dx^\mu = a_0\,dt + a_k\left(\sin^2\theta\,d\varphi + \cos^2\theta\,d\psi\right), \tag{12}$$

while the dilaton field is described by the function $\phi(r)$.

The resulting set of coupled ODEs then consists of first order differential equations for a_0 and n, and second order differential equations for f, m, n, ω, a_k and ϕ. The equation for a_0 allows to eliminate this function from the system.

To obtain asymptotically flat solutions, the metric functions should satisfy the following set of boundary conditions at infinity, $f|_{r=\infty} = m|_{r=\infty} = n|_{r=\infty} = 1$, $\omega|_{r=\infty} = 0$. For the gauge potential we choose a gauge such that $a_0|_{r=\infty} = a_\varphi|_{r=\infty} = 0$. For the dilaton field we choose $\phi|_{r=\infty} = 0$, since we can always make a transformation $\phi \to \phi - \phi|_{r=\infty}$.

In isotropic coordinates the horizon is located at $r_{\rm H} = 0$. An expansion at the horizon yields $f(r) = f_4 r^4 + f_\alpha r^\alpha + o(r^6)$, $m(r) = m_2 r^2 + m_\beta r^\beta + o(r^4)$, $n(r) = n_2 r^2 + n_\gamma r^\gamma + o(r^4)$, $\omega(r) = \omega_1 r + \omega_2 r^2 + o(r^3)$, $a_0(r) = a_{0,0} + a_{0,\lambda} r^\lambda + o(r^2)$, $a_k(r) = a_{k,0} + a_{k,\mu} r^\mu + o(r^2)$, $\phi(r) = \phi_0 + \phi_\nu r^\nu + o(r^2)$. Interestingly, the coefficients α, β, γ, λ, μ and ν are non-integer. Only ω has an integer expansion.

To construct the solutions numerically, we employ a compactified radial coordinate, $x = r/(r+1)$. We then reparametrize the metric in terms of the functions $f = \hat{f} x^2$, $m = \hat{m}$, $n(r) = \hat{n}$, $\omega(r) = \hat{\omega}(1-x)^2$, $a_k = \hat{a}_k/x^2$, and $\phi = \hat{\phi}/x^2$ to properly deal with the non-integer coefficients in the horizon expansion, eliminating possible divergences in the integration of the functions.

We employ a collocation method for boundary-value ordinary differential equations, equipped with an adaptive mesh selection procedure [25]. Typical mesh sizes include 10^3–10^4 points. The solutions have a relative accuracy of 10^{-10}. The estimates of the relative errors of the global charges and other physical quantities are of order 10^{-6}.

Fig. 1 exhibits the ratios $J/A_{\rm H}$ and $J/J_{\rm H}$ versus the charge Q/M for extremal 5*D* EM ($h = 0$) and KK ($h = h_{\rm KK}$) black holes. It clearly reveals the two branches of the extremal EM solutions, together with their matching point. This is in contrast to the single branch of the EMd solutions, shown here for the KK case.

We exhibit in Fig. 2 the domain of existence of the EM and EMd black holes for dilaton coupling constants $h = 0$, 2, 0.5 and $h_{\rm KK}$. Here we display the area $A_{\rm H}/M^{3/2}$ versus the charge Q/M for extremal and static 5*D* black holes. All black holes of the respective theories can be found within these boundaries. Again we note the different structure for the EM case. The EM static extremal solution has finite area, whereas for $h \neq 0$ the static extremal solution is singular with vanishing area.

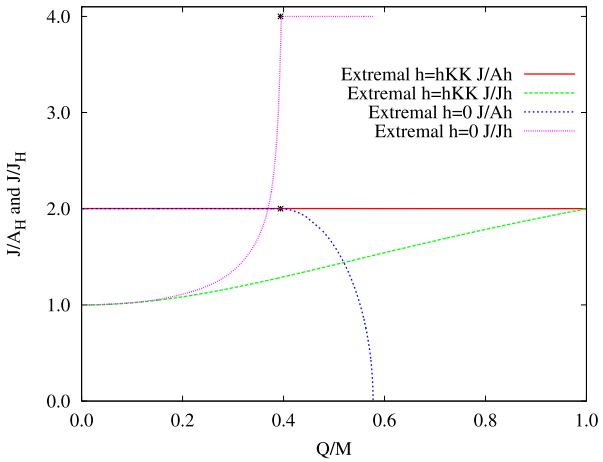

Fig. 1. The ratios $J/A_{\rm H}$ and $J/J_{\rm H}$ are shown versus the charge Q/M for extremal 5*D* EM ($h = 0$) and KK ($h = h_{\rm KK}$) black holes. The asterisks mark the matching point of the two EM branches.

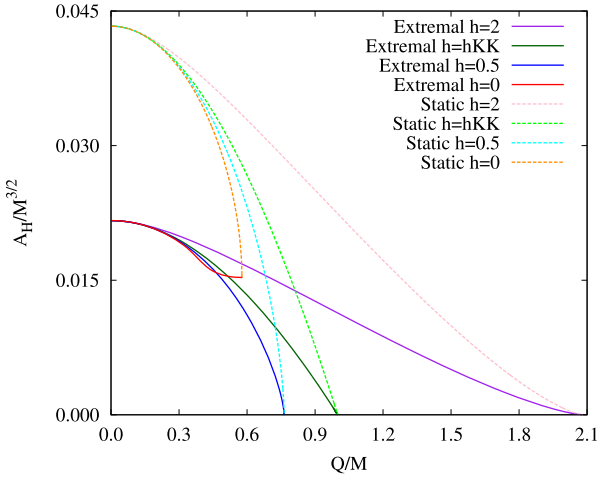

Fig. 2. The area $A_{\rm H}/M^{3/2}$ is shown versus the charge Q/M for extremal and static 5*D* black holes for $h = 0$, 0.5, $h_{\rm KK}$ and 2.

4. EMd black holes in odd $D > 5$

In a straightforward generalization the near horizon solutions can be constructed for arbitrary odd dimensions $D > 5$. In the EM case we retain two branches of solutions, the MP branch with

$$J = \sqrt{2(D-3)}\,A_{\rm H}, \tag{13}$$

and the Tangherlini branch with

$$J = (D-1)\,J_{\rm H}. \tag{14}$$

In the EMd case the near horizon solutions possess only a single branch corresponding to the first branch, with $J = \sqrt{2(D-3)}A_{\rm H}$.

We have performed the respective set of numerical calculations in 7*D* and in 9*D*, and obtained results that are analogous to the 5*D* case.

5. Comparison with other theories

Let us now compare these results with those of two theories whose extremal black holes also exhibit a branch structure

with two distinct branches: the rotating dyonic black holes of 4-dimensional KK theory [26], and the 5-dimensional black holes of Einstein–Maxwell–Chern–Simons (EMCS) theory (minimal $D = 5$ supergravity) [27].

In the first example the 4-dimensional black holes are characterized by their mass M, angular momentum J, electric charge Q and magnetic charge P.[3] In the extremal case, only three of these charges are independent and two distinct surfaces, **S** and **W**, are found. The restriction to $P = Q$ then yields two distinct branches. The **S** branch, $J > PQ$, emerges from the extremal Kerr solution, and presents all the normal characteristics of charged rotating solutions, such as an ergo-region and non-zero angular velocity. On the other hand, the **W** branch, $J < PQ$, possesses no ergo-region and has vanishing horizon angular velocity, although the angular momentum of the black holes along this branch does not vanish. At the matching point of both branches, $J = QP$, the horizon area is zero and the configuration is singular.

Nevertheless, the area-angular momentum relation for these extremal solutions can be written as

$$A_{\rm H}^2 = 64\pi^2 \left| J^2 - Q^2 P^2 \right|. \tag{15}$$

Note, that the electric and magnetic charges are entering the relation for both branches, and that the only difference in the area relation is an overall sign in the expression, depending on whether we are on the **S** ($J > PQ$) or on the **W** ($J < PQ$) branch.

The second example exhibits rather analogous features. Here we consider 5-dimensional black holes in EMCS theory for the supergravity value of the CS coupling constant, $\lambda = 1$ (in an appropriate parametrization). In the extremal case, when both angular momenta possess equal magnitude, the black holes are parametrized by the angular momentum J and the charge Q.[4] Again two branches of extremal black holes are present. The first branch has $J^2 > -\frac{4}{3\sqrt{3}\pi} Q^3$ and is the ordinary branch with an ergo-region, while the second branch has $J^2 < -\frac{4}{3\sqrt{3}\pi} Q^3$ and is ergo-region free with vanishing horizon angular momentum. The area-angular momentum relation for both branches reads

$$A_{\rm H}^2 = 64\pi^2 \left| J^2 + \frac{4}{3\sqrt{3}\pi} Q^3 \right|. \tag{16}$$

At the matching point of both branches the horizon area is again zero and the solution is singular, and again there is a change of sign in the area-angular momentum relation depending on the branch.

Thus in these cases, both charge and angular momentum are entering the area relation. Moreover, the relations (15) and (16) are in accordance with the general expressions obtained in [11], which also depend on both, the charges and the angular momenta.

6. Further remarks

It is interesting to note that for the extremal rotating black holes in EM theory with equal angular momenta, a branch structure with two distinct branches is found, where for one of the branches – the one emerging from the MP solution – the area is independent of the charge of the configuration. Along this branch of solutions, the area remains proportional to the angular momentum and the charge is not entering the relation. This is different from other charged black holes considered before.

However, once the critical extremal EM solution[5] is passed, the charge enters again into the area relation, yielding the expression

$$A_{\rm H} = C_1 J^2 Q^{-3/2} + \frac{1}{16 C_1} Q^{3/2}, \tag{17}$$

where $C_1 = \frac{3^{1/4}\pi}{\sqrt{2}}$ in our normalization.

In contrast to the two branches of global extremal EM black hole solutions, the two branches of EM near horizon solutions do not end at the critical solution. Thus a study of only near horizon solutions is insufficient to clarify the domain of existence of extremal solutions, as was first observed for the extremal dyonic black holes of $D = 4$ Gauß–Bonnet gravity [28].

Interestingly, in the general EMCS theory (with CS coupling constant $\lambda \neq 1$ [29,30]), there appear even more than two branches of extremal black holes for sufficiently large CS coupling [31]. As in the case discussed above, however, the area of these branches of rotating charged black holes always depends on both, the charge and the angular momentum.

Whereas the branch structure of these extremal black holes is very intriguing, their relation with the corresponding near horizon solutions is surprising as well. In particular, a given near horizon solution can correspond to (i) more than one global solution, (ii) precisely one global solution, or (iii) no global solution at all. It would be interesting to perform an analogous study for the general EMd theory (with dilaton coupling constant $h \neq h_{\rm KK}$ [32]), since the analogy between the known black holes of both theories suggests that a similar more complex branch structure would be present for sufficiently large dilaton coupling.

Acknowledgements

We would like to thank B. Kleihaus and E. Radu for helpful discussions. We gratefully acknowledge support by the Spanish Ministerio de Ciencia e Innovacion, research project FIS2011-28013, and by the DFG, in particular, the DFG Research Training Group 1620 “Models of Gravity”. J.L.B. was supported by the Spanish Universidad Complutense de Madrid.

References

[1] F.R. Tangherlini, Nuovo Cimento 27 (1963) 636.
[2] R.C. Myers, M.J. Perry, Ann. Phys. 172 (1986) 304.
[3] A.N. Aliev, V.P. Frolov, Phys. Rev. D 69 (2004) 084022, arXiv:hep-th/0401095.
[4] A.N. Aliev, Phys. Rev. D 74 (2006) 024011, arXiv:hep-th/0604207.
[5] F. Navarro-Lerida, Gen. Relativ. Gravit. 42 (2010) 2891, arXiv:0706.0591 [hep-th].
[6] M. Allahverdizadeh, J. Kunz, F. Navarro-Lerida, Phys. Rev. D 82 (2010) 024030, arXiv:1004.5050 [gr-qc].
[7] M. Allahverdizadeh, J. Kunz, F. Navarro-Lerida, Phys. Rev. D 82 (2010) 064034, arXiv:1007.4250 [gr-qc].
[8] J. Kunz, F. Navarro-Lerida, A.K. Petersen, Phys. Lett. B 614 (2005) 104, arXiv: gr-qc/0503010.
[9] J. Kunz, F. Navarro-Lerida, J. Viebahn, Phys. Lett. B 639 (2006) 362, arXiv: hep-th/0605075.
[10] J. Kunz, D. Maison, F. Navarro-Lerida, J. Viebahn, Phys. Lett. B 639 (2006) 95, arXiv:hep-th/0606005.
[11] M. Cvetic, G.W. Gibbons, C.N. Pope, Phys. Rev. Lett. 106 (2011) 121301, arXiv: 1011.0008 [hep-th].
[12] M. Ansorg, H. Pfister, Class. Quantum Gravity 25 (2008) 035009, arXiv: 0708.4196 [gr-qc].
[13] J. Hennig, M. Ansorg, C. Cederbaum, Class. Quantum Gravity 25 (2008) 162002, arXiv:0805.4320 [gr-qc].
[14] M. Ansorg, J. Hennig, Class. Quantum Gravity 25 (2008) 222001, arXiv: 0810.3998 [gr-qc].
[15] J. Hennig, C. Cederbaum, M. Ansorg, Commun. Math. Phys. 293 (2010) 449, arXiv:0812.2811 [gr-qc].

[3] Note that cohomogeneity-1 is not possible in this theory since it is an even-dimensional one.

[4] The asymmetry in the electric charge of the Chern–Simons term gives rise to different properties for solutions with opposite signs of the electric charge.

[5] Note, that in contrast to the critical solutions of the $4D$ EMd and $5D$ EMCS theories discussed above, the critical EM solution is not singular.

[16] M. Ansorg, J. Hennig, Phys. Rev. Lett. 102 (2009) 221102, arXiv:0903.5405 [gr-qc].
[17] J. Hennig, M. Ansorg, Ann. Henri Poincaré 10 (2009) 1075, arXiv:0904.2071 [gr-qc].
[18] M. Ansorg, J. Hennig, C. Cederbaum, Gen. Relativ. Gravit. 43 (2011) 1205, arXiv:1005.3128 [gr-qc].
[19] A. Castro, M.J. Rodriguez, Phys. Rev. D 86 (2012) 024008, arXiv:1204.1284 [hep-th].
[20] S.S. Yazadjiev, Phys. Rev. D 87 (2013) 024016, arXiv:1210.4684 [gr-qc].
[21] S. Yazadjiev, Class. Quantum Gravity 30 (2013) 115010, arXiv:1301.1548 [hep-th].
[22] D. Astefanesei, K. Goldstein, R.P. Jena, A. Sen, S.P. Trivedi, J. High Energy Phys. 0610 (2006) 058, arXiv:hep-th/0606244.
[23] K. Goldstein, R.P. Jena, J. High Energy Phys. 0711 (2007) 049, arXiv:hep-th/0701221.
[24] H.K. Kunduri, J. Lucietti, arXiv:1306.2517 [hep-th].
[25] U. Ascher, J. Christiansen, R.D. Russell, Math. Comput. 33 (1979) 659;
U. Ascher, J. Christiansen, R.D. Russell, ACM Trans. 7 (1981) 209.
[26] D. Rasheed, Nucl. Phys. B 454 (1995) 379, arXiv:hep-th/9505038.
[27] Z.W. Chong, M. Cvetic, H. Lu, C.N. Pope, Phys. Rev. Lett. 95 (2005) 161301, arXiv:hep-th/0506029.
[28] C.-M. Chen, D.V. Gal'tsov, D.G. Orlov, Phys. Rev. D 78 (2008) 104013, arXiv:0809.1720 [hep-th].
[29] J.P. Gauntlett, R.C. Myers, P.K. Townsend, Class. Quantum Gravity 16 (1999) 1, arXiv:hep-th/9810204.
[30] J. Kunz, F. Navarro-Lerida, Phys. Rev. Lett. 96 (2006) 081101, arXiv:hep-th/0510250.
[31] J.L. Blazquez-Salcedo, J. Kunz, F. Navarro-Lerida, E. Radu, arXiv:1308.0548 [gr-qc].
[32] B. Kleihaus, J. Kunz, F. Navarro-Lerida, Phys. Rev. D 69 (2004) 081501, arXiv:gr-qc/0309082.

3.5.2 Publication: Jose Luis Blázquez-Salcedo, Jutta Kunz, and Francisco Navarro-Lérida, *Properties of rotating Einstein-Maxwell-Dilaton black holes in odd dimensions*, Physical Review D 89 (2014) 024038

PHYSICAL REVIEW D **89,** 024038 (2014)

Properties of rotating Einstein-Maxwell-dilaton black holes in odd dimensions

Jose Luis Blázquez-Salcedo,[1] Jutta Kunz,[2] and Francisco Navarro-Lérida[3]

[1]*Departamento de Física Teórica II, Ciencias Físicas Universidad Complutense de Madrid, E-28040 Madrid, Spain*

[2]*Institut für Physik, Universität Oldenburg Postfach 2503, D-26111 Oldenburg, Germany*

[3]*Departamento de Física Atómica, Molecular y Nuclear, Ciencias Físicas Universidad Complutense de Madrid, E-28040 Madrid, Spain*

(Received 31 October 2013; published 28 January 2014)

We investigate rotating Einstein-Maxwell-dilaton (EMd) black holes in odd dimensions. Focusing on black holes with equal-magnitude angular momenta, we determine the domain of existence of these black holes. Nonextremal black holes reside with the boundaries determined by the static and the extremal rotating black holes. The extremal EMd black holes show proportionality of their horizon area and their angular momenta. Thus the charge does not enter. We also address the Einstein-Maxwell case, where the extremal rotating black holes exhibit two branches. On the branch emerging from the Myers-Perry solutions, their angular momenta are proportional to their horizon area, whereas on the branch emerging from the static solutions their angular momenta are proportional to their horizon angular momenta. Only subsets of the near-horizon solutions are realized globally. Investigating the physical properties of these EMd black holes, we note that one can learn much about the extremal rotating solutions from the much simpler static solutions. The angular momenta of the extremal black holes are proportional to the area of the static ones for the Kaluza-Klein value of the dilaton coupling constant, and remain analogous for other values. The same is found for the horizon angular velocities of the extremal black holes, which possess an analogous behavior to the surface gravity of the static black holes. The gyromagnetic ratio is rather well approximated by the "static" value, obtained perturbatively for small angular momenta.

DOI: 10.1103/PhysRevD.89.024038 PACS numbers: 04.50.Gh, 04.20.-q, 04.40.Nr, 04.50.-h

I. INTRODUCTION

Discovered in 1986 by Myers and Perry (MP) [1,2], the rotating higher-dimensional vacuum black holes have been generalized to include various types of matter fields (see, e.g., [3–5]), as motivated by supergravity and string theory. New analytical black hole solutions can be obtained by a number of solution generation techniques. A straightforward method is based on the Kaluza-Klein (KK) reduction. In the simplest case this leads to electrically charged Einstein-Maxwell-dilaton (EMd) black holes for a particular value of the dilaton coupling constant, $h = h_{KK}$ [6–9]. For general dilaton coupling constant h, however, rotating EMd black hole solutions or their Einstein-Maxwell (EM) counterparts need either perturbative techniques [10–16] or numerical analysis [17–19].

General stationary black holes in D dimensions possess $N = [(D-1)/2]$ independent angular momenta J_i, associated with N orthogonal planes of rotation [1], where N is the integer part of $(D-1)/2$, corresponding to the rank of the rotation group $SO(D-1)$. In odd-D dimensions, when all N angular momenta have equal magnitude, the symmetry of the solutions is enhanced. The EMd equations then simplify, leading to cohomogeneity-1 equations.

Here we consider such cohomogeneity-1 EMd black holes. On the one hand, we solve the coupled system of EMd equations numerically and study the properties of the black holes both for extremal and nonextremal solutions. On the other hand, we derive the near-horizon solutions for the extremal black holes. The physical properties of nonextremal black holes, like the horizon area, the gyromagnetic ratio, or the surface gravity then assume values that are bounded by those of the extremal black holes and those of the static black holes.

For extremal MP black holes in odd-D dimensions the horizon area $A_{\rm H}$ is proportional to the magnitude of the equal angular momenta, $J = |J_i|$, $J = \sqrt{2(D-3)}A_{\rm H}$. This relation for extremal black holes represents the limiting case of a more general relation for MP black holes in terms of the inner and outer horizon areas of nonextremal black holes [20], and was pointed out in four dimensions before [21–27]. In the presence of charge, the relation generalizes, and the product of the horizon areas can typically be written as a sum between the squares of the angular momenta and some powers of the charges [20–28]. Area-angular momentum-charge inequalities for stable marginally outer trapped surfaces were studied for EMd theory in [29,30].

Considering such area-angular momentum relations for extremal EMd and EM black holes, we find that the EM case is special, since there are two branches of extremal solutions. The first branch emerges from the MP black

holes and retains the proportionality between angular momentum and area. Thus the charge does not enter here. The second branch emerges from the higher-dimensional Reissner-Nordström (RN) black holes. Here the proportionality between angular momentum and area is lost. Instead there is a new proportionality between angular momentum and horizon angular momentum along this second branch. As soon as the dilaton is coupled, however, the second branch disappears and the proportionality between angular momentum and area persists for all extremal EMd solutions, independent of the dilaton coupling constant h.

The paper is organized as follows. In Sec. II we present the action, the parametrization for the metric and the fields, as well as the general formulas for the physical properties. In Sec. III we briefly recall the analytically known Kaluza-Klein black holes and their properties. We derive the near-horizon solutions in Sec. IV, discussing in particular the two-branch structure in the EM case. Section V contains our numerical results. Here we exhibit the properties of five-dimensional black holes in detail, and demonstrate subsequently that the pattern observed in five dimensions is generic for higher dimensions. We present our conclusions in Sec. VI.

II. ACTION, ANSÄTZE, AND CHARGES

A. Einstein-Maxwell-dilaton action

We consider the D-dimensional EMd action

$$I = \int d^D x \sqrt{-g}\left[R - \frac{1}{2}\partial_\mu\phi\partial^\mu\phi - \frac{1}{4}e^{-2h\phi}F_{\mu\nu}F^{\mu\nu}\right], \quad (1)$$

with curvature scalar R, dilaton field ϕ, dilaton coupling constant h, and field strength tensor $F_{\mu\nu} = \partial_\mu A_\nu - \partial_\nu A_\mu$, where A_μ denotes the gauge potential. We choose units such that $16\pi G_D = 1$, where G_D is the D-dimensional Newton constant.

Variation of the action with respect to the metric leads to the Einstein equations

$$R_{\mu\nu} - \frac{1}{2}g_{\mu\nu}R = \frac{1}{2}T_{\mu\nu}, \quad (2)$$

with stress-energy tensor

$$T_{\mu\nu} = \partial_\mu\phi\partial_\nu\phi - \frac{1}{2}g_{\mu\nu}\partial_\rho\phi\partial^\rho\phi + e^{-2h\phi}\left(F_{\mu\rho}F_\nu{}^\rho - \frac{1}{4}g_{\mu\nu}F_{\rho\sigma}F^{\rho\sigma}\right), \quad (3)$$

whereas variation with respect to the fields yields for the Maxwell field

$$\nabla_\mu(e^{-2h\phi}F^{\mu\nu}) = 0, \quad (4)$$

and for the dilaton field

$$\nabla_\mu\nabla^\mu\phi = -\frac{h}{2}e^{-2h\phi}F_{\mu\nu}F^{\mu\nu}. \quad (5)$$

Special cases correspond to Einstein-Maxwell theory, where $h = 0$, and to Kaluza-Klein theory, where $h = h_{KK}$,

$$h_{KK} = \sqrt{\frac{D-1}{2(D-2)}}. \quad (6)$$

B. Ansätze

To obtain stationary black hole solutions, which represent generalizations of the Myers-Perry solutions [1] to EMd theory, we consider black hole spacetimes with N-azimuthal symmetries, implying the existence of $N+1$ commuting Killing vectors,

$$\xi \equiv \partial_t, \qquad \eta_{(k)} \equiv \partial_{\varphi_k}, \quad (7)$$

for $k = 1, \ldots, N$. Here we are considering black holes with spherical horizon topology.

While the general EMd black holes possess N independent angular momenta, we now restrict to black holes whose angular momenta have all equal magnitude. In odd dimensions, the metric and the gauge field parametrization then simplify considerably, and the problem reduces to cohomogeneity-1. The EMd equations then form a set of ordinary differential equations, just as in Einstein-Maxwell theory [18].

We parametrize the metric as follows [17,18],

$$\begin{aligned} ds^2 = &-f dt^2 + \frac{m}{f}\left[dr^2 + r^2\sum_{i=1}^{N-1}\left(\prod_{j=0}^{i-1}\cos^2\theta_j\right)d\theta_i^2\right] \\ &+ \frac{n}{f}r^2\sum_{i=1}^{N}\left(\prod_{j=0}^{i-1}\cos^2\theta_j\right)\sin^2\theta_i\left(\varepsilon_i d\varphi_i - \frac{\omega}{r}dt\right)^2 \\ &+ \frac{m-n}{f}r^2\left\{\sum_{i=1}^{N}\left(\prod_{j=0}^{i-1}\cos^2\theta_j\right)\sin^2\theta_i d\varphi_i^2 \right. \\ &\left. - \left[\sum_{i=1}^{N}\left(\prod_{j=0}^{i-1}\cos^2\theta_j\right)\sin^2\theta_i\varepsilon_i d\varphi_i\right]^2\right\}, \end{aligned} \quad (8)$$

where $\theta_0 \equiv 0, \theta_i \in [0, \pi/2]$ for $i = 1, \ldots, N-1, \theta_N \equiv \pi/2$, $\varphi_k \in [0, 2\pi]$ for $k = 1, \ldots, N$, and $\varepsilon_k = \pm 1$ denotes the sense of rotation in the kth orthogonal plane of rotation.

An adequate parametrization for the gauge potential is given by

$$A_\mu dx^\mu = a_0 dt + a_\varphi\sum_{i=1}^{N}\left(\prod_{j=0}^{i-1}\cos^2\theta_j\right)\sin^2\theta_i\varepsilon_i d\varphi_i. \quad (9)$$

Independent of the number of dimensions D, this parametrization involves four functions for the metric, f, m, n, ω, two functions for the gauge field, a_0, a_φ, and one function for the dilaton field, ϕ, all of which depend only on the radial coordinate r.

C. Global charges

We consider asymptotically flat solutions. Thus, asymptotically the metric should approach the Minkowski metric.

The mass M and the angular momenta $J_{(k)}$ of the black holes are obtained from the Komar expressions associated with the respective Killing vector fields

$$M = -\frac{D-2}{D-3}\int_{S^{D-2}_\infty} \alpha, \tag{10}$$

$$J_{(k)} = \int_{S^{D-2}_\infty} \beta_{(k)}, \tag{11}$$

where $\alpha_{\mu_1\ldots\mu_{D-2}} \equiv \epsilon_{\mu_1\ldots\mu_{D-2}\rho\sigma}\nabla^\rho\xi^\sigma$, and $\beta_{(k)\mu_1\ldots\mu_{D-2}} \equiv \epsilon_{\mu_1\ldots\mu_{D-2}\rho\sigma}\nabla^\rho\eta^\sigma_{(k)}$. Equal-magnitude angular momenta then satisfy $|J_{(k)}| = J$, $k = 1, \ldots; , N$.

The electric charge Q is obtained from

$$Q = -\frac{1}{2}\int_{S^{D-2}_\infty} e^{-2h\phi} {}^*F, \tag{12}$$

with ${}^*F_{\mu_1\ldots\mu_{D-2}} \equiv \epsilon_{\mu_1\ldots\mu_{D-2}\rho\sigma}F^{\rho\sigma}$. The magnetic moment $\mu_{\rm mag}$ is determined from the asymptotic expansion of the gauge potential a_φ. The gyromagnetic ratio g is then obtained from the magnetic moment $\mu_{\rm mag}$ via

$$\mu_{\rm mag} = g\frac{QJ}{2M}. \tag{13}$$

The dilaton charge Σ is defined via

$$\Sigma = -A(S^{D-2})\lim_{r\to\infty} r^{D-2}\frac{d\phi}{dr}, \tag{14}$$

where $A(S^{D-2})$ is the area of the S^{D-2} sphere.

D. Horizon properties

The event horizon is located at $r = r_{\rm H}$. Here the Killing vector χ,

$$\chi = \xi + \Omega\sum_{k=1}^{N}\varepsilon_k\eta_{(k)}, \tag{15}$$

is null, and Ω represents the horizon angular velocity. Without loss of generality, Ω is assumed to be nonnegative, any negative sign being included in ε_k.

The area of the horizon $A_{\rm H}$ is given by

$$A_{\rm H} = \int_{\mathcal{H}}\sqrt{|g^{(D-2)}|} = r_{\rm H}^{D-2}A(S^{D-2})\lim_{r\to r_{\rm H}}\sqrt{\frac{m^{D-3}n}{f^{D-2}}}, \tag{16}$$

and the surface gravity κ reads

$$\kappa^2 = -\frac{1}{2}(\nabla_\mu\chi_\nu)(\nabla^\mu\chi^\nu)\big|_{\mathcal{H}} = \lim_{r\to r_{\rm H}}\frac{f}{(r-r_{\rm H})\sqrt{m}}. \tag{17}$$

The horizon mass $M_{\rm H}$ and horizon angular momenta $J_{{\rm H}(k)}$ are given by

$$M_{\rm H} = -\frac{D-2}{D-3}\int_{\mathcal{H}}\alpha, \tag{18}$$

$$J_{{\rm H}(k)} = \int_{\mathcal{H}}\beta_{(k)}, \tag{19}$$

where $\mathcal{H}$ represents the surface of the horizon. For equal-magnitude angular momenta $|J_{{\rm H}(k)}| = J_{\rm H}$, $k = 1, \ldots, N$.

The electric charge Q can also be determined at the horizon via

$$Q = -\frac{1}{2}\int_{\mathcal{H}} e^{-2h\phi} {}^*F. \tag{20}$$

The horizon electrostatic potential $\Phi_{\rm H}$ is defined by

$$\Phi_{\rm H} = \chi^\mu A_\mu\big|_{r=r_{\rm H}}. \tag{21}$$

$\Phi_{\rm H}$ is constant at the horizon. Note that $A \to 0$ for $r \to \infty$ [see Eq. (84)].

E. Mass formula

The Smarr mass formula for Einstein-Maxwell black holes with N equal-magnitude angular momenta reads [17,31]

$$\frac{D-3}{D-2}M = 2\kappa A_{\rm H} + N\Omega J + \frac{D-3}{D-2}\Phi_{\rm H}Q. \tag{22}$$

This mass formula holds also in the presence of a dilaton field [9].

Introducing the dilaton charge into the mass formula via [9]

$$\frac{\Sigma}{h} = -\Phi_{\rm H}Q, \tag{23}$$

Eq. (22) yields the Smarr mass formula

$$M = 2\frac{D-2}{D-3}\kappa A_{\rm H} + \frac{D-2}{D-3}N\Omega J + 2\Phi_{\rm H}Q + \frac{\Sigma}{h}, \tag{24}$$

known to hold also for non-Abelian black holes (in $D = 4$) [32].

F. Scaling symmetry

We note that the solutions have a scaling symmetry, e.g.,

$$\tilde{M} = \tau^{D-3} M \quad \tilde{J}_i = \tau^{D-2} J_i \quad \tilde{Q} = \tau^{D-3} Q, \tag{25}$$

$$\tilde{r}_{\rm H} = \tau r_{\rm H}, \qquad \tilde{\Omega} = \Omega/\tau, \qquad \tilde{\kappa} = \kappa/\tau, \tag{26}$$

etc.

Let us therefore introduce scaled quantities, where we scale with respect to appropriate powers of the mass. These scaled quantities include the scaled angular momentum $j = |J|/M^{(D-2)/(D-3)}$, the scaled charge $q = |Q|/M$, the scaled area $a_{\rm H} = A_{\rm H}/M^{(D-2)/(D-3)}$, the scaled surface gravity $\bar{\kappa} = \kappa M^{1/(D-3)}$, and the scaled horizon angular velocity $\bar{\Omega} = \Omega M^{1/(D-3)}$.

In terms of the scaled quantities, the Smarr relation Eq. (22) reads

$$1 = 2\frac{D-2}{D-3}\bar{\kappa} a_{\rm H} + \frac{D-2}{D-3} N \bar{\Omega} j + \Phi_{\rm H} q. \tag{27}$$

III. KALUZA-KLEIN BLACK HOLES

A straightforward method to obtain charged rotating black hole solutions in D dimensions is based on the Kaluza-Klein reduction. Here one embeds a D-dimensional vacuum solution in $D+1$ dimensions, performs a boost transformation, and then reduces the solution to D dimensions [6–9,33].

The KK black holes, obtained in this way for the particular value of the dilaton coupling constant $h = h_{KK}$,

$$h_{KK} = \frac{D-1}{\sqrt{2(D-1)(D-2)}} = (D-1)\iota, \tag{28}$$

also satisfy the quadratic relation [9,34,35]

$$\frac{Q^2}{M - \frac{2(D-2)\iota}{D-3}\Sigma} = -2(D-3)\iota\Sigma. \tag{29}$$

This relation determines the dilaton charge in terms of the mass and the electric charge, while the angular momenta do not enter.

In contrast, the static black hole solutions are known analytically for arbitrary value of the dilaton coupling constant [36–38]. It should be interesting to find a generalization of relation Eq. (29) for general values of the coupling constant h.

A. Physical properties

Let us briefly recall some properties of these KK black holes. In terms of parameters m, a_i, and α, their mass M, angular momenta J_i, charge Q, magnetic momenta $\mu_{{\rm mag},i}$, and dilaton charge Σ are given by

$$M = m(1 + (D-3)\cosh^2\alpha) A(S^{D-2}), \tag{30}$$

$$J_i = 2 m a_i \cosh\alpha A(S^{D-2}), \tag{31}$$

$$Q = (D-3) m \sinh\alpha \cosh\alpha A(S^{D-2}), \tag{32}$$

$$\mu_{{\rm mag},i} = (D-3) m a_i \sinh\alpha A(S^{D-2}), \tag{33}$$

$$\Sigma = -\frac{(D-3) m \sinh^2\alpha}{2(D-2)\iota} A(S^{D-2}), \tag{34}$$

where m and a_i determine the MP mass and angular momenta in the limit, where the boost parameter vanishes, $\alpha = 0$.

The gyromagnetic ratios g_i are given by

$$g_i = \frac{2M}{Q J_i}\mu_{{\rm mag},i} = (D-3) + \frac{1}{\cosh^2\alpha} \equiv g. \tag{35}$$

Thus the gyromagnetic ratio g depends only on the charge-to-mass ratio, $q = Q/M$. It does not depend on the angular momenta. Therefore, for a given value of q, the gyromagnetic ratio is the same for all rotating black holes. It ranges between $g = D-2$ in the limit of vanishing charge, $q \to 0$, and $g = D-3$ in the limit of maximal charge, $|q| \to 1$.

The event horizon of the KK black holes is characterized as the largest non-negative root $\rho = \rho_{\rm H}$ of

$$\Delta \equiv \prod_{i=1}^{N} (\rho^2 + a_i^2) - m\rho^{2-\varepsilon}, \tag{36}$$

where ε takes the values $\varepsilon = 0$, 1 for odd and even dimensions, respectively. Notice that ρ is a Boyer-Lindquist type of radial coordinate. The (constant) horizon angular velocities Ω_i, the horizon area $A_{\rm H}$, the surface gravity κ, and the horizon electrostatic potential $\Phi_{\rm H}$ are given by

$$\Omega_i = \frac{a_i}{(\rho_{\rm H}^2 + a_i^2)\cosh\alpha}, \tag{37}$$

$$A_{\rm H} = \frac{\cosh\alpha}{\rho_{\rm H}^{1-\varepsilon}} A(S^{D-2}) \prod_{i=1}^{N} (\rho_{\rm H}^2 + a_i^2), \tag{38}$$

$$\kappa = \left. \frac{\Delta_{,\rho}}{2m\rho_{\rm H}^{2-\varepsilon} \cosh\alpha} \right|_{\rho=\rho_{\rm H}}, \tag{39}$$

$$\Phi_{\rm H} = \frac{\sinh\alpha}{\cosh\alpha}. \tag{40}$$

Thus, like g, the horizon electrostatic potential $\Phi_{\rm H}$ depends only on the charge-to-mass ratio q, with $0 \le \Phi_{\rm H} \le 1$.

These KK black holes satisfy the general Smarr formula

$$M = 2\frac{D-2}{D-3}\kappa A_{\rm H} + \frac{D-2}{D-3}\sum_{i=1}^{N} \Omega_i J_i + \Phi_{\rm H} Q, \tag{41}$$

which also holds for arbitrary dilaton coupling constant h.

B. Extremal solutions

We now turn to the extremal rotating KK black holes. We focus on black holes with equal-magnitude angular momenta, $J_i = J$, $i = 1, ..., N$. First, we present the metric

$$ds^2 = \left(1 + \frac{m\sinh^2\alpha}{\rho^\varepsilon(\rho^2+a^2)^{N-1}}\right)^{\frac{1}{D-2}} \left\{ -dt^2 + \frac{\rho^2(\rho^2+a^2)^{N-1}}{(\rho^2+a^2)^N - m\rho^{2-\varepsilon}} d\rho^2 + (\rho^2+a^2)\sum_{i=1}^{N}(d\mu_i^2 + \mu_i^2 d\phi_i^2) + \varepsilon\rho^2 d\nu^2 + \frac{m(\cosh^2\alpha dt - a\sum_{i=1}^{N}\mu_i^2 d\phi_i)^2}{\rho^\varepsilon(\rho^2+a^2)^{N-1} + m\sinh^2\alpha} \right\}, \tag{42}$$

where μ_i, the direction cosines, can be chosen in odd-D dimensions,

$$\mu_i = \sin\theta_i \prod_{j=0}^{i-1} \cos\theta_j, \tag{43}$$

where $\theta_0 = 0$, $\theta_N = \pi/2$, and in even-D dimensions,

$$\mu_i = \sin\theta_{(i+1)} \prod_{j=0}^{i} \cos\theta_j, \tag{44}$$

where $\theta_0 = 0$, $\theta_{N+1} = \pi/2$, and $\mu_0 = \nu$. Note that $\sum_{i=1}^{N}\mu_i^2 + \varepsilon\nu^2 = 1$.

The gauge potential is given by

$$A = \frac{m\sinh\alpha}{\rho^\varepsilon(\rho^2+a^2)^{N-1} + m\sinh^2\alpha}\left(\cosh^2\alpha dt - a\sum_{i=1}^{N}\mu_i d\phi_i\right). \tag{45}$$

Finally, the dilaton is given by the following expression:

$$\phi = -\frac{D-1}{2(D-2)}\log\left(1 + \frac{m\sinh^2\alpha}{\rho^\varepsilon(\rho^2+a^2)^{N-1}}\right). \tag{46}$$

These extremal black holes are characterized only by two free parameters, since the angular momentum parameter a and the mass parameter m can be given in terms of the horizon radius $\rho_{\rm H}$:

$$\begin{aligned} \text{even } D: a^2 &= (2N-1)\rho_{\rm H}^2, \\ m &= (2N)^N \rho_{\rm H}^{2N-1}, \\ \text{odd } D: a^2 &= (N-1)\rho_{\rm H}^2, \\ m &= N^N \rho_{\rm H}^{2N-2}. \end{aligned} \tag{47}$$

The relation between area and angular momentum for extremal black holes then follows:

$$\begin{aligned} \text{even } D: J &= 2\sqrt{D-3}A_{\rm H}, \\ \text{odd } D: J &= \sqrt{2(D-3)}A_{\rm H}. \end{aligned} \tag{48}$$

Considering the Smarr relation Eq. (22), we note that on the one hand for extremal black holes we have vanishing $\bar{\kappa}$, thus

$$1 = \frac{D-2}{D-3} N\bar{\Omega} j\big|_{\rm ex} + \Phi_{\rm H} q. \tag{49}$$

On the other hand, for static black holes we have vanishing $\bar{\Omega}$, thus

$$1 = 2\frac{D-2}{D-3}\bar{\kappa} a_{\rm H}\big|_{\rm st} + \Phi_{\rm H} q. \tag{50}$$

Since the horizon electrostatic potential $\Phi_{\rm H}$ is independent of the angular momentum, we obtain for a given q the interesting relation

$$N\bar{\Omega} j|_{\rm ex} = 2\bar{\kappa} a_{\rm H}|_{\rm st}. \tag{51}$$

The scaled area $a_{\rm H}$ of the static solutions is proportional to the scaled angular momenta j of the extremal solutions, coinciding in five dimensions. For odd dimensions we find

$$j_{\rm ex} = 2N^{\frac{-N}{2(N-1)}}(N-1)^{1/2} a_{\rm H,st}, \tag{52}$$

while for even dimensions

$$j_{\rm ex} = 2^{\frac{N-1}{2N-1}} N^{\frac{-N}{2N-1}} (2N-1)^{1/2} a_{\rm H,st}. \tag{53}$$

Since $j_{\rm ex}$ and $a_{\rm H,st}$ are proportional, we obtain a relation between the scaled horizon velocity $\bar{\Omega}_{\rm ex}$ of the extremal rotating black holes and the scaled surface gravity $\bar{\kappa}_{\rm st}$ of the static black holes. For odd dimensions it reads

$$\bar{\kappa}_{\rm st} = N^{\frac{N-2}{2(N-1)}}(N-1)^{1/2}\bar{\Omega}_{\rm ex}, \tag{54}$$

and for even dimensions

$$\bar{\kappa}_{\rm st} = 2^{\frac{-N}{2N-1}} N^{\frac{N-1}{2N-1}} (2N-1)^{1/2}\bar{\Omega}_{\rm ex}. \tag{55}$$

Again, in five dimensions, $\bar{\kappa}_{\rm st}$ and $\bar{\Omega}_{\rm ex}$ coincide, while they are proportional in higher dimensions.

These KK relations hold also for vacuum black holes, obtained in the limit $q \to 0$.

IV. NEAR-HORIZON SOLUTIONS

The existence of extremal EMd and EM black hole solutions is supported by the existence of exact solutions, describing a rotating squashed $\mathrm{AdS}_2 \times S^{D-2}$ spacetime. These solutions correspond to the neighborhood of the event horizon of extremal black holes.

To obtain these exact near-horizon solutions for odd-D dimensions, we parametrize the metric as follows [39],

$$\begin{aligned} ds^2 = {} & v_1\left(\frac{dr^2}{r^2} - r^2 dt^2\right) + v_2 \sum_{i=1}^{N-1}\left(\prod_{j=0}^{i-1}\cos^2\theta_j\right) d\theta_i^2 \\ & + v_2 v_3 \sum_{i=1}^{N}\left(\prod_{j=0}^{i-1}\cos^2\theta_j\right)\sin^2\theta_i(\varepsilon_i d\varphi_i - k r dt)^2 \\ & + v_2(1-v_3)\left\{\sum_{i=1}^{N}\left(\prod_{j=0}^{i-1}\cos^2\theta_j\right)\sin^2\theta_i d\varphi_i^2 \right. \\ & \left. - \left[\sum_{i=1}^{N}\left(\prod_{j=0}^{i-1}\cos^2\theta_j\right)\sin^2\theta_i\varepsilon_i d\varphi_i\right]^2\right\}. \end{aligned} \tag{56}$$

Here we have employed a new radial coordinate such that the horizon is located at $r = 0$. This position of the horizon can always be obtained by a transformation $r \to r - r_{\rm H}$.

Moreover, we have shifted to a corotating frame such that the angular velocity vanishes on the horizon. The corresponding parametrization for the gauge potential in the corotating frame reads

$$\begin{aligned} A_\mu dx^\mu = {} & (q_1 - q_2 k) r dt \\ & + q_2 \sum_{i=1}^{N}\left(\prod_{j=0}^{i-1}\cos^2\theta_j\right)\sin^2\theta_i\varepsilon_i d\varphi_i. \end{aligned} \tag{57}$$

The dilaton field is simply given by $\phi = u$.

The parameters k, v_i, q_i, and u are constants, which satisfy a set of algebraic relations. In what follows we choose to determine them by using the near-horizon formalism proposed in [40,41].

To that end let us denote by $f(k, v_1, v_2, v_3, q_1, q_2, u)$ the Lagrangian density $\sqrt{-g}\mathcal{L}$ evaluated for the near-horizon geometry Eq. (56) and potential Eq. (57) and integrated over the angular coordinates,

$$f(k, v_1, v_2, v_3, q_1, q_2, u) = \int d\theta_1 \ldots d\theta_{N-1} d\varphi_1 \ldots d\varphi_N \sqrt{-g}\mathcal{L}. \tag{58}$$

The field equations then follow from the variation of this functional. In particular, the derivative with respect to k and q_1 yields the angular momenta and the charge,

$$\frac{\partial f}{\partial k} = 2J, \qquad \frac{\partial f}{\partial q_1} = Q, \tag{59}$$

respectively, while the derivative with respect to the remaining parameters vanishes,

$$\frac{\partial f}{\partial v_i} = 0, \qquad i = 1,2,3, \qquad \frac{\partial f}{\partial q_2} = 0, \qquad \frac{\partial f}{\partial u} = 0. \tag{60}$$

The entropy function is obtained by taking the Legendre transform of the above integral with respect to the parameter k, associated with all equal-magnitude angular momenta, $J_1 = \ldots = J_N = J$, and with respect to the parameter q_1, associated with the charge Q,

$$\begin{aligned} & \mathcal{E}(J, k, Q, q_1, q_2, v_1, v_2, v_3, u) \\ & \quad = 2\pi[NJk + Qq_1 - f(k, v_1, v_2, v_3, q_1, q_2, u)]. \end{aligned} \tag{61}$$

Then the entropy associated with the black holes can be calculated by evaluating this function at the extremum, $S = \mathcal{E}_{\rm extremum}$.

A. Generic dilaton coupling

To obtain the near-horizon solutions, the set of Eqs. (59) and (60) must be solved. For a given spacetime dimension $D = 2N + 1$, the solutions can be expressed in terms of three independent parameters, v_1, q_2, and u,

$$
\begin{aligned}
v_2 &= 2(N-1)Nv_1, \\
v_3 &= N - \frac{2q_2^2 e^{-2hu}}{N(N-1)v_1}, \\
q_1 &= 0, \\
k &= \frac{1}{N\sqrt{N-1}}, \\
J &= \frac{2^{N+1}\sqrt{2N^2(N-1)v_1 - 4q_2^2 e^{-2hu}}}{N(N-1)^{3/2}(N-2)!v1}(\pi N(N-1)v_1)^N, \\
Q &= -\frac{2^{N+2}\sqrt{2N^2(N-1)v_1 - 4q_2^2 e^{-2hu}}}{N(N-1)^{3/2}N!}(\pi N(N-1)v_1)^N \\
&\quad \times \frac{q_2 e^{-2hu}}{v_1^2}.
\end{aligned} \tag{62}
$$

Interestingly, q_1 vanishes and k depends only on the spacetime dimension.

Let us now inspect the horizon quantities obtained from this solution, Eq. (62). The horizon angular momenta are given by

$$
\begin{aligned}
J_{\mathrm{H}} &= 2^N\sqrt{N-1}(N-2)!(N(N-1))^{N-3}\pi^N \\
&\quad \times (2N^2(N-1)v_1 - 4q_2^2 e^{-2hu})^{3/2},
\end{aligned} \tag{63}
$$

and the horizon area is obtained from the entropy function, Eq. (61),

$$
A_{\mathrm{H}} = \frac{\mathcal{E}}{4\pi} = \frac{J}{\sqrt{2(D-3)}}. \tag{64}
$$

Thus relation Eq. (48) holds for generic values of the dilaton coupling constant h ($h \neq 0$). Extremal dilatonic black holes thus show proportionality of their horizon area and their angular momenta.

Since all the asymptotic information is lost in the near-horizon limit, quantities such as the horizon angular velocity do not have a meaning when studying the near-horizon solutions. Consequently, the relation between the horizon angular momenta and the horizon mass,

$$
M_{\mathrm{H}} = \frac{(D-1)(D-2)}{2(D-3)}\Omega J_{\mathrm{H}}, \tag{65}
$$

cannot be derived for the near-horizon geometry. It can only be obtained for global extremal solutions.

The most intriguing feature of Eq. (62) is the presence of three free parameters. However, we know that these extremal black holes possess only two independent parameters (the electric charge Q and the angular momentum J, for instance). One would be tempted to state that the existence of an extra independent parameter in the near-horizon EMd solutions is related to the existence of nonglobally realized near-horizon EMd solutions. Although these nonglobally realized solutions are really present among the near-horizon EMd solutions, as we will show below, the question is more subtle. The key point here is the invariance under a scale transformation associated with the dilaton,

$$
\tilde{x}^\mu = \lambda^{-1}x^\mu, \qquad \tilde{\phi} = \phi + \frac{1}{h}\log\lambda, \qquad \tilde{F}_{\mu\nu} = \lambda^2 F_{\mu\nu}. \tag{66}
$$

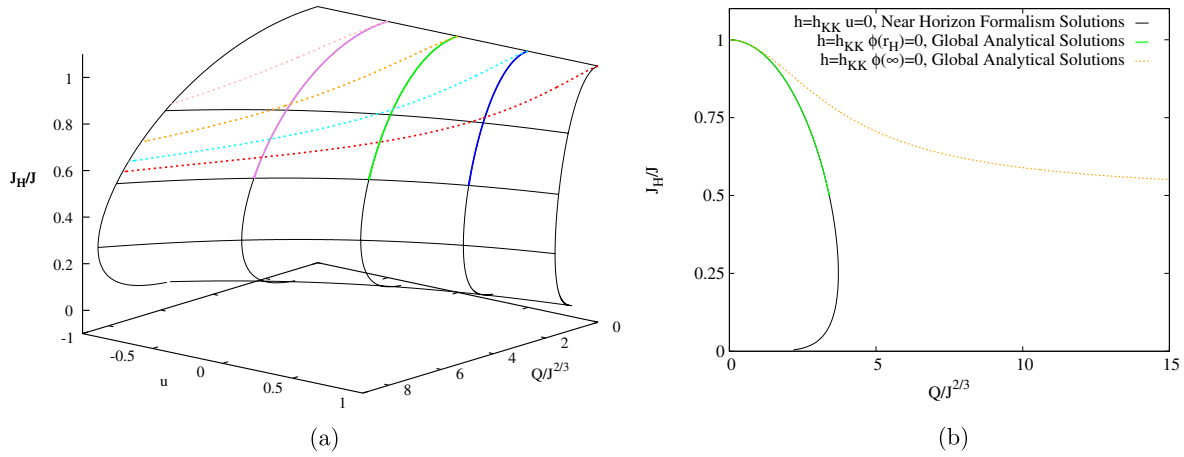

(a) (b)

FIG. 1 (color online). (a) Surface of near-horizon EMd solutions in five dimensions for dilaton coupling constant $h = h_{KK}$, scaled with the angular momentum: the horizon angular momenta J_{H}/J are shown versus the charge $Q/J^{2/3}$ and the dilaton parameter u. The colored solid and colored dotted lines mark the global solutions. (b) Detail of (a) where the global solutions with $\phi(\infty) = 0$ (orange dotted line) and with $u = \phi(r_{\mathrm{H}}) = 0$ (green solid line) are shown, together with the near-horizon EMd solutions with $u = 0$ (black thin line).

Note that under this transformation the value of the dilaton at the horizon may be set to any given value, so the parameter u may be eliminated by such a transformation (i.e., one can set $u = 0$ without loss of generality). We illustrate this fact in Figs. 1. In Fig. 1(a) we plot the scaled horizon angular momenta J_H/J as a function of u and $Q/J^{2/3}$, for the dilaton coupling constant $h = h_{KK}$ in five dimensions. On the surface we show black thin solid curves corresponding to cuts with constant u and cuts with constant J_H/J. We also exhibit with colored solid and colored dotted lines sets of globally realized extremal solutions. The curves in solid-color style (violet, green, and dark blue) are solutions with constant $u = \phi(r_H)$, and the curves in dotted-color style (pink, orange, light blue, and red) are solutions with constant $\phi(\infty)$. All these globally realized curves range from $J_H/J = 1$ to $J_H/J = 1/2$ (this last limit depending on h; its lowest value is $1/4$ for EM $h = 0$). The curves with constant $u = \phi(r_H)$ have finite length while those with constant $\phi(\infty)$ have infinite length. However, all of them are equivalent to each other. The curves with constant $u = \phi(r_H)$ transform into each other under a transformation of the type in Eq. (66) with a constant λ; the same holds among curves with constant $\phi(\infty)$. A transformation among the curves with constant $u = \phi_H$ and the curves with constant $\phi(\infty)$ requires a factor λ that varies with Q. Since J_H/J is invariant under Eq. (66), the requirement for two points on the surface to be equivalent is that they have the same J_H/J value. Note that $Q/J^{2/3}$ is not invariant but transforms as $\tilde{Q}/\tilde{J}^{2/3} = \lambda Q/J^{2/3}$. That means if one changes the $Q/J^{2/3}$ axis to $e^{h\phi(\infty)}Q/J^{2/3}$, all the color curves collapse into the green curve. In fact, the whole upper part of the surface with $J_H/J \geq 1/2$ collapses into the green curve.

Going back to the point of the existence of nonglobally realized near-horizon EMd solutions, we see that solutions with $J_H/J \leq 1/2$ do not exist globally for $h = h_{KK}$. We demonstrate this in Fig. 1(b). There, only the globally realized solutions with $\phi(\infty) = 0$ and $\phi(r_H) = 0$ are included, together with the near-horizon solutions with $u = 0$. Near-horizon EMd solutions (in black) with $J_H/J < 1/2$ are not realized globally. (They correspond to the region where the black and the green curves do not overlap.)

B. Kaluza-Klein case

Since the black hole for the Kaluza-Klein value of the dilaton coupling is explicitly known, we can obtain the near-horizon limit of the analytic solution.

We change the metric Eq. (42) to a corotating frame, shift the radial coordinate to be centered on the horizon, and make the near-horizon limit together with an appropriate gauge transformation on the gauge potential Eq. (45). The resulting metric can be written in a similar form as in Eq. (56). The gauge vector can also be written in the same form as in Eq. (57). The dilaton Eq. (46) is given by a parameter $\phi = u$ in the near-horizon limit. All these parameters satisfy the following relations with the parameters a and α from the Kaluza-Klein solution:

$$\begin{aligned} v_1 &= \frac{1}{2}a^2\frac{(1+N\cosh(\alpha)^2-N)^{\frac{1}{D-2}}}{(N-1)^2}, \\ v_2 &= 2N(N-1)v_1, \\ v_3 &= \frac{N\cosh(\alpha)^2}{1-N+N\cosh(\alpha)^2}, \\ k &= \frac{1}{N\sqrt{N-1}}, \\ q_1 &= 0, \\ q_2 &= -\frac{Na\,\sinh(\alpha)}{1+N\cosh(\alpha)^2-N}. \end{aligned} \tag{67}$$

Note that these relations are compatible with the near-horizon geometry for generic dilaton coupling Eq. (62), in the particular case of $h = h_{KK}$.

In this case, since we derive the near-horizon limit of the global solution, we also obtain a relation for the dilaton parameter,

$$u = -\frac{\sqrt{2(D-1)}}{2\sqrt{D-2}}\,\ln(1+N\cosh(\alpha)^2-N). \tag{68}$$

We note that this relation was not found by employing the near-horizon formalism in the previous Sec. IVA. Here this relation is only found as a result of explicitly knowing the global solution and the fact that the dilaton is required to vanish at infinity. So this solution corresponds to the red curve in Figs. 1.

C. Einstein-Maxwell case

Surprisingly, the EM case is rather different from the EMd case. In particular, there is not only one set of solutions, as in the EMd case, but there are two sets of solutions, which we label currently as the first branch and the second branch of solutions. The five-dimensional case was discussed before [19,42]. Moreover, the EM solutions depend only on two parameters, since there is no dilaton parameter.

For a given spacetime dimension $D = 2N + 1$, the first set of solutions can be expressed in terms of the independent parameters v_1 and q_2. Thus the first branch is given by

$$
\begin{aligned}
v_2 &= 2(N-1)Nv_1,\\
v_3 &= N-\frac{2q_2^2}{N(N-1)v_1},\\
q_1 &= 0,\\
k &= \frac{1}{N\sqrt{N-1}},\\
J &= \frac{2^{N+1}\sqrt{2N^2(N-1)v_1-4q_2^2}}{N(N-1)^{3/2}(N-2)!v1}(\pi N(N-1)v_1)^N,\\
Q &= -\frac{2^{N+2}\sqrt{2N^2(N-1)v_1-4q_2^2}}{N(N-1)^{3/2}N!}(\pi N(N-1)v_1)^N\frac{q_2}{v_1^2}.
\end{aligned}
\tag{69}
$$

As in the EMd case, in this EM solution q_1 vanishes and k is constant. Moreover, by defining $\bar{q}_2 = q_2 e^{-hu}$ and $\bar{Q} = Qe^{hu}$ in the EMd solution Eq. (62), this first EM branch is obtained. Because e^{-2hu} is multiplying q_2 everywhere, we reobtain the MP solution, when setting $q_2 = 0$.

Concerning the horizon quantities obtained from this solution, Eq. (69), the horizon angular momenta are given by

$$
\begin{aligned}
J_{\mathrm{H}} = {} & 2^N\sqrt{N-1}(N-2)!(N(N-1))^{N-3}\pi^N\\
& \times (2N^2(N-1)v_1-4q_2^2)^{3/2},
\end{aligned}
\tag{70}
$$

and the horizon area is obtained from the entropy function, Eq. (61), resulting in

$$
A_{\mathrm{H}} = \frac{\mathcal{E}}{4\pi} = \frac{J}{\sqrt{2(D-3)}}. \tag{71}
$$

Clearly, relation Eq. (48) holds along this first branch, expressing proportionality of the horizon area and the angular momenta.

The near-horizon equations, however, allow for a second set of solutions, which can be expressed in terms of the independent parameters v_1 and v_2. These solutions form the second branch and are given by

$$
\begin{aligned}
v_3 &= \frac{v_2}{4(N-1)(N-2)v_1}-\frac{1}{N-2},\\
k &= \frac{2\sqrt{N-1}v_1}{v_2\sqrt{v_2+4(1-N)v_1}}\sqrt{4(N-1)^2v_1-v_2},\\
q_1 &= \frac{\sqrt{2N-1}}{\sqrt{N-2}}\sqrt{\frac{v_1}{v_2}}\frac{2N(N-1)v_1-v_2}{\sqrt{v_2+4(1-N)v_1}},\\
q_2 &= \frac{\sqrt{2N-1}}{4\sqrt{N-2}(N-1)}\sqrt{\frac{v_2}{v_1}}\sqrt{4(N-1)^3v_1+(1-N)v_2},\\
J &= \frac{(\pi v_2)^N}{(N-1)!}\frac{v2-4(N-1)v_1}{(N-1)^{3/2}(N-2)^{3/2}v_1^{3/2}\sqrt{v_2}}\sqrt{(N-1)(4(N-1)^2v_1-v_2)},\\
Q &= \frac{-2(\pi v_2)^N}{(N-1)!}\frac{\sqrt{2N-1}}{\sqrt{N-1}(N-2)}\frac{4(N-1)v_1-v_2}{v_1v_2}.
\end{aligned}
\tag{72}
$$

Along this second branch the horizon angular momenta are given by

$$
J_{\mathrm{H}} = \frac{J}{D-1}, \tag{73}
$$

and the horizon area is again obtained from the entropy function, Eq. (61),

$$
A_{\mathrm{H}} = \frac{\mathcal{E}}{4\pi} = \frac{(\pi v_2)^N\sqrt{v_2-4(N-1)v_1}}{\sqrt{N-2}\sqrt{N-1}(N-1)!\sqrt{v_1v_2}}. \tag{74}
$$

For this branch of solutions the horizon area is not proportional to the angular momenta. Instead, the horizon angular momenta are proportional to the total angular momenta [19].

Figures 2 exhibit the two branches of solutions for near-horizon solutions in odd dimensions, from five to eleven. In particular, we show the horizon area A_{H} (a) and the horizon angular momenta J_{H} (b) versus the charge Q, scaled by the angular momenta J. The first branch, starting from the MP solution, extends only up to a maximal value of the charge Q, for given angular momenta J. At this critical value it does not end, however, but it continues backwards to smaller charges.

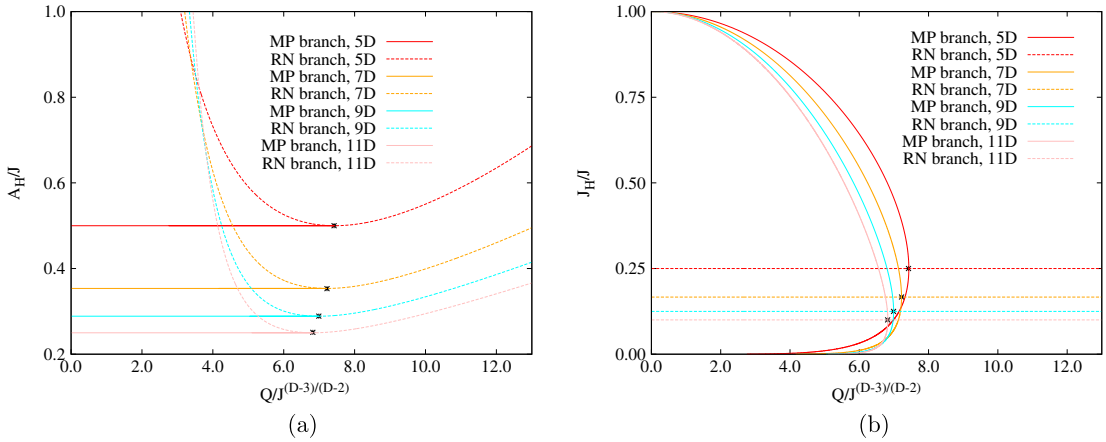

FIG. 2 (color online). Near-horizon EM solutions in several dimensions: the horizon area A_H (a) and the horizon angular momenta J_H (b) are shown versus the charge Q (quantities are scaled by the angular momenta J.) The asterisks mark the matching points of the two branches. The first branch is realized globally from the MP solution to the matching point, while the second branch is realized globally from the matching point to the RN solution.

The second branch, on the other hand, extends over the full axis. It smoothly reaches the extremal static RN solution, when $J \to 0$, but it also extends all the way to vanishing electric charge Q. Most importantly, however, this second branch crosses the first branch precisely at its critical point. Here all physical quantities match for the two branches. This matching point is indicated in the figures by an asterisk. It is this matching point, which also delimits the globally realized parts of these branches of solutions. The first branch is realized globally from the MP solution to the matching point, while the second branch is realized globally from the matching point to the RN solution.

Thus for extremal EM black holes in higher odd dimensions, the branch structure is analogous to the five-dimensional case [19,42]. In the following we will denote the branches as the MP branch and the RN branch, since they start at the extremal MP solution and the extremal RN solution, respectively.

V. NUMERICAL SOLUTIONS

After a short discussion of the numerical procedure and the boundary conditions, we present our results for black holes in five, seven, and nine dimensions. We discuss the domains of existence and the global properties, especially the gyromagnetic ratio and the horizon properties. Here the surface gravity κ and the horizon angular velocity Ω are associated with a critical behavior.

This critical behavior was observed before for static EMd black holes [36]. Here, at the critical value of the dilaton coupling $h_{\rm cr}$,

$$h_{\rm cr} = \frac{D-3}{\sqrt{2(D-2)}}, \tag{75}$$

the surface gravity κ remains finite in the extremal limit. In contrast, κ diverges for $h > h_{\rm cr}$, while $\kappa \to 0$ for $h < h_{\rm cr}$ in the extremal limit. Comparing this critical value $h_{\rm cr}$ to the KK value h_{KK}, we note that

$$\begin{aligned} h_{\rm cr} &= h_{KK} \quad \text{for } D = 5, \\ h_{\rm cr} &> h_{KK} \text{ for } D > 5. \end{aligned} \tag{76}$$

Since the solutions have a scaling symmetry Eq. (26), we typically exhibit scaled physical quantities, where we scale with respect to appropriate powers of the mass M. In particular, we employ the charge to mass ratio q to demonstrate the dependence on the charge.

The domain of existence of these black holes increases with increasing dilaton coupling constant h, since the maximal value of the scaled charge q increases with h according to

$$q_{\rm max} = \sqrt{\frac{D-3}{2(D-2)} + h^2}; \tag{77}$$

i.e., for the Kaluza-Klein coupling constant h_{KK} the maximal value of the scaled charge is given by $q_{\rm max} = 1$, independent of the dimension D.

The gyromagnetic ratio g of higher-dimensional black holes has drawn much interest, ever since perturbations in the charge in the EM case ($h = 0$) yielded for MP black holes the intriguing lowest-order result [10]

$$g_{\delta q} = D - 2 + o(q^2). \tag{78}$$

The same result was obtained when considering first-order perturbations in the angular momentum for the charged static solutions in the EM case ($h = 0$) [14]

$$g_{\delta j} = D - 2 + o(j^2). \tag{79}$$

Nevertheless, this result was shown not to hold in general for higher-order perturbations in the charge [13,15,16], and nonperturbatively for arbitrary values of Q and J [17,18]. However, it still represents an important limiting value for EM and EMd black holes, attained for small values of the charge to mass ratio q. In fact, in the EMd case ($h \neq 0$) first-order perturbations in the angular momentum for the charged static solutions yield, in our conventions in terms of $q = Q/M$ and a generic dilaton coupling h, the expression [14]

$$g_{\delta j} = \frac{(D-1)(D-2)(D-3)[D-3+X]}{4h^2(D-2)^2q^2 + (D-1)(D-3)[D-3+X]}, \tag{80}$$

where

$$X^2 = 2(D-2)[2h^2(D-2) + 3 - D]q^2 + (D-3)^2. \tag{81}$$

A. Numerical procedure and boundary conditions

In order to solve the coupled system of ODEs, we take advantage of the existence of a first integral of that system,

$$\frac{r^{D-2}m^{(D-5)/2}}{f^{(D-3)/2}}\sqrt{\frac{mn}{f}}\left(\frac{da_0}{dr} + \frac{\omega}{r}\frac{da_\varphi}{dr}\right) = -\frac{e^{2h\phi}}{A(S^{D-2})}Q, \tag{82}$$

to eliminate a_0 from the equations, leaving a system of one first-order equation (for n) and four second-order equations.

For the numerical calculations we take units such that $16\pi G_D = 1$. We introduce a compactified radial coordinate. For the nonextremal solutions we take the compactified coordinate to be $\bar{r} = 1 - r_{\rm H}/r$. In the extremal case we employ $\bar{r} = \frac{r}{1+r}$ [43]. (Note that we are using an isotropic coordinate r, so $r_{\rm H} = 0$ in the extremal case.) We employ a collocation method for boundary-value ordinary differential equations, equipped with an adaptive mesh selection procedure [44]. Typical mesh sizes include 10^3–10^4 points. The solutions have a relative accuracy of 10^{-10}. The estimates of the relative errors of the global charges and the magnetic moment are of order 10^{-6}, giving rise to an estimate of the relative error of g of order 10^{-5}.

To obtain asymptotically flat solutions the metric functions should satisfy the boundary conditions

$$f|_{r=\infty} = m|_{r=\infty} = n|_{r=\infty} = 1, \qquad \omega|_{r=\infty} = 0. \tag{83}$$

For the gauge potential we choose a gauge in which it vanishes at infinity,

$$a_0|_{r=\infty} = a_\varphi|_{r=\infty} = 0. \tag{84}$$

For the dilaton field we choose

$$\phi|_{r=\infty} = 0. \tag{85}$$

Note that any finite value of the dilaton field at infinity can always be transformed to zero via $\phi \to \phi - \phi(\infty)$, $r \to re^{h\phi(\infty)}$, $a_0 \to a_0 e^{-h\phi(\infty)}$.

Requiring the horizon to be regular, the metric functions must satisfy the boundary conditions

$$f|_{r=r_{\rm H}} = m|_{r=r_{\rm H}} = n|_{r=r_{\rm H}} = 0, \qquad \omega|_{r=r_{\rm H}} = r_{\rm H}\Omega, \tag{86}$$

where Ω is the horizon angular velocity, defined in terms of the Killing vector χ, Eq. (15).

The gauge potential satisfies at the horizon the conditions,

$$\chi^\mu A_\mu|_{r=r_{\rm H}} = \Phi_{\rm H} = (a_0 + \Omega a_\varphi)|_{r=r_{\rm H}}, \qquad \left.\frac{da_\varphi}{dr}\right|_{r=r_{\rm H}} = 0, \tag{87}$$

with the constant horizon electrostatic potential $\Phi_{\rm H}$. The boundary condition for the dilaton field reads

$$\left.\frac{d\phi}{dr}\right|_{r=r_{\rm H}} = 0. \tag{88}$$

Since the KK solutions are known analytically, we can use them as a test for the accuracy of the numerical calculations, by choosing the dilaton coupling constant $h = h_{KK}$. Other general tests are provided by the Smarr formula Eq. (22) and the relation Eq. (23).

B. Expansions

The asymptotic expansion of the metric, the gauge potential, and the dilaton field reads

$$
\begin{aligned}
f &= 1 - \frac{M}{(D-2)A(S^{D-2})}\frac{1}{r^{D-3}} + \ldots, \\
m &= 1 - \frac{(D-4)M}{(D-2)(D-3)A(S^{D-2})}\frac{1}{r^{D-3}} + \ldots, \\
n &= 1 - \frac{(D-4)M}{(D-2)(D-3)A(S^{D-2})}\frac{1}{r^{D-3}} + \ldots, \\
\omega &= \frac{J}{2A(S^{D-2})}\frac{1}{r^{D-2}} + \ldots, \\
a_0 &= \frac{Q}{(D-3)A(S^{D-2})}\frac{1}{r^{D-3}} + \ldots, \\
a_\varphi &= -\frac{\mu_{\mathrm{mag}}}{(D-3)A(S^{D-2})}\frac{1}{r^{D-3}} + \ldots, \\
\phi &= \frac{\Sigma}{(D-3)A(S^{D-2})}\frac{1}{r^{D-3}} + \ldots.
\end{aligned} \tag{89}
$$

The global mass M, the global angular momenta J, the electric charge Q, the dilaton charge Σ, and the magnetic moment μ_{mag} can be read off from this expansion. Note that in the nonextremal case, only three of these parameters are free. In the extremal case there are only two free parameters.

For the expansion at the horizon we should distinguish explicitly whether the solutions are nonextremal or extremal. In the nonextremal case the expansion of the functions at the horizon reads

$$
\begin{aligned}
f &= f_2\delta^2(1-\delta) + O(\delta^4), \\
m &= m_2\delta^2(1-3\delta) + O(\delta^4), \\
n &= n_2\delta^2(1-3\delta) + O(\delta^4), \\
\omega &= r_{\mathrm{H}}\Omega(1+\delta) + O(\delta^2), \\
a_0 &= a_{0,0} + O(\delta^2), \\
a_\varphi &= a_{\varphi,0} + O(\delta^2), \\
\phi &= \phi_0 + O(\delta^2),
\end{aligned} \tag{90}
$$

where $\delta = r/r_{\mathrm{H}} - 1$ and f_2, m_2, n_2, $a_{0,0}$, $a_{\varphi,0}$, and ϕ_0 are constant.

In the extremal case the situation is very different. The expansion near the horizon $r_{\mathrm{H}} = 0$ is

$$
\begin{aligned}
f &= f_4 r^4 + f_\alpha r^\alpha + o(r^6), \\
m &= m_2 r^2 + m_\beta r^\beta + o(r^4), \\
n &= n_2 r^2 + n_\gamma r^\gamma + o(r^4), \\
\omega &= \omega_1 r + \omega_2 r^2 + o(r^3), \\
a_0 &= a_{0,0} + a_{0,\lambda} r^\lambda + o(r^2), \\
a_\phi &= a_{\phi,0} + a_{\phi,\mu} r^\mu + o(r^2), \\
\phi &= \phi_0 + \phi_\nu r^\nu + o(r^2).
\end{aligned} \tag{91}
$$

It is interesting to note, that, in general, the exponents α, β, γ, λ, μ, and ν are noninteger. Note, that ω is the only function with the usual expansion at the horizon. For the other functions, the next to leading order is given by a term with a noninteger exponent. The ranges are

$$
\begin{aligned}
&4 < \alpha < 6, \qquad 2 < \beta < 4, \qquad 2 < \gamma < 4, \\
&0 < \lambda < 2, \qquad 0 < \mu < 2, \qquad 0 < \nu < 2.
\end{aligned} \tag{92}
$$

In the pure Einstein-Maxwell case ($h = 0$) the expansion contains similarly noninteger exponents (but there is no dilaton function). This feature is found in both EM branches (i.e., in the MP branch and in the RN branch).

For the numerical integration the following reparametrization of the functions was made,

$$
\begin{aligned}
&f = \hat{f}x^2, \qquad m = \hat{m}, \qquad n = \hat{n}, \\
&\omega = \hat{\omega}(1-x)^2, \qquad a_k = \hat{a}_k/x^2, \qquad \phi = \hat{\phi}/x^2.
\end{aligned} \tag{93}
$$

Note that all the redefined functions except for $\hat{\omega}$ now start with an x^2 term in the compactified coordinate $x = r/(r+1)$. (The reparametrization of ω is not related to the expansion at the horizon. It is done in order to be able to fix the angular momentum by a boundary condition). Numerically this reparametrization is used to deal with the possible divergence of the first- and second-order derivatives of any field functions.

C. $D = 5$

Here we present our numerical results for black holes with equal-magnitude angular momenta in five dimensions. We begin with a discussion of the solutions for a generic value of the dilaton coupling constant, $h = 2$. Then we discuss the dependence of the solutions on the dilaton coupling constant, $0 \leq h < \infty$, including the Einstein-Maxwell case ($h = 0$) and the Kaluza-Klein case ($h = h_{KK} = \sqrt{2/3}$). The formulas for the latter are collected in Sec. III. We note that uniqueness of the stationary black holes in five-dimensional Einstein-Maxwell and Einstein-Maxwell-dilaton gravity was discussed by Yazadjiev [45].

1. Dilaton coupling constant $h = 2$

Let us first address the domain of existence of rotating EMd black holes with equal-magnitude angular momenta. For such black holes the domain of existence is always bounded. The boundary is provided by the set of extremal solutions. However, when we consider quantities, that do not depend on the direction of the rotation, the set of static solutions provides a part of the boundary. The nonextremal rotating solutions then reside within this boundary, while solutions outside this boundary exhibit naked singularities.

We illustrate the domain of existence of EMd black holes with dilaton coupling constant $h = 2$ for the scaled horizon

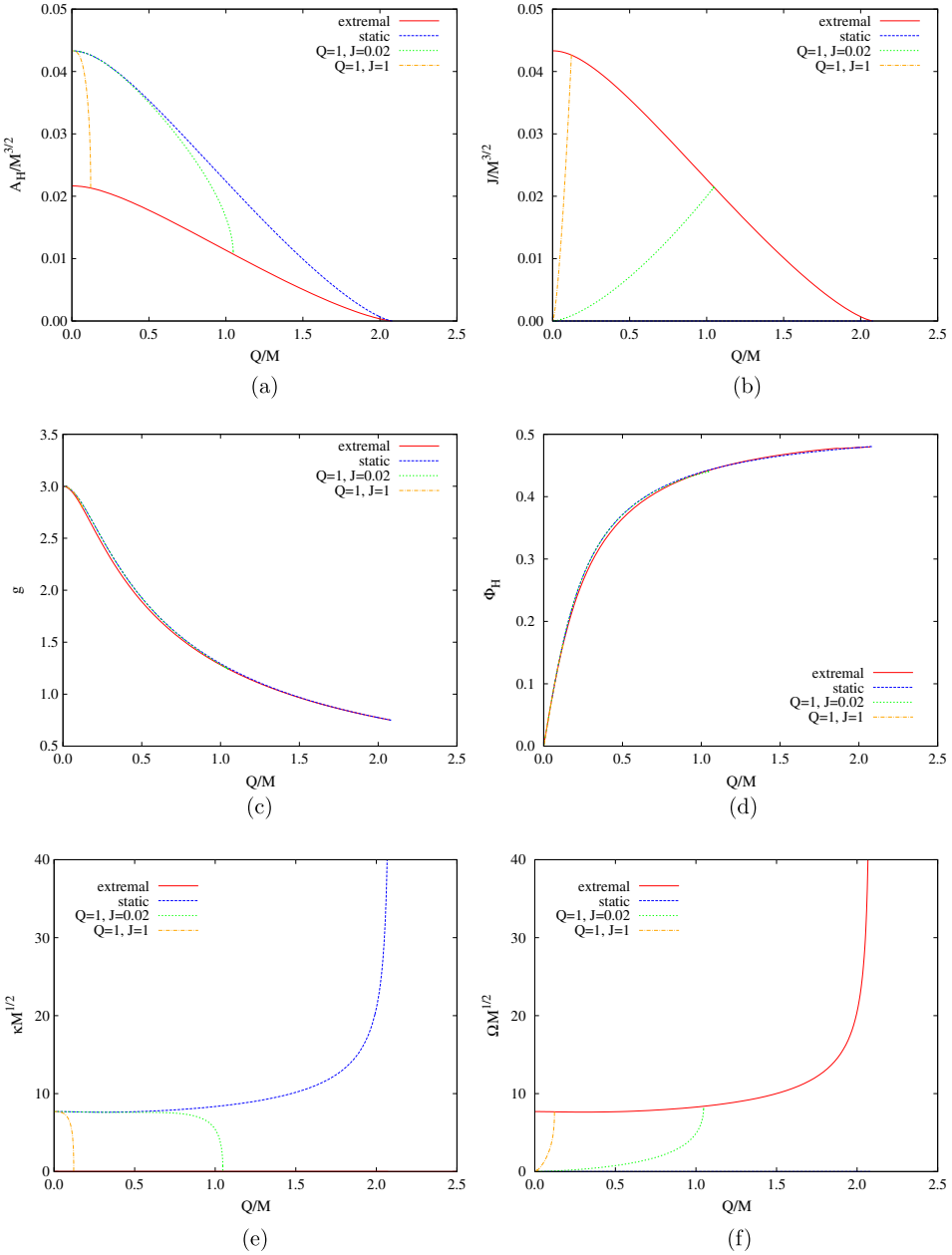

FIG. 3 (color online). Properties of EMd black hole solutions in five dimensions for dilaton coupling constant $h = 2$. (a) The scaled area $a_H = A_H/M^{3/2}$ versus the scaled charge $q = |Q|/M$ for extremal and for static solutions, providing the boundary of the domain of existence. Also shown is a_H versus q for two further sets of nonextremal solutions ($Q = 1$, $J = 0.02$ and $Q = 1$, $J = 1$). For the same sets of (extremal and nonextremal) solutions we exhibit in (b) the scaled angular momenta $j = J/M^{3/2}$ versus q, (c) the gyromagnetic ratio g versus q, (d) the horizon electrostatic potential Φ_H versus q (e) the scaled surface gravity $\bar{\kappa} = \kappa M^{1/2}$ versus q, (f) the scaled horizon angular velocity $\bar{\Omega} = \Omega M^{1/2}$ versus q.

area $a_H = A_H/M^{3/2}$ in Fig. 3(a). Considering a_H versus the scaled charge q, the extremal and static solutions form the lower and upper boundaries of the domain of existence, respectively. In the extremal limit, the horizon area of the static black holes vanishes, while the rotating extremal black holes have finite horizon area. Thus only static extremal black holes have vanishing area, while all other black holes have finite area.

We also exhibit in Fig. 3(a) two further sets of solutions, which are nonextremal, except at their respective endpoints. Here the charge Q and the angular momenta J are kept fixed, in particular, the choices are $Q = 1$, $J = 0.02$ and $Q = 1$, $J = 1$, while the (isotropic) horizon radius $r_{\rm H}$ is varied. These two sets start at a small value of q and end at the respective extremal solutions.

Next to the area we illustrate the scaled angular momenta $j = J/M^{3/2}$ versus q in Fig. 3(b). We note the proportionality of the scaled angular momenta j and the area $a_{\rm H}$, Eq. (48), for the extremal solutions. Since we have chosen $J \geq 0$, the nonextremal rotating solutions reside within the boundary formed by the extremal and the static solutions, which have $j = 0$.

Figure 3(c) exhibits the gyromagnetic ratio g of these black holes. For small charge, the perturbative value $g_{\delta q} = 3$ is found [10], while for larger values of the charge considerable deviations from this value arise, as shown in higher order perturbation theory [13,15,16]. The curves formed by the gyromagnetic ratio g of the extremal black holes and by the gyromagnetic ratio $g_{\delta j}$, Eq. (80), obtained for black holes in the static limit $J \to 0$ [14], enclose the domain, where the gyromagnetic ratio can take its values. Since the extremal and the "static" curve are very close to each other, the static values represent a good approximation for a given value of q. Consequently, the gyromagnetic ratio is not well resolved for the nonextremal sets of solutions in the figure. We recall, that in the KK case, g is given by a single curve, i.e., the KK domain of g is only one dimensional.

The situation is similar for the horizon electrostatic potential $\Phi_{\rm H}$, which we exhibit in Fig. 3(d). Again the static and the extremal solutions forming the boundaries for the admissible values of this quantity are very close to each other, thus the values of the nonextremal black holes are not well discernable here either. In the KK case, $\Phi_{\rm H}$ is again given by a single curve, i.e., its KK domain is only one dimensional.

The surface gravity κ of these black holes is addressed in Fig. 3(e), where the scaled surface gravity $\bar{\kappa} = \kappa M^{1/2}$ is exhibited versus the scaled charge q. The static set of solutions here forms the upper boundary, while the set of extremal solutions, having $\kappa = 0$ (for finite J), forms the lower boundary. At the static extremal black hole, the static curve diverges, $\kappa = \infty$ [36,46], since $h > h_{\rm cr} = \sqrt{2/3}$, Eq. (75). Thus for the set of extremal black holes the surface gravity jumps from zero, its value for finite angular momentum, to infinity in the static limit.

Finally, we exhibit the scaled horizon angular velocity $\bar{\Omega} = \Omega M^{1/2}$ in Fig. 3(f). Here the static black holes, possessing $\Omega = 0$, form the lower boundary, while the extremal black holes form the upper boundary, with all other black holes assuming values in between. Thus the scaled horizon angular velocity and the surface gravity show an analogous behavior, where the static and extremal solutions, however, have switched roles.

2. h dependence

To study the dependence of these black holes on the dilaton coupling constant h, we now consider several fixed values of h: $h = 0$, corresponding to the EM case, $h = 0.5$, $h = \sqrt{2/3}$, corresponding to the KK case, and $h = 2$, the case studied above in more detail. We exhibit properties of these solutions in Figs. 4. In particular, we show the extremal and the static solutions, which form the boundary of the domain of existence for these black holes. All nonextremal rotating black holes are located inside this boundary. The quantities shown are the scaled horizon area $a_{\rm H}$ [Fig. 4(a)], the scaled angular momenta j [Fig. 4(b)], the gyromagnetic ratio g [Fig. 4(c)], the horizon electrostatic potential $\Phi_{\rm H}$ [Fig. 4(d)], the scaled surface gravity $\bar{\kappa}$ (Fig. 4(e)), and the scaled horizon angular velocity $\bar{\Omega}$ [Fig. 4(f)].

For the area and the angular momenta, we note again the proportionality for finite dilaton coupling. For the EM case, $h = 0$, this proportionality holds only along the MP branch, while it is violated on the RN branch of the solutions. We demonstrate this further in Figs. 5, where we exhibit the branch structure for these solutions. In particular, we show the ratio $J/J_{\rm H}$ versus the scaled charge q in Fig. 5(a) for the above set of coupling constants and the ratios $J/A_{\rm H}$ and $J/J_{\rm H}$ versus q for $h = 0$ and $h = 0.5$ in Fig. 5(b).

The figures clearly reveal the two-branch structure of the extremal EM solutions, together with their matching point, and the single-branch structure of the EMd solutions. Comparison with Figs. 2 shows that for the EM solutions only the first part of the near-horizon MP branch and the second part of the near-horizon RN branch are realized globally. For the EMd solutions, on the other hand, the surfaces of near-horizon solutions are reduced to single curves that are—in part—realized globally, for arbitrary finite value of the dilaton coupling h (compare Figs. 1).

In the extremal limit, the horizon area of the static black holes vanishes as long as the dilaton coupling constant h is nonvanishing, no matter how small it is. In contrast, for the static EM black holes, the area remains finite. The EM limit, $h \to 0$, of the extremal static black hole is therefore not smoothly approached.

Turning to the gyromagnetic ratio g, exhibited in Fig. 4(c), we note that it attains the perturbative value $g_{\delta q} = 3$ [10] for small q, independent of the dilaton coupling constant h. For a fixed value of h, the curves formed by the gyromagnetic ratio g of the extremal black holes and by the gyromagnetic ratio $g_{\delta j}$, Eq. (80), obtained for black holes in the static limit $J \to 0$ [14], enclose the domain, where the gyromagnetic ratio can take its values.

In the EM case, the perturbative value obtained for small q, $g_{\delta q} = 3$, coincides with the perturbative value for small j, $g_{\delta j} = 3$, which forms a horizontal line. At the same time, this static limit constitutes a lower bound for the gyromagnetic ratio of all EM black holes with equal-magnitude angular momenta [13,17,18].

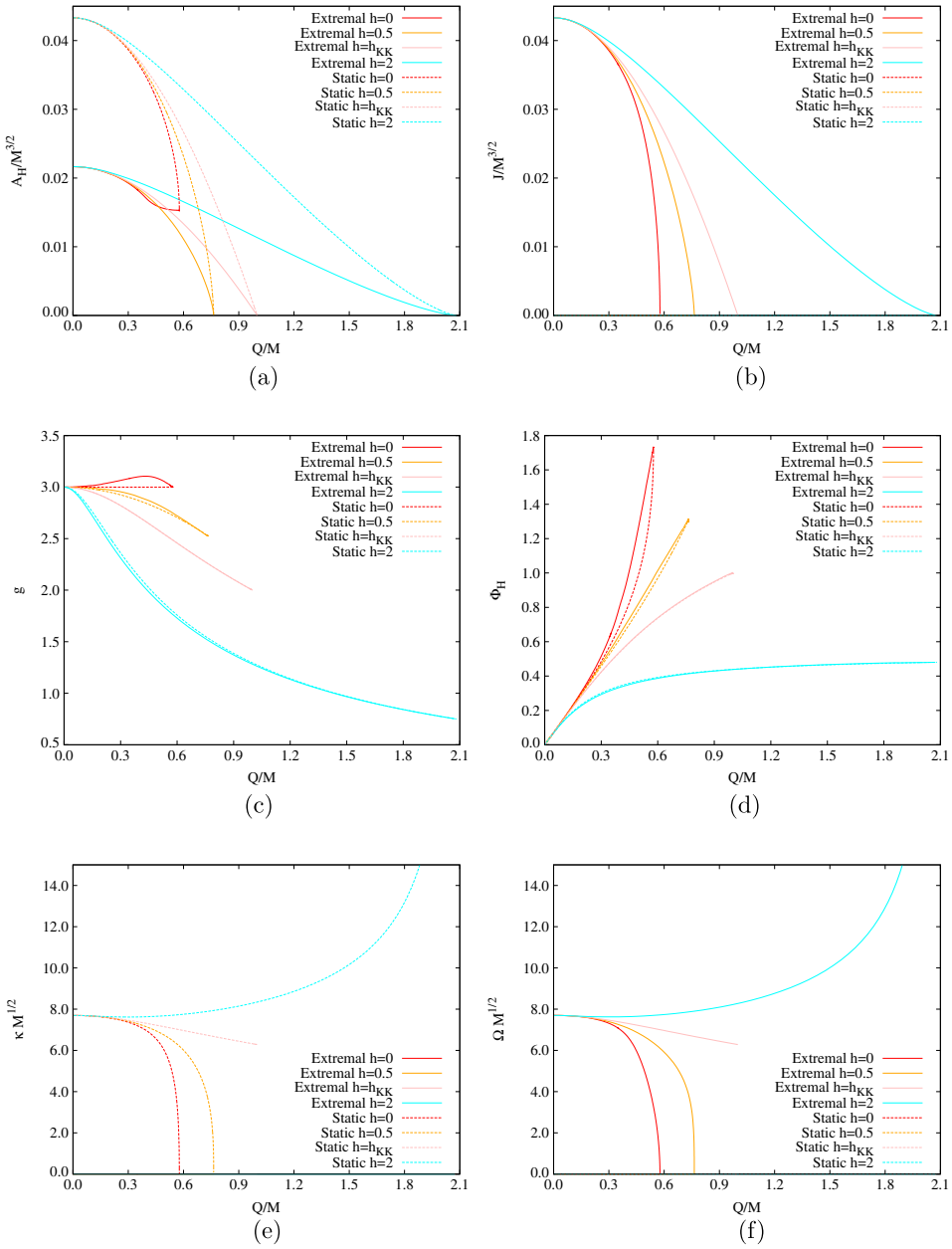

FIG. 4 (color online). Properties of EMd black hole solutions in five dimensions are shown for several values of the dilaton coupling constant h: $h = 0$ (EM), 0.5, $\sqrt{2/3}$ (KK), 2. (a) The scaled area $a_{\mathrm{H}} = A_{\mathrm{H}}/M^{3/2}$ versus the scaled charge $q = |Q|/M$ for extremal and for static solutions, providing the boundary of the domain of existence. For the same sets of (extremal and nonextremal) solutions we exhibit in (b) the scaled angular momenta $j = J/M^{3/2}$ versus q, (c) the gyromagnetic ratio g versus q, (d) the horizon electrostatic potential Φ_{H} versus q, (e) the scaled surface gravity $\bar{\kappa} = \kappa M^{1/2}$ versus q, and (f) the scaled horizon angular velocity $\bar{\Omega} = \Omega M^{1/2}$ versus q.

For small but finite values of the dilaton coupling constant h, the gyromagnetic ratio is no longer constant in the static limit. Instead it decreases monotonically with increasing q, Eq. (80). As the dilaton coupling constant h is increased, the boundary curves of the domain of g approach each other, until at the Kaluza-Klein value h_{KK} both curves coincide, as seen in Eq. (35). Considering the gyromagnetic ratio g versus q, all KK black holes fall on a single curve with $3 \geq g \geq 2$.

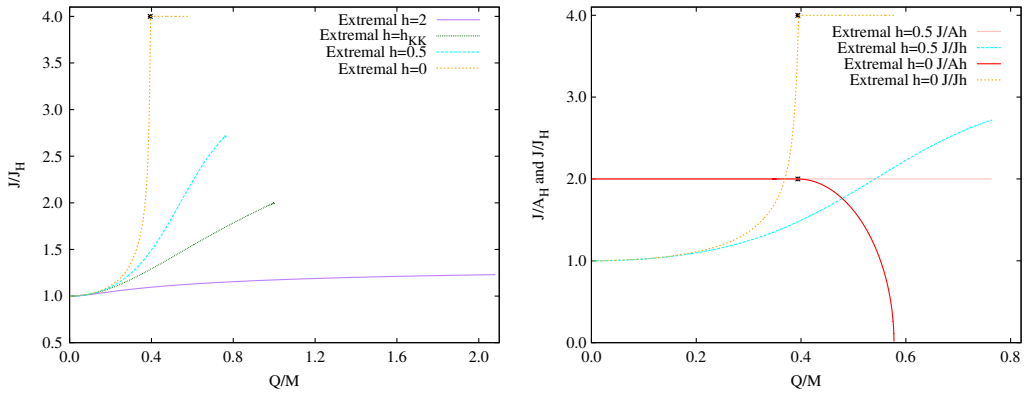

FIG. 5 (color online). (a) J/J_{H} is shown versus the scaled charge q for extremal EMd black hole solutions in five dimensions for $h = 0$ (EM), 0.5, $\sqrt{2/3}$ (KK), and 2. (b) The ratios J/A_{H} and J/J_{H} versus q for $h = 0$ and $h = 0.5$. The asterisks mark the matching point of the two EM branches.

For $h > h_{KK}$, the boundary curves formed by the extremal and the static black holes separate again, retaining common end points. In all cases, however, the static value of g for a given q is a rather good approximation for the true value, which becomes exact in the KK case.

The horizon electrostatic potential Φ_{H} is shown in Fig. 4(d). As always, the static and the extremal solutions form the boundaries for the admissible values of this quantity. Analogous to the case of the gyromagnetic ratio, the two boundary curves are always rather close to each other. They approach each other with increasing h, form a single curve for the Kaluza-Klein value h_{KK} and then separate again. Thus the static value of Φ_{H} for a given q approximates the true value well, and becomes exact in the KK case.

The scaled surface gravity $\bar{\kappa}$ vanishes for the extremal solutions. The curves seen in Fig. 4(e) thus represent the upper boundary of the domain of existence, formed by the static solutions for the various values of the dilaton coupling h. Of particular interest is the extremal endpoint of these static curves. For $h < h_{\mathrm{cr}} = \sqrt{2/3}$ the surface gravity is zero at the endpoint. At the critical value $h = h_{\mathrm{cr}}$ the surface gravity assumes a finite value, κ_{cr}, whereas for $h > h_{\mathrm{cr}}$ the surface gravity diverges at the endpoint [36,46]. Thus for the set of extremal rotating black holes the surface gravity jumps from zero, its value for finite angular momentum, to the finite value κ_{cr} for $h = h_{\mathrm{cr}}$ and to infinity for $h > h_{\mathrm{cr}}$ in the static limit, as indicated in the figure.

The figure for the scaled horizon angular velocity $\bar{\Omega}$, shown in Fig. 4(f), looks completely analogous to the one for the scaled surface gravity. However, here the static solutions form the lower boundary of the domain of existence, since they have $\Omega = 0$, while the upper boundary is formed by the extremal rotating solutions. Inspecting again the endpoint of the set of extremal solutions, we note the same dependence on h. For $h < h_{\mathrm{cr}} = \sqrt{2/3}$ the horizon angular velocity vanishes at the endpoint. At the critical value $h = h_{\mathrm{cr}}$ the horizon angular velocity assumes a finite value, Ω_{cr}, whereas for $h > h_{\mathrm{cr}}$ the horizon angular velocity diverges at the endpoint.

To better understand this analogy, let us inspect Fig. 6(a), where we compare the scaled surface gravity $\bar{\kappa}$ of the static solutions to the scaled horizon angular velocity $\bar{\Omega}$ of the extremal solutions for several values of the dilaton coupling h. We note, that they agree for $h = h_{KK}$, while they are close for other values of h. The situation is analogous, when we compare the scaled area a_{H} of the static solutions to the scaled angular momenta j of the extremal solutions, as seen in Fig. 6(b).

We now recall our discussion in Sec. IIIB. There we showed, that for KK black holes in five dimensions the scaled surface gravity of static black holes indeed agrees with the scaled horizon angular velocity of extremal black holes. Considering the scaled Smarr formula, we furthermore showed relation Eq. (51) for KK black holes, which derived from the fact, that for KK black holes the horizon electrostatic potential only depends on the scaled charge. Since we have seen, that the horizon electrostatic potential depends only little on the angular momenta also for other values of the dilaton coupling h, we conclude that relation Eq. (51) holds approximately also for other values of h. This then leads to the similarity of the static $\bar{\kappa}$ and the extremal $\bar{\Omega}$, as well as the similarity of the static a_{H} and the extremal j, observed in Figs. 6. We conclude, that we can learn much about extremal rotating solutions by only inspecting static solutions.

In Fig. 7(a) we show the scaled charge Q/M versus the scaled relative dilaton charge $\Sigma/(hM)$ for static and extremal solutions and several values of the dilaton coupling. Note that the quadratic relation Eq. (29) is only

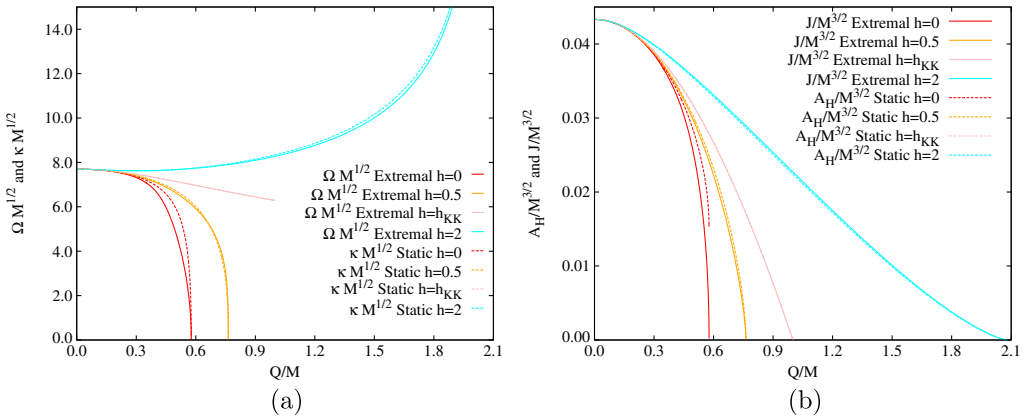

FIG. 6 (color online). Properties of EMd black hole solutions in five dimensions are shown for several values of the dilaton coupling constant h: $h = 0$ (EM), 0.5, $\sqrt{2/3}$ (KK), 2. (a) The scaled surface gravity $\bar{\kappa} = \kappa M^{1/2}$ of the static solutions and the scaled horizon angular velocity $\bar{\Omega} = \Omega M^{1/2}$ of the extremal solutions versus the scaled charge $q = |Q|/M$, (b) the scaled area $a_{\mathrm{H}} = A_{\mathrm{H}}/M^{3/2}$ of the static solutions and the scaled angular momenta $j = J/M^{3/2}$ of the extremal solutions.

fulfilled in the KK case, while the static solutions satisfy a similar quadratic relation,

$$\frac{Q^2}{M + [1 - \frac{2(D-2)h^2}{D-3}]\frac{\Sigma}{2h}} = -\frac{D-3}{D-2}\frac{\Sigma}{h}, \tag{94}$$

valid for arbitrary h. It is interesting to note that this relation coincides with the quadratic relation Eq. (29) of the KK solution, when $h = h_{KK}$. In Fig. 7(a) we see that for extremal solutions with general dilaton coupling, this quadratic relation is almost fulfilled: the extremal curves of Fig. 7(a) are very close to the static curves, where relation Eq. (94) holds exactly. The approximation of the (in general unknown) extremal relation by the static quadratic relation is very good for large dilaton couplings (and exact in the KK case).

In Fig. 7(b) we present the Smarr formula contributions for the extremal and static solutions. Here the situation is similar. Again we note that the extremal and static curves are very close, and we can use the information from the static solutions to gain insight on the extremal solutions.

D. $D > 5$

Let us now turn to black holes in more than five dimensions. Here we show, that the basic features observed for EMd black holes with equal-magnitude angular momenta are retained in higher odd dimensions. To exhibit the dependence on the number of dimensions D, we

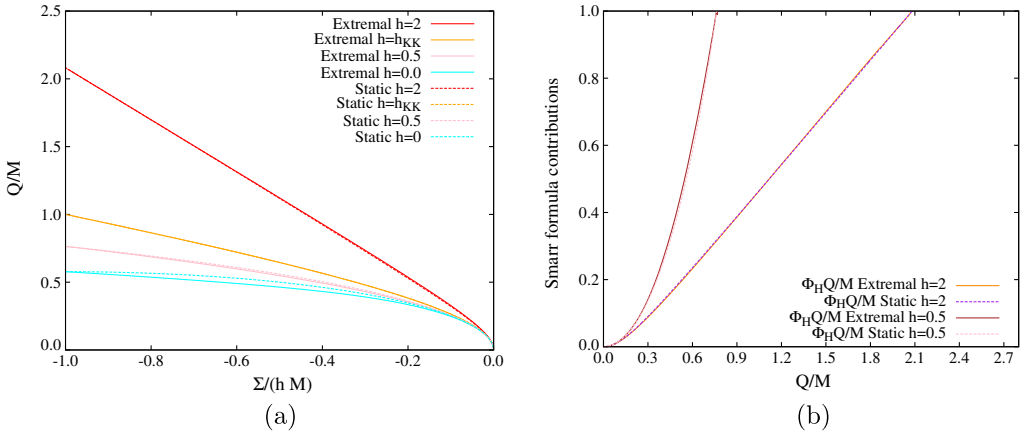

FIG. 7 (color online). (a) The scaled charge $q = Q/M$ versus the scaled relative dilaton charge $\Sigma/(hM)$ for static and extremal solutions with $h = 0$, 0.5, h_{KK} and 2. The quadratic relation Eq. (94) between both scaled charges is fulfilled for every value of h in the static case, and for h_{KK} Eq. (29) in the extremal case. (b) Contributions to the Smarr formula Eq. (27) for static and extremal solutions, for both $h = 0.5$ and $h = 2$.

compare sets of solutions in five, seven, and nine dimensions.

1. $D = 7$

Let us first address the domain of existence again and recall, that unlike the case of a single nonvanishing angular momentum, where no extremal solutions exist in $D > 5$ dimensions [1], extremal solutions always exist for odd-D black holes with equal-magnitude angular momenta.

To study the dependence of these black holes on the dilaton coupling constant h, we again consider several fixed values of h: $h = 0$, corresponding to the EM case, $h_{KK} = \sqrt{3/5}$, corresponding to the KK case, $h_{\rm cr} = \sqrt{8/5}$, corresponding to the critical case of the surface gravity and the horizon angular momentum, and finally $h = 2$.

We exhibit a number of interesting properties of these black hole solutions in Figs. 8. In particular, we show the extremal and the static solutions, which form the boundary of the domain of existence for these seven-dimensional black holes, while all nonextremal rotating black holes are located inside this boundary. The quantities shown are the scaled horizon area $a_{\rm H}$ [Fig. 8(a)], the scaled angular momenta j [Fig. 8(b)], the horizon electrostatic potential $\Phi_{\rm H}$ [Fig. 8(c)], and the scaled surface gravity $\bar{\kappa}$ [Fig. 8(d)].

We note, that the scaled horizon area $a_{\rm H} = A_{\rm H}/M^{5/4}$ is proportional to the scaled angular momenta, as long as h is nonvanishing. For $h = 0$, we find again the two-branch structure of the extremal EM solutions, where only the first part of the near-horizon MP branch and the second part of the near-horizon RN branch are realized globally. For the EMd solutions again the surfaces of near-horizon solutions are reduced to single curves, that are—in part—realized globally, for arbitrary nonvanishing value of the dilaton coupling h.

The gyromagnetic ratio g of these black holes attains the perturbative value $g_{\delta q} = 5$ [10] for small values of q,

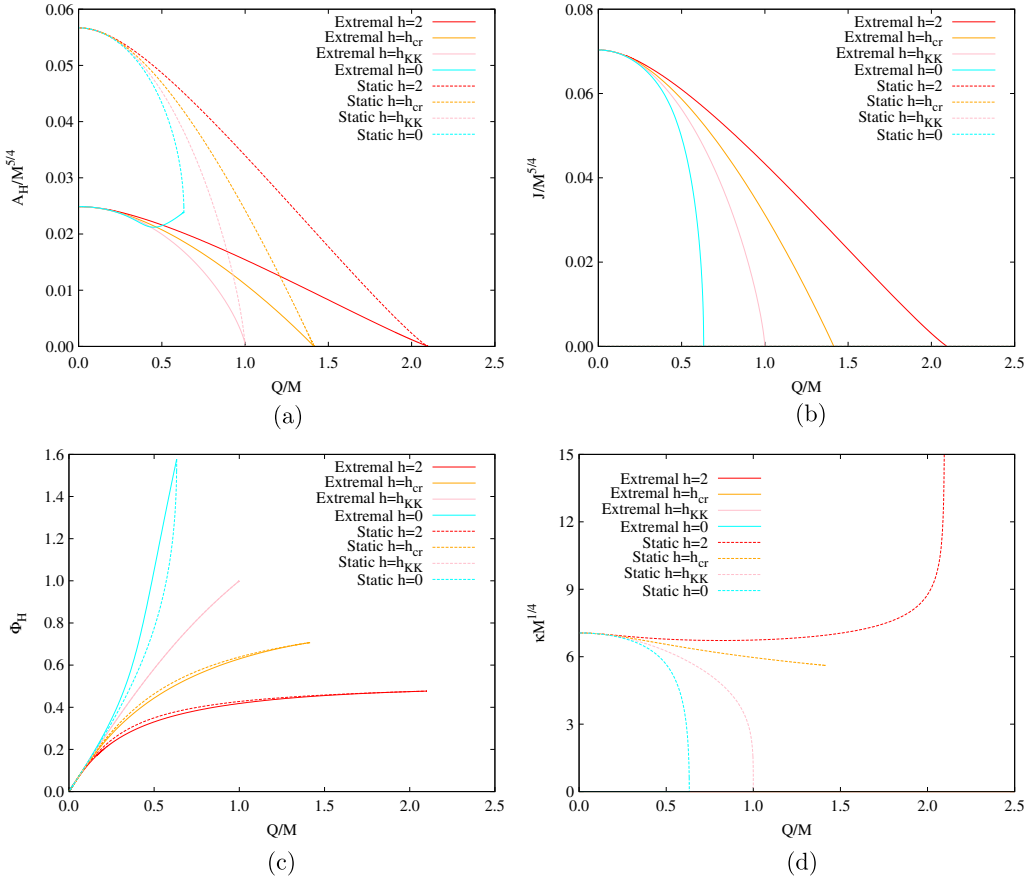

FIG. 8 (color online). Properties of EMd black hole solutions in seven dimensions are shown for several values of the dilaton coupling constant h: $h = 0$ (EM), $h_{KK} = \sqrt{3/5}$, $h_{\rm cr} = \sqrt{8/5}$, and $h = 2$. (a) The scaled area $a_{\rm H} = A_{\rm H}/M^{5/4}$ versus the scaled charge $q = |Q|/M$ for extremal and for static solutions, providing the boundary of the domain of existence. For the same sets of (extremal and static) solutions we exhibit in (b) the scaled angular momenta $j = J/M^{5/4}$ versus q, (c) the horizon electrostatic potential $\Phi_{\rm H}$ versus q, and (d) the scaled surface gravity $\bar{\kappa} = \kappa M^{1/4}$ versus q.

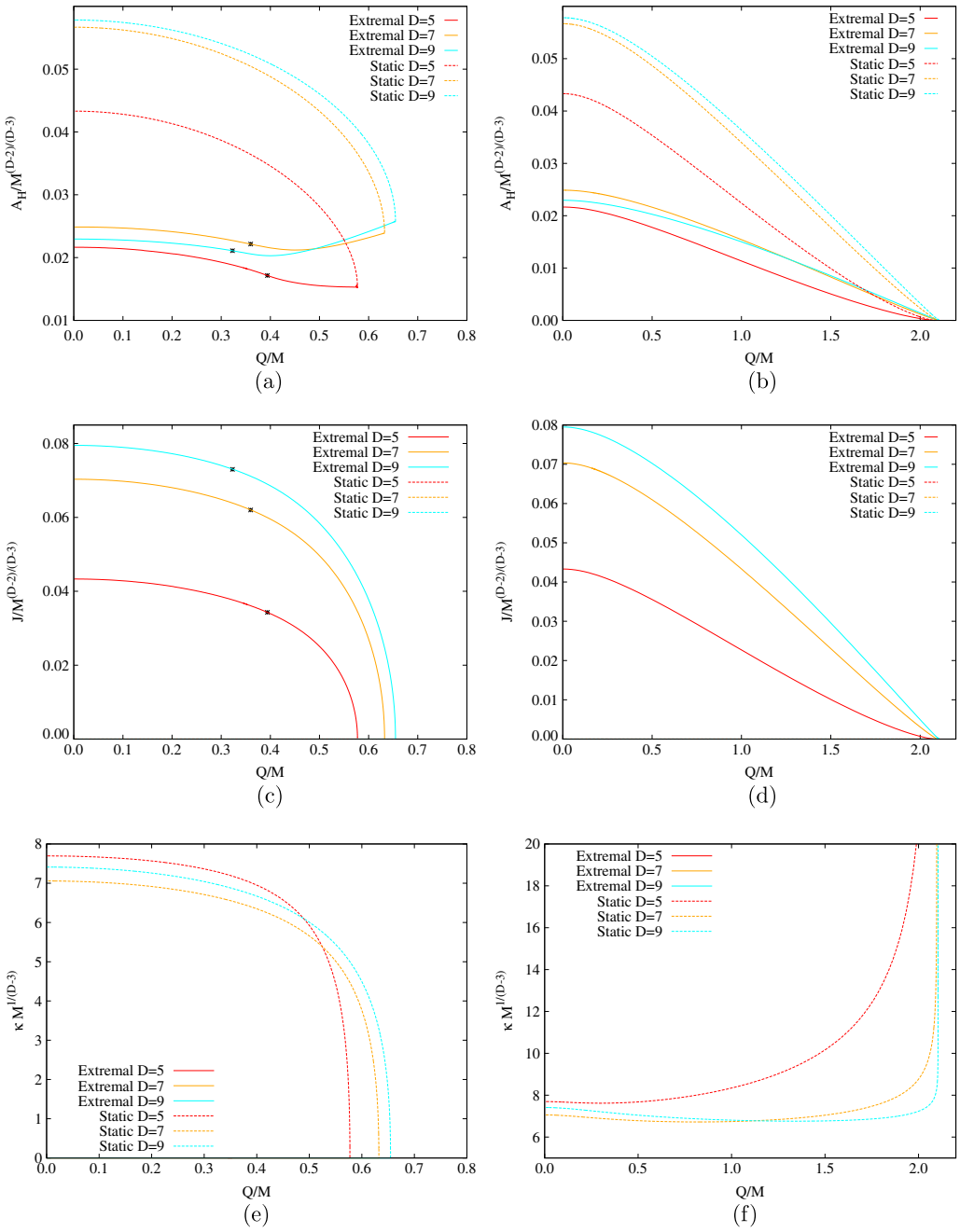

FIG. 9 (color online). Properties of EMd black hole solutions in five, seven, and nine dimensions are shown for the EM case ($h = 0$) (left column) and one example of the EMd case ($h = 2$)(right column). The scaled area $a_{\mathrm{H}} = A_{\mathrm{H}}/M^{(D-2)/(D-3)}$ versus the scaled charge $q = |Q|/M$ (a) for $h = 0$ and (b) for $h = 2$ for extremal and for static solutions, providing the boundary of the domain of existence. For the same sets of solutions we exhibit the scaled angular momenta $j = J/M^{(D-2)/(D-3)}$ versus q, (c) for $h = 0$ and (d) for $h = 2$, and the scaled surface gravity $\bar{\kappa} = \kappa M^{1/(D-3)}$ versus q (e) for $h = 0$ and (f) for $h = 2$. The asterisks mark the matching points of the two EM branches.

independent of the dilaton coupling constant h. In all cases the static value $g_{\delta j}$, Eq. (80), is a rather good approximation for the true value, which becomes exact in the KK case. Likewise, for the horizon electrostatic potential Φ_{H} the static value for a given q approximates the true value well, and becomes exact in the KK case.

The scaled surface gravity $\bar{\kappa} = \kappa M^{1/4}$ of the static solutions forms the upper boundary of the domain of

existence, while the scaled surface gravity of the extremal solutions vanishes. At the extremal endpoints of the static curves the surface gravity is zero for $h < h_{\rm cr} = \sqrt{8/5}$. This includes the KK case in seven dimensions, where $h_{KK} = \sqrt{3/5}$. At the critical value $h = h_{\rm cr}$ the surface gravity assumes a finite value, $\kappa_{\rm cr}$, and for $h > h_{\rm cr}$ the surface gravity diverges at the endpoint [36,46].

As discussed in five dimensions, the situation is analogous for the scaled horizon angular velocity $\bar{\Omega}$ (not shown in the figure). Only here the static solutions form the lower boundary of the domain of existence, since they have $\Omega = 0$, while the upper boundary is formed by the extremal rotating solutions.

Again, we can understand this analogy by recalling our formulas in Sec. IIIB. There we showed that for KK black holes in D dimensions, the scaled surface gravity of static black holes is proportional to the scaled horizon angular velocity of extremal black holes. We furthermore showed relation Eq. (51) for KK black holes, which derived from the fact that for KK black holes the horizon electrostatic potential only depends on the scaled charge.

Since the horizon electrostatic potential depends only little on the angular momenta also for other values of the dilaton coupling h in seven dimensions, relation Eq. (51) holds approximately also for other values of h. The similarity of the static $\bar{\kappa}$ and the extremal $\bar{\Omega}$, as well as the similarity of the static $a_{\rm H}$ and the extremal j thus also holds in seven dimensions. Again we conclude, that we can learn much about extremal rotating solutions from the static solutions.

2. D dependence

The solutions in nine dimensions do not reveal any unexpected behavior, but repeat the pattern observed in five and seven dimensions. Here the special values of the dilaton coupling constant beside the EM case $h = 0$, are the KK case $h_{KK} = \sqrt{4/7}$, known analytically, and the critical case $h_{\rm cr} = \sqrt{18/7}$. As in lower dimensions, for $h = h_{\rm cr}$ the surface gravity of the static solutions and the horizon angular velocity of the extremal rotating solutions remain finite at $q_{\rm max}$, while they diverge at $q_{\rm max}$ for $h > h_{\rm cr}$, and tend to zero at $q_{\rm max}$ for $h < h_{\rm cr}$.

We compare the solutions in five, seven, and nine dimensions in Figs. 9. In particular, we exhibit the EM case ($h = 0$) in the left column and a generic value of the EMd case ($h = 2$) in the right column.

The scaled area $a_{\rm H} = A_{\rm H}/M^{(D-2)/(D-3)}$ of the extremal and static EM solutions is shown in Fig. 9(a), enclosing the domain of existence of the respective sets of black holes. For the extremal solutions it again reveals the two-branch structure, as indicated by the asterisks. As before, the near-horizon solutions are only partly realized globally. The horizon area of the EM solutions is always finite. For the EMd solutions the angular momenta and the horizon area are proportional for all extremal solutions. A single branch of near-horizon solutions is—in part—realized globally. The horizon area of EMd solutions vanishes in the extremal static case.

The gyromagnetic ratio g of these black holes attains the perturbative value $g_{\delta q} = D - 2$ [10] for small q, independent of the dilaton coupling constant h. This indicates already, that g increases with increasing dimension D. For a given q the static value $g_{\delta j}$, Eq. (80), is a rather good approximation for the true value, that becomes exact for h_{KK}. For the EM case $g_{\delta q} = D - 3$ is a rather good approximation in general.

The horizon electrostatic potential $\Phi_{\rm H}$ (not shown in Figs. 9), is remarkably independent of the dimension D, as may be expected from its KK expression, Eq. (40). It is significantly influenced only by the dilaton coupling h. Since its dependence on the angular momenta is small, the horizon electrostatic potential found in the static limit for a given value of q represents a rather good approximation for the horizon electrostatic potential, which becomes exact in the KK case.

The scaled surface gravity $\bar{\kappa} = \kappa M^{1/(D-3)}$ is exhibited in Figs. 9(e) and 9(f). Here the static black holes form the upper boundary of the domain of existence, while the extremal rotating black holes have vanishing $\bar{\kappa}$. At the extremal endpoints of the static curves the surface gravity is zero for $h < h_{\rm cr}$, corresponding to the EM case. At the critical value $h = h_{\rm cr}$ the surface gravity assumes a finite value, $\kappa_{\rm cr}$. For $h > h_{\rm cr}$ the surface gravity diverges at the endpoint, as seen for the EMd case, $h = 2$.

The scaled horizon angular velocity $\bar{\Omega} = \Omega M^{1/(D-3)}$ (not shown in Figs. 9) shows an analogous critical behavior, where the static and the extremal rotating solutions have switched roles. Here the extremal rotating black holes form the upper boundary of the domain of existence, while the static black holes have vanishing $\bar{\Omega}$. For any dimension the scaled horizon angular velocity of the extremal rotating black holes can be inferred to good approximation from the scaled surface gravity of the static black holes.

VI. CONCLUSIONS

We have considered rotating black holes in Einstein-Maxwell-dilaton theory, which are asymptotically flat, and possess a spherical horizon topology. Restricting to odd dimensions, $D = 2N + 1$, and angular momenta with equal magnitude, $J = |J_i|$, $i = 1, ..., N$, the symmetry of the solutions is enhanced, and the resulting cohomogeneity-1 problem is more amenable to approximate analytical treatment and to numerical analysis.

Treating the dilaton coupling constant h as a parameter, we have studied the dependence of these solutions on h. Global analytical solutions for these rotating charged black holes are only available in the Kaluza-Klein case. For extremal solutions, however, the near-horizon formalism can be employed to obtain exact solutions, describing a rotating squashed $\mathrm{AdS}_2 \times S^{D-2}$ spacetime. These near-horizon

solutions are then interpreted as the neighborhood of the event horizon of extremal black holes.

In the EM case, we found two sets of near-horizon solutions for all odd dimensions. Denoting them as the MP branch and the RN branch, since they start at the extremal MP solution and the extremal RN solution, respectively, we noted that the solutions on the MP branch possess proportionality of the angular momenta and the horizon area, whereas the solutions on the RN branch do not. Instead these exhibit proportionality of the angular momenta and the horizon angular momenta.

Interestingly, the branches cross at a critical point, which we denoted as the matching point. Numerical construction of the extremal solutions then revealed, that only parts of these near-horizon solutions are realized globally. The sets of global solutions consist of the first part of the MP branch, reaching up to the matching point, and the second part of the RN branch, starting from the matching point.

For the EMd solutions, on the other hand, we found a single set of near-horizon solutions. But because of the presence of the dilaton field this set depends on one more parameter. However, this parameter can be eliminated by rescaling, so the physical dependence reduces to two independent parameters. Nevertheless, as in the pure EM case, analytical treatment of the extremal KK solutions and numerical construction of the extremal solutions for other values of h have revealed that there are near-horizon solutions that are not realized globally. All extremal EMd solutions possess proportionality of the angular momenta and the horizon area.

We have studied the physical properties of these black holes numerically, in particular their global charges and horizon properties. The scaling symmetry Eqs. (25) and (26) of the solutions has allowed us to give a comprehensive account of all physical properties, by scaling these quantities with the appropriate powers of the mass M or angular momentum J.

For a given dimension D and dilaton coupling constant h, any considered physical property of the corresponding family of black holes then has a domain of existence, which is determined by the set of static black holes on the one hand and the set of extremal rotating black holes on the other hand. A generic nonextremal rotating black hole will be found within this domain of existence, whereas outside this domain singular solutions or no solutions at all should be found.

Addressing some properties, in particular, we note that the gyromagnetic ratio g increases with increasing dimension D. For the EM case, $g = D - 3$ is a rather good approximation in general, while in the EMd case, the gyromagnetic ratio can depend strongly on the scaled charge q. But the static value, obtained perturbatively in the limit $J \to 0$, is a rather good approximation, that becomes exact for h_{KK}.

The horizon electrostatic potential Φ_H, on the other hand, is remarkably independent of the dimension D. It is significantly influenced only by the dilaton coupling h. The static limit for a given q also represents a rather good approximation for the horizon electrostatic potential.

For the scaled surface gravity $\bar{\kappa} = \kappa M^{1/(D-3)}$ the static black holes form the upper boundary of the domain of existence, while the extremal rotating black holes have vanishing $\bar{\kappa}$. At the extremal endpoints of the static curves the surface gravity is zero for $h < h_{cr}$ At the critical value $h = h_{cr}$ the surface gravity assumes a finite value, κ_{cr}, and for $h > h_{cr}$ the surface gravity diverges at the endpoint.

For the scaled horizon angular velocity $\bar{\Omega} = \Omega M^{1/(D-3)}$, on the other hand, the extremal rotating black holes form the upper boundary of the domain of existence, while the static black holes have vanishing $\bar{\Omega}$. Interestingly, the scaled horizon angular velocity of the extremal rotating black holes can be inferred to good approximation from the scaled surface gravity of the static black holes.

While this relation between the scaled horizon angular velocity and the scaled surface gravity is exact in the KK case, for general h it can be seen to arise from the Smarr law, the low dependence of the horizon electrostatic potential on the angular momenta, and the closeness of the horizon area of the static solutions to the angular momenta of the extremal rotating solutions. The surprising finding here is thus, that one can learn much about the extremal rotating solutions from the much simpler static solutions.

We note, that in four dimensions analogous relations hold, when the extremal and the static black hole solutions of EM theory are considered, i.e., the extremal Kerr-Newman (KN) and the static RN solutions, or the KK black holes of four-dimensional EMd theory. We conjecture that these observations hold also for general dilaton coupling h. Since these EMd black holes represent a cohomogeneity-2 problem, we have not yet performed the corresponding numerical calculations to obtain the extremal solutions for general h.

Figure 10(a) shows that the electrostatic potential is rather independent of the angular momentum, also for the four-dimensional EM case, while the KK solutions again have no dependence on the angular momentum. Moreover, for a given scaled charge, the scaled horizon area of the static RN solutions is very close to the scaled angular momentum of the extremal KN solutions, as long as the scaled charge is not too close to its maximal value, as seen in Fig. 10(b). For the KK solutions, on the other hand, the scaled horizon area of the static solutions and the extremal solutions is identical.

Consequently, it follows from the Smarr relation in four dimensions that the scaled surface gravity of the static RN solutions is very close to one-half of the scaled horizon angular velocity of the extremal KN solutions. This is illustrated in Fig. 10(c). For the KK solutions the relation $2\bar{\kappa}_{st} = \bar{\Omega}_{ex}$ holds exactly, and we expect that this relation should hold approximately for all values of the dilaton coupling.

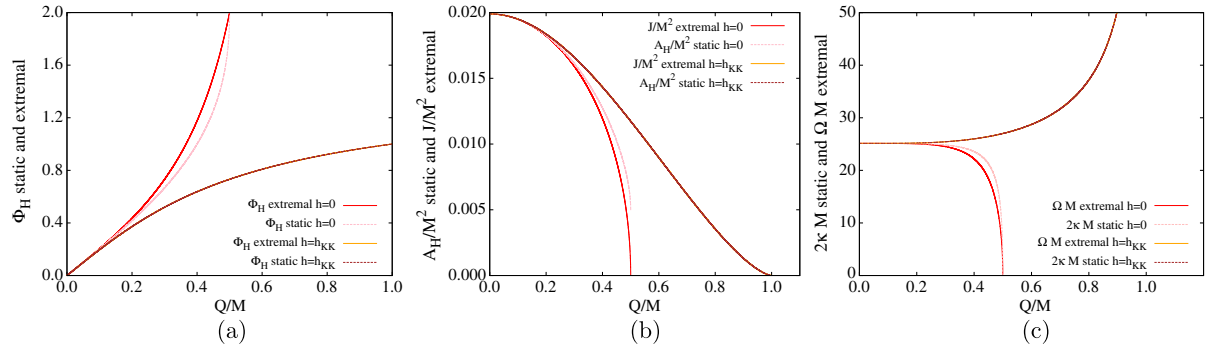

FIG. 10 (color online). Properties of EMd black hole solutions in four dimensions are shown for the values of the dilaton coupling constant h: $h = 0$ (EM), $3/\sqrt{2}$ (KK). The horizon electrostatic potential Φ_H of the extremal and static solutions (a), the scaled horizon area $a_H = A_H/M^2$ of the static solutions and the scaled angular momentum $j = J/M^2$ of the extremal solutions (b), and the scaled surface gravity $\bar{\kappa} = \kappa M$ of the static solutions and the scaled horizon angular velocity $\bar{\Omega} = \Omega M$ (c) versus the scaled charge $q = |Q|/M$.

Concerning the near-horizon geometry, in [40] four-dimensional Kaluza-Klein black holes are studied. However, these solutions possess both electric and magnetic charge [35,47]. Interestingly, here (for fixed magnetic charge) also two branches of black holes are present: the ergo-free branch, which connects to the static RN solution, and the ergo branch, which connects to the extremal Kerr solution.

The near-horizon geometry of the ergo-free branch is independent of the particular value of the dilaton at infinity; therefore, this branch represents an attactor. In contrast, the near-horizon geometry of the ergo branch does depend on the value of the dilaton at infinity and so does the value of the dilaton at the horizon. Of course, for a given angular momentum and charge all these solutions are equivalent under the scaling symmetry. But the scaling relation depends on the asymptotic value of the dilaton.

This property of the ergo branch of four-dimensional EMd black holes is similar to what we have found for the branch of extremal EMd black holes in odd-D dimensions, where the geometry at the horizon also depends on the asymptotic value of the dilaton at infinity. But since the area is proportional to the total angular momentum, if the total angular momentum is fixed, the attractor mechanism works and the entropy does not depend on the value of the dilaton at infinity. We plan to investigate these four-dimensional EMd solutions further, allowing for general values of the dilaton coupling constant [47].

Another case of interest in this connection is represented by the black holes of Einstein-Maxwell-Chern-Simons (EMCS) theory [48–53]. In the supergravity case, these black holes are known analytically. The extremal black holes then again exhibit two branches, an ergo-free branch and an ergo branch. When the Chern-Simons (CS) coupling constant is increased beyond the supergravity value, one of the branches of extremal black holes becomes counter-rotating. When the CS coupling constant is increased even further, beyond a critical value further branches of extremal black holes arise.

Comparing these global EMCS solutions to near-horizon solutions, one realizes that the relation between global solutions and near-horizon solutions becomes even more diverse than observed in EMd theory. In particular, such an EMCS near-horizon solution can correspond to (i) more than one global solution, (ii) precisely one global solution, or (iii) no global solution at all. Clearly, only a study of near-horizon solutions is insufficient to clarify the domain of existence of extremal solutions. Thus the construction of the global solutions is indeed essential, as was first observed for the extremal dyonic black holes of $D = 4$ Gauß-Bonnet gravity [54].

ACKNOWLEDGMENTS

We would like to thank J. Viebahn for initial collaboration on this project, and B. Kleihaus and E. Radu for helpful discussions. We gratefully acknowledge support by the Spanish Ministerio de Ciencia e Innovacion, Research Project No. FIS2011-28013, and by the DFG, in particular, the DFG Research Training Group 1620 "Models of Gravity." J. L. B.-S. was supported by the Spanish Universidad Complutense de Madrid.

[1] R. C. Myers and M. J. Perry, Ann. Phys. (N.Y.) **172**, 304 (1986).
[2] R. C. Myers, arXiv:1111.1903.
[3] D. Youm, Phys. Rep. **316**, 1 (1999).
[4] K.-i. Maeda and M. Nozawa, Prog. Theor. Phys. Suppl. **189**, 310 (2011).
[5] D. Marolf, arXiv:1107.1022.
[6] A. Chodos and S. L. Detweiler, Gen. Relativ. Gravit. **14**, 879 (1982).
[7] V. P. Frolov, A. I. Zelnikov, and U. Bleyer, Ann. Phys. (N.Y.) **44**, 371 (1987).
[8] J. H. Horne and G. T. Horowitz, Phys. Rev. D **46**, 1340 (1992).
[9] J. Kunz, D. Maison, F. Navarro-Lérida, and J. Viebahn, Phys. Lett. B **639**, 95 (2006).
[10] A. N. Aliev and V. P. Frolov, Phys. Rev. D **69**, 084022 (2004).
[11] A. N. Aliev, Mod. Phys. Lett. A **21**, 751 (2006).
[12] A. N. Aliev, Phys. Rev. D **74**, 024011 (2006).
[13] F. Navarro-Lérida, Gen. Relativ. Gravit. **42**, 2891 (2010).
[14] A. Sheykhi, M. Allahverdizadeh, Y. Bahrampour, and M. Rahnama, Phys. Lett. B **666**, 82 (2008).
[15] M. Allahverdizadeh, J. Kunz, and F. Navarro-Lérida, Phys. Rev. D **82**, 024030 (2010).
[16] M. Allahverdizadeh, J. Kunz, and F. Navarro-Lérida, Phys. Rev. D **82**, 064034 (2010).
[17] J. Kunz, F. Navarro-Lérida, and A. K. Petersen, Phys. Lett. B **614**, 104 (2005).
[18] J. Kunz, F. Navarro-Lérida, and J. Viebahn, Phys. Lett. B **639**, 362 (2006).
[19] J. L. Blázquez-Salcedo, J. Kunz, and F. Navarro-Lérida, Phys. Lett. B **727**, 340 (2013).
[20] M. Cvetic, G. W. Gibbons, and C. N. Pope, Phys. Rev. Lett. **106**, 121301 (2011).
[21] M. Ansorg and H. Pfister, Classical Quantum Gravity **25**, 035009 (2008).
[22] J. Hennig, M. Ansorg, and C. Cederbaum, Classical Quantum Gravity **25**, 162002 (2008).
[23] M. Ansorg and J. Hennig, Classical Quantum Gravity **25**, 222001 (2008).
[24] J. Hennig, C. Cederbaum, and M. Ansorg, Commun. Math. Phys. **293**, 449 (2010).
[25] M. Ansorg and J. Hennig, Phys. Rev. Lett. **102**, 221102 (2009).
[26] J. Hennig and M. Ansorg, Ann. Henri Poincare **10**, 1075 (2009).
[27] M. Ansorg, J. Hennig, and C. Cederbaum, Gen. Relativ. Gravit. **43**, 1205 (2011).
[28] A. Castro and M. J. Rodríguez, Phys. Rev. D **86**, 024008 (2012).
[29] S. S. Yazadjiev, Phys. Rev. D **87**, 024016 (2013).
[30] S. Yazadjiev, Classical Quantum Gravity **30**, 115010 (2013).
[31] J. P. Gauntlett, R. C. Myers, and P. K. Townsend, Classical Quantum Gravity **16**, 1 (1999).
[32] B. Kleihaus, J. Kunz, and F. Navarro-Lérida, Phys. Rev. Lett. **90**, 171101 (2003).
[33] P. M. Llatas, Phys. Lett. B **397**, 63 (1997).
[34] G. W. Gibbons and D. L. Wiltshire, Ann. Phys. (N.Y.) **167**, 201 (1986); **176**, 393(E) (1987).
[35] D. Rasheed, Nucl. Phys. **B454**, 379 (1995).
[36] G. W. Gibbons and K.-i. Maeda, Nucl. Phys. **B298**, 741 (1988).
[37] D. Garfinkle, G. T. Horowitz, and A. Strominger, Phys. Rev. D **43**, 3140 (1991); **45**, 3888(E) (1992).
[38] R. Gregory and J. A. Harvey, Phys. Rev. D **47**, 2411 (1993).
[39] P. Figueras, H. K. Kunduri, J. Lucietti, and M. Rangamani, Phys. Rev. D **78**, 044042 (2008).
[40] D. Astefanesei, K. Goldstein, R. P. Jena, A. Sen, and S. P. Trivedi, J. High Energy Phys. 10 (**2006**) 058.
[41] K. Goldstein and R. P. Jena, J. High Energy Phys. 11 (**2007**) 049.
[42] H. K. Kunduri and J. Lucietti, Living Rev. Relativity **16**, 8 (2013).
[43] B. Kleihaus and J. Kunz, Phys. Rev. Lett. **86**, 3704 (2001).
[44] U. Ascher, J. Christiansen, and R. D. Russell, Math. Comput. **33**, 659 (1979); ACM Transactions on Computer Systems **7**, 209 (1981).
[45] S. Yazadjiev, J. High Energy Phys. 06 (**2011**) 083.
[46] G. T. Horowitz and A. Strominger, Nucl. Phys. **B360**, 197 (1991).
[47] B. Kleihaus, J. Kunz, and F. Navarro-Lérida, Phys. Rev. D **69**, 081501 (2004).
[48] J. C. Breckenridge, R. C. Myers, A. W. Peet, and C. Vafa, Phys. Lett. B **391**, 93 (1997).
[49] M. Cvetic, H. Lu, and C. N. Pope, Phys. Lett. B **598**, 273 (2004).
[50] Z. W. Chong, M. Cvetic, H. Lu, and C. N. Pope, Phys. Rev. Lett. **95**, 161301 (2005).
[51] J. Kunz and F. Navarro-Lérida, Phys. Rev. Lett. **96**, 081101 (2006).
[52] J. L. Blázquez-Salcedo, J. Kunz, F. Navarro-Lérida, and E. Radu, Phys. Rev. Lett. **112**, 011101 (2014).
[53] H. K. Kunduri and J. Lucietti, Classical Quantum Gravity **26**, 245010 (2009).
[54] C.-M. Chen, D. V. Gal'tsov, and D. G. Orlov, Phys. Rev. D **78**, 104013 (2008).

3.6 Results on Einstein-Maxwell-Chern-Simons black holes

Let us present now our results on Einstein-Maxwell-Chern-Simons black holes. This is the topic of the paper Physical Review Letters **112** (2014) 011101 [7], presented in the following section 3.6.1. We study 5 dimensional black holes, again with an event horizon of spherical topology, and consider equal-magnitude angular momenta. Like in the EMd case, these black holes are generalizations of the Reissner-Nordström and Myers-Perry solutions. In this case the value of the Chern-Simons coupling parameter is also free. We re-obtain the two-branch structure of the extremal Einstein-Maxwell black holes.

We are again interested in extremal black holes, which can be used to obtain the boundary of the domain of existence. But in this case the situation is much more complicated. The main results can be summarized as follows:

- We again perform the analysis by combining numerical methods with the near-horizon formalism. But in this case the situation is more complicated because of the complex branch structure of the solutions, which can only be seen in the mass and the angular velocity. Hence the near-horizon geometry alone cannot be used to completely characterize the space of solutions of these extremal black holes.

- In particular, we observe that for Chern-Simons couplings above 2 times the supergravity value, non-uniqueness is lost in several ways. First, it can be seen that multiple global solutions correspond to one near-horizon solution. Consider for example extremal solutions with equal angular momentum and electric charge. There is a sequence of these solutions with the same horizon geometry, but which can be distinguised by the internal parameters of their functions. This means that these global solutions have the same values of their horizon area and horizon angular momentum, but can be told apart in their mass or angular velocity.

  On the other hand, there are near-horizon solutions which are not obtained globally. This is similar to what we obtained in EMd theory. Again these non-physical near-horizon solutions are connected to the physical ones.

  We conclude that the near-horizon formalism is very limited at this range of the parameters of Einstein-Maxwell-Chern-Simons theory.

- Non-uniqueness is also lost in the sense that global charges no longer determine completely a black hole: there are black holes of equal mass, electric charge, and angular momentum that have different near-horizon geometry. These black holes can be distinguised by their values of the area or horizon angular momentum. These solutions are associated with the branching point and are found in groups of two solutions, meaning there are two solutions with the same global charges, but two different near-horizon geometries.

- The branch structure obtained in the global parameters gives raise to very exceptional configurations. There is an infinite sequence of non-static configurations with null angular momentum. These configurations can be characterized by the node number of the angular component of the gauge field. Their mass increases with the node number, and asymptotically reach the mass of the static configuration.

- The branch structure also includes extremal solutions with null angular velocity, but non-null angular momentum. Even more, the static configuration is isolated from this non-static solution with vanishing angular velocity or momentum. The static solution is only reached as a limit as the node number of the non-static configurations with null angular momentum is increased to infinity.

- Finally, a very interesting feature is that we can have non-uniqueness between non-extremal and extremal solutions. There are extremal solutions whose global charges are equal to those of a non-extremal configuration.

3.6.1 Publication: Jose Luis Blázquez-Salcedo, Jutta Kunz, Francisco Navarro-Lérida and Eugen Radu, *Sequences of Extremal Radially Excited Rotating Black Holes*, Physical Review Letters 112 (2014) 011101

Sequences of Extremal Radially Excited Rotating Black Holes

Jose Luis Blázquez-Salcedo,[1] Jutta Kunz,[2] Francisco Navarro-Lérida,[3] and Eugen Radu[2]
[1]Department de Física Teórica II, Ciencias Físicas Universidad Complutense de Madrid, E-28040 Madrid, Spain
[2]Institut für Physik, Universität Oldenburg Postfach 2503, D-26111 Oldenburg, Germany
[3]Department de Física Atómica, Molecular y Nuclear, Ciencias Fsicas Universidad Complutense de Madrid, E-28040 Madrid, Spain
(Received 2 August 2013; published 7 January 2014)

In the Einstein-Maxwell-Chern-Simons theory the extremal Reissner-Nordström solution is no longer the single extremal solution with vanishing angular momentum, when the Chern-Simons coupling constant reaches a critical value. Instead a whole sequence of rotating extremal $J = 0$ solutions arises, labeled by the node number of the magnetic U(1) potential. Associated with the same near horizon solution, the mass of these radially excited extremal solutions converges to the mass of the extremal Reissner-Nordström solution. On the other hand, not all near horizon solutions are also realized as global solutions.

DOI: 10.1103/PhysRevLett.112.011101 PACS numbers: 04.40.Nr, 04.20.Jb, 04.50.-h, 04.70.-s

Introduction.—Higher-dimensional black hole spacetimes have received much interest in recent years, associated with various developments in gravity and high energy physics. In particular, the first successful statistical counting of black hole entropy in string theory was performed for an extremal static Reissner-Nordström (RN) black hole in five spacetime dimensions [1].

However, in odd dimensions the Einstein-Maxwell (EM) action may be supplemented by a Chern-Simons (CS) term. In five dimensions, for a certain value of the CS coefficient $\lambda = \lambda_{SG}$, the theory corresponds to the bosonic sector of $D = 5$ supergravity, where rotating black hole solutions are known analytically [2–5]. A particularly interesting subset of these black holes, the Breckenridge-Myers-Peet-Vafa [3] solutions, corresponds to extremal cohomogeneity-1 solutions, where both angular momenta have equal magnitude. These black holes have a nonrotating horizon, although their angular momentum is nonzero. It is stored in the Maxwell field, with a negative fraction of the total angular momentum stored behind the horizon [6–8].

As conjectured in Ref. [6], supersymmetry is associated with the borderline between stability and instability, since for $\lambda > \lambda_{SG}$ a rotational instability arises, where counterrotating black holes appear [9]. Moreover, when the CS coefficient is increased beyond the critical value of $2\lambda_{SG}$, Einstein-Maxwell-Chern-Simons (EMCS) black holes—with the horizon topology of a sphere—are no longer uniquely characterized by their global charges [9].

Focusing on extremal solutions with equal magnitude angular momenta, we here reanalyze five-dimensional EMCS black holes in the vicinity and beyond the critical value of the CS coupling constant $2\lambda_{SG}$. We obtain these cohomogeneity-1 solutions numerically, solving the field equations with appropriate boundary conditions.

These extremal black holes are associated with analytical near horizon solutions, obtained in the entropy function formalism. Surprisingly, however, certain sets of near horizon solutions are associated with more than one global solution, whereas other sets of near horizon solutions do not possess global counterparts. In particular, we find whole sequences of radially excited extremal solutions, all with the same area and angular momenta for a given charge.

The model.—We consider the EMCS action with Lagrangian density [6]

$$\mathcal{L} = \frac{1}{16\pi G_5}\left[\sqrt{-g}(R - F^2) - \frac{2\lambda}{3\sqrt{3}}\varepsilon^{\mu\nu\alpha\beta\gamma}A_\mu F_{\nu\alpha}F_{\beta\gamma}\right] \quad (1)$$

with curvature scalar R, Newton's constant G_5, gauge potential A_μ, field strength tensor $F_{\mu\nu} = \partial_\mu A_\nu - \partial_\nu A_\mu$, and CS coupling constant λ (with $\lambda_{SG} = 1$).

To obtain stationary cohomogeneity-1 solutions we employ for the metric the parametrization [10]

$$\begin{aligned} ds^2 = &-f dt^2 + \frac{m}{f}(dr^2 + r^2 d\theta^2) \\ &+ \frac{lr^2}{f}\left[\sin^2\theta\left(d\varphi_1 - \frac{\omega}{r}dt\right)^2 + \cos^2\theta\left(d\varphi_2 - \frac{\omega}{r}dt\right)^2\right] \\ &+ \frac{m-l}{f}r^2\sin^2\theta\cos^2\theta(d\varphi_1 - d\varphi_2)^2, \end{aligned} \quad (2)$$

and for the gauge potential

$$A_\mu dx^\mu = a_0 dt + a_\varphi(\sin^2\theta d\varphi_1 + \cos^2\theta d\varphi_2). \quad (3)$$

To obtain asymptotically flat solutions, the metric functions should satisfy the following set of boundary conditions at infinity: $f|_{r=\infty} = m|_{r=\infty} = l|_{r=\infty} = 1$, $\omega|_{r=\infty} = 0$. We choose a gauge such that $a_0|_{r=\infty} = a_\varphi|_{r=\infty} = 0$. In isotropic coordinates the horizon is located at $r_{\rm H} = 0$. An expansion at the horizon yields $f = f_4 r^4 + f_\alpha r^\alpha + \cdots$, $m = m_2 r^2 + m_\beta r^\beta + \cdots$, $l = l_2 r^2 + l_\gamma r^\gamma + \cdots$, $\omega = \Omega_{\rm H} r + \omega_2 r^2 + \cdots$, $a_0 = a_{0,0} + a_{0,\epsilon} r^\epsilon + \cdots$, $a_\varphi = a_{\varphi,0} + a_{\varphi,\mu} r^\mu + \cdots$.

Interestingly, the coefficients α, β, γ, ϵ, μ, and ν can be noninteger.

The global charges of these solutions can be read from the asymptotic expansion [9]

$$f = 1 - \frac{8G_5 M}{3\pi r^2} + \cdots, \qquad \omega = \frac{4G_5 J}{\pi r^3} + \cdots,$$
$$a_0 = \frac{4G_5 Q}{\pi r^2} + \cdots, \qquad a_\varphi = -\frac{4G_5 \mu_{\rm mag}}{\pi r^2} + \cdots, \tag{4}$$

together with their magnetic moment $\mu_{\rm mag}$. These extremal solutions satisfy the Smarr formula [6] $M = 3\Omega_{\rm H} J + \Phi_{\rm H} Q$, and the first law $dM = 2\Omega_{\rm H} dJ + \Phi_{\rm H} dQ$, where $A_{\rm H} = 2\pi^2 \sqrt{l_2} m_2 / {f_4}^{3/2}$ is the horizon area, $\Omega_{\rm H}$ is the horizon angular velocity, and $\Phi_{\rm H} = -(a_{0,0} + \Omega_{\rm H} a_{\varphi,0})$ is the horizon electrostatic potential.

The near horizon solutions.—A partial analytical understanding of the properties of the solutions can be achieved by studying their near horizon expression in conjunction with the attractor mechanism [11]. The advantage of the latter is that we can compute the physical charges and obtain semianalytic expressions for the entropy as a function of the electric charge and the angular momentum.

To apply the entropy function for the near horizon geometry of the extremal EMCS solutions, one uses the ansatz [12]

$$ds^2 = v_1 \left(\frac{d\rho^2}{\rho^2} - \rho^2 dt^2 \right) + v_2 [\sigma_1^2 + \sigma_2^2 + v_3 (\sigma_3 - \alpha \rho dt)^2],$$
$$A_\mu dx^\mu = -e\rho dt + p(\sigma_3 - \alpha \rho dt), \tag{5}$$

where $\sigma_1^2 + \sigma_2^2 = d\bar{\theta}^2 + \sin^2\bar{\theta} d\psi^2$, $\sigma_3 = d\phi + \cos\bar{\theta} d\psi$, with $\bar{\theta} = 2\theta$, $\phi = \varphi_1 + \varphi_2$, $\psi = \varphi_2 - \varphi_1$, with constants v_1, v_2, e, p, and α; ρ is the radial coordinate.

In the entropy function formalism, the entropy can be found from the extremum of the entropy function $S = 2\pi(2\alpha J + e\hat{q} - h)$ in which $h = \int d\theta d\varphi_1 d\varphi_2 \sqrt{-g}\mathcal{L}$ and $2J = \partial h / \partial \alpha$, $\hat{q} = \partial h / \partial e$. However, the analysis is somehow intricate due to the presence of the CS term. For example, for $\lambda \neq 0$, the constant $\hat{q}$ cannot be identified with the electric charge and the extremization equations $\partial S / \partial v_a = \partial S / \partial e = \partial S / \partial \alpha = 0$ should be used together with the Maxwell-Chern-Simons equations [13]. The near horizon solutions are found in terms of p and v_1 (this holds also for S, J, and Q). However, for a generic nonzero $\lambda \neq \lambda_{SC}$, it is not possible to write an explicit expression of $S = A_{\rm H}/4G_5$ as a function of Q and J, and one has to resort to solving the algebraic relations numerically. In Fig. 1 we present the horizon area $A_{\rm H}$ versus the angular momentum J for extremal black holes with $\lambda = 5$ and $|Q| = 8\sqrt{3}\pi^2$. The near horizon values are represented by thick solid lines. One can see, for instance, that three different near horizon solutions may exist with the same global charges J and Q, for not very large values of J.

However, the existence of near horizon solutions does not guarantee, in general, their existence as global solutions. Moreover, it is not ruled out that one near horizon solution may correspond to several different global solutions. This lack of a one-to-one correspondence between near horizon solutions and global solutions implies that a complete analysis of the solutions in this theory requires the computation of the global solutions.

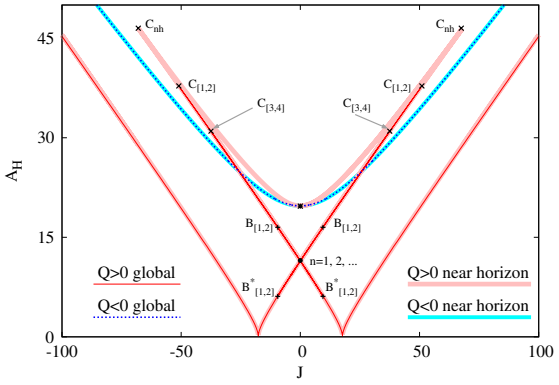

FIG. 1 (color online). Horizon area $A_{\rm H}$ versus angular momentum J for extremal black holes with $\lambda = 5$ and $|Q| = 8\sqrt{3}\pi^2$. Both near horizon and global solutions are included. The asterisk marks the extremal static solution.

The numerical results.—The global solutions are found by solving numerically the EMCS equations subject to the boundary conditions described above. In the numerical calculations [14], we introduce a compactified radial coordinate $\bar{r} = r/(1+r)$ and employ units such that $16\pi G_5 = 1$.

Coming back again to Fig. 1, we also exhibit there the curves corresponding to the global solutions computed numerically (thin lines). For $Q < 0$ the near horizon and the global solutions agree, indicating that the near horizon solutions are realized globally. The situation completely changes for $Q > 0$. First of all, we observe that the cusp present for the near horizon solutions $C_{\rm nh}$ does not coincide with the corresponding one for the global solutions $C_{[1,2]}$. As a consequence, the near horizon solutions between both cusps are not realized globally. Moreover, all of the near horizon branch that connects the static extremal solution (marked by an asterisk in the figure) with the cusp $C_{\rm nh}$ is not globally realized either, except for the static extremal solution. In that sense, we can state that for $\lambda > 2$ the static extremal solution with $Q > 0$ is rotationally isolated from the rest of the extremal solutions, since its horizon area is significantly larger than that of any extremal solutions with $Q > 0$ and small angular momentum. Thus there are sets of near horizon solutions that do not possess counterparts in the sets of global solutions [15]. However, when looking at the global charges we see that the situation is more subtle and the static extremal solution can be infinitesimally approached, concerning its global charges, by an intricate pattern of rotating extremal black hole branches.

In order to show that pattern, we present in Fig. 2 the mass M versus the angular momentum J for global

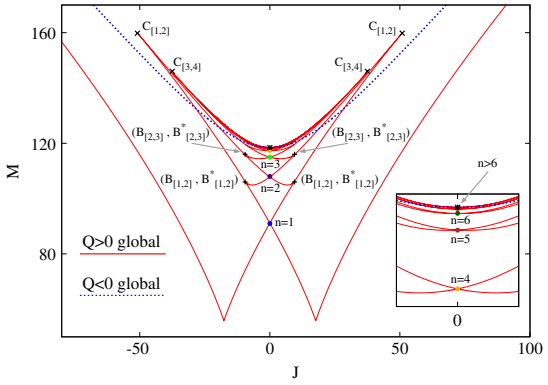

FIG. 2 (color online). Mass M versus angular momentum J for global extremal black holes with $\lambda = 5$ and $|Q| = 8\sqrt{3}\pi^2$.

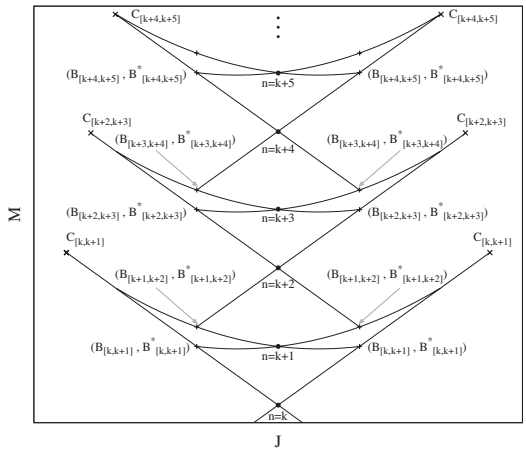

FIG. 3. Schematic representation of the branch structure around the extremal rotating $J = 0$ solution with $n = k$.

extremal black holes with $\lambda = 5$ and $|Q| = 8\sqrt{3}\pi^2$. The points with minimal mass correspond to the singular solutions with vanishing area in Fig. 1. Choosing as the starting point, for instance, the singular point with $J < 0$, if we decrease the angular momentum from this point, we obtain a whole branch of extremal solutions, whose mass increases monotonically with increasing $|J|$. However, if we start increasing J from that point, we first cross the $n = 1$ nonstatic $J = 0$ solution. If we keep increasing J, we cross a certain solution $B_{[1,2]}$, and eventually we get to a solution for which a maximal value of J is reached and beyond which the branch ceases to exist. In fact, the branch bends backwards with decreasing J, forming a cusp $C_{[1,2]}$. Note that the solutions at these cusps are not singular. On its way down this branch crosses the next nonstatic $J = 0$ solution, $n = 2$. This branch ends when it reaches the symmetric first branch, at the solution $B^*_{[1,2]}$. In fact, this point, where the two branches meet, constitutes a bifurcation point where the two solutions $B^*_{[1,2]}$ and $B_{[1,2]}$ possess the same global charges. However, their horizon area and horizon angular momentum are different, as can be seen in Fig. 1 for the horizon area. This provides us with an example of uniqueness violation for extremal black holes in the EMCS theory when $\lambda > 2$.

This structure of cusps and bifurcation points repeats indefinitely towards the corresponding extremal RN solution. At the bifurcation points new branches start and they extend up to the corresponding cusps and then they bend backwards until the following bifurcation point is reached. Uniqueness is violated at the bifurcation points. The width of the branches decreases and subsequent branches get closer and closer to each other as the static solution is approached, making the structure almost indistinguishable. In Fig. 3 we have included a schematic representation of the M-J diagram around the k-th branch structure to clarify the picture. Since the cusps $C_{[n,n+1]}$ occur at decreasing values of $|J|$, the number of extremal global solutions for fixed $|J|$ decreases with increasing $|J|$, whenever a cusp is passed.

It is worth emphasizing that the points denoted by $n = 1, 2, 3, \ldots$ in the figures correspond to extremal rotating solutions with vanishing angular momentum. Investigating this sequence of extremal $J = 0$ solutions for fixed charge Q in more detail, we realize that these solutions constitute a set of radially excited extremal solutions that can be labeled by the node number n of the magnetic gauge potential a_φ, as seen in Fig. 4, or equivalently, of the metric function ω. The first node always refers to spatial infinity. We have constructed solutions with up to 30 nodes, from the whole infinite sequence. As expected, sequences of radially excited solutions [16] exist also for nonzero J.

With increasing node number n, the mass M_n converges monotonically from below to the mass of the extremal static black hole M_{RN} (see Fig. 2). Surprisingly, however, the horizon area has the same value for all solutions of the sequence, as is clearly seen in Fig. 1, and the same holds

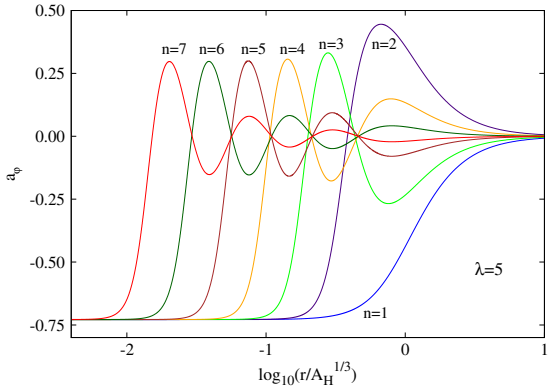

FIG. 4 (color online). Function a_φ for rotating extremal solutions with $J = 0$ and same electric charge $Q = 8\sqrt{3}\pi^2$ ($\lambda = 5$), for several node numbers.

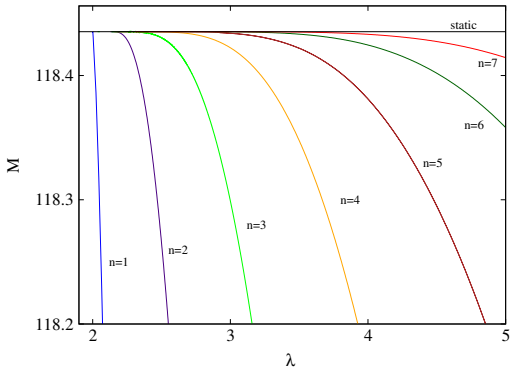

FIG. 5 (color online). Mass M versus λ for rotating $J = 0$ solutions with several nodes.

for the magnitude of the horizon angular momentum. In that sense, an infinite sequence of globally realized solutions corresponds to just one near horizon solution.

Also of interest is the λ dependence of the observed pattern of extremal solutions. This is shown in Fig. 5 where we exhibit the mass M versus the CS coupling λ of the rotating $J = 0$ solutions with one to seven nodes. We note, that we do not find rotating $J = 0$ solutions below $\lambda = 2$, and the mass M_n of the solutions with n nodes approaches the mass M_{RN} of the static extremal solution, as λ is decreased towards $\lambda = 2\lambda_{SG}$.

Let us finally address the domain of existence of these solutions. In principle, extremal solutions are expected to form the boundary of the domain of existence. In order to study this boundary, we exhibit in Fig. 6 the scaled angular momentum $j = J/M^{3/2}$ versus the scaled charge $q = Q/M$ for extremal solutions. Again the results are for a CS coupling constant $\lambda = 5$, although a similar picture has been found for other values of $\lambda > 2$. Bifurcation

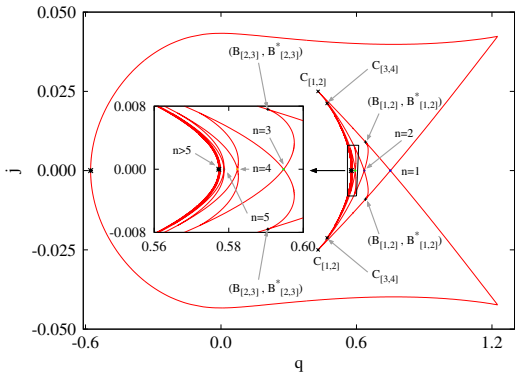

FIG. 6 (color online). Scaled angular momentum $j = J/M^{3/2}$ versus scaled electric charge $q = Q/M$ for extremal black holes ($\lambda = 5$).

points, cusps, and rotating $J = 0$ solutions have been included in the figure for completeness, allowing us to track down the locations of those solutions in the previous figures. The domain of existence is delimited by the outer lines of extremal solutions, which constitute its boundary. For spinning solutions, the CS term breaks the symmetry $Q \to -Q$. The extremal solutions with negative charge form the left outer boundary. This contains the extremal static solution where J vanishes. The extremal solutions with positive charge, on the other hand, represent a much more interesting set of solutions, associated with the branch structure we have described above. There are two remarkable things to mention. First, the maximal value of $|q|$ occurs at the two peaks for $q > 0$ with $J \neq 0$. These solutions correspond to the singular solutions with vanishing horizon area in Fig. 1. This value of $|q|$ is larger than that of the RN solution. Second, there are extremal solutions in the interior of the domain of existence. In other theories (pure EM, Einstein-Maxwell-dilaton, …) only nonextremal solutions are in the interior of the domain of existence, the extremal ones being only on the boundary. This fact allows for a strange type of uniqueness violation: the existence of both extremal and nonextremal solutions with the same values of their global charges M, J, and Q.

Further remarks.—The results in this work show that the intuition based on known exact solutions cannot be safely applied in the general case. Working in the EMCS theory, we have shown that beyond a critical value of the CS coupling λ, for fixed charge Q, a sequence of branches of extremal radially excited black holes arises. To our knowledge, this is the first example of black holes with Abelian fields that form excited states reminiscent of radial excitations of atoms [17].

Also, these black holes clearly illustrate that the relation between global solutions and near horizon solutions may be rather intricate since there are near horizon solutions that do not correspond to global solutions, while other near horizon solutions correspond to one or more global solutions.

As we decrease the CS coupling below the critical value, this intriguing pattern of global solutions disappears. However, in the limit $\lambda \to 0$ when the EM theory is obtained, we again encounter two branches of extremal solutions. The first branch is connected to the static RN black hole and has horizon area $A_{\mathrm{H}} = (\pi 3^{3/4} J^2 Q^{-3/2})/\sqrt{2} + (3^{1/4}\sqrt{2} Q^{3/2})/(48\pi)$. The second branch originates at the Myers-Perry solution, and has the rather unusual property to possess an entropy independent of the electric charge, $A_{\mathrm{H}} = J/2$. Both branches are associated with near horizon solutions, which are only partly realized as global configurations.

Finally, we conjecture that extremal black holes with similar properties may also exist in other theories, in particular in a $D = 4$ Einstein-Maxwell-dilaton theory.

We gratefully acknowledge support by the Spanish Ministerio de Ciencia e Innovacion, research project

FIS2011-28013, and by the DFG, in particular, the DFG Research Training Group 1620 "Models of Gravity." J. L. B. is supported by the Spanish Universidad Complutense de Madrid.

[1] A. Strominger and C. Vafa, Phys. Lett. B **379**, 99 (1996).
[2] J. C. Breckenridge, D. A. Lowe, R. C. Myers, A. W. Peet, A. Strominger, and C. Vafa, Phys. Lett. B **381**, 423 (1996).
[3] J. C. Breckenridge, R. C. Myers, A. W. Peet, and C. Vafa, Phys. Lett. B **391**, 93 (1997).
[4] M. Cvetic, H. Lu, and C. N. Pope, Phys. Lett. B **598**, 273 (2004).
[5] Z. W. Chong, M. Cvetic, H. Lu, and C. N. Pope, Phys. Rev. Lett. **95**, 161301 (2005).
[6] J. P. Gauntlett, R. C. Myers, and P. K. Townsend, Classical Quantum Gravity **16**, 1 (1999).
[7] C. A. R. Herdeiro, Nucl. Phys. **B582**, 363 (2000).
[8] P. K. Townsend, Annales Henri Poincare **4**, S183 (2003).
[9] J. Kunz and F. Navarro-Lérida, Phys. Rev. Lett. **96**, 081101 (2006).
[10] J. Kunz, F. Navarro-Lérida, and J. Viebahn, Phys. Lett. B **639**, 362 (2006).
[11] D. Astefanesei, K. Goldstein, R. P. Jena, A. Sen, and S. P. Trivedi, J. High Energy Phys. 10 (**2006**) 058.
[12] H. K. Kunduri and J. Lucietti, J. High Energy Phys. 12 (**2007**) 015.
[13] N. V. Suryanarayana and M. C. Wapler, Classical Quantum Gravity **24**, 5047 (2007).
[14] We employ a collocation method for boundary-value ordinary differential equations, equipped with an adaptive mesh selection procedure (COLSYS) [18]. Typical mesh sizes include $10^3 - 10^4$ points, the solutions having a relative accuracy of 10^{-8}.
[15] This feature was also found for extremal black holes in $D = 4$ Gauss-Bonnet gravity [19].
[16] A family of radially excited solutions exists also in the nonextremal case for large enough values of λ, though with a finite maximal value of n.
[17] This resembles also the case of black holes with non-Abelian gauge fields [20].
[18] U. Ascher, J. Christiansen, and R. D. Russell, Math. Comput. **33**, 659 (1979); ACM Transactions on Computer Systems **7**, 209 (1981).
[19] C.-M. Chen, D. V. Gal'tsov, and D. G. Orlov, Phys. Rev. D **78**, 104013 (2008).
[20] M. S. Volkov and D. V. Gal'tsov, Phys. Rep. **319**, 1 (1999).

CHAPTER 4

VORTICES

4.1 Outline and objectives

In this chapter we will present our results on Chern-Simons-Higgs vortices in 2+1 dimensions. The results of this study can be found in the published paper Physical Review D **88** (2013) 025026 [8], which is appended in Section 4.4.1.

We have considered the Abelian and non-Abelian vortices of a scalar Higgs field coupled to a $SU(2)$ gauge field. The Higgs field is in the adjoint representation and the coupling to the gauge field is made via a Chern-Simons term. A fourth-order Higgs self-interaction potential has been considered.

Let us start by making a brief introduction to the subject of Yang-Mills-Higgs vortices. In particular we will present the ANO vortex and the 't Hooft-Polyakov monopole before discussing our results.

4.2 Vortices in Yang-Mills-Higgs theories

Vortex solutions of Yang-Mills-Higgs (YMH) theories correspond to a more general class of topological objects that can be found in these classical field theories: instantons, monopoles, and vortices [87]. These solutions present non-trivial topological properties.

An instanton [88], also known as pseudo particle, is a classical solution of the field equations in Yang-Mills (YM) theories in a Riemannian manifold. They are related to point-like topological singularities of the space-time manifold, and possess finite action and minimal energy. They describe, in the path integral of a classical system,

the leading term of the quantum correction. They can be found in the Euclidean version of a YM theory, which can be understood as the analytic continuation of the original Lorentzian theory into the complex plane (taking the time coordinate as a complex variable).

Monopoles [89], on the other hand, are related to topological singularities on a world-line, and could have infinite action. Monopoles can be found as topological defects of gauge fields on Lorentzian manifolds. Maybe the most simple example is the Dirac monopole, which is found as a point like magnetic charge associated to the $U(1)$ gauge vector (the magnetic field) coupled to a scalar electric potential.

Vortices are typically related to excitations of a scalar field (Higgs field) coupled to a gauge field with non-trivial topological properties. The topological singularity of a vortex extends on a world-sheet of a Lorentzian manifold [89].

In this work, we will be interested in vortices in theories where a scalar Higgs field is coupled to an $SU(2)$ gauge field. Let us recall some interesting results in this particular class of theories.

4.2.1 Abrikosov-Nielsen-Olesen vortices

The Abrikosov-Nielsen-Olesen vortex (ANO vortex) [90] is a topological excitation of the Higgs field (meaning that the excitation has some non-trivial topological property) when coupled to an Abelian gauge field. The ANO vortex owes its existence to vacuum degeneracy, i.e., to the presence of multiple, energetically degenerate solutions of minimal energy due to some self-interacting Higgs potential.

This model of Higgs scalar coupled to an Abelian gauge field is a very interesting model in field theory, due to its important applications in Particle Physics and Condensed Matter Physics. It provides a useful framework for the description of phenomena related to superconductivity [91] ("Ginzburg-Landau model") and its topological excitations ("Abrikosov vortices"). At the same time, it provides the simplest setting for the mass generation mechanism in the electro-weak interaction.

The Higgs field Φ is minimally coupled to a $U(1)$ gauge field A_μ. We will give a brief introduction to the $2+1$ dimensional ANO vortices. The Lagrangian density is the following:

$$\mathcal{L} = -\frac{1}{2}F_{\mu\nu}^2 + (D_\mu\Phi)^*(D^\mu\Phi) - V(\Phi), \tag{4.1}$$

where the used signature is $(+,-,-)$ and we have defined the gauge field tensor

$$F_{\mu\nu} = \partial_\mu A_\nu - \partial_\nu A_\mu \tag{4.2}$$

and the covariant derivative minimally couples the gauge field to the Higgs field,

$$D_\mu = \partial_\mu + iA_\mu. \tag{4.3}$$

The symmetry breaking Higgs self-interaction potential is

$$V(\Phi) = \frac{1}{4}\lambda(|\Phi|^2 - a^2)^2, \tag{4.4}$$

which is a quartic potential. The Higgs is a complex scalar field. Note that the minimum of the Higgs potential is degenerated, $|\Phi| = a$, which is a circumference in the complex plane of the Higgs space of solutions. We can always rescale and consider $a = 1$.

Variating the Lagrangian with respect to the gauge potential and the Higgs fields, we obtain the Euler-Lagrange equations of motion. The field equations and the Lagrangian are invariants under a gauge transformation of both the gauge field and the scalar field under an $U(1)$ transformation

$$U(x) = e^{i\alpha(x)}, \tag{4.5}$$

yielding

$$\bar{\Phi} = U(x)\Phi \ , \tag{4.6}$$

$$\bar{A_\mu} = A_\mu + U(x)\frac{1}{i}\partial_\mu U^*(x) \ , \tag{4.7}$$

where x are some system of coordinates of the space, for example polar coordinates $x = (r, \varphi)$. In particular, if $\theta(x)$ is the phase of the Higgs field $\Phi(x) = \rho(x)e^{i\theta(x)}$, we could choose the gauge so that $U(x) = e^{-i\theta(x)}$, hence fixing the phase of the Higgs field. In order words, the phase of the Higgs field is pure gauge [89].

The ground state is not unique due to the Higgs vacuum degeneracy. In general, we can characterize the degree of this degeneracy by parameterizing the manifold of field configurations of minimal energy (manifold of zeroes of the potential energy). In this case it is characterized by a manifold, $\Phi = ae^{i\beta}$, which has the topological properties of a circumference S^1. This vacuum degeneracy is the source of the non-trivial topological

properties of the Abelian Higgs model.

Let us consider a static field solution. The energy of a configuration can be calculated from the Hamiltonian related to the Lagrangian (4.1). It can be demonstrated that finite energy is only achieved if asymptotically, when $r \to \infty$,

$$\Phi(x) \to a e^{i\theta(x)}, \tag{4.8}$$

$$A_\mu(x) \to \nabla_\mu \theta(x). \tag{4.9}$$

Hence, the gauge vector is bounded to the phase of the Higgs field asymptotically, and the gauge vector becomes pure gauge.

Let us calculate the magnetic flux of a possible finite energy solution to this theory. In an inertial frame, we can define the electric field component $E^i = F^{i0}$, and the magnetic field component $B^i = -\frac{1}{2}\varepsilon^{ijk}F^{jk}$. By applying the Stokes theorem to the magnetic field on the (r, φ) plane $\Re^2$ we have

$$\int_{\Re^2} B \mathrm{d}^2x = \oint_C \mathbf{A} \cdot \mathrm{d}\mathbf{s} = \oint_C \nabla\theta(x) \cdot \mathrm{d}\mathbf{s} = 2\pi n, \tag{4.10}$$

where C denotes a closed curve which becomes the boundary of $\Re^2$ in the asymptotical limit $r \to \infty$. The magnetic flux is proportional to an integer number n. Hence it is conserved in time. This conserved quantity does not have its origin in any symmetries. It is a topological invariant.

Let us assume that C is a circumference centered at $r = 0$. On this circumference the Higgs field becomes $\Phi = a e^{i\theta(\varphi)}$. Note $e^{i\theta(\varphi)} = e^{i(\theta(\varphi)+2k\pi)}$ (the phase must be continuous), where k is some integer. The phase defines a non-trivial mapping between the circumference C defined at spatial infinity of the $\Re^2$ plane, into the circumference $|\Phi| = a$, defined in the complex space of Φ.

$$\theta \ : \ S^1 \to S^1. \tag{4.11}$$

The key-point is that this mapping is naturally divided into equivalence classes θ_n, modulo the winding number n,

$$\theta_n(\varphi + 2\phi) = \theta(\varphi) + 2n\pi. \tag{4.12}$$

The phase of the Higgs field belongs to one of the equivalence classes (the homotopy group). If the phase belongs to the θ_n equivalence class, then the magnetic flux is $2n\pi$. The winding number n is just the number of times that the phase curls around the

S^1 circumference on the complex plane, as one circles around the S^1 circumference at asymptotically spatial infinity.

The field equations can be solved using the static spherically symmetric Ansatz. When written in polar coordinates (r, φ) the expression is simply given by

$$\Phi = |\Phi(r)|e^{in\varphi}, A = n\frac{\alpha(r)}{r}\partial_\varphi. \tag{4.13}$$

The requirement of finite energy asymptotically and in the center of the vortex leads to the following boundary conditions $\alpha(\infty) = 1,\ |\Phi(\infty)| = 1$ and $\alpha(0) = |\Phi(0)| = 0$, where we have rescaled so that $a = 1$.

The behavior of the ANO vortices depends on the value of the coupling parameter λ. If $\lambda \leq 8$, then we have

$$\alpha - 1 \propto \sqrt{r}e^{-\sqrt{2}r}, |\Phi| - 1 \propto r^{-1/2}e^{-\sqrt{\lambda}r}. \tag{4.14}$$

But if $\lambda > 8$, then

$$\alpha - 1 \propto \sqrt{r}e^{-\sqrt{2}r}, |\Phi| - 1 \propto r^{-1}e^{-2\sqrt{2}r}. \tag{4.15}$$

Hence the scale of the penetration of the gauge field into the Higgs field is controlled by the Higgs potential parameter λ.

ANO vortices are of special interest as an effective model of superconductivity. These 2-dimensional vortices we have briefly commented, can be seen as 3-dimensional tubes of vortices, assuming independence on the third coordinate. The parameter λ is essentially the Ginzburg-Landau parameter, which depends on the superconductor material. When $\lambda \leq 8$, the model describes type I superconductors, while $\lambda > 8$ corresponds to type II superconductors. In type I superconductors, not enough Cooper pairs are formed inside the superconductor, and the magnetic flux does not penetrate it. In type II superconductors, Cooper pairs can be formed for strong enough magnetic fields, and the magnetic flux can permeate the superconductor.

4.2.2 't Hooft-Polyakov monopole and non-Abelian vortices

The ANO vortices we have presented are an example of vortex solution in an Abelian theory. But these topological solutions can be found in non-Abelian gauge theories as well, also known as Yang-Mills theories.

In non-Abelian gauge theories, the gauge fields have their internal symmetry defined in some non-Abelian group. The components of the gauge field take their values on the Lie algebra of the group. For gauge fields in the $SU(N)$ group, the gauge

potential can be expanded in terms of the generators of the corresponding $su(N)$ Lie algebra

$$A_\mu = A_\mu^a T_a \ . \tag{4.16}$$

In $SU(2)$, $T_a = \frac{1}{2i}\tau_a$ where τ_a are the Pauli matrices. The generators of the non-Abelian group will in general satisfy some non-trivial commutation relations $[T_a, T_b] = if_{abc}T_c$, where f_{abc} are the structure constants of the Lie algebra. In $SU(2)$, these structure constants are $f_{abc} = \varepsilon_{abc}$, the completely antisymmetric symbol.

The covariant derivative which minimally couples to the gauge vector can be written as

$$D_\mu = \partial_\mu + [A_\mu, \circ] \ , \tag{4.17}$$

and the field strength tensor

$$F_{\mu\nu} = \partial_\mu A_\nu - \partial_\nu A_\mu + [A_\mu, A_\nu] \ , \tag{4.18}$$

that is, there is an additional self-interacting term $[A_\mu, A_\nu]$ with respect to the Abelian gauge field.

The Yang-Mills action (without any further fields) can be written

$$\mathcal{L} = -\frac{1}{4}F_{\mu\nu a}F_a^{\mu\nu} = -\frac{1}{2}Tr(F_{\mu\nu}^2) = \frac{1}{2}(E^2 - B^2). \tag{4.19}$$

In the last equality we have introduced the electric field component $E_a^i = F_a^{i0}$, and the magnetic field component $B_a^i = -\frac{1}{2}\varepsilon^{ijk}F_a^{jk}$, as defined in a given inertial frame.

When considering variations, the terms resulting from the Yang-Mills action will give us the dynamics of the gauge field.

Typically, the Yang-Mills action is usually coupled to other fields. One application is Quantum Chromodynamics (QCD). In this theory, the gauge fields are coupled to some fermionic fields. The gauge fields are the gluons and the fermions are the quarks. Quarks are in the fundamental representation (spinors).

The Yang-Mills action can also be coupled to a Higgs field (Yang-Mills-Higgs action, or Georgi-Glashow model), where the Higgs is chosen in the adjoint representation. The action is equivalent to the ANO action (4.1) but with non-Abelian gauge fields

$$\mathcal{L} = -\frac{1}{2}Tr(F_{\mu\nu}^2) + Tr(D_\mu\Phi D^\mu\Phi) - V(\Phi). \tag{4.20}$$

For example, in $SU(2)$, the Higgs field is a 3-vector in $SU(2)$, $\Phi = \Phi^a T_a$.

There is a number of interesting topological solutions in $SU(2)$ Yang-Mills-Higgs theories (monopoles, vortices, etc).

The 't Hooft-Polyakov monopole [92, 93] is a topological solution of $SU(2)$ YMH theory in three spatial dimensions, with the Higgs field in the adjoint representation. It is a topologically stable and finite energy solution. The Higgs field takes its values in the Lie algebra, and hence it is an isovector $\Phi = (\Phi_1, \Phi_2, \Phi_3)$, invariant under $SO(3)$ rotations of the internal space.

This extra symmetry of the Higgs field can be seen in the vacuum selection. The Higgs potential is of the form $V(\Phi) = V(\Phi^2)$, where $\Phi^2 = \sum_{a=1}^{3} \Phi_a^2$. The vacuum values of the Higgs satisfy $V = 0$. This fixes the modulus of the Higgs field to some constant a, $|\Phi| = a$. This defines an S^2 sphere in the internal space where the Higgs is defined. We can freely select the orientation of Φ in this sphere. We choose this orientation by selecting some vector $\bar{\Phi}$, so that $\Phi = a\bar{\Phi}$, with $|\bar{\Phi}| = 1$. But note that there is still a residual symmetry that we have not fixed: rotations whose axis coincide with $\bar{\Phi}$. We can fix this symmetry with some extra symmetry condition to the internal degrees of freedom of the Higgs field (for example, the vanishing of some combination of components orthogonal to the vacuum direction), but of course this condition must be consistent with the modulus of the Higgs field and its orientation.

Nevertheless, since the fields are in $\Re^3$ space, the topological charge is related to the mapping of an S^2 sphere (defined on the internal space of the Higgs field), into the asymptotical sphere of spatial infinite S^2. It can be demonstrated that the homotopy group in this case is $\mathbb{Z}$, like in the ANO vortices.

To finalize with this section, let us make some comments on the construction of non-Abelian YMH vortices on $\Re^2$.

Nielsen and Olesen constructed $SU(2)$ non-Abelian vortices on $\Re^2$ by including two Higgs fields, each of them with different potential and vacuum value [90]. Each of the Higgs fields must point in different directions of the internal S^2 space in order to have non-Abelian gauge fields. The simplest case is obtained for orthogonal directions. This type of solutions can be extended for $SU(N)$ gauge fields if N different Higgs are included [94].

Non-Abelian vortices on $\Re^2$ in $SU(2)$ YMH theory, for a single Higgs field, were obtained in [95] using numerical methods. Interestingly, the analysis showed that the non-Abelian vortices branch off from the Abelian ANO vortices for certain values of the Higgs potential coupling parameter λ. There is an infinite, discrete number of this branching points, which also depend on the topological charge n. Hence, for

a given topological charge, there are branches of non-Abelian solutions that can be labeled by an integer number m. In the limit of large coupling $\lambda \to \infty$, the energy is proportional to this non-Abelian branch number m, and the energy gap between each branch becomes constant.

4.3 Chern-Simons theory

When vortices on $\Re^2$ are considered, there is also an important contribution to the action that can be supplemented: the Chern-Simons term [96, 97, 98]. A Chern-Simons term in 2+1 dimensions is Lorentz invariant and is locally defined. It can be written as

$$\mathcal{L}_{CS} = \frac{\kappa}{2}\varepsilon^{\rho\mu\nu} Tr\left[A_\rho(F_{\mu\nu} - \frac{2}{3}A_\mu A_\nu)\right] = \tag{4.21}$$

$$\kappa\varepsilon^{\rho\mu\nu} Tr\left[A_\rho\partial_\mu A_\nu + \frac{2}{3}A_\rho A_\mu A_\nu)\right] \ . \tag{4.22}$$

In an Abelian theory, the trilineal term of the action vanishes because of the commutation of the gauge potential. Under a gauge transformation $\bar{A_\mu} = A_\mu + g^{-1}\partial_\mu g$, the Chern-Simons term changes like

$$\delta\mathcal{L}_{CS} = \kappa\varepsilon^{\rho\mu\nu}\partial_\rho Tr\left[\partial_\mu g g^{-1} A_\nu\right] + \frac{\kappa}{3}\varepsilon^{\rho\mu\nu} Tr\left[g^{-1}\partial_\rho g g^{-1}\partial_\mu g g^{-1}\partial_\nu g\right] \ . \tag{4.23}$$

The first term is a total derivative, and can be made null with appropriate boundary conditions. But the second term does not vanish in a non-Abelian theory, and in fact gives rise to a constant term in the Chern-Simons action

$$\bar{\mathcal{S}}_{CS} = \mathcal{S}_{CS} + 8\pi^2\kappa N \ , \tag{4.24}$$

where N is some integer number. This constant term has some implications on the quantized non-Abelian CS theory, because in order to have a gauge invariant quantum amplitude $e^{i\mathcal{S}}$, the CS coupling constant κ must be quantized so that $8\pi^2\kappa N$ is a multiple of 2π.

There are some interesting results on vortices with a Chern-Simons term. In particular, the ANO vortices of YMH theory can be generalized to the case in which the Higgs field is coupled to the gauge field via a Chern-Simons term instead of a Yang-Mills coupling. This theory is usually called Chern-Simons-Higgs (CSH).

Let us first comment that under variations of the action, the Chern-Simons term gives first-order differential equations of the gauge field, unlike the Yang-Mills action, which gives second-order differential equations. Hence, in a purely Chern-Simons theory, the gauge field has no dynamics. In fact, the gauge field is completely determined by the dynamics of the mass fields it is coupled to.

Hence in CSH vortices, the gauge field acquires its dynamics from the Higgs field. Abelian vortices due to topological excitations of the Higgs field (the equivalent to ANO vortices in YMH) were discovered independently by Hong, Kim [99], and Pac and Jackiw and Weinberg [100] (HKP-JW vortex). These solutions are obtained for a sixth-order Higgs potential, which grants self-duality of the gauge vector. The corresponding non-Abelian generalizations of these vortices were obtained using numerical procedures in [101].

In this Thesis we will study CSH vortices with the standard fourth-order Higgs potential. Hence our vortex solutions do not grant self-duality of the gauge vector. We will see that this leads to interesting features like non-uniqueness.

4.4 Results on Chern-Simons vortices

We will briefly introduce our results on Chern-Simons vortices. The results have been published in Physical Review D **88** (2013) 025026 [8], and will be presented in the next section 4.4.1. Here we have studied vortices in $SU(2)$ Chern-Simons-Higgs theory. The $SU(2)$ gauge field is coupled to the scalar Higgs field (which is in the adjoint representation) via a Chern-Simons term in the action. Hence the gauge field has no dynamics, and can be determined by a set of constraints that bound the gauge field to the Higgs field. Since we will be considering the standard quartic symmetry-breaking Higgs potential, self-duality of the solutions is lost.

- To build non-Abelian configurations, we start from the corresponding Abelian solutions. By changing the value of some internal parameters of the solution we can generate non-Abelian solutions. For example, p_1 and p_2, which are related to the amplitude of two of the internal isotriplets, and are null in the Abelian case. Nevertheless, it can become null again for certain non-Abelian configurations. The non-Abelian, $p_2 = 0$ configurations have specially interesting properties.

- For a given number of vortices, the number of non-Abelian solutions with $p_2 = 0$ depends on the Higgs self-coupling parameter. As the Higgs self-coupling is increased, the number of these non-Abelian branches with $p_2 = 0$ increases.

- The energy of the Abelian branch is always greater or equal than the non-Abelian solutions. The same holds for the angular momentum. The energy and the angular momentum of a non-Abelian solution increases with the non-Abelian branch number.

- For large values of the Higgs self-coupling parameter, the energy gap between the non-Abelian $p_2 = 0$ branches becomes constant. The angular momentum tends to zero. Interestingly, the non-Abelian $p_2 = 0$ branch number also determines the number of pieces of the step-like structure of the gauge potential functions.

- On the other hand, for large values of the Higgs self-coupling parameter, the relation between the energy and the angular momentum of the non-Abelian solutions (general value of p_2) becomes a Regge-like quadratic relation. All these solutions tend to behave like step-like functions in the limit.

- For topological number equal to 3, there is non-uniqueness of the solutions with respect the global parameters. We have found two distinct solutions with the

same angular momentum and energy, but different values of other invariant quantities, like the Higgs amplitude. Surprisingly, the value of the Higgs self-interaction parameter is relatively low, and the non-uniqueness is related to a complicated relation between the internal parameters and the total energy and angular momentum (interestingly, the p_1 parameter is null in both solutions, while the p_2 parameter is different).

4.4.1 Publication: Jose Luis Blázquez-Salcedo, Luis Manuel González-Romero, Francisco Navarro-Lérida, and D. H. Tchrakian, *Non-Abelian Chern-Simons-Higgs vortices with a quartic potential*, Physical Review D 88 (2013) 025026

PHYSICAL REVIEW D **88,** 025026 (2013)

Non-Abelian Chern-Simons-Higgs vortices with a quartic potential

J. L. Blázquez-Salcedo,[1] L. M. González-Romero,[1] F. Navarro-Lérida,[2] and D. H. Tchrakian[3,4]
[1]*Departamento de Física Teórica II, Universidad Complutense de Madrid, E-28040 Madrid, Spain*
[2]*Departamento de Física Atómica, Molecular y Nuclear, Universidad Complutense de Madrid, E-28040 Madrid, Spain*
[3]*School of Theoretical Physics, Dublin Institute for Advanced Studies, 10 Burlington Road, Dublin 4, Ireland*
[4]*Department of Computer Science, NUI, Maynooth, Maynooth, Ireland*
(Received 21 June 2013; published 16 July 2013)

We have constructed numerically non-Abelian vortices in an $SU(2)$ Chern-Simons-Higgs theory with a quartic Higgs potential. We have analyzed these solutions in detail by means of improved numerical codes and found some unexpected features we did not find when a sixth-order Higgs potential was used. The generic non-Abelian solutions have been generated by using their corresponding Abelian counterparts as initial guess. Typically, the energy of the non-Abelian solutions is lower than that of the corresponding Abelian one (except in certain regions of the parameter space). Regarding the angular momentum, the Abelian solutions possess the maximal value, although there exist non-Abelian solutions which reach that maximal value too. In order to classify the solutions it is useful to consider the non-Abelian solutions with asymptotically vanishing A_t component of the gauge potential, which may be labeled by an integer number m. For vortex number $n = 3$ and above, we have found uniqueness violation: two different non-Abelian solutions with all the global charges equal. Finally, we have investigated the limit of infinite Higgs self-coupling parameter and found a piecewise Regge-like relation between the energy and the angular momentum.

DOI: 10.1103/PhysRevD.88.025026 PACS numbers: 11.15.−q, 11.10.Kk, 11.15.Kc

I. INTRODUCTION

Vortices on $\Re^2$ have attracted interest for a very long time. They arise in spontaneously broken gauge theories in two dimensions and possess a quantized magnetic flux due to their topological properties. When a Chern-Simons (CS) term is added to the action, vortices acquire electric charge while keeping a finite energy [1]. The inclusion of CS terms in Higgs models in $2+1$ dimensions was motivated by the discovery in [2] of topologically massive non-Abelian Yang-Mills (YM) theories augmented by a CS term, where the CS provides a gauge-invariant mechanism of mass generation.

Vortex solutions in an Abelian Chern-Simons-Higgs (CSH) theory were studied in [3,4] by Hong *et al.* and Jackiw and Weinberg (HKP-JW), independently. There, a sixth-order Higgs potential was used to ensure self-duality. Non-Abelian generalizations of these solutions were considered later [1,5,6] with a simple gauge group [$SU(2)$ and $SU(N)$]. In contrast to our model, these models feature at least two adjoint representation Higgs fields in addition to other scalar multiplets. Owing to that these solutions are topologically stable.

The non-Abelian generalization of the Abelian vortices introduced in [3,4] was presented in [7], where only one Higgs field is considered. There a sixth-order Higgs potential is employed. In this paper we investigate an $SU(2)$ CSH model with the Higgs field in the adjoint representation but using the standard quartic potential for the Higgs field. Due to that we will not have self-dual solutions in the Abelian sector of the theory. By using improved numerics we are able to analyze the solutions very accurately and explore the limit of a large Higgs self-coupling constant.

The paper is organized as follows: in the next section we present the model. Then in Sec. III we introduce the ansatz and the gauge choice we will employ and derive the field equations for that ansatz in Sec. IV. Due to their special relevance in the construction of the vortex solutions we devote Sec. V to the Abelian case. We carry out the numerical construction of the non-Abelian vortex solutions in Sec. VI and summarize our results in Sec. VII.

II. FIELD EQUATIONS

We will use the Lagrangian density

$$\mathcal{L} = \frac{\kappa}{2}\varepsilon^{\rho\mu\nu}\mathrm{Tr}\left[A_\rho\left(F_{\mu\nu} - \frac{2}{3}A_\mu A_\nu\right)\right] + \mathrm{Tr}[D_\mu\Phi D^\mu\Phi] - V(\Phi), \tag{1}$$

where $\varepsilon^{\alpha\mu\nu}$ is the three dimensional Levi-Civita tensor, A_μ is an $SU(2)$ gauge potential, and Φ is the Higgs field in the adjoint representation. We have defined the gauge field by

$$F_{\mu\nu} = \partial_\mu A_\nu - \partial_\nu A_\mu + [A_\mu, A_\nu], \tag{2}$$

and the gauge covariant derivative by

$$D_\mu = \partial_\mu + [A_\mu, \circ]. \tag{3}$$

Both the gauge potential and the Higgs field can be written in terms of combinations of $su(2)$ matrices

$$A_\mu = A_\mu^a T_a, \tag{4}$$

$$\Phi = \Phi^a T_a, \tag{5}$$

with $T_a = \frac{1}{2i}\tau_a$ $(a = 1, 2, 3)$, $\{\tau_a\}$ being the Pauli matrices.

The Lagrangian density Eq. (1) describes the coupling between the gauge field and the Higgs field. There is no dynamical term for the gauge field; we are considering a CS coupling term though. For the potential $V(\Phi)$ we will employ the standard quartic symmetry-breaking Higgs self-interaction potential

$$V(\Phi) = -(4\lambda)^2 \mathrm{Tr}\left[\frac{1}{4}v^2 + \Phi^2\right]^2. \tag{6}$$

By taking variations of the Lagrangian with respect to the gauge potential and the Higgs field, we obtain the Euler-Lagrange equations of motion. These general equations read

$$D_\mu(D^\mu\Phi) - 2(4\lambda)^2\Phi\left(\frac{1}{4}v^2 + \Phi^2\right) = 0, \tag{7}$$

$$\frac{\kappa}{2}\varepsilon^{\alpha\mu\nu}F_{\mu\nu} + [\Phi, D^\alpha\Phi] = 0. \tag{8}$$

Note that Eq. (7) gives the Higgs field dynamics and Eq. (8) can be seen as a set of constraint equations that bounds the gauge field to the Higgs field.

From the Lagrangian Eq. (1) we may also obtain the stress-energy tensor:

$$T_{\mu\nu} = \eta_{\mu\nu}\,\mathrm{Tr}[(D_\alpha\Phi)^2] - 2\,\mathrm{Tr}[D_\mu\Phi D_\nu\Phi] + 16\lambda^2\eta_{\mu\nu}\,\mathrm{Tr}\left[\frac{1}{4}v^2 + \Phi^2\right], \tag{9}$$

from which we will obtain the energy and the angular momentum of the vortex configurations. Here $\eta_{\mu\nu}$ denotes the Minkowski metric.

III. ANSATZ AND GAUGE CHOICE

We will restrict to a rotationally symmetric ansatz for the Higgs field and the Yang-Mills (YM) connection. They may be written in the following form [7]:

$$\Phi = \phi^{(3)}T_r^{(n)} + \phi^{(4)}T_\varphi^{(n)} - \phi^{(5)}T_3, \tag{10}$$

$$A_t = \chi^{(3)}T_r^{(n)} + \chi^{(4)}T_\varphi^{(n)} - \chi^{(5)}T_3, \tag{11}$$

$$A_1 = -\left[\frac{\xi^{(3)}}{r}\hat{x}_2 + A_r^{(3)}\hat{x}_1\right]T_r^{(n)} - \left[\frac{\xi^{(4)}}{r}\hat{x}_2 + A_r^{(4)}\hat{x}_1\right]T_\varphi^{(n)} + \left[A_r^{(5)}\hat{x}_1 + \left(\frac{\xi^{(5)} + n}{r}\right)\hat{x}_1\right]T_3, \tag{12}$$

$$A_2 = \left[\frac{\xi^{(3)}}{r}\hat{x}_1 - A_r^{(3)}\hat{x}_2\right]T_r^{(n)} + \left[\frac{\xi^{(4)}}{r}\hat{x}_1 - A_r^{(4)}\hat{x}_2\right]T_\varphi^{(n)} + \left[A_r^{(5)}\hat{x}_2 - \left(\frac{\xi^{(5)} + n}{r}\right)\hat{x}_2\right]T_3, \tag{13}$$

where we have defined $\hat{x}_1 = \cos\varphi$, $\hat{x}_2 = \sin\varphi$, and the $su(2)$-valued matrices

$$T_r^{(n)} = \cos n\varphi T_1 + \sin n\varphi T_2, \tag{14}$$

$$T_\varphi^{(n)} = \cos n\varphi T_2 - \sin n\varphi T_1. \tag{15}$$

n denotes an integer number, representing the winding (vortex) number. The ansatz functions $\phi^{(i)}$, $\chi^{(i)}$, $\xi^{(i)}$, and $A_r^{(i)}$ $(i = 3, 4, 5)$ depend on the radial coordinate r only.

Equations (10)–(13) represent the most general expression for the ansatz, which describes configurations of n vortices pinned up at the origin $(r = 0)$. But we still have a complete $SU(2)$ gauge symmetry that can be used to simplify the ansatz.

Part of that gauge freedom may be removed by setting $A_r^{(i)}(r) = 0$. Furthermore, we simplify a bit more the ansatz by introducing the consistent truncation $\phi^{(4)} = 0$, $\chi^{(4)} = 0$, and $\xi^{(4)} = 0$ [7].

Then, the only functions we have in our truncated ansatz are $\phi^{(3)} = vh$, $\phi^{(5)} = vg$, $\xi^{(3)} = c$, $\xi^{(5)} = a$, $\chi^{(3)} = \frac{v^2}{\kappa}d$, $\chi^{(5)} = \frac{v^2}{\kappa}b$, where a, b, c, d, g, and h are functions of r. In these variables the ansatz reads

$$\Phi = vhT_r^{(n)} - vgT_3, \tag{16}$$

$$A_t = \frac{v^2}{\kappa}dT_r^{(n)} - \frac{v^2}{\kappa}bT_3, \tag{17}$$

$$A_r = 0, \tag{18}$$

$$A_\varphi = -\frac{2c}{r}\cos\varphi\sin\varphi T_r^{(n)} - \frac{2(a+n)}{r}\cos\varphi\sin\varphi T_3, \tag{19}$$

where we have introduced the (r, φ) components of the gauge connection

$$A_r = \cos\varphi A_1 + \sin\varphi A_2, \tag{20}$$

$$A_\varphi = \cos\varphi A_2 - \sin\varphi A_1. \tag{21}$$

IV. DIFFERENTIAL EQUATIONS, ENERGY, AND ANGULAR MOMENTUM OF THE SOLUTIONS

If we redefine the parameters of the theory the following way

$$\kappa = \frac{v^2}{\beta}, \qquad \lambda = \frac{\beta\mu}{2v}, \tag{22}$$

and rescale the radial coordinate by $r \to \beta r$, the only parameter of the theory that can be found explicitly in the differential equations is μ (the scaled Higgs self-coupling parameter). In these rescaled variables the field equations read

$$a_{,r} = (gd - hb)hr, \tag{23}$$

$$b_{,r} = -(ah - gc)h/r, \tag{24}$$

$$c_{,r} = -(gd - hb)gr, \tag{25}$$

$$d_{,r} = (ah - gc)g/r, \tag{26}$$

$$h_{,rr} = -\frac{1}{r}h_{,r} + \frac{a}{r^2}(ah - gc) + b(gd - bh) + 2\mu^2 h(g^2 + h^2 - 1), \tag{27}$$

$$g_{,rr} = -\frac{1}{r}g_{,r} - \frac{c}{r^2}(ah - gc) - d(gd - bh) + 2\mu^2 g(g^2 + h^2 - 1), \tag{28}$$

together with the constraint

$$rhg_{,r} - rgh_{,r} + ad - bc = 0. \tag{29}$$

Here the subindex $,r$ denotes the derivative with respect to the rescaled radial coordinate r.

The constraint equation (29) is compatible with the system of differential equations (23)–(28), so we can take Eqs. (23)–(27) and (29) as the minimal system of equations of the problem.

The total energy of a given solution can be calculated from the (t, t) component of the stress-energy tensor:

$$E = \int_{\Re^2} T_{tt} = 2\pi \int_0^\infty drrT_{tt}. \tag{30}$$

Note that $2\pi rT_{tt} = H$, the Hamiltonian. For the ansatz we are considering, the expression of the Hamiltonian is

$$H = \pi r[(g_{,r})^2 + (h_{,r})^2] + \frac{\pi}{r}(gc - ha)^2 + \pi r(bh - gd)^2 + \mu^2 \pi r(1 - g^2 - h^2)^2. \tag{31}$$

Using the expression of the total energy of the configurations, we may obtain the set of boundary conditions that allows us to generate solutions. Since we are interested in vortex solutions, we must impose regularity of the solutions at the origin and a finite value of the energy.

The expansion at the origin of a general vortex solution with vorticity n reads

$$a = -n - \frac{h_n^2}{2(n+1)}(b_0 + g_0^2)r^{2n+2} + O(r^{2n+4}), \tag{32}$$

$$b = b_0 + \frac{h_n^2}{2}r^{2n} + O(r^{2n+2}), \tag{33}$$

$$c = \frac{b_0 + g_0^2}{n+2}g_0 h_n r^{n+2} + O(r^{n+4}), \tag{34}$$

$$d = -g_0 h_n r^n + O(r^{n+2}), \tag{35}$$

$$g = g_0 + \mu^2 \frac{g_0}{2}(g_0 - 1)(g_0 + 1)r^2 + O(r^4), \tag{36}$$

$$h = h_n r^n + O(r^{n+2}), \tag{37}$$

and all the higher order terms can be written in terms of g_0, b_0, and h_n. Note that, although the vorticity number does not appear explicitly in the equations, it is a fundamental parameter in the expansion at the origin.

Finiteness of the energy Eq. (30) imposes the following asymptotic values for the functions:

$$\lim_{r\to+\infty} a = p_1 \cos\alpha, \qquad \lim_{r\to+\infty} b = p_2 \cos\alpha, \tag{38}$$

$$\lim_{r\to+\infty} c = p_1 \sin\alpha, \qquad \lim_{r\to+\infty} d = p_2 \sin\alpha, \tag{39}$$

$$\lim_{r\to+\infty} g = \cos\alpha, \qquad \lim_{r\to+\infty} h = \sin\alpha. \tag{40}$$

p_1 is related to the amplitude of the electric isotriplet $\vec{\chi}$, and p_2 to the amplitude of $\vec{\xi}$. α is related to the angle between the directions of the non-Abelian isotriplets and their Abelian counterparts.

From all the parameters involved in the expansion at the origin and the behavior at infinity, g_0, b_0, h_n, p_1, p_2, and α, it can be numerically proven that only one is free and the remaining ones are numerically fixed by the system. In our computations we have chosen either p_1 or p_2 as the free numerical parameter, depending on the numerical convenience of one or the other.

Another physical quantity that will turn out to be useful in the analysis of the solutions is the angular momentum J. From the (t, φ) component of the stress-energy tensor we obtain the total angular momentum of the configuration:

$$J = \int_{\Re^2} T_{t\varphi} = 2\pi \int_0^\infty drrT_{t\varphi}, \tag{41}$$

which results to be

$$J = 2\pi \int_0^\infty drr(gd - hb)(gc - ha). \tag{42}$$

Using Eqs. (23) and (25) and the values of the functions at the origin and infinity, the total angular momentum of a configuration may be shown to depend only on the vorticity n and the asymptotic parameter p_1 [7]

$$J = -2\pi \int_0^\infty dr(cc_{,r} + aa_{,r}) = \pi(n^2 - p_1^2). \tag{43}$$

V. ABELIAN CASE

Due to their essential role in the construction of the non-Abelian vortices, we will analyze the embedded Abelian solutions. The ansatz, Eqs. (16)–(19), becomes Abelian when

$$c = d = g = 0. \tag{44}$$

The equations for the Abelian case are greatly simplified. It should be noticed that the constraint equation Eq. (29) is identically satisfied in this Abelian case, so the minimal system of equations reduces to

$$a_{,r} = -bh^2 r, \tag{45}$$

$$b_{,r} = -ah^2/r, \tag{46}$$

$$h_{,rr} = -\frac{1}{r}h_{,r} + \frac{a^2}{r^2}h - b^2 h + 2\mu^2 h(h^2 - 1). \tag{47}$$

These equations are the analogue to the equations used by HKP-JW [3,4], with a quartic potential instead. The Hamiltonian for these Abelian configurations is

$$H = \pi r(h_{,r})^2 + \frac{\pi}{r}(ha)^2 + \pi r(bh)^2 + \mu^2 \pi r(1 - h^2)^2. \tag{48}$$

Now imposing regularity at the origin and finite energy, we obtain that there is no free integration parameter for the Abelian configurations, once μ is given. In fact, comparing the parameters with the general non-Abelian case, one finds that

$$p_1 = p_2 = 0, \qquad \alpha = \pi/2, \tag{49}$$

for Abelian solutions. Note that due to Eq. (43), the Abelian solutions possess maximal angular momentum.

These embedded Abelian solutions constitute the starting point in the construction of non-Abelian vortices, since the non-Abelian $p_2 = 0$ branches bifurcate from the Abelian branch at certain values of the rescaled Higgs self-coupling parameter μ. The remaining non-Abelian $p_2 \neq 0$ solutions may be computed from these non-Abelian $p_2 = 0$ counterparts.

VI. NUMERICAL RESULTS

The complexity of the system of equations Eqs. (23)–(27) and (29) prevents us from using analytical methods to solve it. On the contrary, numerical schemes may be successfully employed. The set of boundary conditions for numerics can be easily derived from the expansion at the origin Eqs. (32)–(37) and asymptotic behavior Eqs. (38)–(40) of the functions. In fact, several choices are possible that ensure convergence of the codes.

Compared to our previous paper [7], we have improved our numerical accuracy, which has allowed us to analyze vast regions of the parameter space in detail, including the limit $\mu \to \infty$. We have applied a collocation method for boundary-value ordinary differential equations, equipped with an adaptive mesh selection procedure [8]. Typical mesh sizes include 10^3–10^4 points. The solutions have a relative accuracy of 10^{-8}.

After a detailed analysis of the equations, one finds that for a fixed integer value of the vortex number n and a nonvanishing real value of the Higgs self-coupling constant μ, the regular solutions to Eqs. (23)–(27) and (29) depend on just one numerical parameter which we have chosen to be either p_1 or p_2. Usually p_2 is the most efficient numerical parameter, but in certain regions of the parameter space the system becomes extremely sensitive to changes in p_2 and using p_1 as the free parameter improves the efficiency of the numerical codes.

Our procedure to generate non-Abelian vortices in the $\{n, \mu, p_2\}$ parameter space was as follows: for fixed integer n, we start from a small value of μ and generate the corresponding Abelian solution ($p_2 = 0$); this may be done easily by using a shooting method; after that, the p_2 parameter is moved from zero while keeping n and μ; this generates non-Abelian solutions, as c, d, and g functions get excited; once the non-Abelian solutions are generated, one may study the parameter space moving p_2 and μ. In order to generate solutions with a different value of the vortex number n, one has to start from the corresponding Abelian solution as n cannot be varied smoothly from an integer value to another.

The profiles of the functions a, b, c, d, g, and h for a typical non-Abelian solution ($n = 1$, $\mu = 50$, $p_2 = 0.6$) are shown in Fig. 1. The deviation of c, d, and g from zero is clearly seen, which illustrates the non-Abelian nature of the solution.

As one moves p_2 away from zero, the solutions become more non-Abelian. This feature has consequences on the global charges such as the energy and the angular momentum. In Fig. 2 we exhibit the energy E and the angular momentum J versus the asymptotic parameter p_2 for $n = 1$, $\mu = 50$ solutions. We observe that the energy decreases as we separate from the Abelian solution. In fact, for wide

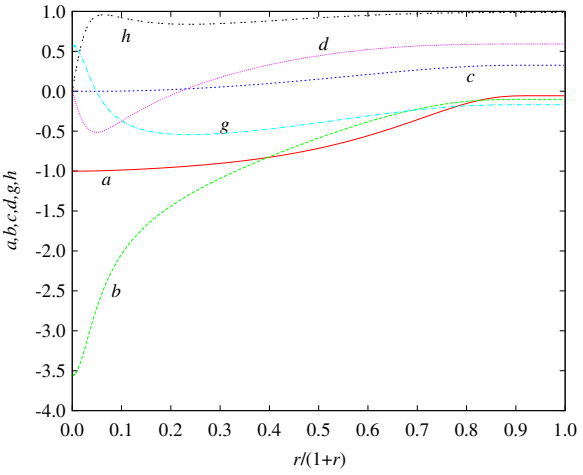

FIG. 1 (color online). Functions a, b, c, d, g, and h for a typical non-Abelian solution ($n = 1$, $\mu = 50$, $p_2 = 0.6$).

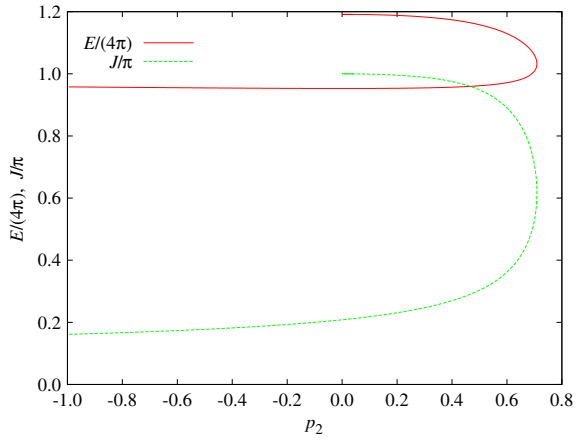

FIG. 2 (color online). Energy E and angular momentum J versus the p_2 parameter for $n = 1$, $\mu = 50$ vortices.

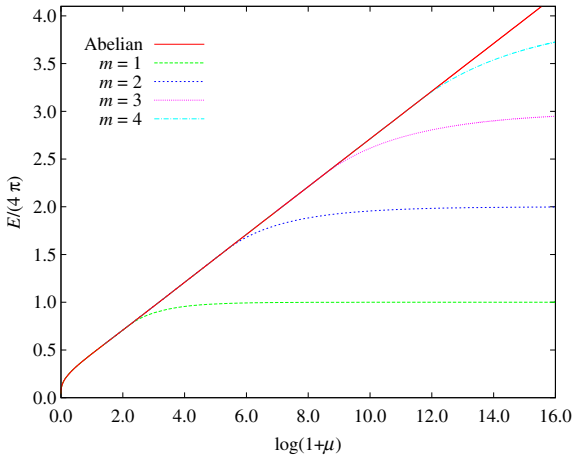

FIG. 3 (color online). Energy E versus the Higgs potential coupling constant μ for CSH vortices with $n = 1$, $p_2 = 0$.

ranges of μ the corresponding Abelian solution always has the largest value of the energy along the branches with fixed n and μ, although for small values of μ there exist non-Abelian solutions with energy greater than that of their Abelian counterpart. For the angular momentum the Abelian solutions always have the maximal value, as can be easily seen from Eq. (43) ($p_1 = 0$ for Abelian solutions).

The theory possesses the symmetry $p_2 \to -p_2$, leaving the global charges invariant. Then, the mirror image of the curves presented in Fig. 2 might be plotted, although we will not include those mirror images in our figures for the sake of clarity.

The non-Abelian branch may be extended by moving p_2 until the limit $|p_2| \to 1$ is reached. In that limit the solutions tend pointwise to a trivial solution [7].

A. Abelian and non-Abelian $p_2 = 0$ branches

Although Abelian vortices imply $p_2 = 0$, the opposite does not hold. In fact, in Fig. 2 the existence of one non-Abelian solution with $p_2 = 0$ is clearly seen. These non-Abelian $p_2 = 0$ solutions will be shown to be crucial in understanding the structure of the solution space.

For any nonvanishing integer value of n and nonvanishing real value of μ there exists a unique Abelian vortex solution. For low values of μ this solution is the only one with $p_2 = 0$. As μ is increased non-Abelian $p_2 = 0$ solutions branch off the Abelian ones. These new non-Abelian $p_2 = 0$ branches can be enumerated by using an integer number m, that labels them. For fixed μ the number of non-Abelian $p_2 = 0$ branches is finite, this number increasing with increasing μ (in the limit $\mu \to \infty$ the number of these branches becomes infinite). The values of μ where the non-Abelian $p_2 = 0$ branches bifurcate from the Abelian one depend on the vortex number n, and they are roughly equidistant on a logarithmic scale for μ. For example, for $n = 1$, the first non-Abelian $p_2 = 0$ branching points are $\mu = 8.023$ ($m = 1$), $\mu = 2.063 \times 10^2$ ($m = 2$), $\mu = 4.769 \times 10^3$ ($m = 3$), and $\mu = 1.108 \times 10^5$ ($m = 4$).

The general structure of these $p_2 = 0$ solutions is exhibited in Fig. 3 for $n = 1$ solutions. As happened for their YMH analogues [9], the energy of non-Abelian $p_2 = 0$ solutions is always smaller than that of the corresponding Abelian solution. Notice this was not the case for CSH solutions with a sixth-order potential [7]. Then, this fact seems to be a consequence of the quartic Higgs potential. For other values of the vorticity number, the behaviors of the Abelian and non-Abelian branches are quite similar.

In the limit $\mu \to \infty$ the energy of the non-Abelian $p_2 = 0$ solutions tends to $E_{n,m} \to 4\pi mn$ asymptotically. The energy of the Abelian configuration diverges logarithmically, though [10].

The angular momentum J of these non-Abelian $p_2 = 0$ configurations is also below the angular momentum of their Abelian counterparts, and tends asymptotically to zero in the limit $\mu \to \infty$. This is exhibited in Fig. 4, where J is plotted versus μ both for Abelian and for non-Abelian $p_2 = 0$ solutions.

The lack of self-duality of the Abelian configurations of this theory can be shown by representing the energy per vortex for some Abelian configurations for different vortex numbers. In Fig. 5 we represent the energy per vortex as a function of μ. If the theory were self-dual, there would be a value of μ where the energy per vortex number E/n would not depend on n. We clearly see in Fig. 5 that value does not exist.

B. Configurations with $p_2 \neq 0$

In this section we explore the solutions with $p_2 \neq 0$. These solutions are always non-Abelian configurations and connect non-Abelian configurations with $p_2 = 0$ to the corresponding Abelian solutions. Note that, once a branch

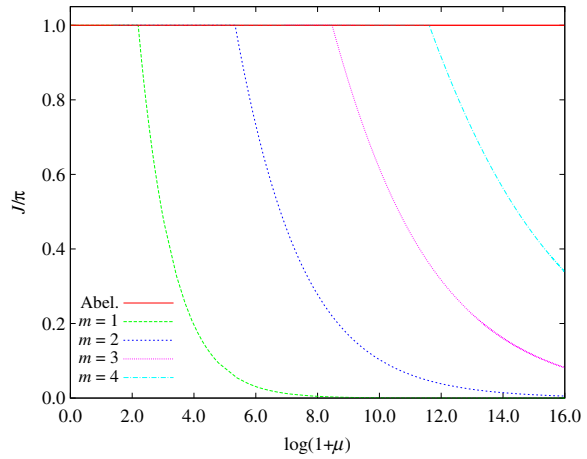

FIG. 4 (color online). Angular momentum J versus the Higgs potential coupling constant μ for CSH vortices with $n = 1$, $p_2 = 0$.

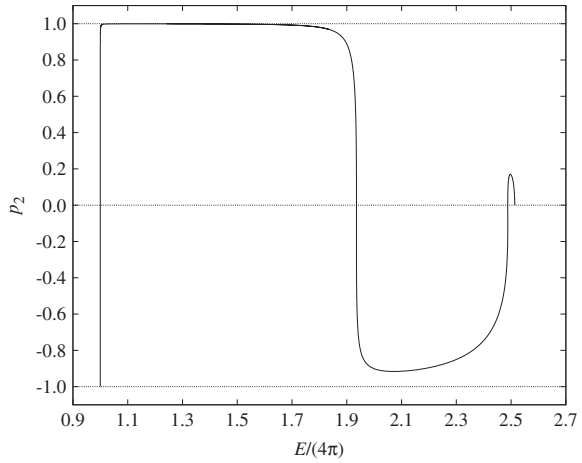

FIG. 6. p_2 parameter versus the energy E for $n = 1$, $\mu = 10^4$ solutions.

of configurations with parameters (p_1, p_2) is known, an equivalent branch can be constructed by making an appropriate sign reverse: $(p_1, p_2) \rightarrow (-p_1, -p_2)$. For the sake of clarity, we will only present one of the branches in our figures, although the other one can be obtained by mirroring the figures on the p_1/p_2 axis.

In Fig. 6 we represent the p_2 parameter versus the energy E for $n = 1$, $\mu = 10^4$ solutions. The corresponding Abelian solution possesses the highest value of E (at the right end of the curve). Starting from that point we make p_2 deviate from zero and non-Abelian solutions ($p_2 \neq 0$) are generated. At some point, the $p_2 = 0$ value is reached again, now corresponding to a non-Abelian solution, namely, that of the $m = 3$, $p_2 = 0$ branch. If one continues varying p_2, more non-Abelian solutions are produced. Two more $p_2 = 0$ solutions are found on the way, corresponding to $m = 2$ and $m = 1$, respectively. The curve can be extended until the trivial limiting solution with $|p_2| = 1$ is reached.

The other parameter we discussed, p_1, has been represented in Fig. 7. It is clear that the behaviors of p_1 and p_2 are quite different: in the regions where p_2 varies rapidly, p_1 changes slowly, and vice versa. We take advantage of that fact from a numerical point of view, since it allows us to overcome a convergence problem in certain regions of the parameter space. The relation between the energy and p_1 gets more and more piecewise linear as μ increases.

The angular momentum J is represented versus the energy E in Fig. 8 for the same set of parameters. The maximal value of the angular momentum ($J_{\max} = \pi n^2$) is

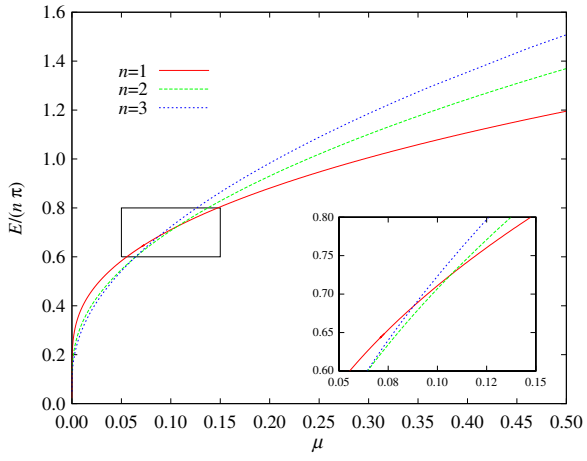

FIG. 5 (color online). Energy per vortex E/n versus the Higgs potential coupling constant μ for CSH vortices with $n = 1, 2, 3$, $p_2 = 0$.

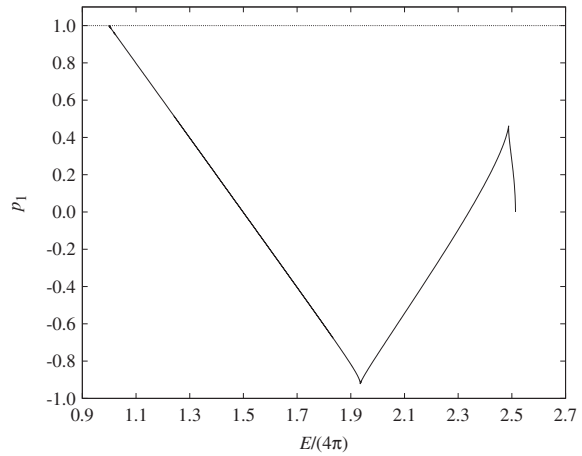

FIG. 7. p_1 parameter versus the energy E for $n = 1$, $\mu = 10^4$ solutions.

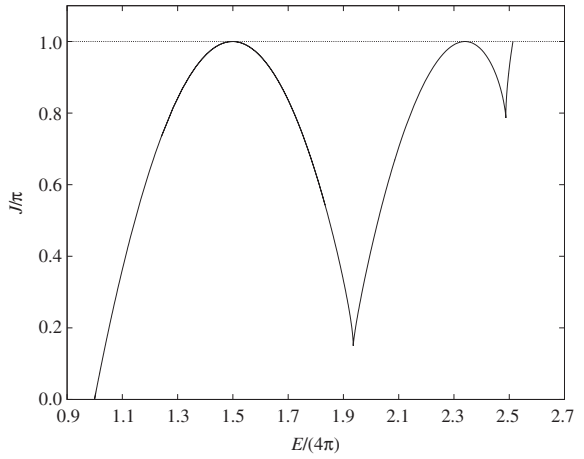

FIG. 8. Angular momentum J versus the energy E for $n = 1$, $\mu = 10^4$ solutions.

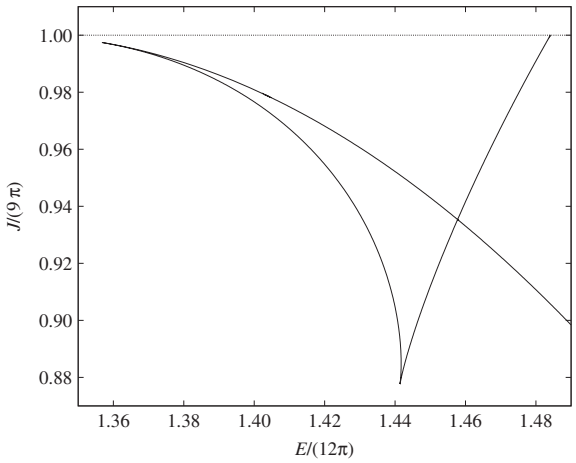

FIG. 9. Angular momentum J versus the energy E for $n = 3$, $\mu = 10$ (detail of the whole curve). The intersection of the curve shows the violation of uniqueness in configurations with $n = 3$.

reached at solutions with $p_1 = 0$ [see Eq. (43)]. Together with the Abelian solution, for these parameters, we have two non-Abelian solutions with maximal angular momentum. It is interesting to realize the archlike structure of the figure. This is something characteristic of large values of μ and we will discuss it in more detail later.

Although the results presented here are for $n = 1$, $\mu = 10^4$, these features are general for other values of μ and n. However, for $n = 3$ (and beyond), we find some peculiarities we will discuss in the next section.

C. Uniqueness violation for $n = 3$

Even though the situation explained in the last section is quite similar to the situations found for other values of μ and n (except for the number of non-Abelian branches and the branching points) for $n = 3$ a peculiar behavior has been found for relatively low values of the coupling constant: we find configurations with the same energy and angular momentum, but different internal parameters.

In Fig. 9 we present this feature for $n = 3$, $\mu = 10$. The curve begins at the Abelian configuration (at the right end with maximal angular momentum). When we move away from the Abelian solution, we obtain two non-Abelian configurations that possess the same energy and angular momentum ($E/12\pi = 1.459$, $J/9\pi = 0.9353$), but different internal p_2 parameter [$p_2^{(1)} = 0.3592$ and $p_2^{(2)} = -0.9986$]. Not all the internal parameters are different: because the angular momentum is equal for both solutions, the p_1 parameter is also equal.

To be sure that both solutions are not related by a gauge transformation we can consider a gauge-invariant quantity and evaluate it for both solutions. In Fig. 10 we represent the Higgs field density $\mathrm{Tr}[|\Phi|^2]$ and we can see that they are clearly different solutions.

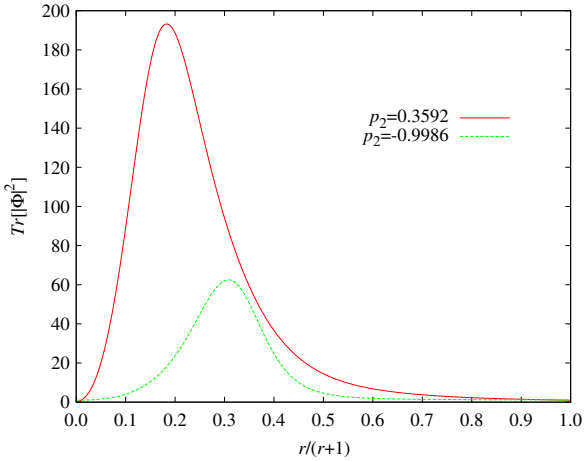

FIG. 10 (color online). $\mathrm{Tr}[|\Phi|^2]$ versus the compactified radial coordinate for $n = 3$, $\mu = 10$ for different configurations with equal energy and angular momentum ($E/12\pi = 1.459$, $J/9\pi = 0.9353$).

For lower values of the vorticity number, this phenomenon has not been observed. In fact, for $n = 3$ and high enough μ, this phenomenon also disappears. This lack of uniqueness in certain regions of the parameter space may lead us to introduce another quantity that allows us to classify uniquely the solutions by means of μ, n, E, J, and this new quantity. That quantity has to be gauge invariant. In order to propose one, further research needs to be done.

D. The $\mu \to \infty$ limit

In this section we will analyze the behavior of the configurations when the Higgs self-coupling parameter

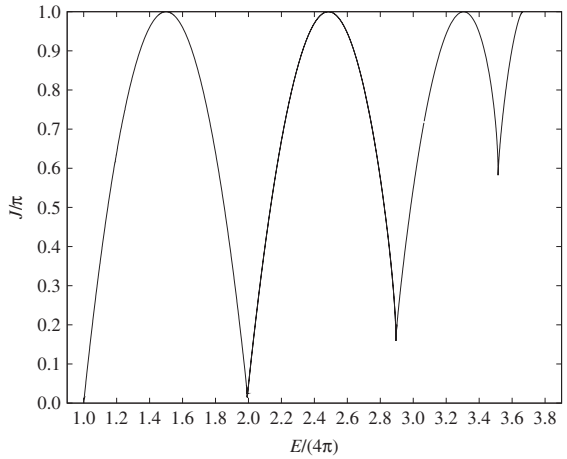

FIG. 11. Angular momentum J versus the energy E for $n = 1$, $\mu = 10^6$ solutions.

tends to infinity. In that limit the theory becomes a gauged σ-model, with $\mathrm{Tr}[F^2] \neq 0$.

The main feature in the $\mu \to \infty$ limit is that the energy becomes piecewise linear in p_1, which results in a piecewise quadratic relation between the energy and the angular momentum [as a consequence of Eq. (43)]. One can see this result for $n = 1$, $\mu = 10^6$ in Fig. 11. The arch structure that can be seen in this figure can be written explicitly for the general case when $\mu = \infty$:

$$J = n^2\pi - \frac{1}{4\pi}\left[E - 4n\pi\left(m + \frac{1}{2}\right)\right]^2, \qquad (50)$$

for $E \in [4\pi mn, 4\pi(m+1)n]$.

One can notice that in the limit $\mu \to \infty$ the angular momentum J is a piecewise quadratic polynomial in E. This reminds us of Regge-like dispersion relations where the angular momentum is a function of the square of the mass (when referred to maximal angular momentum configurations).

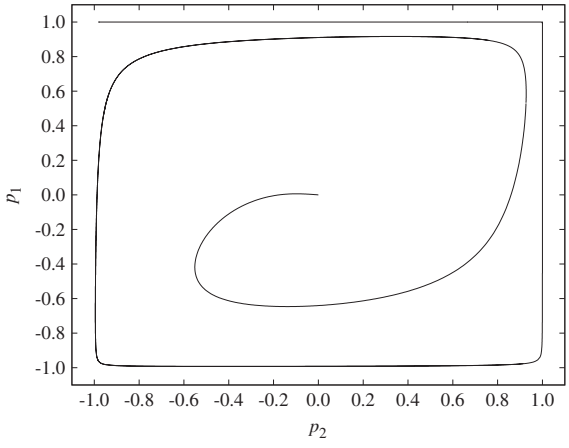

FIG. 12. p_1 parameter versus p_2 for $n = 1$, $\mu = 10^6$ solutions.

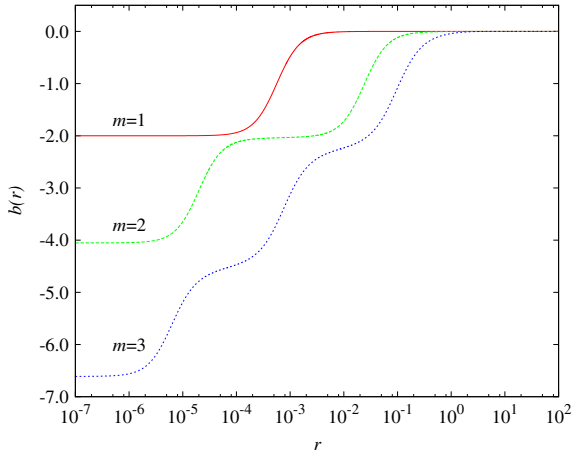

FIG. 13 (color online). The gauge field function $b(r)$ versus r for the $n = 1$, $\mu = 10^6$, $p_2 = 0$, $m = 1, 2, 3$ solutions.

In that limit, neither the energy nor the angular momentum depends on the p_2 parameter. The reason for this can be seen numerically: in the limit $\mu \to \infty$, for $p_2 \in (-1, 1)$ we have $|p_1| = n$. On the other side, for $p_1 \in (-n, n)$, we have $|p_2| = 1$. So in the limit, all the solutions with $p_2 \in (-1, 1)$ are degenerated into the minimal angular momentum solutions. We present this result for $n = 1$, $\mu = 10^6$ in Fig. 12. Note that the $p_1 = p_2 = 0$ configuration corresponds to the Abelian solution. In the limit $\mu \to \infty$ there is no such solution (the energy of the Abelian configuration diverges). What is left are the limiting non-Abelian configurations with $\{|p_1| = n, p_2 \in (-1, 1)\} \cup \{|p_2| = 1, p_1 \in (-n, n)\}$.

This behavior of the configurations is closely related to the structure of the functions when $\mu \to \infty$. In Fig. 13 we show the structure for the gauge field function $b(r)$, for $n = 1$, $\mu = 10^6$, and $m = 1, 2, 3$, that is, the three non-Abelian $p_2 = 0$ branches. In general, $b(r)$ presents a tendency to become overlapping step functions as $\mu \to \infty$, where the number of steps of the function is given by the branch number m.

VII. SUMMARY AND DISCUSSION

In this paper we have constructed non-Abelian vortices in an $SU(2)$ CSH theory in $2 + 1$ dimensions with a quartic Higgs potential. Contrary to what happens for HKP-JW solutions [3,4], in the Abelian sector of this theory no self-dual limit is present. However, we have investigated this model since the Higgs potential we have used is the standard quartic one. This fact makes the non-Abelian solutions presented here very different from the ones described in [7], where a sixth-order potential was used instead.

In order to generate these solutions we start from their corresponding Abelian counterparts. We observe that for certain values of μ non-Abelian branches with $p_2 = 0$

appear. These non-Abelian $p_2 = 0$ solutions are important to understand the structure of the solution space. These solutions may be labeled by an integer number m, which results to be related to the steplike structure of function b. All these non-Abelian $p_2 = 0$ solutions possess lower energy than their corresponding Abelian one, something that has not always happened for the sixth-order potential. The same holds for the angular momentum, which is maximal for the Abelian solutions. The structure of the energy levels of these non-Abelian $p_2 = 0$ solutions is quite regular, becoming completely equidistant in the limit $\mu \to \infty$.

Apart from the Abelian and the non-Abelian $p_2 = 0$ solutions there are generic non-Abelian $p_2 \neq 0$ solutions which connect both types of solutions. In fact, starting from an Abelian solution (for fixed values of n and μ) one can move p_2 and generate a whole branch of non-Abelian solutions, which ends when the limiting solution (with $|p_2| = 1$) is reached.

In this theory we observe an interesting feature for vortex number $n = 3$ (and beyond): the violation of uniqueness. For $n = 3$ there are regions in the parameter space where the solutions are no longer characterized by their global charges n, E, J, for a given μ. It is possible to find different solutions with the same values for all these quantities. This lack of uniqueness brings us to look for another (gauge-invariant) quantity that allows us to characterize uniquely the solutions. Although we have some candidates we have not yet decided which one is more appropriate to do the job.

Finally, we have addressed the theory in the limit $\mu \to \infty$, when it changes from a Higgs model to an $O(3)$ gauged sigma model. In such a limit one can extract the exact relation between the energy E and the angular momentum J, Eq. (50), which results to be a Regge-like relation when the energies are referred to the energies of the solutions with maximal angular momentum ($|p_1| = n$ solutions).

ACKNOWLEDGMENTS

We thank E. Radu for useful discussions and comments on this paper. This work was carried out in the framework of the Spanish Education and Science Ministry under Project No. FIS2011-28013 and the Science Foundation Ireland under Project No. RFP07-330PHY. J. L. B.-S. was supported by Universidad Complutense de Madrid.

[1] H. J. de Vega and F. A. Schaposnik, Phys. Rev. Lett. **56**, 2564 (1986).
[2] S. Deser, R. Jackiw, and S. Templeton, Phys. Rev. Lett. **48**, 975 (1982).
[3] J. Hong, Y. Kim, and P. Y. Pac, Phys. Rev. Lett. **64**, 2230 (1990).
[4] R. Jackiw and E. J. Weinberg, Phys. Rev. Lett. **64**, 2234 (1990).
[5] H. J. de Vega and F. A. Schaposnik, Phys. Rev. D **34**, 3206 (1986).
[6] C. N. Kumar and A. Khare, Phys. Lett. B **178**, 395 (1986).
[7] F. Navarro-Lérida, E. Radu, and D. H. Tchrakian, Phys. Rev. D **79**, 065036 (2009).
[8] U. Ascher, J. Christiansen, and R. D. Russell, Math. Comput. **33**, 659 (1979); ACM Trans. Math. Softw. **7**, 209 (1981).
[9] F. Navarro-Lérida and D. H. Tchrakian, Phys. Rev. D **81**, 127702 (2010).
[10] J. Burzlaff and F. Navarro-Lérida, Phys. Rev. D **82**, 125033 (2010).

CHAPTER 5

CONCLUSIONS

Throughout this Thesis we have studied several objects in classical field theories. These objects have been: neutron stars in Einstein theory, black holes in different higher dimensional models of gravity, and vortices in Yang-Mills-Higgs theories.

All these objects present a high degree of symmetries. Hence, under the proper mathematical steps, all the problems could be reduced to a system of ordinary differential equations, where some suitable boundary conditions, which are specific of each object, had to be imposed. These boundary conditions were obtained by several procedures: for example, by studying regularity conditions at the origin of the system of coordinates, or the asymptotical behavior of the expected solutions, or the matching conditions if the solutions were defined in several regions, etc.

In general we had no available analytic solutions, except for very specific cases. Hence we had to rely on numerical methods to generate the configurations. We used the Colsys package to solve the system of ordinary differential equations. Colsys also allowed us to impose the boundary conditions, which were typically defined at different points of the domain of integration, and usually were expressed as relations among the functions and/or their derivatives. Colsys allowed us to generate new configurations by continuation of a previously known solution.

Neutron stars are stellar objects composed of matter at extreme conditions. Their properties can be used to estimate the behavior of matter at densities higher than nuclear, where very little experimental knowledge is available. We have studied quasi-normal modes of neutron stars, which are expected to describe the resonant frequencies of gravitational waves emitted from these objects.

It is very important to have an, up-to-date, study of the physical properties of neutron stars composed by the latest equations of state available. A good part of the old equations of state which incorporated exotic matter has been ruled out by the detection of 2 $M_\odot$ pulsars. But in the last years, new equations of state have been proposed which include exotic matter like hyperonic matter and quarks, and are able to sustain neutron stars with more than 2 $M_\odot$. We have used some of these equations in our studies.

The idea behind the study of the quasi-normal mode spectrum was to obtain some universal phenomenological relations. These relations should relate the quasi-normal modes to some global properties of the star, like the mass, radius, compacity, and mean density. If a gravitational wave originated at a neutron star is detected, and if some other parameter of the neutron star is known (say for example the mass), then these phenomenological relations could be used to estimate other unknown parameters (i.e. the radius). Combining measurements of quasi-normal modes from the same neutron star, or even measurements from other stars, it should be possible to constrain greatly the equation of state.

There are several well-known phenomenological relations that have been obtained for polytropes and some older equations of state. We have studied these phenomenological relations for the new equations of state. We have also proposed a couple of new empirical relations, which we think are more useful since are more independent of the equation of state.

We have studied space-time modes of the axial and polar components of the spectrum. These modes are highly independent of the composition of the neutron star. We propose a new empirical relation for the w modes, which relate the frequency and the damping time to the central pressure. In principle, a detection of a w mode could be used to estimate the central pressure of the star.

We have also studied the fluid modes. These modes are obviously more dependent on the composition of the star. In particular, the fundamental pressure mode is very dependent on the particular equation of state. The fundamental mode is also very dependent on the equation of state (in particular for the frequencies of the highest mass configurations). We propose a new empirical relation which is independent of the equation of state. This relation, together with the previous new relation of the w modes, could be used to estimate the radius of the neutron star.

Interestingly, for pure quark stars, both old and new phenomenological relations are quite different. The reason is in the different structure of the outer layers. Quark stars present a density jump at the surface of the star. They can be understood as

naked cores, with an abrupt interface between the interior and the exterior.

Neutron stars have always been observed in rotation. They are in fact the most precise natural clock in the universe. But nevertheless glitches (sudden jumps in the angular velocity) have been observed in most pulsars. If glitches are related to some phenomena altering the properties of the outer layers of the star, then they could be used to gain information of the state of matter at those densities.

We have used the slow rotation formalism, together with an study of the junction conditions at the border of the star. We have treated the case of a surface energy density enveloping the core of the star. We have found that this configuration allows us to approximate in a proper way the outer layers of the star as a surface energy density. This simple model allows us to obtain an estimation of the variation of the core-crust transition pressure that could be related to the jump in the angular velocity during the glitch. The variation of pressure is associated to a rise in the temperature of the outer layers, that could be the product of a thermal energy deposition from a phase transition in this region.

Another topic in this Thesis has been higher dimensional black holes. These objects are very interesting in the context of new models of gravity. String theory predicts more than 3 space dimensions. Even more, the AdS/CFT correspondence suggests that black holes, as fundamental solutions of a gravitational theory, are dual to non-perturbative quantum states. Hence these objects are interesting both as fundamental objects of a unified theory, or because of their possible practical application as dual of strongly interacting quantum systems.

We have studied higher dimensional black holes in odd dimensional Einstein-Maxwell-dilaton theory. We have considered black holes with event horizons of spherical topology, and the cohomogeneity-1 case, when all the angular momenta are of equal magnitude.

In particular we have studied Einstein-Maxwell black holes without dilaton field. In the extremal case, two branches of black holes are found, one emerging from the Myers-Perry configurations, and the other from the Reissner-Nordtrüm configuration. The Myers-Perry branch has entropy proportional to the angular momentum, while the horizon angular momentum is dependent on both the angular momentum and the electric charge. The Reissner-Nordstrüm branch interchanges the behavior of these quantities, and has the horizon angular velocity proportional to the angular momentum, and the entropy dependent on both the angular velocity and the electric charge. Both branches meet at a non-singular configuration.

We have used the near-horizon formalism to complement the numerical analysis. We have found that not all the allowed near-horizon solutions are realized globally. The asymptotic behavior of the global solution constrains the set of near-horizon solutions.

Extremal Einstein-Maxwell-dilaton black holes do not present this two-branch structure. Instead, only the Myers-Perry branch is present and the entropy is always independent of the electric charge. We find a very interesting relation between the horizon angular velocity of the extremal solutions and the surface gravity of the static ones. A similar relation between the angular momentum of the extremal solutions and the area of the static solutions is found.

We have also studied higher dimensional black holes in 5 dimensional Einstein-Maxwell-Chern-Simons theory. The black holes considered are similar to the ones considered in EMd theory: spherical topology and cohomogeneity-1.

A rather complicated branch structure has been found for extremal black holes (when the Chern-Simons coupling constant exceeds 2 times the supergravity value). This branch structure is not present in the near-horizon geometry. Instead, it is observed in the mass and the angular velocity.

There are infinite branches which bend back and forth towards the static configuration. The static configuration is otherwise isolated, meaning that it can only be reached as a limit point of the infinite branch structure.

These branches have several interesting properties. For example, there is uniqueness violation. There are black holes with the same global parameters (mass, electric charge, angular momentum), that can only be distinguished by its near-horizon geometry, and in particular, the horizon area and horizon angular momentum.

There is an infinite number of black holes with the same near-horizon geometry, but different mass. There are also near-horizon solutions which are not realized globally, like in the EMd case.

Maybe the most interesting feature of these extremal branches are the non-static solutions with null angular momentum. There are an infinite number of them. They have the same near-horizon geometry, but different mass. In fact, their mass increases towards the static mass. On the other hand, the static solution has a completely different near-horizon geometry.

These non-static $J = 0$ solutions can be characterized by the number of nodes of the angular component of the gauge field, and hence are a set of radially excited black holes.

Another interesting feature is the non-uniqueness between extremal solutions and non-extremal ones. That is, there are non-extremal black holes with exactly the same

global charges than an extremal solution.

Vortices of Chern-Simons-Higgs theories have also been studied. We have obtained Abelian and non-Abelian solutions of vortices of a scalar Higgs field coupled to a $SU(2)$ gauge field. The Higgs field, in the adjoint representation, had a self-coupling potential of fourth order. Hence no self-dual solutions were contained in the theory.

To build the non-Abelian configuration, we start from the corresponding Abelian solutions. By changing the value of some internal parameters (p_1 and p_2) of the solution we can generate non-Abelian solutions. For a given value of the topological number, the number of non-Abelian solutions depends on the Higgs self-coupling parameter. As the Higgs self-coupling is increased, the extension of these non-Abelian solutions increases.

The energy of the Abelian branch and the angular momentum are always greater than or equal to those of the non-Abelian solutions. For large values of the Higgs self-coupling parameter, the energy gap between the non-Abelian $p_2 = 0$ branches becomes constant. The angular momentum tends to zero. Interestingly, the non-Abelian $p_2 = 0$ branch number also determines the number of pieces of the step-like structure of one of the gauge potential functions. For large values of the Higgs self-coupling parameter, we obtain a Regge-like quadratic relation between the energy and the angular momentum of the non-Abelian solutions. These solutions become step-like functions.

When we have three vortices pinned at the origin, there is non-uniqueness of the solutions with respect the global parameters. We have found two distinct solutions with the same angular momentum and energy, but different values of other invariant quantities like the Higgs amplitude. Surprisingly, the value of the Higgs self-interaction parameter is relatively low.

The various topics treated in this Thesis have opened several lines of future research. It is our purpose to continue with the following lines of investigation:

- The adaptation of the techniques used in this Thesis in the study of quasi-normal modes of higher dimensional black holes. This is a very active area of research since the gauge/gravity duality was proposed [102]. Quasi-normal modes are a standard tool used to study, in the context of the dual gravity, the near-equilibrium behavior of gauge theory plasmas. Quasi-normal modes also appear in some approaches to the information-loss paradox.

- Higher dimensional black holes in anti-de-Sitter space-time. An ongoing project is the study of black holes in Einstein-Maxwell-Chern-Simons theory with a negative cosmological constant (hence asymptotically anti-de-Sitter). It would be very interesting to see if the complex branch structure obtained in the asymptotically flat case is preserved, and if radially excited extremal black holes do also inhabit this theory. The numerical analysis will be supplemented with the application of the near-horizon formalism.

- Stability of Yang-Mills-Higgs vortices. Another ongoing project is the study of the stability of the vortices obtained in [95]. In this case the perturbation can have two possible behaviors. It can oscillate around the vortex configuration, or it can explode exponentially, meaning that the solution is unstable. The perturbations are studied for both Abelian and non-Abelian vortices, considering non-Abelian perturbations.

RESUMEN EN CASTELLANO

Introducción

En esta Tesis hemos estudiado distintas configuraciones, todas ellas soluciones de teorías clásicas de campos. Estas configuraciones son estrellas de neutrones, agujeros negros y vórtices. La interpretación física de todos estos objetos, así como de las teorías de campos en las que se encuentran, son muy variadas. Las estrellas de neutrones son soluciones de las ecuaciones de Einstein, y se corresponden con objetos astrofísicos que nos permiten estudiar las propiedades del espacio-tiempo y la materia a alta densidad de energía. Los agujeros negros en altas dimensiones que hemos estudiado son soluciones muy interesantes de teorías de campos efectivas que se obtienen en los límites de baja energía de teoría de cuerdas. Por otra parte, los vórtices de teorías de Yang-Mills-Higgs son muy útiles como descripción fenomenológica de la superconductividad.

Hemos dividido estos tres estudios (estrellas de neutrones, agujeros negros y vórtices) en tres secciones. El nexo entre estos tres estudios está principalmente en los métodos matemáticos que se han utilizado para generar estas soluciones, y en las herramientas empleadas para estudiar sus propiedades. Aunque, como veremos, cada problema particular tiene sus propias peculiaridades, las herramientas que hemos usado son prácticamente las mismas. En particular, como hemos tratado configuraciones axialmente simétricas y estacionarias, o perturbaciones pequeñas de estos objetos, nos encontraremos con que los problemas son muy similares en los tres casos desde un punto de vista matemático.

Nuestras investigaciones nos han conducido a resultados originales e interesantes, que han sido publicados en revistas internacionales de primera línea. A continuación

comentaremos brevemente los resultados principales de esta Tesis y los artículos resultantes que han sido publicados, y que se han adjuntado en las secciones anteriores.

Estrellas de neutrones. En los artículos Physical Review D **87** (2013) 104042 [1] (incluido en la sección 2.3.2) y Physical Review D **89** (2014) 044006 [2] (incluido en la sección 2.3.3), hemos estudiado las componentes axial y polar del espectro de modos cuasi-normales de estrellas de neutrones realistas. Para ello, hemos considerado diversas composiciones con respecto a la materia que compone el interior de la estrella. Hemos estudiado diversas relaciones fenomenológicas para el espectro de modos cuasi-normales, y hemos obtenido nuevas relaciones empíricas, que por ser menos dependientes de la composición interna de la estrella, pueden ser más útiles en su aplicación en asteroseismología.

También para estrellas de neutrones, hemos tratado la aproximación de rotación lenta, en el caso en que una densidad superficial de energía envuelve a la estrella de neutrones. Este modelo tan sencillo es apropiado para estudiar variaciones en el estado de las capas superficiales de la estrella. De esta forma podemos interpretar saltos en la velocidad de rotación del pulsar (glitches) como variaciones en la presión de transición entre el núcleo de la estrella y las capas externas. El resultado de estos trabajos se pueden encontrar en los artículos AIP Conference Proceedings **1458** (2012) 419-422 [4] y Journal of Physics: Conference Series **314** (2011) 012088 [3], que están incluidos en las secciones 2.4.2 y 2.4.3, respectivamente.

Agujeros negros. Hemos estudiado agujeros negros en altas dimensiones en dos teorías distintas. En la teoría Einstein-Maxwell-dilaton, hemos estudiado agujeros negros de dimensión impar, con topología esférica y momentos angulares de la misma magnitud. Hemos considerado un acoplo con el dilatón general y, por tanto, en el estudio se incluye el caso Einstein-Maxwell. Cuando nos ceñimos al caso Einstein-Maxwell, y consideramos agujeros negros extremos, obtenemos dos ramas de agujeros negros. Las relaciones entre la entropía y las cargas en estas ramas es bastante especial (en una de ellas la entropía es independiente de la carga eléctrica). En la teoría Einstein-Maxwell-dilatón, sólo una de las ramas permanece, siendo la entropía siempre independiente de la carga eléctrica. El análisis numérico que realizamos se complementa con un estudio analítico de la geometría cercana al horizonte. Este trabajo puede encontrarse en las referencias Physics Letters B **727** (2013) 340-344 [5] (incluido en la sección 3.5.1) y Physical Review D **89** (2014) 024038 [6] (incluido en la sección 3.5.2).

También tratamos el caso de agujeros negros en 5 dimensiones en la teoría Einstein-Maxwell-Chern-Simons, donde también consideramos topología esférica y cohomogeneidad-

1. Tratamos el término de Chern-Simons con acoplo general. Sorprendentemente, obtenemos una estructura de ramas infinita en el caso de agujeros negros extremos, para ciertos valores de la constante de acoplo. Esta secuencia de agujeros negros radialmente excitados implica que infinitas soluciones de la teoría violan unicidad con respecto a las cargas globales. El estudio de la geometría cercana al horizonte también ha sido utilizado para complementar el análisis numérico. Los resultados pueden encontrarse en la referencia Physical Review Letters **112** (2014) 011101 [7], que ha sido incluida en la sección 3.6.1.

Vórtices. Hemos estudiado vórtices no abelianos en la teoría $SU(2)$ Chern-Simons-Higgs con potencial de cuarto orden. Hemos obtenido una estructura de ramas que es dependiente del índice topológico n, y también encontramos pérdida de unicidad cuando $n > 3$. Estos resultados pueden encontrarse en el artículo Physical Review D **88** (2013) 025026 [8], que ha sido incluido en la sección 4.4.1.

Comenzamos este resumen de la Tesis comentando brevemente los métodos numéricos utilizados. Después pasaremos a describir con más detalle los resultados obtenidos para estrellas de neutrones, agujeros negros en altas dimensiones y vórtices.

Métodos numéricos

Ecuaciones diferenciales ordinarias

En todos los casos que hemos considerado en esta Tesis, hemos sido capaces de reducir el problema a un sistema de ecuaciones diferenciales ordinarias. Las teorías que hemos considerado se pueden expresar en términos de un lagrangiano, que es un funcional de los campos y la métrica del espacio-tiempo. Variaciones con respecto a estos campos conducen a las ecuaciones de Euler-Lagrange, de donde se pueden extraer las ecuaciones diferenciales a resolver.

Esencialmente obtenemos las ecuaciones de Einstein junto con ecuaciones para los campos y la materia acoplada, en los casos en que consideramos gravedad (estrellas de neutrones y agujeros negros), o solamente ecuaciones para los campos gauge y de Higgs en el caso de vórtices.

En cualquier caso todas las teorías que hemos tratado dan lugar a ecuaciones diferenciales de segundo orden.

En esta Tesis se ha estado interesado en obtener soluciones a estas ecuaciones, pero también hemos tratado casos en los que hemos estado interesados en estudiar perturbaciones sobre una solución conocida.

En el primer caso, buscamos soluciones con ciertas condiciones de simetría, de manera que somos capaces de escribir un Ansatz que delimita la estructura funcional de la solución en unas coordenadas apropiadas. Por ejemplo éste ha sido el caso de agujeros negros en altas dimensiones, donde hemos buscado configuraciones de topología esférica, cohomogeneidad-1, estacionarias y axisimétricas. En la aproximación de rotación lenta de estrellas de neutrones también somos capaces de escribir explícitamente la dependencia angular, ya que la configuración esférica se deforma a cada orden perturbativo con un número finito de términos del desarrollo en armónicos esféricos. Los vórtices de Chern-Simons-Higgs también satisfacen una serie de condiciones de simetría (simetría rotacional en el plano) que nos permiten escribir la dependencia angular explícitamente. En todos los casos podemos encontrar unas coordenadas en las que somos capaces de escribir explícitamente la dependencia angular de las funciones. Además, las funciones son independientes de la coordenada temporal ya que consideramos configuraciones estacionarias. Por tanto, la única incógnita es la dependencia de las funciones que parametrizan el Ansatz con la coordenada radial.

En el caso en que consideramos perturbaciones dependientes del tiempo de estrellas de neutrones, también podemos reducir el problema a un sistema de ecuaciones diferenciales ordinarias. La idea esencial es que las perturbaciones se pueden desarrollar en armónicos esféricos. Nosotros nos hemos limitado a estudiar perturbaciones con $l = 2$. En consecuencia, la dependencia angular de estos modos es conocida. Como estamos interesados en el estudio de modos cuasi-normales, la dependencia temporal puede ser extraída por medio de una transformada de Laplace (ya que los autovalores de los modos cuasi-normales son números complejos). De esta manera la ecuación de propagación de la perturbación (1.1) puede reescribirse como una ecuación similar a la de Schrödinger (1.3), donde la auto-energía es un número complejo, desconocido. En consecuencia, se reduce a un sistema de ecuaciones diferenciales ordinarias, donde las condiciones de contorno y de pegado determinarán cuándo este auto-valor corresponde a un modo cuasi-normal.

Condiciones de contorno.

El sistema de ecuaciones diferenciales debe ser complementado con un sistema de condiciones de contorno. Estas condiciones de contorno son las que definen el tipo específico de solución que se está buscando (estrellas, agujeros negros, vórtices). El dominio de integración tanto de estrellas como de vórtices es todo el espacio-tiempo, mientras que para generar agujeros negros nos bastará con integrar la configuración en la parte externa al horizonte de sucesos.

Todas las configuraciones estarán definidas en espacio-tiempos asintóticamente planos (estrellas de neutrones y agujeros negros) o espacio-tiempo plano (vórtices). Esto impone un cierto tipo de decaimiento a las funciones al alejarnos del objeto, que se estudia con detalle en cada caso.

Las soluciones deben ser regulares en el origen de coordenadas cuando se trate de estrellas de neutrones o vórtices, o deberán satisfacer las condiciones de horizonte de Killing en el caso de agujeros negros. En cualquier caso, las condiciones de contorno en este extremo del dominio de integración se obtienen realizando una expansión en serie de potencias. Sobre esta serie se imponen las ecuaciones diferenciales, y las relaciones deseadas para las funciones. Esto limita los términos del desarrollo y proporciona relaciones entre sus coeficientes. El desarrollo en serie resultante se puede imponer en forma de condiciones de contorno si se realiza una parametrización correcta de las funciones a integrar.

En algunas ocasiones el número de condiciones que impone el desarrollo en serie es mayor que el número de condiciones de contorno que se pueden pedir al sistema de ecuaciones diferenciales. Se debe realizar un análisis para determinar qué conjunto de condiciones de contorno es más pertinente (mayor precisión, menor tiempo de integración, mayor estabilidad del código), mientras que las condiciones extra se deben de satisfacer una vez generada la configuración.

Método de continuación.

Como comentaremos a continuación, generamos la solución numérica deseada a partir de una solución inicial de las ecuaciones diferenciales. La solución inicial se deforma poco a poco hasta la solución deseada. La solución inicial debe encontrarse en un entorno cercano a la solución deseada en el espacio de soluciones de la teoría. Esta solución inicial se conoce previamente, bien porque es una solución analítica de un caso conocido que esté contenido en el caso que estudiamos, o bien por ser una solución numérica previamente generada.

La solución inicial satisface las condiciones iniciales evaluadas para cierto valor de los parámetros que describen la configuración (piénsese en la masa, carga eléctrica y momento angular). Si variamos alguno o algunos de estos parámetros levemente, en principio el algoritmo será capaz de converger hacia la nueva solución que posee los parámetros modificados. A este método se le conoce como el método de continuación. Los parámetros que se utilizan para definir la configuración pueden ser parámetros internos como derivadas definidas en ciertos puntos, o parámetros del desarrollo en potencias. El algoritmo sólo convergerá si estos parámetros definen unívocamente una

única configuración, y si la solución final está lo suficientemente próxima a la solución inicial.

Colsys.

Para resolver numéricamente el sistema de ecuaciones diferenciales, utilizaremos el software Colsys. Nos permitirá resolver numéricamente problemas de condiciones de contorno. A Colsys se le puede especificar un sistema de ecuaciones diferenciales ordinarias donde cada ecuación puede tener un orden diferente, aunque en nuestro caso siempre se trataran de sistemas con ecuaciones diferenciales de primer y segundo orden.

Las ecuaciones de contorno en nuestro caso serán separadas, queriendo decir que las condiciones de contorno sólo dependen del valor de las funciones y derivadas evaluadas en un mismo punto del dominio de integración, pese a que podrán ser no lineales en las funciones y las derivadas.

Lo interesante de Colsys es que es capaz de estimar el error cometido en la solución en cada paso de la iteración. La forma en que Colsys realiza cada iteración es la siguiente.

Por el método de colocación, Colsys divide el dominio de integración en una malla de puntos, entre los que se encuentran los puntos donde se definen las condiciones de contorno. Cada intervalo de la malla es a su vez dividido en puntos usando una distribución de Gauss-Legendre.

La solución es aproximada en cada uno de los puntos de la malla completa por una serie de polinomios. La serie está dada en términos de unos coeficientes que en principio están indeterminados. Estos coeficientes se deben determinar por imposición de las condiciones de contorno y por requerimiento de las ecuaciones diferenciales en el resto de los puntos de la malla.

Colsys requiere que la iteración actual satisfaga a primer orden las ecuaciones y las condiciones de contorno. El problema de colocación se convierte en un sistema de ecuaciones lineales no homogéneas, en el que los coeficientes lineales estan determinados por los jacobianos de las ecuaciones diferenciales y las condiciones de contorno. Los términos no homogéneos se determinan estimando con la anterior iteración la parte no lineal de las ecuaciones diferenciales y las condiciones de contorno. Además Colsys usa el método de Newton amortiguado con parámetro libre a la hora de realizar la siguiente iteración.

Colsys es capaz de estimar el error cometido, y seleccionar un nuevo mallado en iteraciones posteriores, con más o menos puntos en distintas regiones que resulten más

o menos problemáticas. Esencialmente Colsys obtiene dos soluciones en cada iteración, una de ellas con la mitad de puntos. El error local y global puede estimarse evaluando estas dos soluciones en las ecuaciones diferenciales. El usuario introduce una tolerancia (un error deseado mínimo), y Colsys procede a iterar, modificando el mallado, hasta que consigue un error menor a la tolerancia introducida. Pueden especificarse tolerancias distintas para cada función y derivada. Si la tolerancia no se satisface, Colsys redistribuye la malla por distintos procedimientos intentando redistribuir el error local en cada paso de la iteración. Eventualmente el error global satisface la tolerancia, y Colsys devuelve la correspondiente solución.

Estrellas de neutrones

En esta sección vamos a discutir brevemente los estudios realizados sobre estrellas de neutrones. Estos estudios se pueden separar en dos bloques: modos cuasi-normales de oscilación, y aproximación de rotación lenta.

Modos cuasi-normales

Es muy probable que en los próximos cinco años se detecten las primeras ondas gravitacionales utilizando grandes detectores de ondas gravitacionales como LIGO, GEO, TAMA y VIRGO. Recordemos que una onda gravitacional es una oscilación del espacio-tiempo, típicamente producida por oscilaciones de materia, pero que se propaga por el espacio-tiempo. Son el ejemplo más claro de que en Relatividad General el espacio-tiempo tiene su propia dinámica. Las posibles fuentes de ondas gravitacionales son agujeros negros en colisión, coalescencia de estrellas binarias compactas, colapsos estelares y púlsares.

En ese sentido, las estrellas de neutrones son buenos candidatos a emitir ondas gravitacionales detectables. Las estrellas de neutrones se encuentran en el interior de los pulsares y son el resultado del colapso de estrellas masivas. Tras la explosión de una supernova, la protoestrella de neutrones se encuentra en un estado de fuertes oscilaciones, que se amortiguan según va radiando ondas gravitacionales. De la misma manera, la coalescencia de enanas blancas puede dar lugar a una estrella de neutrones oscilante, que emita ondas gravitacionales.

Las oscilaciones de materia de la estrella de neutrones se acoplan al espacio-tiempo, y provocan que éste también oscile. La oscilación se escapa de la estrella de neutrones en forma de radiación gravitatoria: oscilación del espacio-tiempo que se propaga hacia

infinito, mantenida por la propia dinámica del espacio-tiempo. Por tanto, las oscilaciones de una estrella de neutrones no sólo presentarán frecuencia de oscilación, sino tiempo de decaimiento (similar a la viscosidad en el caso Newtoniano).

El espectro de resonancias de estas ondas gravitacionales puede transportar información sobre la estructura y la composición de las estrellas de neutrones. Es por ello que estamos interesados en realizar un estudio de los modos cuasi-normales de estrellas de neutrones realistas, compuestas por ecuaciones de estado modernas que incluyan estados exóticos de la materia. La comparación entre detecciones y estudios teóricos podría arrojar luz sobre el estado de la materia a las densidades tan altas que se encuentran en una estrella de neutrones (superior a la nuclear).

La manera apropiada de estudiar matemáticamente estas oscilaciones amortiguadas es utilizando un desarrollo en modos cuasi-normales. Consideraremos perturbaciones sobre una configuración esférica y estática. Asumiremos que la materia en el interior de la estrella se puede describir como un barótropo, lo cual es una excelente aproximación para las estrellas de neutrones.

Utilizando teoría de perturbaciones a primer orden, y desarrollando las perturbaciones en armónicos tensoriales, se puede encontrar un sistema de ecuaciones diferenciales para el conjunto de perturbaciones de la métrica del espacio-tiempo y de la densidad y presión de la materia. Este conjunto de perturbaciones se desacopla en dos componentes. Una de ellas (componente axial) no se acopla a perturbaciones materiales. La otra (polar) se acopla a perturbaciones de la densidad y la presión en el interior de la estrella.

Puede demostrarse que en el exterior de las estrella, tanto las perturbaciones axiales como las polares satisfacen (2.10). En el caso axial, esta ecuación se conoce como ecuación de Zerilli, y también se satisface en el interior de la estrella, dado que las perturbaciones no se acoplan a las variaciones de presión y densidad. En el caso polar, se le conoce como ecuación de Regge-Wheeler, y sólo es válida en el exterior. Las perturbaciones polares en el interior de la estrella están determinadas por un conjunto de ecuaciones diferenciales de segundo y primer orden.

Podemos estudiar los modos resonantes de estas ecuaciones diferenciales si estudiamos la transformada de Laplace de las perturbaciones (2.14). De esta forma pasamos de estudiar un sistema de ecuaciones diferenciales en derivadas parciales a un sistema de ecuaciones diferenciales ordinarias, con un parámetro por determinar ω. Este parámetro es complejo, su parte real es la frecuencia de oscilación, y su parte imaginaria el tiempo de decaimiento.

Dado que estamos interesados en ondas gravitacionales producidas en la estrella,

y que viajan desde ella hasta el infinito espacial (ondas salientes), debemos exigir un cierto comportamiento asintótico de las perturbaciones en infinito (2.17). Nótese que este comportamiento provoca que la perturbación diverja en infinito. La componente entrante de la solución sin embargo, tiende a cero en infinito. Ésto provoca que sea fácil generar soluciones que tengan una componente entrante, y que no sirven por tanto como modos cuasi-normales.

Existen diversos métodos para obtener modos cuasi-normales que satisfagan, al menos aproximadamente, la condición de onda saliente. El método WKB [37, 38] y el método de las fracciones continuas [39, 40, 41, 42, 43] han sido utilizadas extensivamente y con resultados bastante buenos, especialmente para modos cuasi-normales lentamente amortiguados, donde es más fácil no tener contaminación de onda entrante. Otros métodos más sofisticados estudian la función fase de la perturbación [44] y sus condiciones de contorno. Se puede realizar una continuación analítica de la perturbación en el plano complejo [45, 38, 46, 47], de manera que el comportamiento de onda entrante se pueda controlar mejor e incluso imponer como condición de contorno.

El procedimiento que hemos desarrollado es una amalgama de métodos conocidos y otros no utilizados antes en este contexto. Utilizamos la función fase de la perturbación en el exterior de la estrella. Además estudiamos una continuación analítica de esta función en el plano complejo, de manera que el radio es ahora una variable compleja. Parametrizamos el dominio de integración como una línea recta en el plano complejo. Esta recta tiene un cierto ángulo α con la recta real. Este ángulo es libre, y puede ser ajustado de manera que el comportamiento de onda saliente sea una condición de contorno para la fase de la perturbación en el infinito de la recta de ángulo α. A este método se le conoce como Exterior Complex Scaling. Así pues, una solución de las ecuaciones con esta condición de contorno no puede tener contaminación de onda entrante, y si se efectúa correctamente el pegado con una solución interior, habremos determinado un modo cuasi-normal.

De esta manera, generamos una perturbación en el interior de la estrella. Estudiamos las condiciones de pegado de la solución completa. La perturbación en el interior debe pegar con la fase en el exterior. El pegado que se realiza es estándar: continuidad de las formas fundamentales a través del borde de la estrella. Permitimos que existan saltos en la densidad y presión (ecuaciones de estado generales). Finalmente, las condiciones de pegado se escriben en forma de determinante (wroskiano) que debe anularse cuando la perturbación integrada es un modo cuasi-normal (i.e. cuando la parte real y la parte imaginaria de ω son efectivamente la frecuencia y el tiempo de decaimiento de una perturbación).

Como se ha dicho, esto se ha realizado tanto para modos cuasi-normales axiales como para polares, y cuyos resultados se encuentran publicados en dos artículos que se adjuntan en las Secciones 2.3.2 y 2.3.3.

Referente al primer artículo, Physical Review D **87** (2013) 104042 [1], donde se tratan los modos axiales:

- Como estamos interesados en modos cuasi-normales (axiales) para estrellas de neutrones realistas, debemos utilizar métodos numéricos para integrar las ecuaciones diferenciales. Como se ha explicado, esto implica integrar la ecuación de Zerilli. Sin embargo, decidimos integrar esta ecuación a la vez que integramos las ecuaciones a orden cero (ecuaciones de Tolman-Openheimer-Volkov). De esta forma la solución estática se adapta a la precisión que deseemos obtener en la perturbación.

- Como la función perturbación es una función compleja que diverge en infinito espacial si imponemos comportamiento de onda saliente, utilizamos el método que hemos presentado de forma breve anteriormente. Utilizamos Exterior Complex Scaling en la fase de la perturbación fuera de la estrella.

- Los modos axiales son modos puramente espacio-temporales de oscilación. Esto quiere decir que no se acoplan a oscilaciones de la materia. Hemos estudiado los modos w (modos de espacio-tiempo), y en particular nos hemos concentrado en el fundamental y el primer excitado. También hemos estudiado el modo fundamental wII (modo de interfaz). Las ecuaciones de estado consideradas no dan lugar a modos atrapados (que aparecen sólo cuando la compacidad es muy alta, y por tanto, poco realista en estrellas de neutrones).

- Utilizamos 18 ecuaciones de estado realistas, y dos métodos diferentes para implementarlas. Uno de ellos es una interpolación politrópica a trozos (diferentes regiones de la ecuación de estado son aproximados por polítropos de ciertos parámetros). Esta interpolación fue desarrollada en [33]. El otro método es una interpolación a trozos por polinomios cúbicos de Hermite, que satisface condiciones locales termodinámicas. Esta interpolación se realiza sobre tablas numéricas de valores de densidad de energía y presión. Las ecuaciones de estado consideradas satisfacen todas el límite inferior de 2 $M_\odot$ (es decir, como existen pulsares con masas de 2 $M_\odot$, la masa máxima mínima que la ecuación de estado debe permitir debe ser mayor a dos masas solares). Sólo hemos incluido dos casos en los que la masa no supera el límite, para comparar los resultados.

Las ecuaciones de estado incluyen materia nuclear, materia nuclear mezclada con hyperones, materia nuclear mezclada con quarks, y materia quark pura. La mayoría de las ecuaciones de estado han sido propuestas muy recientemente (últimos dos años) en Física Nuclear.

- Hemos estudiado relaciones fenomenológicas, siguiendo [49, 50, 51, 41]. Si estas relaciones son independientes de la ecuación de estado, entonces pueden ser muy útiles a la hora de determinar, en caso de detección, otros parámetros de la estrella como el radio, la masa o la compacidad. Para modos axiales obtenemos que son bastante independientes de la ecuación de estado, excepto para estrellas de quarks, que presentan diferentes relaciones escaladas (la misma expresión pero con diferentes parámetros).

- También hemos estudiado nuevas relaciones fenomenológicas. En este caso la idea es relacionar la frecuencia con el tiempo de decaimiento. Si escalamos ambas cantidades a la presión central, encontramos que entre ellas existe una relación bastante independiente de la ecuación de estado. Proponemos estas nuevas relaciones empíricas para estimar la presión central de la estrella.

En un artículo posterior, Physical Review D **89** (2014) 044006 [2], incluido en la Sección 2.3.3, hemos desarrollado un estudio similar para modos polares.

- El procedimiento numérico es equivalente al realizado para modos axiales. Integramos el sistema de ecuaciones de TOV junto con el sistema de ecuaciones para perturbaciones polares. La diferencia es que el sistema de ecuaciones necesario para describir la perturbación en el interior de la estrella es más complicado, ya que no se puede reformular en una única ecuación diferencial como en el exterior, donde sólo tenemos que integrar la ecuación de Regge-Wheeler.

- Sin embargo, en la región exterior, como la ecuación diferencial es esencialmente la misma que en el caso axial, podemos aplicar el método de Exterior Complex Scaling a la fase de la función de Regge-Wheeler. Imponemos como condición de contorno el comportamiento de onda saliente.

- En el artículo tratamos 15 ecuaciones de estado realistas diferentes. Son las mismas ecuaciones de estado que se tratan en el artículo 2.3.2 y todas ellas satisfacen la condición de 2 $M_{\odot}$. Se utilizand los mismos procedimientos para la interpolación de la ecuación de estado que en el caso axial.

- Estudiamos los modos fundamentales wI de la componente polar, el modo fundamental de presión, y el modo fundamental. De nuevo siguiendo [49, 50, 51, 41] estudiamos relaciones escaladas. En este caso las relaciones escaladas no son tan útiles como en la componente axial, ya que el espectro de los modos de fluido es mucho más dependiente de la ecuación de estado. Las estrellas de quarks son las más diferentes.

- Proponemos nuevas relaciones fenomenológicas que relacionan la frecuencia con el tiempo de decaimiento. Escalamos ambas cantidades a la presión central. Obtenemos relaciones para los modos w y los modos f. Las relaciones obtenidas son muy independientes de la ecuación de estado. Proponemos que estas relaciones fenomenológicas pueden utilizarse para estimar la presión central y el radio de la estrella (suponiendo que la masa es conocida, y que la detección es suficientemente buena como para que la parte real e imaginaria de los modos w y f se conozcan).

Los resultados de estos dos trabajos son muy útiles para la futura asteroseismología de estrellas de neutrones. Como el análisis se realiza en un rango muy amplio de ecuaciones de estado actuales, la información contenida en estos artículos se podría usar junto con futuras detecciones de ondas gravitacionales para restringir la ecuación de estado a altas densidades.

Rotación Lenta

Como las estrellas de neutrones se encuentran en la naturaleza en forma de pulsares, es importante considerar el caso de estrellas de neutrones en rotación. En Relatividad General la rotación tiene un efecto en el espacio-tiempo que no se observa en gravedad Newtoniana. Este efecto es el arrastre de los sistemas de referencia inerciales: un observador en caída libre desde el infinito adquiere una velocidad de rotación en torno a la estrella a medida que se acerca a ésta.

Nosotros supondremos que la estrella se mueve con rotación rígida lenta. La aproximación de rotación lenta se realiza desarrollando las funciones de la métrica y del fluido a primer orden en la velocidad angular de la estrella Ω.

En los artículos AIP Conference Proceedings **1458** (2012) 419-422 [4] y Journal of Physics: Conference Series **314** (2011) 012088 [3], que están incluidos en las secciones 2.4.2 y 2.4.3, aplicamos el límite de rotación lenta al estudio de los glitches. Los glitches son pequeñas variaciones en la velocidad angular de los pulsares, que probablemente tienen su origen en cambios en las capas más externas de la estrella. En nuestro

plantemamiento del problema, el estudio de las condiciones de pegado en el borde de la estrella es fundamental:

- Estas condiciones de contorno se formulan de manera intrínseca, usando formas fundamentales de la hipersuperficie que forma el borde de la estrella. Esto proporciona condiciones que la métrica y las funciones del fluido del interior de la estrella deben satisfacer en el borde de la estrella. De esta manera la solución interior y la exterior pegan correctamente, y podemos garantizar que la configuración es una solución de las ecuaciones de Einstein. Además consideramos el caso en que la estrella está envuelta por una densidad superficial de energía. El modelo resultante puede interpretarse como una aproximación para las capas exteriores de la estrella. Si el crust de la estrella de neutrones tiene un tamaño pequeño en comparación con el resto de la estrella, y su masa es también pequeña en comparación con la masa total, esta capa externa puede aproximarse como una superficie infinitesimal que envuelve el resto de la estrella.

- El parámetro esencial de este modelo de estrella de neutrones con crust superficial es la presión de transición entre el núcleo y el crust de la estrella (además de la densidad central y la velocidad angular de la estrella).

- Variaciones en la presión de transición de la estrella están relacionadas con saltos en la velocidad angular de la configuración. En consecuencia, podemos aplicar este modelo sencillo a la descripción de los glitches gigantes de un pulsar. Como los glitches son probablemente producto de variaciones térmicas en las capas exteriores de la estrella de neutrones, podemos relacionar el salto en la velocidad angular con cambios en la presión de transición, asumiendo que el núcleo interior de la estrella no se ve modificado. Este cambio en la presión de transición estaría relacionado con una transición de fase. Las variaciones obtenidas en la presión de transición son compatibles con los cambios de temperatura esperados en el crust interno de la estrella.

Agujeros negros

Objetivos

En esta sección trataremos brevemente los estudios realizados sobre agujeros negros en altas dimensiones. El estudio se ha realizado en dos teorías diferentes: Einstein-Maxwell-dilatón y Einstein-Maxwell-Chern-Simons. Hemos realizado tanto análisis numérico como estudio de la geometría cercana al horizonte.

En la teoría Einstein-Maxwell-dilatón, se han considerado agujeros negros en dimensión impar. Nos hemos limitado al caso en que las soluciones poseen topología esférica del horizonte. Además asumimos que todos los momentos angulares tienen la misma magnitud. En particular, consideraremos el caso en que los agujeros negros son extremos. Veremos que en el caso sin dilatón encontramos dos ramas de soluciones, en una de las cuales la entropía es independiente de la carga eléctrica del agujero negro. Cuando se incluye un campo de dilatón, con independencia de la constante de acoplo, la entropía mantiene este comportamiento. Este estudio ha dado como resultado los artículos Physics Letters B **727** (2013) 340-344 [5] (incluido en la sección 3.5.1) y Physical Review D **89** (2014) 024038 [6] (incluido en la sección 3.5.2)

También hemos considerado agujeros negros en Einstein-Maxwell-Chern-Simons, pero en este caso nos restringimos a 5 dimensiones. Hemos encontrado resultados muy interesantes como por ejemplo: soluciones con momento angular nulo, pero que no son estáticas; y pérdida de unicidad con respecto a las cargas globales. Estos resultados han sido publicados en Physical Review Letters **112** (2014) 011101 [7] (incluido en la sección 3.6.1).

Motivación

Los agujeros negros son predicciones de la Relatividad General. Se trata de regiones especiales del espacio de las cuales ni siquiera la luz puede escapar clasicamente. La métrica del espacio-tiempo que describe un agujero negro estático (sin carga eléctrica) en 3+1 dimensiones fue descubierta por Schwarzschild en 1915. Un par de años después se generalizó para incluir un campo eléctrico de Maxwell (solución de Reissner-Nordström). Al comienzo estas soluciones de las ecuaciones de Einstein se consideraban como soluciones singulares, con únicamente interés académico. No fue hasta los años sesenta cuando la naturaleza del horizonte de sucesos de un agujero negro fue realmente comprendida (singularidad de las coordenadas). En 1963 Kerr

hace el descubrimiento de los agujeros negros en rotación sin carga eléctrica, y posteriormente se generaliza para incluir un campo de Maxwell (solución de Kerr-Newman) [103].

La evidencia astrofísica de la presencia de agujeros negros masivos en el núcleo de las galaxias espirales es muy fuerte. Otros objetos astrofísicos de nuestra galaxia, con fuerte emisión de rayos X y masas del orden de la de nuestro Sol, son candidatos importantes a agujeros negros, probablemente resultado del colapso de estrellas masivas [17].

Los agujeros negros asintóticamente planos en 4 dimensiones en Einstein-Maxwell tienen propiedades muy especiales. Deben ser topológicamente esféricos, y no pueden darse otras topologías si se asume estabilidad y la condición de energía se satisface. Una solución de agujero negro en Einstein-Maxwell en 4 dimensiones se caracteriza por sus cargas globales, i.e., su masa, su momento angular y su carga eléctrica. Dados estos tres parámetros, sólo existe una solución de agujero negro [55].

Sin embargo, en más de 4 dimensiones, o cuando otros campos más generales se acoplan a la gravedad (campos de Yang-Mills, dilatón) los agujeros negros dejan de poseer estas características [56]. En altas dimensiones existen dos diferencias fundamentales: los horizontes de sucesos de los agujeros negros pueden ser objetos extensos, con topologías diferentes a la esférica; y existe más de un plano de rotación.

La primera propiedad es fácil de ver si tomamos agujeros negros en D dimensiones, con un cierto horizonte de sucesos Σ_H. Podemos construir inmediatamente una solución perfectamente válida en $D+1$ dimensiones, simplemente añadiendo una dimensión espacial adicional [57]. Este nuevo agujero negro tiene horizonte $\Sigma_H \times \Re$. Nótese que este horizonte de sucesos es un objeto extenso, con topología no esférica. En general para $D > 4$ dimensiones podemos encontrar soluciones con horizonte de suceso más generales, como black strings, y en general, p-branas en más de 4 dimensiones.

Por supuesto, estos agujeros negros no son asintóticamente planos. Sin embargo podemos pensar en tomar una solución tipo cuerda en $D+1$ dimensiones y horizonte $\Sigma_H \times \Re$ y doblarlo de manera que el horizonte adquiera topología $\Sigma_H \times S^1$ [57]. Con un ajuste apropiado de los momentos angulares de cada plano de rotación, podemos estabilizar la solución, y obtener una solución tipo anillo negro estable. Estos anillos negros estables pueden encontrarse para más de 4 dimensiones [56].

Los agujeros negros en altas dimensiones tienen más de un plano de rotación. En general, para $D-1$ dimensiones espaciales, el grupo de rotación es $SO(D-1)$ y tiene $N = [(D-1)/2]$ planos de rotación independientes, donde N es la parte entera de $(D-1)/2$. Un momento angular puede asociarse a cada uno de los planos de rotación.

Comentemos brevemente las razones por las que los modelos de gravedad con más de 3 dimensiones espaciales, y en especial soluciones tipo agujero negro de estas teorías, son interesantes.

Tras la formulación de la teoría de la Relatividad por Einstein, Kaluza en 1921 [58] y Klein en 1926 [59] descubrieron que si una dimensión espacial extra se añadía a la gravedad de Einstein, en una rebanada de 4 dimensiones de esta teoría extendida, la gravedad resultante poseía un campo electromagnético extra acoplado de manera natural a la métrica de la rebanada [56]. De esta forma, surgía la posibilidad de interpretar la teoría de Einstein-Maxwell en 4 dimensiones como una teoría de Einstein en cinco dimensiones. Esta fue la primera pista hacia la idea de que las interacciones naturales (en este caso el electromagnetismo y la gravedad) podrían unificarse en una única fuerza (en este caso la gravedad de Einstein) actuando sobre un espacio-tiempo de dimensiones más elevadas.

Más tarde, la teoría de cuerdas, una posible aproximación a la gravedad cuántica, ha predicho la existencia de más de 4 dimensiones espacio-temporales (la llamada teoría M tiene 11 dimensiones). Las dimensiones espaciales extra son compactas y mucho menores en escala que las 3 dimensiones espaciales usuales de nuestra experiencia cotidiana. Estas dimensiones extra están enrolladas en volúmenes pequeños (compactificación).

Otras teorías, como la idea del mundo-brana, sugieren que nuestras 3 dimensiones espaciales son una rebanada de un espacio-tiempo de dimensión más alta. En estas teorías, el espacio podría tener dimensiones espaciales extra mucho más extensas, en adición a dimensiones compactas extra.

Algunas de estas teorías predicen la posibilidad de producir agujeros negros de altas dimensiones en el LHC y futuros colisionadores TeV.

Una aplicación interesante de los agujeros negros en altas dimensiones, y que guarda relación con teoría de cuerdas, es la dualidad gauge-gravedad [56]. Esta conjetura propuesta por Maldacena en 1997 [60] propone que existe una correspondencia entre el espacio-tiempo de Anti-de Sitter y una teoría conforme de campos. De esta forma teorías cuánticas de campos podrían relacionarse con teorías de gravedad en altas dimensiones. Sistemas no gravitatorios en equilibrio térmico en 3+1 dimensiones, podrían ser duales a agujeros negros de altas dimensiones. Sistemas fuertemente interactuantes podrían estudiarse utilizando su dual como agujeros negros.

Como las propiedades de los agujeros negros en altas dimensiones son muy diferentes a los de 4 dimensiones, su estudio también tiene mucho interés por sí mismo. Su estudio puede arrojar luz en porque la topología, la unicidad, y la estabilidad de los

agujeros negros en 4 dimensiones es tan especial [57].

La primera generalización de agujero negro a dimensiones más altas, la solución estática en gravedad de Einstein (generalización de la métrica de Schwarzschild), se realizó por Tangherlini [53], quien también generalizo la métrica de Reissner-Nordström. La correspondiente generalización del agujero negro de Kerr se realizó por Myers y Perry [52]. Otras soluciones acopladas a distintos campos, estacionarias y con distintas propiedades han sido obtenidas en el contexto de teorías efectivas relacionadas con límites de baja energía de teoría de cuerdas [61, 62, 63]. En [57] se puede encontrar una revisión completa de las soluciones de agujero negro en altas dimensiones conocidas hasta ahora analíticamente.

Geometría cercana al horizonte

En el formalismo cercano al horizonte, se asume que el espacio-tiempo exterior al horizonte de sucesos se puede dividir en dos regiones [77]. Una de ella es cercana al horizonte de sucesos (geometría cercana al horizonte), y la otra región corresponde al espacio-tiempo que se extiende desde la geometría cercana al horizonte hasta el infinito asintóticamente plano.

La geometría cercana al horizonte se puede obtener mediante un límite aplicado a una transformación de coordenadas concreto, que elimina el resto de la geometría. En general, esta transformación de coordenadas selecciona un sistema de referencia corrotante con el horizonte de sucesos, y centra la coordenada radial en el horizonte. La transformación depende de un parámetro de escala, Λ, que cuando es tomado en el límite $\Lambda \to 0$, suprime el resto del espacio-tiempo, pero mantiene la región cercana al horizonte de sucesos.

Comentaremos a continuación algunas propiedades de la geometría cercana al horizonte [78]. Como estamos considerando horizontes de sucesos con topología esférica, el espacio-tiempo cerca del horizonte se puede describir como el producto de dos espacios independientes. Uno de ellos se puede cubrir con coordenadas angulares (θ_i, ϕ_j) (que dependen de la dimensión considerada) y describen una esfera (achatada en el caso rotante) en $D-2$ dimensiones: S^{D-2}. El otro factor del espacio-tiempo puede cubrirse con coordenadas temporal y radial (t, r), y describe un espacio tiempo de anti-de-Sitter en dos dimensiones: AdS_2 (recuérdese que esto es la gravedad de Einstein en dos dimensiones con constante cosmológica negativa). Cabe destacar que este espacio-tiempo factorizado es una solución exacta de las ecuaciones de Einstein. Pero nótese que esta factorización del espacio-tiempo no es válida en el resto de la geometría de la solución total, que es asintóticamente plana. En otras palabras, esta factorización nunca describe soluciones globales de las que estamos interesados.

El espacio-tiempo cerca del horizonte de sucesos tiene una gran cantidad de simetría. Efectivamente, sobre la esfera S^{D-2} actúa el grupo de isometría $SO(D-1)$ en el caso estático, y el grupo $U(1)^N$ de isometría actúa sobre la esfera achatada en el caso de rotación (rotación independiente en cada uno de sus N planos axiales) [79]. Si todos los momentos angulares tienen la misma magnitud, entonces la simetría aumenta al grupo de cohomogeneidad-1, y tenemos una esfera achatada factorizada con isometría $U(N)$. El otro factor del espacio-tiempo, la componente anti-de-Sitter, tiene isometría $SO(2,1)$ generada por tres vectores de Killing independientes. Nótese que los posibles campos gauge y escalar acoplados al espacio-tiempo son invariantes bajo todas las isometrías que actúan sobre $AdS_2 \times S^{D-2}$.

Todos los ejemplos conocidos de agujeros negros extremos, con topología esférica y horizontes no singulares, tienen geometría cercana al horizonte factorizada como $AdS_2 \times S^{D-2}$ y isometrías asociadas $SO(2,1) \times SO(D-1)$ en el caso esféricamente simétrico, y $SO(2,1) \times U(1)^N$ en el caso rotante [78]. Una factorización similar en términos de AdS_2 se encuentra también en agujeros negros con otras topologías, como los anillos negros [77].

Por supuesto que en la geometría cercana al horizonte toda la información asociada a la estructura asintótica de la solución global se pierde. Sin embargo hay mucha información útil en la geometría cercana al horizonte [80].

En particular, como la geometría cercana al horizonte se obtiene en un sistema de referencia corrotante con el horizonte, la conexión con el sistema de referencia asintóticamente plano de la solución global desaparece. La velocidad angular y la masa no pueden ser calculadas utilizando la geometría cercana al horizonte. Si es posible calcular cargas conservadas relacionadas con flujos conservados de los campos gauge, y asociadas a la simetría rotacional. Es decir, podremos calcular, utilizando las cargas de Noether, la carga eléctrica y el momento angular.

Agujeros negros en la teoría Einstein-Maxwell-dilatón

Aquí comentaremos los estudios realizados sobre agujeros negros en la teoría Einstein-Maxwell-dilatón. Éste es el tema que se ha tratado en los artículos adjuntos en 3.5.1 y 3.5.2, publicados respectivamente en Physics Letters B **727** (2013) 340-344 [5] y Physical Review D **89** (2014) 024038 [6].

Hemos estudiado agujeros negros de dimensión impar y cuyo horizonte de sucesos tiene topología esférica. Nos hemos restringido al caso en que los agujeros negros tienen todos los momentos angulares de la misma magnitud. Esto incrementa la simetría a cohomogeneidad-1, lo que nos proporciona un conocimiento analítico para

la dependencia angular de las funciones. Los agujeros negros que estudiamos son generalización de las soluciones de Reissner-Nordström y Myer-Perry, donde la carga eléctrica, el momento angular y la masa, en principio, serán parámetros libres.

Para el caso de agujeros negros extremos, podremos emplear el formalismo cercano al horizonte.

- En el caso en que no incluimos dilatón (teoría Einstein-Maxwell) encontramos dos ramas de soluciones extremas. Una de ellas emerge desde la solución de Myers-Perry (rama MP). La segunda rama está compuesta por generalizaciones rotantes de la configuración de Reissner-Nordström (rama RN). Las dos ramas se encuentran en una cierta solución no singular.

- En la rama MP, el área es proporcional al momento angular. La carga no entra en la relación. En consecuencia, la entropía es proporcional al momento angular del agujero negro. Por otro lado, el momento angular del horizonte de sucesos sí que depende tanto del momento angular como de la carga.

- En la rama RN, el área depende tanto del momento angular como de la carga. Sin embargo, el momento angular en el horizonte es proporcional al momento angular total. Por tanto, hay un intercambio de comportamientos entre la rama RN y la rama MP.

- Estos resultados se obtienen tanto utilizando métodos numéricos como el formalismo cercano al horizonte. Sin embargo, el formalismo cercano al horizonte presenta soluciones que no se encuentran globalmente. Concluimos que no todas las geometrías cercanas al horizonte se corresponden con soluciones globales.

- Cuando introducimos un campo dilatón, con constante de acoplo libre, la estructura de doble rama se pierde. Sólo hay una rama, que es la generalización con dilatón de la rama MP. La entropía de estas soluciones es proporcional al momento angular, sin dependencia con la carga.

- El borde del dominio de existencia de estos agujeros negros está formado por agujeros negros extremos. Representamos este borde en los artículos escalando los diferentes parámetros a la masa. Existe una cierta dualidad entre la velocidad angular escalada de agujeros extremos y la gravedad superficial de agujeros estáticos (cuando estas cantidades se representan en función de la carga eléctrica escalada). Una relación similar se puede encontrar entre el área escalada para configuraciones estáticas y el momento angular para configuraciones extremas.

Estas relaciones aproximadas se satisfacen idénticamente en el caso de agujeros negros de Kaluza-Klein, correspondiente al valor de acoplo h_{KK}. Estos agujeros negros de Kaluza-Klein se conocen analíticamente, y son utilizados para testear los resultados.

Agujeros negros en la teoría Einstein-Maxwell-Chern-Simons

A continuación presentamos un resumen del estudio realizado a los agujeros negros en la teoría Einstein-Maxwell-Chern-Simons, y que se encuentra publicado en Physical Review Letters **112** (2014) 011101 [7], y que adjuntamos en 3.6.1. Estudiamos agujeros negros en 5 dimensiones, de nuevo con horizonte de sucesos con topología esférica, y considerando todos los momentos angulares con la misma magnitud. Como en el caso anterior, estos agujeros negros son generalizaciones de las soluciones de Reissner-Nordström y Myers-Perry. El valor de la constante de acoplo del termino de Chern-Simons es un parámetro libre. Por supuesto, reobtenemos todos los resultados para el caso Einstein-Maxwell en el caso en que el término de Chern-Simons se desacopla.

Nos interesan especialmente los agujeros negros extremos, que en principio se pueden utilizar para estudiar el borde del dominio de existencia. Pero en este caso la situación resulta ser mucho más complicada que en el caso EMd:

- De nuevo realizamos el análisis combinando métodos numéricos con el formalismo cercano al horizonte. Pero en este caso las soluciones globales forman una estructura de ramas complicada, que no puede ser obtenida utilizando únicamente la geometría cercana al horizonte. La razón es que la estructura de ramas está presente en términos de las cargas globales (masa, velocidad angular). La geometría cercana al horizonte no caracteriza completamente el espacio de soluciones de estos agujeros negros extremos. Dicho de otra forma, existe no unicidad de la geometría cercana al horizonte. Una misma solución de la geometría cerca del horizonte corresponde a más de una (incluso infinitas) soluciones globales. Encontramos esta propiedad en agujeros negros cuyo valor de la constante de acoplo de Chern-Simons es superior a 2 veces el valor de supergravedad. Además hay soluciones cerca del horizonte que no son obtenidas globalmente, similar a lo observado en la teoría Einstein-Maxwell-dilatón.

- Encontramos no unicidad con respecto a las cargas globales: existen soluciones con las mismas cargas globales, pero con geometrías cercanas al horizonte distintas. De manera que para caracterizar a estos agujeros negros extremos, debemos

conocer además de sus cargas globales, algún parámetro del horizonte, como el área o el momento angular del horizonte.

- La estructura de ramas obtenida en los parámetros globales da lugar a configuraciones excepcionales. Por ejemplo, existe una secuencia infinita de configuraciones extremas no estáticas, pero cuyo momento angular es nulo. Estas configuraciones son excitaciones radiales: pueden caracterizarse por el número de nodos de las funciones del campo gauge. A medida que el número de nodos de estas funciones aumenta, la masa aumenta. La masa tiende al valor de la configuración estática cuando el número de nodos tiende a infinito.

- La estructura de ramas también incluye soluciones extremas con velocidad angular nula, pero momento angular no nulo.

- Una propiedad interesante es que podemos tener no unicidad entre soluciones extremas y no extremas. Es decir, hay soluciones extremas cuyas cargas globales coinciden con las cargas globales de soluciones no extremas.

  El borde del dominio de existencia de estos agujeros negros se compone de agujeros negros extremos. Representamos este borde escalando los parámetros de los agujeros negros a la masa.

Vórtices

En este capítulo vamos a presentar nuestros resultados para vórtices de Chern-Simons-Higgs en 2+1 dimensiones. Los resultados de este estudio pueden encontrarse en el artículo Physical Review D **88** (2013) 025026 [8], adjunto en la Sección 4.4.1.

A continuación comentaremos nuestros resultados en vórtices de Chern-Simons-Higgs. Estos vórtices se han obtenido en la teoría $SU(2)$ Chern-Simons-Higgs. El campo gauge $SU(2)$ se acopla al campo de Higgs (que se encuentra en la representación adjunta) vía un término de Chern-Simons en la acción. Por tanto el campo gauge no tiene dinámica, y se determina por un conjunto de condiciones que ligan el campo gauge con el campo de Higgs. Como el campo de Higgs tiene un potencial de cuarto orden, la auto-dualidad de los vórtices en el caso abeliano se pierde.

- Para construir las configuraciones no abelianas, empezamos con las correspondientes configuraciones abelianas. Cambiando los valores de los parámetros internos de la solución, podemos generar las soluciones no abelianas. Por ejemplo, los

parámetros p_1 y p_2, que están relacionados con la amplitud de los dos isotripletes internos, y que son nulos en el caso abeliano. Sin embargo, se pueden anular de nuevo para ciertas configuraciones no abelianas.

- Para un número dado de vórtices, el número de soluciones no abelianas que satisfacen $p_2 = 0$ depende del parámetro de acoplo del Higgs. A medida que el parámetro de acoplo del Higgs se incrementa, el número de estas ramas no abelianas con $p_2 = 0$ incrementa.

- La energía de la rama abeliana es siempre mayor o igual que la energía de las soluciones no abelianas. Lo mismo se cumple para el momento angular. La energía y el momento angular de una solución no abeliana aumentan con el número de la rama.

- Para valores grandes del parámetro de acoplo del Higgs, la energía del gap entre las sucesivas ramas no abelianas con $p_2 = 0$ se hace constante. Es interesante observar que el número de rama no abeliana con $p_2 = 0$ también determina el número de trozos de la función paso a la que tienden las funciones del potencial gauge.

- Por otro lado, para valores grandes del parámetro de acoplo del Higgs, la relación entre la energía y el momento angular de las soluciones no abelianas resulta ser una relación tipo Regge cuadrática. Las soluciones se pueden describir con funciones paso, como hemos dicho.

- Para número topológico igual a 3, existe no unicidad de las soluciones con respecto a los parámetros globales. Hemos encontrado dos soluciones distintas con el mismo momento angular y energía, pero con diferentes valores de otras cantidades invariantes, como la amplitud del campo Higgs. Sorprendentemente, el valor del acoplo del Higgs es relativamente pequeño. La no unicidad es consecuencia de una relación complicada entre los parámetros internos y la energía y el momento angular de la configuración (el parámetro p_1 se anula en ambas soluciones, pero el parámetro p_2 tiene un valor diferente en cada caso).

Conclusiones

En esta Tesis hemos considerado diversos objetos pertenecientes a distintas teorías clásicas de campos: estrellas de neutrones, agujeros negros en altas dimensiones y

vórtices de teorías de Yang-Mills-Higgs.

Todos estos objetos presentan un alto grado de simetría. Por tanto, todos los problemas se podían reducir a un sistema de ecuaciones diferenciales ordinarias, donde un cierto conjunto de condiciones de contorno, específico de cada objeto, debía ser impuesto. Estas condiciones de contorno se obtienen por distintos procedimientos, como condiciones de regularidad, pegado o comportamiento asintótico.

En general, no disponemos de solución analítica, excepto para valores particulares de los parámetros de la teoría. En consecuencia, hemos tenido que emplear métodos numéricos para generar las configuraciones. Hemos utilizado el software Colsys para ello. Colsys nos permite resolver ecuaciones diferenciales ordinarias, donde las condiciones de contorno se podían definir en distintos puntos del dominio de integración. Colsys permite el uso del método de continuación por lo que podemos explorar el espacio de soluciones de la teoría a partir de una solución inicial conocida, bien sea analítica o numérica aproximada.

Con respecto a estrellas de neutrones, hemos estudiado modos cuasi-normales y rotación lenta. El estudio de los modos cuasi-normales de estrellas realistas incluye ecuaciones de estado modernas que satisfacen el límite de 2 $M_{\odot}$. Se han tratado distintas composiciones de materia (nuclear, hyperones, quark). Relaciones muy interesantes con aplicación a asteroseismología han sido obtenidas. La rotación lenta, junto con un modelo de crust superficial, nos ha permitido modelar de manera sencilla el cambio en la presión de transición del pulsar Vela durante un glitch, pudiendo estimar variaciones de la temperatura de las capas exteriores de la estrella.

Otro tema de estudio han sido los agujeros negros en altas dimensiones. Con respecto a EMd, se han considerado agujeros negros en dimensión impar, topológicamente esféricos y cohomogeneidad-1. El estudio numérico se suplementa con el estudio de la geometría cercana al horizonte. La entropía resulta ser independiente de la carga eléctrica y proporcional al momento angular, en el caso extremo en presencia de un dilatón. En el caso EM puro, existen dos ramas de agujeros negros extremos, una de ellas de entropía proporcional al momento angular. No todas las soluciones cercanas al horizonte se corresponden con una solución global.

Con respecto a EMCS, la situación es bastante mas complicada. En el caso extremo, una estructura de ramas infinita aparece cuando el valor del parámetro acoplo del término de Chern-Simons es mayor a dos veces el valor de supergravedad. Esta estructura de ramas es rica en propiedades: secuencia infinita de configuraciones $J = 0$ no estáticas, radialmente excitadas y que se diferencian por el número de nodos de la función del vector gauge; configuraciones no estáticas con velocidad angular nula;

pérdida de unicidad global entre soluciones extremas; pérdida de unicidad de la geometría cercana al horizonte; soluciones cercanas al horizonte que no se corresponden con soluciones globales; y pérdida de unicidad global entre soluciones extremas y no extremas.

Finalmente hemos estudiado vórtices en teorías de Chern-Simons-Higgs. Estas soluciones son de interés en descripciones efectivas de fenómenos de superconductividad. Hemos obtenidos soluciones abelianas y no abelianas de vórtices de campo escalar Higgs acoplado a un campo gauge $SU(2)$, donde el Higgs se encuentra en la representación adjunta, y el potencial de auto-acoplo del Higgs es de orden cuarto. La falta de auto-dualidad de las soluciones da lugar a propiedades interesantes. El comportamiento de las soluciones no abelianas con los parámetros internos es estudiada en detalle, junto con el límite en el que el parámetro de acoplo del Higgs es alto. Para índice topológico mayor que 3, existe pérdida de unicidad.

Los diversos temas tratados en esta Tesis han abierto diversas líneas de investigación que se están desarrollando, o se planean desarrollar. Por ejemplo:

- La adaptación de las técnicas utilizadas en esta Tesis al estudio de modos cuasi-normales de agujeros negros en altas dimensiones. Este área de investigación es muy activa a consecuencia de la dualidad gauge/gravedad [102]. En este contexto, modos cuasi-normales son una herramienta apropiada para estudiar el comportamiento cercano al equilibrio de plasmas en teorías gauge. Además, modos cuasi-normales aparecen en algunos enfoques de la paradoja de la pérdida de información en agujeros negros.

- Agujeros negros en altas dimensiones en espacio-tiempo de anti-de-Sitter. Un proyecto en desarrollo es el estudio de agujeros negros en la teoría Einstein-Maxwell-Chern-Simons con constante cosmológica negativa. Sería interesante ver si la estructura de ramas tan compleja que obtenemos en el caso asintóticamente plano se conserva en el caso asintóticamente anti-de-Sitter. El estudio numérico se complementará con el estudio de la geometría cercana al horizonte.

- Estabilidad de vórtices de Yang-Mills-Higgs. Otro proyecto en curso es el estudio de la estabilidad de los vórtices obtenidos en [95]. En este caso una perturbación tiene dos posibles comportamientos. Puede oscilar entorno a la configuración vórtice. O puede explotar exponencialmente, lo que significa que la solución es inestable. La perturbación se considera en general no abeliana, y se efectúa tanto en vórtices no abelianos como en abelianos.

SUMMARY IN ENGLISH

Introduction

In this Thesis we have studied different configurations which are solutions of classical field theories. These objects are neutron stars, black holes, and vortices. The physical interpretation of these objects, and the field theories where they are found, is very different. Neutron stars are solutions of the Einstein equations, and correspond to astrophysical objects which allow us to study the properties of space-time and matter at extremely high densities. The higher dimensional black holes we have studied are very interesting solutions of state-of-the-art low energy effective field theories coming from string theory. Vortices of Yang-Mill-Higgs theories are useful in the phenomenological description of superconductivity.

We have divided these three studies (neutron stars, black holes, and vortices) in three sections. The link among these three studies is the methods we have used to generate the solutions, and the tools we have used to study their properties. Although, as we will see, each particular problem has its own peculiarities, the tools used are almost the same ones. In particular, since we have treated axially symmetric and stationary objects, or small perturbations of such objects, we will find that the mathematical problems are very similar in the three cases.

Our investigation has led to interesting, original results, which have been published in international front-line journals. Let us enumerate the main results of this Thesis and the corresponding papers where they have been published.

Neutron stars. In papers [1] and [2] (which are included in sections 2.3.2 and 2.3.3, respectively) we have studied axial and polar quasi-normal modes of neutron stars. To do so, we have considered several realistic matter compositions of the neutron

star. That is, realistic equations of state that include exotic matter. These equations of state have never been considered before in this context. We have studied several phenomenological relations concerning the spectrum of neutron stars, and we have obtained new ones which are highly independent of the model, and hence could be very useful for asteroseismology.

Regarding neutron stars, we have also studied the slow rotation limit in the presence of a surface energy density enveloping the star. We have applied this model to the study of pulsar glitches. This model allows us to interpret jumps in the rotation velocity of the pulsar as variations in the transition pressure of the core-crust interface. The results of this work can be found in the references [3] and [4], which are included in sections 2.4.2 and 2.4.3, respectively.

Black Holes. Higher-dimensional black holes have been obtained in two different theories. In Einstein-Maxwell-dilaton theory, we have studied odd-dimensional black holes, with spherical topology and equal-magnitude angular momenta. We have considered a general dilaton coupling, and hence we also include the case of pure Einstein-Maxwell theory. We have obtained that in the extremal case, Einstein-Maxwell theory features two branches of black holes, with very special relations between the entropy and the global charges (in one of them the entropy is independent of the electric charge). In Einstein-Maxwell-dilaton theory, only the branch of black holes with entropy independent of the electric charge is found. The numerical analysis is supplemented with the use of the near-horizon formalism. This work can be found in references [5] and [6], and are included in sections 3.5.1 and 3.5.2, respectively.

In Einstein-Maxwell-Chern-Simons theory we have studied five dimensional black holes, where we also assumed spherical topology and equal-magnitude angular momenta. We have considered a general Chern-Simons coupling constant. Surprisingly, we have obtained an infinite branch structure in the extremal case for certain values of this coupling constant. In this branch structure we find a sequence of radially excited extremal solutions. We also find infinite non-uniqueness of some solutions with respect to the global charges. The study of the near-horizon geometry has also been used to complement the numerical analysis. The results can be found in [7], which is included in section 3.6.1.

Vortices. We have studied non-Abelian vortices in an $SU(2)$ Chern-Simons-Higgs theory with a quartic Higgs potential. We have obtained a branch structure which is dependent on the topological index n, and non-uniqueness with respect the global charges for $n > 3$. This results can be found in paper [8], which is included in section 4.4.1.

We start this summary of the Thesis by commenting very briefly the numerical methods we have used. Then we will describe the results we have obtained for neutron stars, black holes, and vortices.

Numerical methods

Ordinary differential equations

In all the cases we have considered in this Thesis, we have been able to reduce the problem to a system of ordinary differential equations. The theories we have considered can be expressed in terms of a Lagrangian, which is a functional of the matter fields and metric of the space-time. Variations with respect to these fields yield the Euler-Lagrange equations, from where we can obtain the differential equations that we need to solve.

Essentially, when gravity is considered (neutron stars and black holes) we obtain the Einstein equations with some equations for the matter fields coupled, and in the case of vortices we just obtain the equations for the gauge fields and the Higgs field (since we will consider flat 2+1 space-time). All the theories we have considered yield second-order differential equations.

In this Thesis we have been interested in solutions to these equations, but we have also been interested in perturbations over some known solutions.

In the first case, we look for solutions with certain symmetry requirements, so that we are able to write an Ansatz which delimits the functional structure of the solutions in some appropriate coordinates. This has been the case of higher-dimensional black holes, where we have considered stationary and axisymmetric configurations with spherical topology and cohomogeneity-1. In the slow rotation approximation we are able to write explicitly the angular dependence, since the spherical configuration is deformed at each one of the perturbative orders with some finite amount of terms from the expansion in spherical harmonics. Vortices of Chern-Simons-Higgs theory also satisfy some symmetry conditions (rotational symmetry in the plane) which allow us to write explicitly the angular dependence of the functions. In every case we are able to find some coordinates where we are able to write explicitly the angular dependence of the functions, and where the functions are independent of the time coordinate (stationary configurations). Hence, the only unknown is in the dependence of the functions with the radial coordinate.

When we consider time-dependent perturbations in neutron stars, we can reduce the problem to a system of ordinary differential equations. The perturbations can

be expanded in spherical harmonics. We have limited to $l = 2$ perturbations. As a consequence, the angular dependence of the perturbation functions is known. The temporal dependence can be extracted by a Laplace transformation (since the eigenvalues of the quasi-normal modes are complex numbers). In this way, the propagation equation for the perturbation (1.1) can be rewritten as a Schrödinger-like equation (1.3), where the eigen-energy is an unknown complex number. The system of equations we need to solve is composed by ordinary differential equations, where the boundary conditions and the junction conditions will determine when the eigen-value corresponds to a quasi-normal mode solution of the system.

Boundary conditions.

The system of differential equations must be supplemented by a system of boundary conditions. These boundary conditions determine which kinds of solutions are going to be generated (star, black hole, vortex). The domain of integration of vortices and neutron stars is all the space-time, while for black holes it will be enough for us to integrate the configuration outside of the event horizon.

All the configurations will be defined in asymptotically flat space-time (neutron stars and black holes) or flat space-time (vortices). This imposes a certain type of decay to the functions, which will be studied in each case.

The solutions must be regular at the origin of coordinates (neutron stars and vortices), or satisfy the Killing horizon condition (black holes). In any case, the boundary conditions at this side of the domain of integration are obtained by a power series expansion. On this series the desired relations for the functions are imposed, together with the differential equations. This constrains the terms of the expansion and yields relations between the coefficients. The resulting series expansion can be imposed as a boundary condition if an appropriate parametrization of the functions is done.

In some cases, the number of conditions that the expansion imposes is bigger than the number of boundary conditions that can be imposed on the system of differential equations. An analysis must be performed in order to determine which set of boundary conditions is more appropriate (better precision, less integration time), while all the remaining extra conditions must be satisfied by the generated configuration.

Continuation method.

We generate a numerical solution using a previously known solution of the differential equations. This initial solution is slowly deformed towards the target solution. The initial solution must be close enough to the final solution in the space of solutions

of the theory. The initial solution is known as an analytic solution of the theory for some particular values of the charges, or as a numerical solution previously generated.

The initial solution satisfies the boundary conditions for some particular values of the parameters that describe the configuration (for example mass, electric charge and angular momentum). If we change by a small amount some of these parameters, in principle the algorithm will be able to converge to a new solution of the differential equations with these modified parameters. This method is known as continuation method. The parameters used to define the configuration can be some internal parameters, like derivatives defined at some points, or parameters of the series expansion. The algorithm will only converge if these parameters uniquely define a configuration and if the final solution is close enough to the initial solution.

Colsys.

In order to solve numerically the system of differential equations, we will use the Colsys package. It will allow us to solve numerically boundary value problems. Colsys can handle systems of ordinary differential equations with different orders, even though in our case they will always be first-order and second-order differential equations.

The boundary conditions are separated, meaning that they only depend on the value of the functions and derivatives at a single point of the domain of integration, although they can be non-linear in the functions and derivatives.

The interesting feature of Colsys is that it is able to estimate the error of the numerical solution at each iteration step. Colsys performs the iteration in the following form.

Using the collocation method, Colsys divides the domain of integration into a mesh of points, including the points where the boundary conditions are defined. Each interval of the mesh is subdivided using a Gauss-Legendre distribution.

The solution is approximated at each one of the points of the complete mesh by a polynomial series. This series is given in terms of some coefficients which are in principle undetermined. These coefficients must be determined by imposing the boundary conditions and by requiring that the differential equations are fulfilled at the rest of the mesh points.

Colsys uses a linearized system of equations. This means that, from a solution of a previous iteration, Colsys requires that the current iteration satisfies at first order the equations and the boundary conditions (that is, in terms of the Jacobians of the differential equations and the boundary conditions). Colsys uses a damped Newton method with free parameter.

Colsys is able to estimate the error of the solution, and selects a new mesh for the next iteration, with more or less points introduced at regions more or less problematic. Essentially Colsys obtains two solutions at each iteration, one of them with half the points. The local and global error can be estimated by evaluating the two solutions in the differential equations. The user introduces a tolerance (a desired minimum error), and Colsys proceeds to iterate, modifying the mesh, until it obtains an error smaller than the tolerance required. Different tolerances can be introduced for each function and derivative. If the tolerance is not satisfied, Colsys redistributes the mesh making use of different procedures, trying to equidistribute the local error at each step of the iteration. Eventually, the estimated global error satisfies the tolerance, and Colsys returns the corresponding solution.

Neutron stars

In this section we will briefly discuss our studies on neutron stars. We have studied quasi-normal modes and the slow rotation approximation.

Quasi-normal modes

The first detection of gravitational waves is expected to happen in the next five years by large-scale detectors like LIGO, GEO, TAMA and VIRGO. Gravitational waves are oscillations of space-time, typically produced by matter oscillations, which propagates throughout empty space-time. This is a result of space-time in General Relativity having its own dynamics. The possible sources of gravitational waves are interacting black holes, coalescing compact binary systems, stellar collapses and pulsars.

Hence neutron stars are good candidates as sources of detectable gravitational waves. Neutron stars are found in the interior of pulsars and are the results of collapsing stars. After the supernova explosion, the protoneutron star presents strong oscillations, that are damped because of the emission of gravitational waves. In the same way, the coalescence of white dwarfs can give as a result an oscillating neutron star, with gravitational wave emission.

The matter oscillations in the neutron star are coupled to space-time, and cause the space-time to oscillate. The oscillation energy of the matter escapes from the neutron star in the form of a gravitational waves: space-time oscillations which propagate towards infinity, which are maintained by the dynamics of space-time. Hence, the oscillations of a neutron star do not only present a frequency, they also present a

decay time (similar to the viscosity in the Newtonian regime).

The spectrum of resonances of these gravitational waves can transport information on the structure and composition of neutron stars. This is the reason we are interested in performing the study of quasi-normal modes for realistic neutron stars. We will use state-of-the-art equations of state, including exotic matter. The comparison between measurements and theoretical studies could give some insight into the state of matter at such high densities (above nuclear).

The appropriate mathematical tool to study these damped oscillations is the quasi-normal mode expansion. We will consider perturbations over a spherical and static configuration. We will assume that matter inside the star can be described with a barotropic equation of state, which is a good approximation for neutron stars.

By using perturbation theory up to first order, and expanding the perturbations in spherical harmonics, a system of differential equations for the metric and matter perturbations can be found. This set of perturbations can be decoupled into two components. One of them (axial modes) does not couple to matter perturbations. The other one (polar modes) couples to density and pressure oscillations inside the star.

It can be demonstrated that in the exterior of the star, both axial and polar perturbations satisfy the equation (2.10). This equation is known as the Zerilli equation in the axial case, and is also satisfied inside the star, since the perturbations do not couple to pressure or density oscillations. It is known as the Regge-Wheeler equation in the polar case, where it is only valid outside the star. The perturbations inside the star are determined by a set of second-order and first-order differential equation.

We can study the resonant modes of these differential equations if we study the Laplace transform of the perturbations (2.14). The system of partial differential equations becomes a system of ordinary differential equations, with a parameter to determine ω. This parameter is complex, being the real part the oscillation frequency, and the imaginary part the decay time.

Since we are interested in gravitational waves produced inside the star and traveling towards infinity (outgoing waves), we must impose this asymptotic behavior to the perturbations at infinity (2.17). Note that this behavior causes the perturbation to diverge at infinity. The incoming wave solution nonetheless tends to zero at infinity. As a result, it is easy to generate a solution with some incoming component, which are not useful in the quasi-normal mode analysis.

There are several methods to obtain quasi-normal modes which satisfy, at least approximately, the outgoing wave condition. The WKB method [37, 38] and the

continuous fraction method [39, 40, 41, 42, 43] have been extensively used and with quite good results, specially for slowly damped modes, where it is easier to deal with the incoming wave component. Other methods, more sophisticated, study the phase function of the perturbation [44] and their boundary conditions. An analytic continuation of the perturbation into the complex plane can be performed [45, 38, 46, 47], so that the ingoing wave behavior can be much better controlled and the outgoing wave behavior can even be imposed as a boundary condition.

The procedure we have developed make use of previously used methods together with new techniques not used before in this context. We study the phase function of the perturbation outside the star. In addition we perform an analytic continuation of the function into the complex plane, so that the radius is a complex variable. We parametrize the domain of integration with a line in this complex plane. The line has an angle α with the real line. This angle is free, and can be adjusted so that the outgoing wave behavior can be imposed as a boundary condition to the phase function. This method is known as Exterior Complex Scaling. Hence, the solution to the equations with this boundary condition cannot have any incoming wave contamination, and if we perform the matching with an interior solution, we will have determined a quasi-normal mode.

We generate a perturbation inside the star. We study the matching conditions, for both the real and imaginary parts. The interior perturbation must match with the exterior phase. The matching conditions are standard: continuity of the fundamental forms across the border of the star. We allow for jumps in density and pressure (general equations of state). Finally, the matching conditions can be described as a determinant (Wroskian) which must be null when the perturbation is a quasi-normal mode (i.e. when the real and imaginary parts ω area the frequency and damping time of the perturbation).

As we said, this has been performed for axial and polar modes, and the results have been published in two papers that can be found in sections 2.3.2 and 2.3.3.

Concerning the first paper, Physical Review D **87** (2013) 104042 [1], where axial modes are studied:

- Since we are interested in axial quasi-normal modes of neutron stars including realistic equations of state, we have to rely on numerical methods in order to integrate the differential equations. We have to integrate the Tolman-Openheimer-Volkov (TOV) equations for the zeroth-order, and the Zerilli equation for the perturbations. We integrate both systems of equations at the same time. This allows us to adapt the static solution to the precision we need for the perturba-

tion.

- The perturbation function is a complex function which diverges towards infinity (outgoing wave). We use the exterior complex scaling method. This method allows us to study an analytical extension of the perturbation function, where well-defined boundary conditions for the phase function of the perturbation, more appropriate for the numerical integration, can be obtained.

- We have studied the fundamental wI mode (space-time mode), and its first excitation. We have also studied the fundamental wII mode (interface mode). No trapped modes are found for these equations of state.

- We use 18 realistic equations of state and two different methods of interpolation in order to implement them. One of them is a piecewise polytropic interpolation (different regions of the equation of state are approximated as specific polytropes). This interpolation was developed in [33]. The other method consist of a piecewise monotone cubic Hermite interpolation satisfying the local thermodynamic condition. This interpolation is performed on a numerical table of density-pressure values. The equations of state considered satisfy the 2 $M_\odot$ condition (except in two cases included for comparison), and include various compositions: plain nuclear matter, mixed hyperon-nuclear matter, hybrid quark-nuclear matter, and pure quark matter. Most of the equations of state are state-of-the-art results of high energy nuclear theory.

- We have studied phenomenological scaled relations, following [49, 50, 51, 41]. If these relations are independent of the equation of state, then they can be very useful in order to determine, from a quasi-normal mode measurement, other parameters of the star, like the radius, the mass or the compacity. For axial modes we obtain that they are quite independent of the equation of state, except in the case of pure quark matter stars, which present different scaled phenomenological relations (the same functional dependence but with different parameters).

- We have also studied new phenomenological relations. In this case the idea is to relate the frequency with the damping time of a quasi-normal mode. We scale both quantities to the central pressure. The relations obtained are very independent of the equation of state. We propose that these phenomenological relations can be used to estimate the central pressure of the neutron star.

In the paper Physical Review D **89** (2014) 044006 [2], we have performed the analysis of the polar quasi-normal modes. It is included in Section 2.3.3.

- Essentially the numerical procedure is equivalent to the one performed on axial modes. We integrate the TOV system of equations together with the polar perturbation equations. The difference is that the system of equations necessary to describe the perturbation is more complicated in the interior region, because the system of equations cannot be redefined into a single ordinary differential equation like it can be done in the exterior region (Regge-Wheeler equation).

- Nevertheless, in the exterior region, since the ordinary differential equation is basically the same one as in the axial case, we apply the exterior complex scaling method to the Regge-Wheeler function, so that we can impose boundary conditions to the phase function and obtain pure outgoing wave functions.

- In this paper we use 15 realistic equations of state, which are the same equations of state of 2.3.2 that satisfy the 2 $M_{\odot}$ condition. The same procedures of equation of state interpolation are used.

- We study the fundamental wI mode of the polar spectrum, the fundamental pressure mode, and the fundamental mode. Again, we follow [49, 50, 51, 41] and study scaled phenomenological relation. In this case the scaled relations are not as useful as in the axial component since the spectrum is more dependent on the physics of the equation of state (except of course, for the w modes). Again the pure quark stars are the most different ones.

- We propose new phenomenological relations that relate the frequency to the damping time of a quasi-normal mode. We scale both quantities to the central pressure. We obtain relations for the w modes and the fundamental modes. The relations obtained are very independent of the equation of state. We propose that this phenomenological relations can be used to estimate the central pressure of the neutron star, and the radius (provided that the mass is known, and the detection is good enough to have the real and the imaginary part of both the w mode and the fundamental mode).

We think that the results of these works could be very useful in future neutron star asteroseismology. Because the analysis is realized on a wide range of realistic state-of-the-art equations of state, the information contained in these papers could be used in future gravitational wave measurements in order to constrain the equation of state of neutron stars.

Slow rotation

Since neutron stars are found in nature as pulsars, it is important to consider the case of neutron stars in rotation. We have to use General Relativity in order to describe them. The effect of rotation in space-time is the dragging of the inertial systems. A free falling observer will acquires a rotational velocity around the star as it falls towards the star.

We will assume slow and rigid rotation of the neutron star. The slow rotation approximation can be done by expanding the metric and fluid functions in terms of the angular velocity Ω.

In the papers AIP Conference Proceedings **1458** (2012) 419-422 [4] and Journal of Physics: Conference Series **314** (2011) 012088 [3], which are included in Sections 2.4.2 and 2.4.3, we study the slow rotation approximation and apply it to the study of glitches. Glitches are small variations of the angular velocity of pulsars, which probably have their origin in the outer layers of the star. The matching conditions are essential in our model:

- The junction conditions are formulated intrinsically, using the fundamental forms. This provides the junction conditions that the metric and matter functions must satisfy between the interior and the exterior solutions. We will also consider the introduction of a surface energy density. The resulting model can be interpreted as an approximation of the outer layers of the star, assuming that the mass of the outer layers and its size are small.

- The essential parameters of this model of neutron star, enveloped by a surface energy density, are the core-crust transition pressure, the central pressure and the angular velocity of the star.

- Variations in the transition pressure are related to jumps in the angular velocity of the configuration. Hence we can apply this simple model to the description of giant glitches of pulsars (in particular to the Vela pulsar glitches). Since glitches are probably related to thermal variations in the outer layers of the neutron stars, we can relate the jump in the angular velocity to a variation of the core-crust transition pressure, assuming that the inner core is not changed. This change in the transition pressure would probably be related to a phase transition. The variations of the transition pressure are compatible with the expected temperature variations of the inner crust during the glitch.

Black holes

Objectives

In Einstein-Maxwell-dilaton theory, we have considered odd-dimensional black holes. We have considered black holes with spherical topology. We also assume that all the angular momenta are of equal magnitude. In particular, we will consider extremal black holes. We will see that in the case without dilaton, we find two branches of solutions. In one of them the entropy is independent of the electric charge of the black hole. When a dilaton field is included, with independence of the coupling constant, this behavior is retained. The study has given as results the papers Physics Letters B **727** (2013) 340-344 [5] (included in section 3.5.1) and Physical Review D **89** (2014) 024038 [6] (included in section 3.5.2)

We have also considered black holes in Einstein-Maxwell-Chern-Simons, but in this case we restrict ourselves to five-dimensional black holes. We have found very interesting results: non-static solutions with non-zero angular momentum and non-uniqueness with respect the global charges. The results have been published in Physical Review Letters **112** (2014) 011101 [7] (included in section 3.6.1).

Motivation

One of the most striking predictions in General Relativity are black holes, special regions of space where not even light can classically scape from. The space-time metric describing the static uncharged black hole in 3+1 dimensions was discovered by Schwarzschild in 1915, and a couple of years later it was generalized to include a Maxwell electric field (Reissner-Nordström solution). In the beginnings these solutions of Einstein equations were considered as singular solutions with only academic interest. It was not until the sixties that the nature of the black hole horizon was fully understood (coordinate singularity). In 1963 Kerr makes the very important discovery of the rotating uncharged black hole, and a couple of years later the Kerr solution is generalized to include a Maxwell electromagnetic field (Kerr-Newmann solution) [54].

There is strong astrophysical evidence for the presence of massive black holes at the core of spiral galaxies. Other astrophysical objects within our galaxy, with strong X-ray emission and a few times the mass of the Sun, are very strong candidates to astrophysical black holes, resulting probably from supernova explosions of very massive stars [17].

Asymptotically flat stationary black holes of Einstein-Maxwell theory in 4 dimensions have very special properties. They must be spherical, with no other topologies

allowed for stable solutions, if the dominant energy condition is satisfied. Then a black hole solution is uniquely characterized by a set of global charges, i.e., the mass M, the angular momentum J, and the electric charge Q. Given these three parameters, there is only one black hole solution of Einstein-Maxwell equations in 4 dimensions [55].

In more than 4 dimensions, or when more general fields are coupled to gravity (Yang-Mills fields, dilaton fields), black holes do not posses these special features [56]. In higher dimensions there are two main differences: the black hole horizon can have topologies different from spherical, or even be an extended object; and there is more than one independent plane of rotation.

Concerning the first feature, it is easy to see that given a black hole in D dimensions with a certain horizon Σ_H, a perfectly valid black hole solution in $D+1$ dimensions can be constructed just by adding an additional space dimension [57]. The new black hole has horizon $\Sigma_H \times \Re$. Note that now the black hole horizon is an extended object, with a topology different from spherical. Black strings, and in general, extended black p-branes, can be found for arbitrary higher than 4 dimensions.

Nevertheless, these black holes are not asymptotically flat. But we can think about taking the $D+1$ dimensions black string of horizon $\Sigma_H \times \Re$ and bend it so that the horizon becomes $\Sigma_H \times S^1$ [57]. The resulting black ring is unstable and tends to contract. But appropriately choosing the angular momentum of each rotation plane, we can re-equilibrate the black ring, obtaining a stable solution. Stable black holes solutions with ring-like topologies can be found for arbitrary higher than 4 dimensions [56].

Even more, black p-branes with compact horizon can in principle be constructed in a similar way. The topology of the resulting p-branes can become very complicated [56].

Black holes in higher dimensions have more than one independent plane of rotation. In general, for $D-1$ space-like dimensions, the rotation group $SO(D-1)$ has $N = [(D-1)/2]$ independent planes of rotation, where N is the integer part of $(D-1)/2$. An angular momentum can be associated with each plane of rotation.

There are a number of reasons why gravity models with more than 3 space dimensions, and specially black hole solutions of these theories, are interesting. Let us briefly enumerate some of them.

After general theory of Relativity was formulated by Einstein, Kaluza in 1921 [58] and Klein in 1926 [59] noticed that if one extra space dimension was added to Einstein's gravity, in a four dimensional slice of this extended theory, gravity on this slice was naturally coupled to an extra electro-magnetic field [56]. Hence one could interpret

Einstein-Maxwell theory in four dimensions as Einstein theory in five dimensions. This was the first hint towards the idea that natural interactions (in this case electromagnetism and gravity) could be unified to one unique force (in this case Einstein gravity) acting in a higher dimensional space-time.

More lately, string theory, a very successful approach to quantum gravity, predicts the existence of more than 4 space-time dimensions (M-theory has 11 dimensions). The extra space dimensions are compact and much smaller in scale than our usual 3 space dimensions. These extra space dimensions are curled up into small volumes (compactification).

Other theories, like the brane-world idea, suggest that our 3 dimensional space is just an slice of a higher dimensional space-time. In these theories, space could have extended extra dimensions, as well as compact extra dimensions.

Some of these theories present as a possible scenario the production of higher dimensional black holes in the LHC and future TeV colliders, so falsifiability of some of these theories could be made.

Another interesting application of higher-dimensional black holes can be found, in the context of string theory, in the gauge-gravity duality [56]. This conjecture proposed by Maldacena in 1997 [60] as a correspondence between Anti-de Sitter space-time and two conformal field theories, tells us that quantum field theories could be related to higher dimensional theories of gravity. Thermal equilibrium in 3+1 dimensional non-gravitational systems could be dual to higher dimensional black holes. Strongly interacting systems could be studied using their duals as black holes solutions.

Since the properties of higher dimensional black holes are very different to those of $3+1$ dimensional black holes, their study has a lot of interest. Insight on why the topology, uniqueness, and stability of 4 dimensional black holes are so special can be gained by the dependence of these properties with the space-time dimension [57].

The first generalization of a black hole solution to higher dimensions, the static black hole in Einstein gravity (generalization of the Schwarzschild metric), was pioneered by Tangherlini [53], who also generalized the Reissner-Nordström solution. The corresponding generalization of the Kerr black hole to higher dimensions was found by Myers and Perry [52]. Other stationary non-vacuum solutions have been obtained in effective theories whose low-energy actions are related to string theory [61, 62, 63]. See [57] for a complete review on known higher dimensional black hole solutions.

Near-horizon geometry

In the near-horizon formalism, it is assumed that the space-time outside the event horizon can be divided in two regions [77]. One of them is closed to the event horizon

(near-horizon geometry), and the other region correspond to the space-time which extends from the near-horizon geometry towards, in our case, the asymptotically flat infinity.

The near-horizon geometry can be obtained as a limit of a coordinate transformation, which allows us to remove the bulk geometry. In general, this coordinate transformation selects a reference frame in corrotation with the event horizon, and centers the radial coordinate to the horizon. The transformation depends on a scale parameter Λ, and when it is taken to the limit $\Lambda \to 0$, remove the space-time bulk keeping the near-horizon region.

Let us comment some properties of the near horizon geometry [78]. Since we are considering horizons with spherical topology, the space-time near the horizon can be described as the product of two independent spaces. One of them can be described with angular coordinates (θ_i, ϕ_j) (which depends on the dimension considered) and describes the sphere (squashed if rotating) in $D-2$ dimensions: S^{D-2}. The other factor of space-time can be mapped by a temporal and a radial coordinate (t, r), and describes the anti-de-Sitter space-time in two dimensions: AdS_2 (recall that this is Einstein gravity in two dimensions with a negative cosmological constant). It is worth mentioning that this factorized space-time is an exact solution of the Einstein equations. But the factorization is of course not valid in the bulk of the black hole, which is asymptotically flat. In other words, this factorization never describes global solutions, which are the ones we are ultimately interested in.

The space-time near the event horizon of a black hole has a very high amount of symmetry. The near-horizon geometry has $SO(D-1)$ isometry acting on the S^{D-2} sphere in the case of a static black hole, and $U(1)^N$ isometry group acting on a squashed sphere in the case of a rotating black hole, with independent rotation in each one of its N axial planes [79]. This symmetry is inherited from the global solution, which has spherical horizon topology. In the near-horizon limit, the coordinates are adapted to the event horizon squashed sphere geometry. If the angular momenta have equal magnitude, the symmetry increases into a cohomogeneity-1 group, and we have a factorized squashed sphere with $U(N)$ isometry. The other space-time factor, the anti-de-Sitter component, has a $SO(2,1)$ isometry generated by three independent Killing vectors. Note that the gauge and scalar fields are also invariant under the isometries acting on the $AdS_2 \times S^{D-2}$ metric.

All the known examples of extremal black holes, with spherical topology and non-singular horizons, have near-horizon geometry factorized as $AdS_2 \times S^{D-2}$ and associated $SO(2,1) \times SO(D-1)$ isometry for the spherically symmetric case, and

$SO(2,1) \times U(1)^N$ if rotation is considered [78]. AdS_2 factorization is also found in the near-horizon geometry of black holes with different topologies, like black rings. A classification of near-horizon geometries can be found in [77].

Although all the information from the bulk space-time, and in particular its asymptotical structure, is lost when considering the near-horizon limit, there is still a lot of information from the global solution encoded in the near-horizon geometry [80].

In particular, since the near-horizon geometry is obtained in a comoving frame with the horizon, and the connection with the asymptotically flat coordinate frame is lost, the horizon angular velocity and the mass cannot be calculated with the near-horizon geometry alone. It is possible to calculate conserved charges associated to conserved fluxed of the gauge fields and to the rotational symmetry (electric charge and angular momentum). The horizon charges of the black hole can be safely calculated with the near-horizon geometry. In particular, the horizon angular momentum and the area of the event horizon can be calculated.

Black holes in Einstein-Maxwell-dilaton

Here we will present the results on Einstein-Maxwell-dilaton black holes. This is the topic of the papers Physics Letters B **727** (2013) 340-344 [5] (included in the following section 3.5.1) and Physical Review D **89** (2014) 024038 [6] (included in the following section 3.5.2).

We study odd-dimensional black holes, with event horizon of spherical topology, and consider equal-magnitude angular momenta. This increases the symmetry to cohomogeneity-1, and allows us to write explicitly the angular dependence of the functions. These black holes are generalizations of the Reissner-Nordström and Myers-Perry solutions, meaning that in principle they can have arbitrary values of the electric charge and angular momentum. The value of the dilaton coupling parameter is also free.

For the extremal case, we can use the near-horizon formalism.

- In the Einstein-Maxwell case, that is, when there is no dilaton field, two distinct branches appear when extremal black holes are considered. One of them emerges from the Myers-Perry solution (MP branch). This branch is composed of charged generalizations of the Myers-Perry solution. The second branch is composed by rotating generalizations of the Reissner-Nordström solution (RN branch). Both branches meet at a certain non-singular configuration.

- In the MP branch, the area is proportional to the angular momentum. The charge does not enter the relation. Hence the entropy is independent of the charge. On the other hand, the horizon angular momentum is dependent on both the angular momentum and the charge.

- In the RN branch, the area depends on the angular momentum and the charge. But the horizon angular velocity is proportional to the angular momentum. Hence, there is a switch in the behavior of the area with the horizon angular momentum between the MP branch and the RN branch.

- These results have been obtained both using numerical methods (for the full solution), and using the near-horizon formalism (where only the near-horizon geometry can be studied). Nevertheless, in the near-horizon formalism, there are solutions to the equations that are not found globally. Hence we conclude that not all the near-horizon solutions correspond to global solutions. The branch of non-physical near-horizon solutions is connected to the branch of physical ones.

- When a dilaton field is included, for arbitrary values of the dilaton coupling, the two-branch structure is lost. There is only one branch of solutions that corresponds to the MP branch. These solutions have entropy proportional to the angular momentum, with independence of the charge.

- The boundary of the domain of existence of these black holes is composed by extremal black holes. We plot this boundary by scaling the different parameters of the black holes to the mass. There is a certain duality between the scaled angular velocity for extremal black holes, and the surface gravity for the static black holes, when these quantities are plotted as a function of the scaled charge of the black holes. A similar relation is found between the scaled area of static configurations and the scaled angular momentum of extremal black holes. The approximate similarity of these relations becomes an equality in the case of Kaluza-Klein black holes (when the value of the dilaton coupling becomes $h_{KK} = \sqrt{\frac{D-1}{2(D-2)}}$). Note that these Kaluza-Klein black holes are known analytically, and we have used them to test our numerical results.

Black holes in Einstein-Maxwell-Chern-Simons

Let us present now our results on Einstein-Maxwell-Chern-Simons black holes. This is the topic of the paper Physical Review Letters **112** (2014) 011101 [7], presented

in the following section 3.6.1. We study 5 dimensional black holes, again with event horizon of spherical topology, and consider equal-magnitude angular momenta. Like in the EMd case, these black holes are generalizations of the Reissner-Nordström and Myers-Perry solutions. In this case the value of the Chern-Simons coupling parameter is also free. We re-obtain the two-branch structure of the extremal Einstein-Maxwell black holes.

We are again interested in extremal black holes, which can be used to obtain the boundary of the domain of existence. But in this case the situation is much more complicated.

- We again perform the analysis by combining numerical methods with the near-horizon formalism. But in this case the situation is more complicated because of the complex branch structure of the solutions, which can only be seen in the mass and the angular velocity. Hence the near-horizon geometry alone cannot be used to completely characterize the space of solutions of these extremal black holes.

- In particular, we observe that for Chern-Simons couplings above 2 times the supergravity value, non-uniqueness is lost in several ways. First, it can be seen that multiple global solutions correspond to one near-horizon solution. Consider for example extremal solutions with equal angular momentum and electric charge. There is a sequence of these solutions with the same horizon geometry, but which can be differentiated by the internal parameters of their functions. This means that these global solutions have the same values of their horizon area and horizon angular momentum, but can be distinguished by their mass or angular velocity.

  On the other hand, there are near-horizon solutions which are not obtained globally. This is similar to what we obtained in EMd theory. Again these non-physical near-horizon solutions are connected to the physical ones.

  We conclude that the near-horizon formalism is very limited at this range of the parameters of Einstein-Maxwell-Chern-Simons theory.

- Uniqueness is also lost in the sense that global charges no longer determine completely a black hole: there are black holes of equal mass, electric charge, and angular momentum that have different near-horizon geometry. These black holes can be distinguised by their values of the area or horizon angular momentum. These solutions are associated with the branching point and are found in groups

of two solutions, meaning there are two solutions with the same global charges, but two different near-horizon geometries.

- The branch structure obtained in the global parameters gives raise to very exceptional configurations. There is an infinite sequence of non-static configurations with null angular momentum. These configurations can be characterized by the node number of the angular component of the gauge field. Their mass increases with the node number, and asymptotically reach the mass of the static configuration.

- The branch structure also includes extremal solutions with null angular velocity, but non-null angular momentum. Even more, the static configuration is isolated from these non-static solutions with vanishing angular velocity or momentum. The static solution is only reached as a limit as the node number of the non-static configurations with null angular momentum is increased to infinity.

- Finally, a very interesting feature is that we can have non-uniqueness between non-extremal and extremal solutions. There are extremal solutions whose global charges are equal to those of a non-extremal configuration.

Vortices

We will present our results on Chern-Simons-Higgs vortices in 2+1 dimensions. The results of this study can be found in the published paper Physical Review D **88** (2013) 025026 [8], which is appended in Section 4.4.1.

We have considered the Abelian and non-Abelian vortices of a scalar Higgs field coupled to an $SU(2)$ gauge field. The Higgs field is in the adjoint representation and the coupling to the gauge field is made via a Chern-Simons term.

We have studied vortices in an $SU(2)$ Chern-Simons-Higgs theory. The $SU(2)$ gauge field is coupled to the scalar Higgs field (which is in the adjoint representation) via a Chern-Simons term in the action. A fourth-order Higgs self-interaction potential has been considered, so self-duality of the solutions is lost. The gauge field has no dynamics, and can be determined by a set of constraints that bound the gauge field to the Higgs field via the Chern-Simons term.

- To build non-Abelian configurations, we start from the corresponding Abelian solutions. By changing the value of some internal parameters of the solution we

can generate non-Abelian solutions (for example, p_1 and p_2, which are related to the amplitude of two of the internal isotriplets, and are null in the Abelian case). Nevertheless, it can become null again for certain non-Abelian configurations. The non-Abelian, $p_2 = 0$ configurations have specially interesting properties.

- For a given number of vortices, the number of non-Abelian solutions with $p_2 = 0$ depends on the Higgs self-coupling parameter. As the Higgs self-coupling is increased, the number of these non-Abelian branches with $p_2 = 0$ increases.

- The energy of the Abelian branch is always greater or equal than that of the non-Abelian solutions. The same holds for the angular momentum. The energy and the angular momentum of a non-Abelian solution increase with the non-Abelian branch number.

- For large values of the Higgs self-coupling parameter, the energy gap between the non-Abelian $p_2 = 0$ branches becomes constant. The angular momentum tends to zero. Interestingly, the non-Abelian $p_2 = 0$ branch number also determines the number of pieces of the step-like structure of the gauge potential functions.

- On the other hand, for large values of the Higgs self-coupling parameter, the relation between the energy and the angular momentum of the non-Abelian solutions (general value of p_2) becomes a Regge-like quadratic relation. All these solutions tend to behave like step-like functions in the limit.

- For topological number equal to 3, there is non-uniqueness of the solutions with respect the global parameters. We have found two distinct solutions with the same angular momentum and energy, but different values of other invariant quantities, like the Higgs amplitude. Surprisingly, the value of the Higgs self-interaction parameter is relatively low, and the non-uniqueness is related to a complicated relation between the internal parameters and the total energy and angular momentum (interestingly, the p_1 parameter is null in both solutions, while the p_2 parameter is different).

Conclusions

In this Thesis we have considered different solutions of classical field theories: neutron stars, higher dimensional black holes, and vortices.

All these objects present a high degree of symmetry. Hence, all the problems can be reduced to a system of ordinary differential equations, where a certain set of boundary conditions, specific of each object, must be imposed. These boundary conditions are obtained by several procedures, like regularity conditions, junction conditions, and asymptotic behavior.

In general, we do not know an analytic solution, except for particular values of the parameters of the theory. In consequence, we have to rely on numerical methods to generate the configurations. We have used the Colsys package. Colsys allows us to solve ordinary differential equations, where the boundary conditions can be defined at different points of the domain of integration. We use the continuation method in order to explore faster the space of solutions of the theory, using as a starting point a known solution (analytical or numerically approximated).

With respect neutron stars, we have studied quasi-normal modes and slow rotation. The study of quasi-normal modes or realistic neutron stars includes state-of-the-art equations of state which satisfy the 2 $M_{\odot}$ condition. Several matter compositions have been treated (nuclear, hyperons, quarks). Interesting phenomenological relations, useful in the context of asteroseismology, have been obtained. The slow rotation, together with a model of surface crust, allowed us to study in a simple way the changes in the transition pressure associated to glitches of the Vela pulsar. We are able to estimate temperature changes in the exterior layers of the star.

Another topic in this Thesis has been higher dimensional black holes. With respect to EMd, we have considered black holes with event horizons of spherical topology, and the cohomogeneity-1 case, when all the angular momenta are of equal magnitude. We have used the near-horizon formalism to complement the numerical analysis. In the extremal case, when a dilaton field is present, the entropy is independent of the electric charge, and proportional to the angular momentum. In pure EM case, there are two branches of extremal black holes, one of them similar to the EMd branch. Not every near-horizon solution corresponds to a global solution.

With respect to EMCS theory, the situation is more complicated. In the extremal case, an infinite branch structure appears when the value of the Chern-Simons coupling parameter is greater than twice the supergravity value. This branch structure is rich in properties: infinite sequence of non-static $J = 0$ solutions, radially excited which are distinguised by the node number of the gauge field function; non-static configurations with null angular velocity; non-uniqueness of extremal solutions; non-uniqueness of the near-horizon geometry; near-horizon solutions which do not correspond to global solutions; and non-uniqueness between non-extremal and extremal solutions.

Finally, we have studied vortices of Chern-Simons-Higgs theories. These solutions are of interest in effective theories of superconductivity. We have obtained Abelian and non-Abelian vortices of a Higgs scalar field coupled to an $SU(2)$ gauge field, where the Higgs is in the adjoint representation, and the self-coupling potential or the Higgs field is of fourth order. The lack of self-duality gives rise to interesting properties. The behavior of the non-Abelian solutions is studied in detail, together with the large Higgs coupling parameter limit. For topological index greater than 3, there is non-uniqueness.

The various topics treated in this Thesis have opened several lines of future research. It is our purpose to continue with the following lines of investigation:

- The adaptation of the techniques used in this Thesis in the study of quasi-normal modes of higher dimensional black holes. This is a very active area of research since the gauge/gravity duality was proposed [102]. Quasi-normal modes are a standard tool used to study, in the context of the dual gravity, the near-equilibrium behavior of gauge theory plasmas. Quasi-normal modes also appear in some approaches to the information loss paradox.

- Higher dimensional black holes in anti-de-Sitter space-time. An ongoing project is the study of black holes in Einstein-Maxwell-Chern-Simons theory with a negative cosmological constant (hence asymptotically anti-de-Sitter). It would be very interesting to see if the complex branch structure obtained in the asymptotically flat case is preserved, and if radially excited extremal black holes do also inhabit this theory. The numerical analysis will be supplemented with the application of the near-horizon formalism.

- Stability of Yang-Mills-Higgs vortices. Another ongoing project is the study of the stability of the vortices obtained in [95]. In this case the perturbation can have two possible behaviors. It can oscillate around the vortex configuration, or it can explode exponentially, meaning that the solution is unstable. The perturbations are studied for both Abelian and non-Abelian vortices, considering non-Abelian perturbations.

BIBLIOGRAPHY

[1] J. L. Blázquez-Salcedo, L. M. González-Romero, and F. Navarro-Lérida, "Phenomenological relations for axial quasinormal modes of neutron stars with realistic equations of state," Phys. Rev. D **87** (2013) 104042, arXiv:1207.4651 [gr-qc].

[2] J. L. Blázquez-Salcedo, L. M. González-Romero, and F. Navarro-Lérida, "Polar quasi-normal modes of neutron stars with equations of state satisfying the $2M_{\odot}$ constraint," Phys. Rev. D **89** (2014) 044006, arXiv:1307.1063 [gr-qc].

[3] L. M. González-Romero and J. L. Blázquez-Salcedo, "New model of relativistic slowly rotating neutron stars with surface layer crust: application to giant glitches of vela pulsar," *Journal of Physics: Conference Series* **314** (2011) 012088, arXiv:1101.3179 [gr-qc].

[4] L. M. González-Romero and J. L. Blázquez-Salcedo, "Core-crust transition pressure for relativistic slowly rotating neutron stars," *AIP Conference Proceedings* **1458** (2012) 419–422, arXiv:1307.1566 [gr-qc].

[5] J. L. Blázquez-Salcedo, J. Kunz, and F. Navarro-Lérida, "Angular momentum – area – proportionality of extremal charged black holes in odd dimensions," *Physics Letters B* **727** (2013) 340 – 344, arXiv:1309.2088 [gr-qc].

[6] J. L. Blázquez-Salcedo, J. Kunz, and F. Navarro-Lérida, "Properties of rotating einstein-maxwell-dilaton black holes in odd dimensions," *Phys. Rev. D* **89** (2014) 024038, arXiv:1311.0062 [gr-qc].

[7] J. L. Blázquez-Salcedo, J. Kunz, F. Navarro-Lérida, and E. Radu, "Sequences

of extremal radially excited rotating black holes," *Phys. Rev. Lett.* **112** (2014) 011101, arXiv:1308.0548 [gr-qc].

[8] J. L. Blázquez-Salcedo, L. M. González-Romero, F. Navarro-Lérida, and D. H. Tchrakian, "Non-abelian chern-simons-higgs vortices with a quartic potential," *Phys. Rev. D* **88** (2013) 025026, arXiv:1306.5146 [gr-qc].

[9] J. B. Hartle, "Slowly Rotating Relativistic Stars. I. Equations of Structure," ApJ **150** (1967) 1005.

[10] U. Ascher, J. Christiansen, and R. D. Russell, "Collocation software for boundary-value odes," *ACM Trans. Math. Softw.* **7** no. 2, (1981) 209–222.

[11] U. M. Ascher and L. R. Petzold, *Computer Methods for Ordinary Differential Equations and Differential-Algebraic Equations*. Society for Industrial and Applied Mathematics, Philadelphia, PA, USA, 1st ed., 1998.

[12] J. Cash and F. Mazzia, "Efficient global methods for the numerical solution of nonlinear systems of two point boundary value problems," in *Recent Advances in Computational and Applied Mathematics*, T. E. Simos, ed., pp. 23–39. Springer Netherlands, 2011.

[13] U. M. Ascher, J. Christiansen, and R. D. Russell, "Colsys - - a collocation code for boundary - value problems," in *Codes for Boundary-Value Problems in Ordinary Differential Equations*, B. Childs, M. R. Scott, J. W. Daniel, E. D. Denman, and P. Nelson, eds., vol. 76 of *Lecture Notes in Computer Science*, pp. 164–185. Springer, 1978.

[14] U. Ascher, J. Christiansen, and R. D. Russell, "A collocation solver for mixed order systems of boundary value problems," *Math. Comp.* **33** no. 146, (1979) 659–679.

[15] T. Padmanabhan, *Theoretical Astrophysics: Volume 2, Stars and Stellar Systems*. Theoretical Astrophysics. Cambridge University Press, 2000.

[16] A. Unsöld and B. Baschek, *The New Cosmos: An Introduction to Astronomy and Astrophysics*. Physics and astronomy online library. Springer, 2001.

[17] N. Glendenning, *Compact Stars: Nuclear Physics, Particle Physics, and General Relativity*. Astronomy and astrophysics library. Springer US, 2000.

[18] D. Arnett, *Supernovae and Nucleosynthesis: An Investigation of the History of Matter, from the Big Bang to the Present*. Princeton series in astrophysics. Princeton University Press, 1996.

[19] A. Lyne and F. Graham-Smith, *Pulsar Astronomy*. Cambridge Astrophysics. Cambridge University Press, 2006.

[20] W. Lewin and M. van der Klis, *Compact Stellar X-ray Sources*. Cambridge Astrophysics. Cambridge University Press, 2006.

[21] P. Goldreich and W. H. Julian, "Pulsar Electrodynamics," ApJ **157** (1969) 869.

[22] R. C. Kapoor and C. S. Shukre, "Kinematics of pulsar beams," ApJ **501** (1998) 228.

[23] P. Haensel, P. Haensel, A. Potekhin, and D. Yakovlev, *Neutron Stars 1: Equation of State and Structure*. Astrophysics and Space Science Library. Springer, 2007.

[24] M. Demiański, *Relativistic astrophysics*. International series in natural philosophy. Pergamon Press, 1985.

[25] M. Camenzind, *Compact Objects in Astrophysics: White Dwarfs, Neutron Stars and Black Holes*. Astronomy and astrophysics library. Springer, 2007.

[26] P. B. Demorest, T. Pennucci, S. M. Ransom, M. S. E. Roberts, and J. W. T. Hessels, "A two-solar-mass neutron star measured using Shapiro delay," *Nature* **467** (2010) 1081–1083, arXiv:1010.5788 [astro-ph.HE].

[27] J. Antoniadis, P. C. C. Freire, N. Wex, T. M. Tauris, R. S. Lynch, M. H. van Kerkwijk, M. Kramer, C. Bassa, V. S. Dhillon, T. Driebe, J. W. T. Hessels, V. M. Kaspi, V. I. Kondratiev, N. Langer, T. R. Marsh, M. A. McLaughlin, T. T. Pennucci, S. M. Ransom, I. H. Stairs, J. van Leeuwen, J. P. W. Verbiest, and D. G. Whelan, "A massive pulsar in a compact relativistic binary," *Science* **340** (2013) , arXiv:1304.6875 [astro-ph.HE].

[28] M. Prakash and J. M. Lattimer, "What a two solar mass neutron star really means," in *From Nuclei to Stars*, S. Lee, ed., ch. 12, pp. 275–304. Worldscientific, 2011. arXiv:1012.3208 [astro-ph.SR].

[29] I. Bednarek, P. Haensel, J. L. Zdunik, M. Bejger, and R. Ma´nka, "Hyperons in neutron-star cores and a $2m_{\odot}$," *A&A* **543** (2012) A157, arXiv:1111.6942 [astro-ph.SR].

[30] L. Bonanno and A. Sedrakian, "Composition and stability of hybrid stars with hyperons and quark color-superconductivity," *A&A* **539** (2012) A16, arXiv:1108.0559 [astro-ph.SR].

[31] S. Weissenborn, D. Chatterjee, and J. Schaffner-Bielich, "Hyperons and massive neutron stars: Vector repulsion and su(3) symmetry," *Phys. Rev. C* **85** (2012) 065802, arXiv:1112.0234 [astro-ph.HE].

[32] S. Weissenborn, I. Sagert, G. Pagliara, M. Hempel, and J. Schaffner-Bielich, "Quark matter in massive compact stars," ApJ*Letters* **740** (2011) L14, arXiv:1102.2869 [astro-ph.HE].

[33] J. S. Read, B. D. Lackey, B. J. Owen, and J. L. Friedman, "Constraints on a phenomenologically parametrized neutron-star equation of state," *Phys. Rev. D* **79** (2009) 124032, arXiv:0812.2163 [astro-ph].

[34] K. D. Kokkotas and B. Schmidt, "Quasi-normal modes of stars and black holes," *Living Reviews in Relativity* **2** (1999) .

[35] B. Sathyaprakash and B. F. Schutz, "Physics, astrophysics and cosmology with gravitational waves," *Living Reviews in Relativity* **12** (2009) .

[36] H.-P. Nollert, "Quasinormal modes: the characteristic 'sound' of black holes and neutron stars," *Classical and Quantum Gravity* **16** (1999) R159, arXiv:1304.6875 [astro-ph.HE].

[37] K. D. Kokkotas and B. F. Schutz, "W-modes - A new family of normal modes of pulsating relativistic stars," *MNRAS* **255** (1992) 119–128.

[38] N. Andersson, K. D. Kokkotas, and B. F. Schutz, "A new numerical approach to the oscillation modes of relativistic stars," *MNRAS* **274** (1995) 9.

[39] E. W. Leaver, "An analytic representation for the quasinormal modes of Kerr black holes," *Proc. R. Soc. A* **402** (1985) 285–298.

[40] M. Leins, H. P. Nollert, and M. H. Soffel, "Nonradial oscillations of neutron stars: A new branch of strongly damped normal modes," *Phys. Rev. D* **48** (1993) 3467–3472.

[41] O. Benhar, E. Berti, and V. Ferrari, "The imprint of the equation of state on the axial w-modes of oscillating neutron stars," *MNRAS* **310** (1999) 9, arXiv:gr-qc/9901037 [gr-qc].

[42] O. Benhar, V. Ferrari, and L. Gualtieri, "Gravitational wave asteroseismology reexamined," Phys. Rev. D **70** (2004) 124015.

[43] D.-H. Wen, B.-A. Li, and P. G. Krastev, "Imprints of the nuclear symmetry energy on gravitational waves from the axial w-modes of neutron stars," *Phys.Rev.* **C80** (2009) 025801, arXiv:0902.4702 [nucl-th].

[44] S. Chandrasekhar and S. Detweiler, "The quasi-normal modes of the schwarzschild black hole," *Proc. R. Soc. A* **344** (1975) 441–452.

[45] N. Andersson, "A numerically accurate investigation of black-hole normal modes," *Proc. R. Soc. A* **439** (1992) 47–58.

[46] N. Andersson, Y. Kojima, and K. D. Kokkotas, "On the oscillation spectra of ultra compact stars: an extensive survey of gravitational-wave modes," ApJ **462** (1996) 855–864, arXiv:gr-qc/9512048 [gr-qc].

[47] L. Samuelsson, N. Andersson, and A. Maniopoulou, "A characteristic approach to the quasi-normal mode problem," *Classical and Quantum Gravity* **24** (2007) 4147, arXiv:0705.4585 [gr-qc].

[48] L. M. González-Romero, "Rotating relativistic stars: Matching conditions and kinematical properties," *Phys. Rev. D* **67** (2003) 064011.

[49] N. Andersson and K. D. Kokkotas, "Gravitational waves and pulsating stars: What can we learn from future observations?," *Phys. Rev. Lett.* **77** (1996) 4134–4137.

[50] K. D. Kokkotas, T. A. Apostolatos, and N. Andersson, "The inverse problem for pulsating neutron stars: a 'fingerprint analysis' for the supranuclear equation of state," *Monthly Notices of the Royal Astronomical Society* **320** (2001) 307–315, arXiv:gr-qc/9901072 [gr-qc].

[51] N. Andersson and K. D. Kokkotas, "Towards gravitational wave asteroseismology," *Monthly Notices of the Royal Astronomical Society* **299** (1998) 1059–1068, arXiv:gr-qc/9711088 [gr-qc].

[52] R. Myers and M. Perry, "Black holes in higher dimensional space-times," *Ann. Phys. (N.Y.)* **172** (1986) 304–347.

[53] F. Tangherlini, "Schwarzschild field in n dimensions and the dimensionality of space problem," *Nuovo Cimento* **27** (1963) 636.

[54] S. Hawking and G. Ellis, *The Large Scale Structure of Space-Time*. Cambridge Monographs on Mathematical Physics. Cambridge University Press, 1973.

[55] M. Heusler, *Black Hole Uniqueness Theorems*. Cambridge Cultural Social Studies. Cambridge University Press, 1996.

[56] G. Horowitz, *Black Holes in Higher Dimensions*. Cambridge University Press, 2012.

[57] R. Emparan and H. S. Reall, "Black holes in higher dimensions," *Living Reviews in Relativity* **11** (2008) .

[58] T. Kaluza, "On the Problem of Unity in Physics," *Sitzungsber.Preuss.Akad.Wiss.Berlin (Math.Phys.)* **1921** (1921) 966–972.

[59] O. Klein, "Quantum Theory and Five-Dimensional Theory of Relativity. (In German and English)," *Z.Phys.* **37** (1926) 895–906.

[60] J. Maldacena, "The large-n limit of superconformal field theories and supergravity," *International Journal of Theoretical Physics* **38** (1999) 1113–1133, `arXiv:hep-th/9711200 [hep-th]`.

[61] J. Breckenridge, R. Myers, A. Peet, and C. Vafa, "D-branes and spinning black holes," *Physics Letters B* **391** (1997) 93 – 98, `arXiv:hep-th/9602065 [hep-th]`.

[62] M. Cvetič and D. Youm, "Near-bps-saturated rotating electrically charged black holes as string states," *Nucl. Phys. B* **477** (1996) 449, `arXiv:hep-th/9605051 [hep-th]`.

[63] M. Cvetič and C. Hull, "Black holes and u-duality," *Nucl. Phys. B* **480** (1996) 296, `arXiv:hep-th/9606193 [hep-th]`.

[64] J. Kunz, F. Navarro-Lérida, and A. K. Petersen, "Five-dimensional charged rotating black holes," *Physics Letters B* **614** (2005) 104 – 112, `arXiv:gr-qc/0503010 [gr-qc]`.

[65] J. Kunz, F. Navarro-Lérida, and J. Viebahn, "Charged rotating black holes in odd dimensions," *Physics Letters B* **639** (2006) 362 – 367, arXiv:hep-th/0605075 [hep-th].

[66] S. Hollands, J. Holland, and A. Ishibashi, "Further restrictions on the topology of stationary black holes in five dimensions," *Annales Henri Poincaré* **12** (2011) 279–301, arXiv:1002.0490 [gr-qc].

[67] S. Hollands, A. Ishibashi, and R. Wald, "A higher dimensional stationary rotating black hole must be axisymmetric," *Communications in Mathematical Physics* **271** (2007) 699–722, arXiv:gr-qc/0605106 [gr-qc].

[68] S. Hollands and A. Ishibashi, "On the 'stationary implies axisymmetric' theorem for extremal black holes in higher dimensions," *Communications in Mathematical Physics* **291** (2009) 443–471, arXiv:0809.2659 [gr-qc].

[69] S. Hollands and A. Ishibashi, "Black hole uniqueness theorems in higher dimensional spacetimes," *Classical and Quantum Gravity* **29** (2012) 163001, arXiv:1206.1164 [gr-qc].

[70] C. Misner, K. Thorne, and J. Wheeler, *Gravitation*. Gravitation. W. H. Freeman, 1973.

[71] G. Gibbons and K. ichi Maeda, "Black holes and membranes in higher-dimensional theories with dilaton fields," *Nuclear Physics B* **298** (1988) 741 – 775.

[72] A. Strominger and C. Vafa, "Microscopic origin of the bekenstein-hawking entropy," *Phys. Lett. B* **379** (1996) 99–104, arXiv:hep-th/9601029 [hep-th].

[73] A. Komar, "Covariant conservation laws in general relativity," *Phys. Rev.* **113** (1959) 934–936.

[74] J. P. Gauntlett, R. C. Myers, and P. K. Townsend, "Black holes of d = 5 supergravity," *Classical and Quantum Gravity* **16** (1999) 1, arXiv:hep-th/9810204 [hep-th].

[75] J. Kunz, D. Maison, F. Navarro-Lérida, and J. Viebahn, "Rotating einstein–maxwell–dilaton black holes in d dimensions," *Physics Letters B* **639** (2006) 95 – 100, arXiv:hep-th/0606005 [hep-th].

[76] M. Cvetič and D. Youm, "General rotating five-dimensional black holes of toroidally compactified heterotic string," *Nuclear Physics B* **476** (1996) 118 – 132, arXiv:hep-th/9603100 [hep-th].

[77] H. K. Kunduri and J. Lucietti, "Classification of near-horizon geometries of extremal black holes," *Living Reviews in Relativity* **16** (2013) .

[78] A. Sen, "Black hole entropy function, attractors and precision counting of microstates," *General Relativity and Gravitation* **40** (2008) 2249–2431, arXiv:0708.1270 [hep-th].

[79] D. Astefanesei, K. Goldstein, R. P. Jena, A. Sen, and S. P. Trivedi, "Rotating attractors," *Journal of High Energy Physics* **2006** (2006) 058, arXiv:hep-th/0606244 [hep-th].

[80] D. Astefanesei and H. Yavartanoo, "Stationary black holes and attractor mechanism," *Nuclear Physics B* **794** (2008) 13 – 27, arXiv:0706.1847 [hep-th].

[81] N. V. Suryanarayana and M. C. Wapler, "Charges from attractors," *Classical and Quantum Gravity* **24** (2007) 5047, arXiv:0704.0955 [hep-th].

[82] K. Hanaki, K. Ohashi, and Y. Tachikawa, "Comments on charges and near-horizon data of black rings," *Journal of High Energy Physics* **2007** (2007) 057, arXiv:0704.1819 [hep-th].

[83] D. Marolf, "Chern-Simons terms and the three notions of charge," arXiv:hep-th/0006117 [hep-th].

[84] X. D. Arsiwalla, "Entropy functions with 5d chern-simons terms," *Journal of High Energy Physics* **2009** (2009) 059, arXiv:0807.2246 [hep-th].

[85] P. Figueras, H. K. Kunduri, J. Lucietti, and M. Rangamani, "Extremal vacuum black holes in higher dimensions," *Phys. Rev. D* **78** (2008) 044042, arXiv:0803.2998 [hep-th].

[86] K. Goldstein and R. P. Jena, "One entropy function to rule them all...," *Journal of High Energy Physics* **2007** (2007) 049, arXiv:hep-th/0701221 [hep-th].

[87] A. Jaffe and C. Taubes, *Vortices and monopoles: structure of static gauge theories*. Progress in physics. Birkhäuser, 1980.

[88] R. Rajaraman, *Solitons and Instantons: An Introduction to Solitons and Instantons in Quantum Field Theory*. North-Holland personal library. North-Holland Publishing Company, 1982.

[89] F. Lenz, "Topological concepts in gauge theories," in *Topology and Geometry in Physics*, E. Bick and F. Steffen, eds., vol. 659 of *Lecture Notes in Physics*, pp. 7–98. Springer Berlin Heidelberg, 2005. arXiv:hep-th/0403286 [hep-th].

[90] H. Nielsen and P. Olesen, "Vortex-line models for dual strings," *Nuclear Physics B* **61** (1973) 45 – 61.

[91] M. Tinkham, *Introduction to Superconductivity*. Dover books on physics and chemistry. Dover Publications, 2004.

[92] G. Hooft, "Magnetic monopoles in unified gauge theories," *Nuclear Physics B* **79** (1974) 276 – 284.

[93] A. M. Polyakov, "Particle Spectrum in the Quantum Field Theory," *JETP Lett.* **20** (1974) 194–195.

[94] H. J. de Vega and F. A. Schaposnik, "Vortices and electrically charged vortices in non-abelian gauge theories," *Phys. Rev. D* **34** (1986) 3206–3213.

[95] F. Navarro-Lérida and D. H. Tchrakian, "Non-abelian yang-mills–higgs vortices," *Phys. Rev. D* **81** (2010) 127702, arXiv:0909.4220 [hep-th].

[96] G. V. Dunne, "Selfdual Chern-Simons theories," arXiv:hep-th/9410065 [hep-th].

[97] G. V. Dunne, "Aspects of Chern-Simons theory," arXiv:hep-th/9902115 [hep-th].

[98] P. A. Horvathy and P. Zhang, "Vortices in (abelian) Chern-Simons gauge theory," *Phys.Rept.* **481** (2009) 83–142, arXiv:0811.2094 [hep-th].

[99] J. Hong, Y. Kim, and P. Y. Pac, "Multivortex solutions of the abelian chern-simons-higgs theory," *Phys. Rev. Lett.* **64** (1990) 2230–2233.

[100] R. Jackiw and E. J. Weinberg, "Self-dual chern-simons vortices," *Phys. Rev. Lett.* **64** (1990) 2234–2237.

[101] F. Navarro-Lérida, E. Radu, and D. H. Tchrakian, "Non-abelian chern-simons-higgs solutions in 2+1 dimensions," *Phys. Rev. D* **79** (2009) 065036, arXiv:0811.3524 [hep-th].

[102] E. Berti, V. Cardoso, and A. O. Starinets, "Quasinormal modes of black holes and black branes," *Class.Quant.Grav.* **26** (2009) 163001, arXiv:0905.2975 [gr-qc].

[103] T. Padmanabhan, *Gravitation: Foundations and Frontiers*. Gravitation: Foundations and Frontiers. Cambridge University Press, 2010.